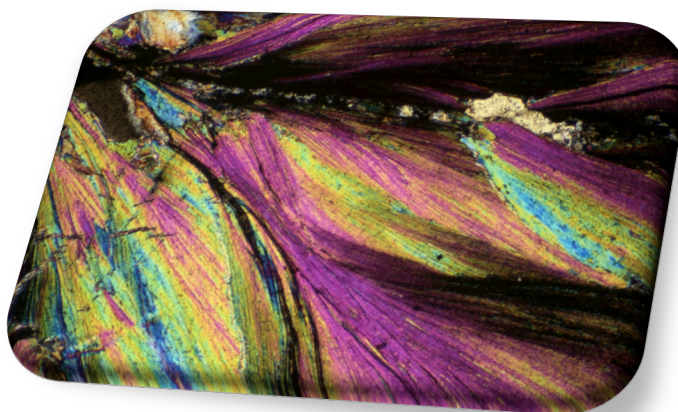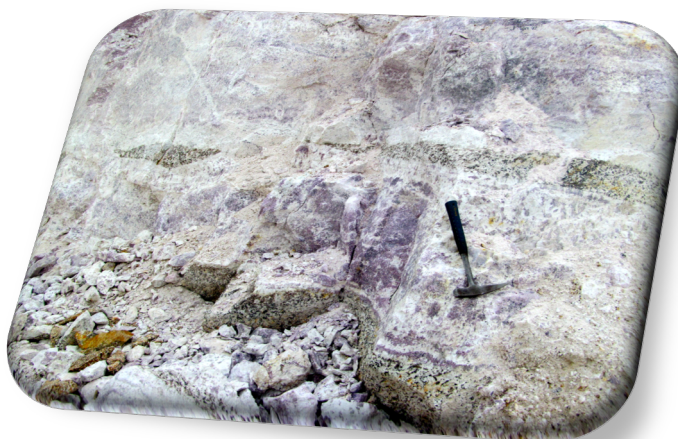# PEGMATITAS DE LA ZONA CENTRO IBÉRICA
(España y Portugal)

PEGMATITES FROM THE CENTRAL IBERIAN ZONE (SPAIN & PORTUGAL)

4ª Reunión de la Comisión de Petrología, Geoquímica y Geocronología de Rocas Ígneas y Metamórficas (PGG-RIM)

SOCIEDAD GEOLÓGICA DE ESPAÑA

Saucelle (Salamanca) 12 al 14 de septiembre de 2017
Organización y Guía de Campo: Encarnación Roda Robles

Comisión de Petrología, Geoquímica y
Geocronología de Rocas Ígneas y Metamórficas
de la Sociedad Geológica de España

Fotografías de la portada/*Cover pictures*:
- Bandeado con alternacia de niveles ricos en lepidolita con otros ricos en albita en un sill aplopegmatítico subhorizontal, encajado en un granito de dos micas, del campo de Gonçalo (Guarda, Portugal).
  Aplite-pegmatites sill with alternating lepidolite-rich and albite-rich bands, intruded into a two-mica granite. Gonçalo pegmatitic field (Guarda, Portugal).
- Foto de microscopo de luz transmitida de cristales de moscovita litinífera de la mina Feli (Campo Fregeneda-Almendra, Salamanca)
  Microphotograph of fan-shaped Li-muscovite crystals from the Feli open-pit (Fregeneda-Almendra pegmatite field, Salamanca, Spain).

LIST OF PARTICIPANTS

1. Saida Alikouss (alikouss@gmail.com)
2. Pilar Andonaegui (andonaeg@ucm.es)
3. Ricardo Arenas (rarenas@geo.ucm.es)
4. César Casquet (casquet@ucm.es)
5. Fernando Colombo (fosfatos@yahoo.com.ar)
6. Andrés Cuesta Fernández (acuesta@geol.uniovi.es)
7. Jon Errandonea Martin (jon.errandonea@ehu.eus)
8. Peter Floor (floo0117@planet.nl)
9. Mª Piedad Franco González (piti@usal.es)
10. Carmen Galindo (cgalindo@ucm.es)
11. Gloria Gallastegui Suárez (g.gallastegui@igme.es)
12. Idoia Garate Olave (idoia.garate@ehu.eus)
13. Antonio García Casco (agcasco@ugr.es)
14. Luis González Menéndez (l.gonzalez@igme.es)
15. Faouziya Haissen (faouziya.haissen@gmail.com)
16. Alexandre Lima (allima@fc.up.pt)
17. David Orejana (dorejana@ucm.es)
18. Alfonso Pesquera (npppepea@lg.ehu.es)
19. Encar Roda Robles (encar.roda@ehu.es)
20. Joana Rita Rodrigues de Freitas
21. Álvaro Rubio Ordoñez (arubio@geol.uniovi.es)
22. Sonía Sánchez Martínez (s.sanchez@geo.ucm.es)
23. Eligiusz Szeleg (eligiusz.szeleg@us.edu.pl)
24. Adam Szuszkiewizc (adam.szuszkiewicz@uwr.edu.pl)
25. Romeu Vieira (romeuvieira@gmail.com)
26. Carlos Villaseca (granito@ucm.es)

FIELD LOCATIONS

- Locality 1: Fregeneda-Almendra aplite-pegmatite field (Salamanca, Spain)

Stop 1 (12th of September, afternoon) Feli open pit

Stop 4 (14th of September, morning) Alberto I open-pit
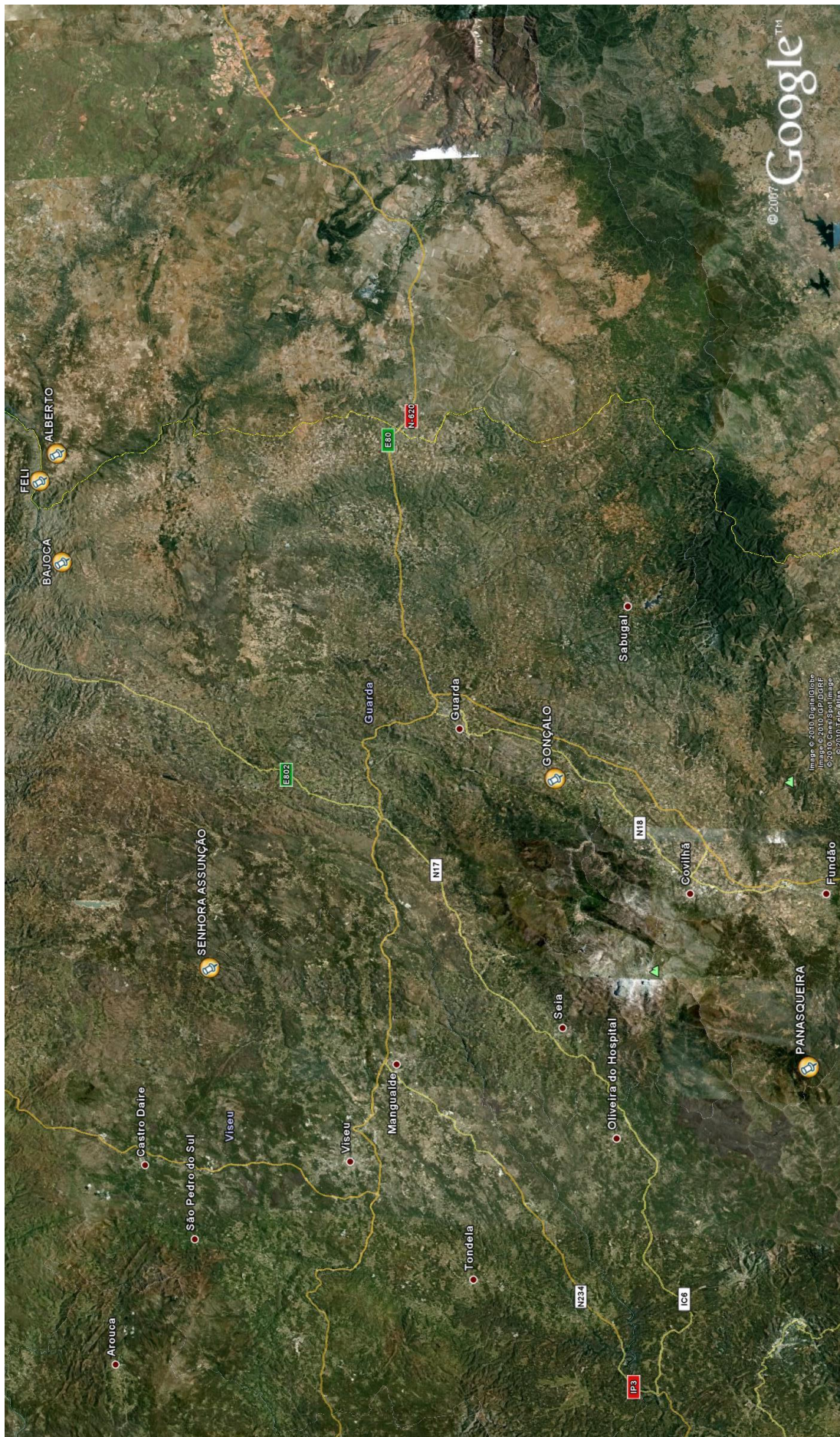
- Locality 2: The Senhora da Assunçao beryl-phosphate pegmatites (Sátão, Portugal)

Stop 2 (13th of September, morning)

- Locality 3: Gonçalo aplite-pegmatite field (Guarda-Belmonte, Portugal)

Stop 3 (13th of September, afternoon)

Field locations

Itinerary for the whole field-trip

PROGRAM

SEPTEMBER 12TH

15:00-16:00 - Reception at the Hotel Oca Aldeaduero (Salto de Saucelle, Salamanca)

16:15 - Departure from the Hotel to Stop 1 (≈30 km, 45 min + ≈ 2km by feet on a steep slope): Fregeneda-Almendra aplite-pegmatite field (Salamanca, Spain), FELI OPEN PIT

20:15 - Introductory conferences:
- **Dr. Carlos Villaseca (UCM): "Clasificación de los granitos de la ZCI"**
- **Dr. Encarnación Roda (EHU): "Introducción sobre las pegmatitas de la ZCI"**
- **Dr. Romeu Vieira (Universidade do Porto y Consultor Independente especialista en mineralizaciones de Li): "A Fregeneda-Almendra como possível fonte de lítio - petalite, espodumena ou lepidolite?"**

21:30: Dinner

SEPTEMBER 13TH

08:00 - Departure from the Hotel to Stop 2 (trip by bus, ≈154km, 2h40min)

09:45 (Portuguese time) - Arrival to Stop 2 and visit to the SENHORA DA ASSUNÇAO BERYL-PHOSPHATE PEGMATITES (Aldeia Nova, Sátão, Portugal)

12:15 (Portuguese time) - Departure from Stop 2 and Trip to Stop 3 (≈100km; 1h30min), with a stop on the way for lunch ("pic-nic").

14:45 (Portuguese time) - Visit to <u>GONÇALO APLITE-PEGMATITE FIELD</u> (Guarda-Belmonte, Portugal)

17:15 (Portuguese time) - Departure to the hotel (≈141 km, 2h)

20:45 – Students conferences:
- **Dr. Fernando Colombo (CONICET-Universidad Nacional de Córdoba, Argentina): "Cristaloquímica de fosfatos pegmatíticos: un estudio con microsonda de electrones y difracción de rayos X de monocristal a través del sustrato (tts-micro-XRD)".**
- **Idoia Garate Olave (Universidad del País Vasco UPV/EHU): "Evolución del sistema granito-pegmatita de Tres Arroyos (Badajoz) documentado por las variaciones composicionales del cuarzo"**
- **Jon Errandonea (Universidad del País Vasco UPV/EHU): "Petrología de granitoides alóctonos peraluminosos con cordierita. Ejemplo: el plutón de Sierra Bermeja (Zona Centro Ibérica)"**

21:30: Dinner

SEPTEMBER 14TH

08:30 - Departure from the Hotel to Stop 4 (≈26 km, 35 min + ≈ 1km by feet on a steep slope): Fregeneda-Almendra aplite-pegmatite field (Salamanca, Spain), <u>ALBERTO I OPEN PIT</u>

11:30 – Departure to Aldeadavila de la Rivera (≈ 63 km, 1h10min)

13:00 - Trip along the Duero river (≈1h30min)
**14:30 - Lunch at "El Zebadero" restaurant and end of the field-trip.**

THE PEGMATITES FROM THE CENTRAL IBERIAN ZONE

Introduction

Pegmatites are relatively common in the Central Iberian Zone (CIZ) of the Iberian Massif, in a NNW-SSE striking belt, ≈500 km long and ≈150 km wide, being particularly abundant in the provinces of Salamanca, Cáceres, Pontevedra, south of Zamora and north of Badajoz in Spain, and in the Viana do Castelo, Porto, Vila Real, Guarda, Castelo Branco and Viseu districts in Portugal (Fig. 1, Table 1) (Roda-Robles et al., 2016). These pegmatites are often barren, with none or just a slight enrichment in incompatible elements. However, rare-element pegmatites, mainly enriched in Li±F±P±Nb±Ta±Sn±Be±B may be also locally abundant. The pegmatites exhibit varying degrees of evolution and can show distinct patterns of regional zonation. In some cases these pegmatites form a pegmatite field around a granitic body. This is the case for the Li-Sn-rich Fregeneda-Almendra aplite-pegmatite field (Salamanca-Guarda) (Roda *et al.* 1999; Vieira *et al.* 2011), the Barroso-Alvão field (Northern Portugal) (Lima, 2000; Martins *et al.*, 2012), and the Tres Arroyos field (Badajoz) (Garate-Olave et al., 2017), among others. In other cases, Li-rich aplite-pegmatitic facies are observed in the marginal and/or apical parts of leucogranites, as in the Pinilla de Fermoselle pegmatite (Zamora) (Roda-Robles *et al.*, 2012b) and the Castillejo de Dos Casas cupola (Roda-Robles et al., 2015). Lithium enrichment can also occur in the intermediate zones of coarse-grained beryl-phosphate pegmatites, usually hosted by granites, such as the Cañada (Salamanca) (Roda *et al.*, 2004) and Mangualde (Viseu) (Carvalho and Farinha, 2004) pegmatites. Geological and mineralogical data indicate that all these types of pegmatites belong to a metallogenetic province related to the Variscan orogeny. Field, geochemical and structural relationships, as well as the available geochronological data (Roda-Robles *et al.*, 2009), indicate that the origin of the pegmatites is most probably related to the major Variscan granitic magmatism occurring between 320 and 290 Ma. The crystallization of the residual melts generated by high degrees of fractional crystallization of P-rich and Ca-poor, S-type, highly peraluminous granites is the most likely origin for most of the Li-richest bodies from the CIZ (Roda-Robles et al., 2016; Roda-Robles et al., submitted).

The Regional Geology of the Central Iberian Zone

The CIZ constitutes the westernmost region of the Variscan European Belt. It is composed of metasedimentary rocks in a great extent. In the southern CIZ (S-CIZ), Neoproterozoic to Early Cambrian define a thick succession of shales and sandstones with scarce interlayered volcanoclastic rocks (up to 11,000 m), known as the Schist-Greywacke Complex (SGC). The correlative metasedimentary sequences of the northern CIZ (N-CIZ) are chemically different to the SGC, being richer in LILE, REE and some HFSE, and having lower P contents. The CIZ is characterized by a large volume of syn- to post-tectonic granitic intrusions outcropping from central to NW Iberian Peninsula. The progressive thermal maturity of the orogenically thickened crust combined with the change from a compressional to a transtensional/transpressional regime resulted in extensive crustal melting (e.g., Bea et al., 1999; Dias et al., 2002). The CIZ granite magmatism is mostly late- to post-kinematic with respect to the regional D3 phase. Thus, CIZ granites intrude after the main phases of ductile deformation, which are coeval with migmatization and low-pressure/high temperature M2 metamorphism in some CIZ sectors. According to their emplacement ages, the CIZ granites have been classified as syn-D3 (320-310 Ma), late-D3 (310-306 Ma) and post-D3 (305-290 Ma) (e.g., Dias et al., 1998). According to Villaseca (2011) the granitic rocks from the CIZ can be grouped into five geochemically different series: (1) two-mica peraluminous leucogranites (S1); (2) P-rich highly peraluminous granites (S2); (3) P-poor moderately peraluminous granites (S3); (4) moderately to low peraluminous granites (S4); and (5) I-type low peraluminous granites (I).
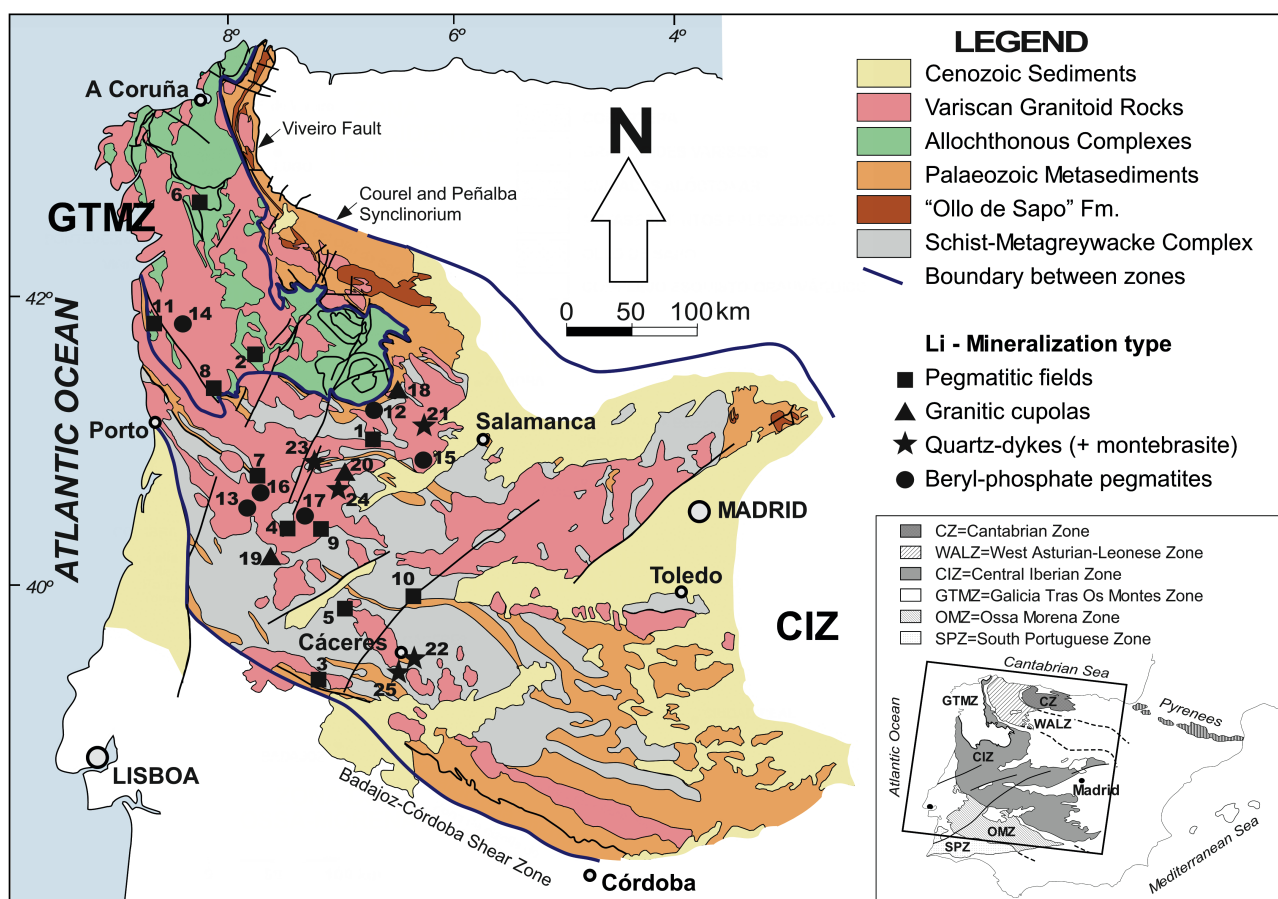
Fig. 1: Schematic geological map of the Central Iberian Zone (CIZ) and the Galicia-Trás-Os Montes Zone (GTMZ) (Spain and Portugal) (modified from Martinez-Catalán et al., 2004, with the permission of the SGE and authors) with the location of the different Li-mineralization. Numbers as in Table 1 (Roda-Robles et al., 2016).

General Geology of the Pegmatites

Pegmatites are rocks commonly characterized by their coarse, sometimes giant grain size, and often by an internal zoning with the development of a massive quartz-core, intermediate(s) zone(s) and a wall zone, in the simplest case. Pegmatitic bodies showing these features are common in the CIZ, as for example the Puentemocha pegmatite (Salamanca, Spain) (Roda-Robles et al., 2012b) or the Senhora da Assunção pegmatite (Viseu, Portugal) (Trabulo et al., 1995; Roda-Robles et al. 2014). These are Be-P-rich pegmatites, belonging to the beryl-phosphate subtype of the Černý and Ercit classification (2005). However, the rare-elements-richest bodies (mainly Li) occurring in the CIZ are texturally and chemically quite different from these more commonly observed LCT (Li-Cs-Ta) pegmatites. On the one hand, many of these Li-rich bodies show an aplitic texture, frequently with the development of line-rock units. Coarse crystals are also common, but usually smaller than 10 cm long; and internal zoning of the pegmatites, if present, usually does not show the development of a core nor intermediate zones. On the other hand, the Li-richest bodies usually show an important overall enrichment in this element, locally even with values in Li2O > 2 wt%. The main features of the three Li-rich pegmatite types from the CIZ are explained in the following (Table 1, Fig. 1):

Aplite-pegmatite fields

This is the most common type of Li-mineralization found in the CIZ. Lithium-bearing pegmatites outcrop in groups of up to one hundred dykes, hosted in granites and in metasediments. These dykes are usually thin (from a few centimeters up to 20 m thick),

and lengths from a few meters up to a 1.5km, with very variable dipping, from subhorizontal (e.g. Gonçalo and Tres Arroyos fields) to subvertical (e.g. Fregeneda-Almendra field). Not all of the pegmatites in each field are enriched in Li. Actually, it is not rare that pegmatites display a regional zoning, where barren, intermediate and Li-rich pegmatites are located in different areas of the field, with a clear sense of enrichment in rare-metals mainly including Li and F, but also Sn, P, Nb, Ta, Rb and Cs in some cases (e.g. Fregeneda-Almendra and Tres Arroyos fields). Usually no internal zoning is observed in these Li-bearing dykes. The grain size may be very homogeneous (aplitic or pegmatitic), with crystals only exceptionally >12 cm in length; or pretty heterogeneous, with aplitic and pegmatitic facies occurring in the same pegmatite body. It is also relatively common to observe layered units, usually parallel to the contacts with the host-rocks. In such case, the layering is often developed from wall to wall (e.g. Fregeneda-Almendra, Gonçalo, and Tres Arroyos fields). In the simplest case, the layering consists of two alternating mineral associations (e.g. Li-mica + quartz alternating with albite + quartz as it is observed in the Gonçalo and Fregeneda-Almendra fields) (Fig. 2a); whereas in other cases there are different layers following distinct and complex patterns across the dyke. The occurrence of wedge-shaped crystals of K-feldspar that grow perpendicular to the contacts with the host-rock and with their vertex pointing to the walls is also common. Mineralogy of these pegmatites is quite simple, including albite, quartz, K-feldspar and muscovite in the barren dykes, and spodumene, petalite, Li-muscovite and/or lepidolite, in different proportions, in the Li-rich dykes. Those showing the highest fractionation levels are rich in Li-micas. Amblygonite-montebrasite, cassiterite, and Nb-Ta oxides are the most common accessory minerals in all the dykes of the pegmatite fields. Overall, these pegmatites are highly peraluminous, with a high Na content, and usually lower K values. In the Li-rich pegmatite bodies, the volume of Li-bearing minerals may achieve high concentrations (e.g. up to ≈ 50 % of spodumene modal proportion across some dykes of the Fregeneda-Almendra field).
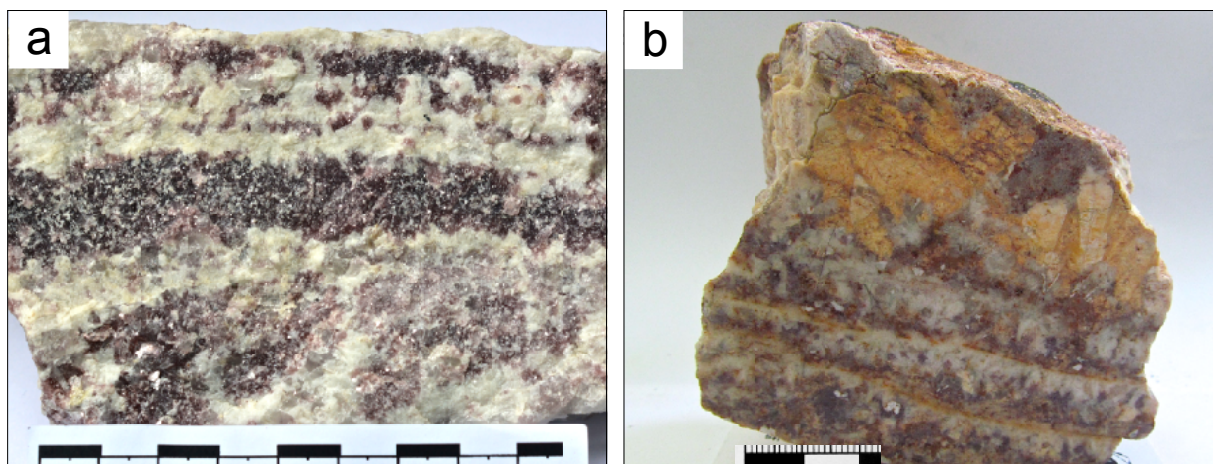

Fig. 2: (a) Rythmic layering with alternating lepidolite-rich and albite-rich bands in an aplite-pegmatite dyke from the Gonçalo field; (b) similar texture as (a) in the lower part, plus some wedge-shaped crystals of K-feldspar in the upper part, from the stockscheider of Castillejo de Dos Casas (Roda-Robles et al., 2016).

Beryl-phosphate pegmatites
The beryl-phosphate pegmatites occur usually as intragranitic bodies in the CIZ. Their fractionation degree is in general lower than that of the Li-richest aplite-pegmatites from the fields. Main enrichment in these pegmatites are in Li±Be±Nb±Ta. Li is mainly contained in subrounded masses (>1.5 m Ø) of Fe-Mn phosphates, usually of the triphylite-lithiophilite series (e.g. Cañada, Pedra da Moura, Senhora da Assunção). These pegmatites show a well-developed internal structure and a coarse grain size. Main minerals include quartz, K-feldspar, plagioclase, beryl, muscovite, biotite, with schorl, Nb-Ta-oxides and apatite as minor or accessory phases. The shape of these bodies goes

from tabular to turnip-shaped. Similarly to the rest of the Li-rich pegmatites, these are peraluminous rocks, with high Na contents, and with the highest K values. The overall chemical composition of these dykes reveals that they are the less enriched in Li, F and other rare-elements, as the volume of phosphates is usually < 10%.

Highly fractionated pegmatitic leucogranitic cupolas
This kind of occurrence is not as common as the ones decribed previously. They occur in the apical or marginal areas of quite fractionated leucogranites, hosted by metasediments of the SGC. The associated leucogranites are usually fine grained and enriched in B, Li and F. The apical/marginal zones are quite heterogeneous, including different mineral associations. The most common facies consists of a fine-grained matrix of quartz, albite and Li-mica, where coarser crystals of K-feldspar grow perpendicularly to the contacts, and topaz, montebrasite, petalite, cassiterite and columbite group minerals are accessory. Another typical facies includes fine- to medium-sized layered, subhorizontal textures (stockscheider), with lepidolite-rich bands alternating rhythmically with feldspars-rich bands (e.g. Castillejo de Dos Casas) (Fig. 2b). Overall, the chemical composition of these bodies is quite similar to that of the dykes in the pegmatite fields, with mean ASI ≈1.70; high Na (from 3.1 to 5.6 wt% Na2O); and lower K values in the range 2.1 - 5.1 wt% K2O (data from Martín-Izard et al. 1992 and this study).

Table 1: Localities and main characteristics of Li-pegmatites from the CIZ (Roda-Robles et al., 2016).

	LOCALITY	MINERALIZATION TYPE (country rocks)	MINERAL ASSOCIATION*	Li-MINERALS
1	**Fregeneda-Almendra** (Salamanca, Spain- Guarda, Portugal) Vieira et al., 2011	Several pegmatites, some Li-rich (micaschists)	Qtz, Fsp, Li-Ms, Spd, Ptl, Cst, Mtb	**Spodumene Petalite** Li-Muscovite Montebrasite
2	**Barroso-Alvão** (Vila Real, Northern Portugal) Lima, 2000 Martins et al., 2012	Several pegmatites, some Li-rich (micaschists)	Qtz, Fsp, Ms, Spd, Ptl, Cst, Nb-Ta oxides	**Spodumene Petalite** Lepidolite Montebrasite
3	**Tres Arroyos** (Badajoz, Spain) Garate-Olave et al., 2014	Aplite-pegmatites, some Li-rich (metasediments)	Qtz, Fsp, Ms, Li-Ms, Mtb, Tpz, Cst, Nb-Ta oxides	**Li-Muscovite** Montebrasite
4	**Gonçalo** (Belmonte-Guarda, Portugal) Neiva and Ramos, 2010	Li-rich pegmatites (granite)	Qtz, Fsp, Ms, Li-Ms, Amb, Ptl, Tpz, Tur, Cst, Nb-Ta oxides+Zwd in country rock	**Li-Muscovite Amblygonite** Zinnwaldite
5	**Segura** (Central Portugal) Antunes et al. 2013	Li-rich aplite-pegmatites (michaschists)	Qtz, Fsp, Lpd, Mtb, Tpz, Cst, Nb-Ta oxides	**Lepidolite** Montebrasite
6	**Lalin-Forcarei** (Galicia, Spain) Fuertes-Fuente and Martín-Izard, 1998	Aplite-pegmatites, some Li-rich (metasediments)	Fsp, Qtz, Spd, Ms, Mtb, Cst, Nb-Ta oxides	**Spodumene** Montebrasite
7	**Queiriga** (Alto Vouga, Portugal) Dias et al. 2013	Perigranitic pegmatites (andalusite schists)	Qtz, Fsp, Ptl, Lpd, Spd, Tpz, Brl, Cst, Nb-Ta oxides	**Petalite**, Lepidolite, Spodumene
8	**Seixoso-Vieiros** (Vila Real, Northern Portugal) Lima et al. 2009	Aplite-pegmatites + leucogranitic cupola (metasediments)	Qtz, Fsp, Ptl, Mtb, Spd	**Petalite** Montebrasite, Spodumene
9	**Cabeço dos Poupos** (Sabugal, Portugal) Neiva et al. 2011	Li-rich aplite-pegmatites (granite)	Qtz, Fsp, Ms, Li-Ms, Zwd, Tur, Cst, Nb-Ta oxides, Ap, triplite	**Li-Muscovite**, Zinnwaldite
10	**Las Navas** (Cáceres, Spain) Gallego Garrido, 1992	Li-rich aplite-pegmatites, (metasediments)	Qtz, Fsp, Ms, Li-Ms, Mtb, Tpz, Spd, Cst, Nb-Ta oxides	**Li-Muscovite** Montebrasite Spodumene
11	**Serra de Arga** (Viana do Castelo, Portugal) Leal Gomes, 1994	Li-rich aplite-pegmatites, (metasediments)	Qtz, Fsp, Ms, Ptl, Lpd, Spd, Cst, Nb-Ta oxides	**Petalite Lepidolite** Spodumene Montebrasite
12	**Puentemocha (Salamanca, Spain) Roda-Robles et al., 2013**	Beryl- phosphates subtype pegmatites (granite)	Qtz, Ms, Fsp, Bt, Brl, Fe-Mn phosp, sulphides	**Ferrisicklerite**
13	**Senhora da Assunçao** (Alto Vouga, Portugal) Dias et al. 2013	Beryl- phosphates subtype pegmatites (granite)	Qtz, Fsp, Ms, Brl, Bt, Fe-Mn phosp, Al-phosp, Nb-Ta oxides, sulphides	**Triphylite**
14	**Pedra da Moura** (Ponte da Barca, Portugal) Leal Gomes et al. 2009	Beryl- phosphates subtype pegmatites (granite)	Qtz, Ms, Fsp, Brl, Fe-Mn phosp, sulphides	**Triphylite**
15	**Cañada** (Salamanca, Spain) Roda et al. 2004	Beryl- phosphates subtype pegmatite (gabbro and granite)	Qtz, Ms, Fsp, Tur, Bt, Grt, Brl, Fe-Mn phosp, Nb-Ta oxides, sulphides	**Triphylite Ferrisicklerite**
16	**Mangualde** (Viseu, Portugal) Carvalho and Farinha, 2004	Beryl- phosphates subtype pegmatites (granite)	Qtz, Fsp, Ms, Brl, Bt, Grt, Tur, Fe-Mn phosp, Nb-Ta oxides, sulphides	**Triphylite** Ferrisicklerite
17	**Seixeira-Fonte da Cal** (Guarda, Portugal) Roda-Robles et al. 2008	Beryl- phosphates subtype pegmatites (granite)	Qtz, Fsp, Ms, Brl, Fe-Mn phosp	**Ferrisicklerite**
18	**Pinilla de Fermoselle** (Zamora, Spain) Roda-Robles et al. 2012a	Pegmatitic cupola over a granite, Li-rich in its upper part	Qtz, Ms, Fsp, Tur, Lpd, Bt, Zwd, Fe-Mn phosph	**Lepidolite Ferrisicklerite** Elbaite Zinnwaldite
19	**Argemela** (Guarda, Portugal) Charoy and Noronha, 1996	Microgranite + Quartz-Albite-dykes with montebrasite	Qtz, Fsp, Ms, Lpd, Mtb, Cst, Nb-Ta oxides	**Lepidolite** Montebrasite
20	**Castillejo de Dos Casas** (Salamanca, Spain) Martín-Izard et al. 1992; Roda-Robles et al. 2013	Stockscheider over a leucogranitic cupola in contact to the micaschists	Qtz, Fsp, Li-Ms, Ptl, Cst, Mtb, Tpz, Fe-Mn phosp	**Li-Muscovite** Petalite Montebrasite Lithiophilite

Geology and mineralogy of Li mineralization in the Central Iberian Zone (Spain and Portugal)

E. Roda-Robles[1,*], A. Pesquera[1], P. P. Gil-Crespo[1], R. Vieira[2,3], A. Lima[3,4], I. Garate-Olave[1], T. Martins[5] and J. Torres-Ruiz[6]

[1] Departamento Mineralogía y Petrología, Univ. País Vasco (UPV/EHU), Apdo. 644, 48080-Bilbao, Spain
[2] Sojitz Beralt Tin & Wolfram (Portugal) S.A., Portugal
[3] Instituto Ciências da Terra (Pólo da UP), Porto, Portugal
[4] Departamento Geociências, Ambiente e Ordenamento do Território, Faculdade de Ciências, Universidade do Porto, Portugal
[5] Manitoba Geological Survey, 360-1395 Ellice Av., Winnipeg, Manitoba R3G 3P2, Canada
[6] Departamento de Mineralogía y Petrología, Universidad de Granada, 18071 Granada, Spain

ABSTRACT

Lithium mineralization is common in the Central Iberian Zone and, to a lesser extent, in the Galizia-Trás-Os-Montes Zone of Spain and Portugal, occurring along a ~500 km-long NNW-SSE striking belt. There are different styles of Li mineralization along this belt; they are mainly associated with aplite-pegmatite bodies and, to a much lesser extent, with veins of quartz and phosphate. Lithium mineralization in the Central Iberian Zone may be classified into four types: aplite-pegmatite dykes occurring in pegmatitic fields, Li mineralization associated with leucogranitic cupolas, beryl-phosphate pegmatites and quartz-montebrasite veins. The main Li minerals of these bodies include Li-mica, spodumene and/or petalite in the pegmatitic fields and leucogranitic cupolas; triphylite–lithiophilite in the beryl-phosphate pegmatites, and amblygonite–montebrasite in the quartz-montebrasite veins. The origin of these different styles of mineralization is considered to be related to differentiation of peraluminous melts, which were generated by partial melting of metasedimentary rocks during the Variscan orogeny. On the basis of paragenesis and chemical composition, the pegmatitic fields and Li mineralization associated with granitic cupolas record the highest fractionation levels, whereas the beryl-phosphate pegmatites and quartz-montebrasite veins show lower degrees of fractionation. There are a number of textural and mineralogical indicators for Li exploration in the Central Iberian Zone and in the Galizia-Trás-Os-Montes Zone, with the highest economic potential for Li being in the pegmatite fields.

Keywords: lithium, pegmatites, hydrothermal veins, granites, Variscan orogeny, Central Iberian Zone, Spain, Portugal.

Introduction

Lithium is a relatively rare element in the Earth´s crust. Its uses and, consequently, its price, have increased considerably during the last decade. Among its many uses, the high demand for high-efficiency Li-batteries contributes to the increasing importance of Li as a strategic element (Christmann *et al.*, 2015). Lithium (±Sn, Nb and Ta) mineralization is common in the Central Iberian Zone and, to a lesser extent, in the Galizia-Trás-Os-Montes Zone, both in the Iberian Massif of Spain and Portugal. The Li-rich rocks occur in a NNW-SSE striking belt, ~500 km long and ~150 km wide, being particularly abundant in the provinces of Salamanca, Cáceres, Badajoz and Pontevedra in Spain, and in the Viana do Castelo, Porto, Vila Real, Guarda, Castelo Branco and Viseu districts in

Portugal (Fig. 1, Table 1). The mineralization occurs principally in aplite-pegmatite bodies and, to a much lesser extent, in hydrothermal veins with quartz and phosphates. The first Li ore was mined in the Central Iberian Zone in Portugal, for a short period during the 1920s and 1930s (Garção, 1927), and consisted of material rich in montebrasite–amblygonite from hydrothermal veins. Subsequently, from the 1970s, lepidolite-rich aplite-pegmatite dykes were exploited. More recently, petalite and spodumene-bearing pegmatites have become the main source of lithium ore in this region. Mineralization in the Portuguese part of these zones is nowadays mined intensively, and since 2009 Portugal has become the world's sixth largest producer of Li raw material (Christmann *et al.,* 2015). With the exception of the first-mined amblygonite–montebrasite assemblage that was used for alkaline accumulators, the main application of lithium extracted in the Central Iberian Zone has been in the ceramics and glass industries.

The aplite-pegmatites exhibit varying degrees of evolution and can show distinct patterns of regional zonation. In some cases these pegmatites form a pegmatite field around a granitic body. This is the case for the Li-Sn-rich Fregeneda-Almendra pegmatite field (Salamanca-Guarda) (Roda *et al.,* 1999; Vieira *et al.,* 2011) and the Barroso-Alvão field (Northern Portugal) (Lima, 2000; Martins *et al*., 2012), among others. In other cases, Li enrichment is observed in the marginal and/or apical parts of leucogranites, as in the Pinilla de Fermoselle pegmatite (Zamora) (Roda-Robles *et al*., 2012*b*). Lithium enrichment can also occur in the intermediate zones of coarse-grained beryl-phosphate pegmatites, usually hosted by granites, such as the Cañada (Salamanca) (Roda *et al*., 2004) and Mangualde (Viseu) (Carvalho and Farinha, 2004) pegmatites. In addition to pegmatites *sensu stricto*, other Li-enriched dyke-like bodies related to granitic rocks, are also observed in the Central Iberian Zone, both in Spain and Portugal. These are very rich in quartz and amblygonite–montebrasite, and are considered as hydrothermal veins. Examples include those occurring at Valdeflores (Cáceres) (Pesquera *et al*., 1999), Golpejas (Salamanca) (Matín-Izard *et al*., 1992) and Massueime (Guarda) (Carvalho and Farinha, 2004, Roda-Robles *et al*., 2012*c*). Geological and mineralogical data indicate that all these types of Li mineralization belong to a metallogenetic province related to the Variscan orogeny. Field, geochemical and structural relationships, as well as the available geochronological data (Roda-Robles *et al*., 2009),

indicate that the origin of the mineralization is most probably related to the major Variscan granitic magmatism occurring between 330 and 290 Ma.

The main Li-rich minerals occurring in the mineralization described here include the silicates spodumene, petalite, Li-rich micas, and the phosphates amblygonite–montebrasite and triphylite–lithiophilite. Elbaite is only found as a minor mineral in a few pegmatites. Some, or all, of these minerals have been identified in each of these bodies, in varying modal proportions. In this paper we present a detailed petrographic and compositional description of the Li-bearing minerals in the different types of mineralization, discuss their origin, and their potential for Li-exploration.

Geological setting

Lithium-rich mineralization in the Iberian Massif is located mainly in the Central Iberian Zone and, in a lesser extent, in the Galizia-Trás-Os-Montes Zone to the north-west (Fig. 1). This zone, allocthonous to parautochonous over the Central Iberian Zone, has been considered a subzone of the Central Iberian Zone by some authors (e.g. Julivert *et al*., 1972), whereas others consider it a separate zone (e.g. Farias *et al*., 1987; Arenas *et al*., 2004). In the Galicia-Trás-Os-Montes Zone, however, pegmatites only occur in materials that have similar ages and character to those occurring further south in the Central Iberian Zone. For this reason, we include both areas in this study, although it should be noted that Li mineralization is much less abundant in the Galicia-Trás-Os-Montes Zone than in the Central Iberian Zone. The Central Iberian Zone and the Galicia-Trás-Os-Montes Zone together represent the westernmost segment of the European Variscan Belt that was formed in the Upper Paleozoic during the collision of Gondwana and Laurentia (Martínez Catalán *et al*., 1996), with three main phases of variscan deformation (Martínez-Fernández, 1974; Noronha *et al*., 1981). The Central Iberian Zone is characterized by extensive granitic magmatism and by the occurrence of high-grade metamorphic complexes (Martínez *et al*., 1988). It is limited by the Viveiro Fault and its continuation along the Courel and Peñalba Synclinoriums to the north (Martínez Catalán, 1985), in contact with the West Asturian-Leonese Zone. The Ossa Morena Zone occurs to the south west of the Central Iberian Zone, with the Central Unit of the Badajoz-Córdoba Shear Zone separating both zones (Díez Balda *et al*., 1990; Azor *et al*., 1994). The Central Iberian
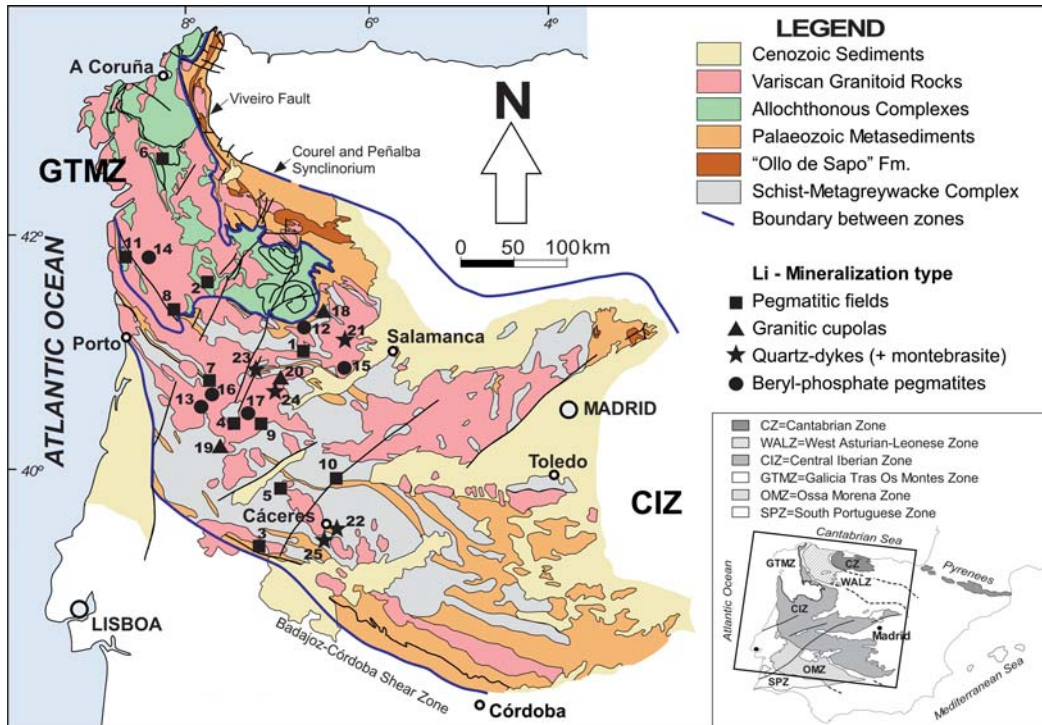
FIG. 1. Schematic geological map of the Central Iberian Zone (CIZ) and the Galicia-Trás-Os Montes Zone (GTMZ) (Spain and Portugal) (modified from Martinez-Catalán *et al.*, 2004, with the permission of the SGE and authors) with the location of the different Li mineralization areas. Numbers as in Table 1.

Zone is divided into two subdomains (Pérez-Estaún *et al.*, 2004): (1) the Ollo de Sapo Domain to the north, characterized by broad outcrops of gneisses with coarse ovoid megacrystals of feldspar (augen gneisses), syntectonic granites and high-degree regional metamorphism in some areas; and, (2) the Schist-Metagreywacke Complex Domain to the south, where Neoproterozoic to Lower Palaeozoic metasedimentary rocks including metamorphosed shales, sandstones, and minor conglomerates and limestones, are intruded by abundant granitoids (Fig. 1). The central parts of the Iberian Massif are characterized by voluminous, syn- to late-D_2, S-type, granitic magmatism (330–290 Ma). Recycling of meta-sediments and meta-igneous materials from the continental crust is the most plausible protolith for most of the granites in the Central Iberian Zone (Bea, 2004). The granitoids can be grouped into four categories (for an overview see Bea, 2004): (G1) early granodiorites and monzogranites; (G2) granites and leucogranites from anatectic complexes; (G3) allochthonous granites and leucogranites; and (G4) late granodiorites and monzogranites.

Data collection and analyses

Over 700 samples were collected from the different types of Li mineralization and from their country rocks. Identification of the silicates and phosphates was achieved by studying their optical properties in thin section under the polarizing microscope, powder X-ray diffraction techniques and electron-microprobe analyses. Over 1400 microprobe analyses of micas, 120 of Li-aluminosilicates, 150 of amblygonite–montebrasite and 340 of Li-bearing Fe-Mn phosphates were obtained. Representative micas and Li-aluminosilicates were analysed at the University of Granada, using a Cameca SX50 microprobe equipped with four wavelength-dispersive spectrometers. Operating conditions were 20 kV accelerating voltage, 20 nA beam current and a beam diameter of ~2 μm. Both

TABLE 1. Localities and main characteristics of Li mineralization in the Central Iberian Zone and in the Galizia-Trás-Os-Montes Zone.

	Locality	Mineralization type (country rocks)	Mineral association*	Li minerals
1	Fregeneda-Almendra (Salamanca, Spain-Guarda, Portugal) Roda *et al.* (1999) Vieira *et al.* (2011)	Several pegmatites, some Li rich (micaschists)	Qtz, Fsp, Li-Ms, Spd, Ptl, Cst, Mtb	**Spodumene** **Petalite** Li-Muscovite Montebrasite
2	Barroso-Alvão (Vila Real, Northern Portugal) Lima (2000) Martins *et al.* (2012)	Several pegmatites, some Li rich (micaschists)	Qtz, Fsp, Ms, Spd, Ptl, Cst, Nb-Ta oxides	**Spodumene** **Petalite** Lepidolite Montebrasite
3	Tres Arroyos (Badajoz, Spain) Garate-Olave *et al.* (2014)	Aplite-pegmatites, some Li rich (metasediments)	Qtz, Fsp, Ms, Li-Ms, Mtb, Tpz, Cst, Nb-Ta oxides	**Li-Muscovite** Montebrasite
4	Gonçalo (Belmonte-Guarda, Portugal) Neiva and Ramos (2010)	Li-rich pegmatites (granite)	Qtz, Fsp, Ms, Li-Ms, Amb, Ptl, Tpz, Tur, Cst, Nb-Ta oxides + Zwd in country rock	**Li-Muscovite** **Amblygonite** Zinnwaldite
5	Segura (Central Portugal) Antunes *et al.* (2013)	Li-rich aplite-pegmatites (michaschists)	Qtz, Fsp, Lpd, Mtb, Tpz, Cst, Nb-Ta oxides	**Lepidolite** Montebrasite
6	Lalin-Forcarei (Galicia, Spain) Fuertes-Fuente and Martín-Izard (1998)	Aplite-pegmatites, some Li rich (metasediments)	Fsp, Qtz, Spd, Ms, Mtb, Cst, Nb-Ta oxides	**Spodumene** Montebrasite
7	Queiriga (Alto Vouga, Portugal) Dias *et al.* (2013)	Perigranitic pegmatites (andalusite schists)	Qtz, Fsp, Ptl, Lpd, Spd, Tpz, Brl, Cst, Nb-Ta oxides	**Petalite**, Lepidolite, Spodumene
8	Seixoso-Vieiros (Vila Real, Northern Portugal) Lima *et al.* (2009)	Aplite-pegmatites + leucogranitic cupola (metasediments)	Qtz, Fsp, Ptl, Mtb, Spd	**Petalite** Montebrasite, Spodumene
9	Cabeço dos Poupos (Sabugal, Portugal) Neiva *et al.* (2011)	Li-rich aplite-pegmatites (granite)	Qtz, Fsp, Ms, Li-Ms, Zwd, Tur, Cst, Nb-Ta oxides, Ap, triplite	**Li-Muscovite**, Zinnwaldite
10	Las Navas (Cáceres, Spain) Gallego Garrido (1992)	Li-rich aplite-pegmatites, (metasediments)	Qtz, Fsp, Ms, Li-Ms, Mtb, Tpz, Spd, Cst, Nb-Ta oxides	**Li-Muscovite** Montebrasite Spodumene
11	Serra de Arga (Viana do Castelo, Portugal) Leal Gomes (1994)	Li-rich aplite-pegmatites, (metasediments)	Qtz, Fsp, Ms, Ptl, Lpd, Spd, Cst, Nb-Ta oxides	**Petalite** **Lepidolite** Spodumene Montebrasite
12	Puentemocha (Salamanca, Spain) Roda-Robles *et al.* (2012*a*)	Beryl-phosphates subtype pegmatites (granite)	Qtz, Ms, Fsp, Bt, Brl, Fe-Mn phosp, sulfides	**Ferrisicklerite**
13	Nossa Senhora da Assunção (Alto Vouga, Portugal) Dias *et al.* (2013)	Beryl-phosphates subtype pegmatites (granite)	Qtz, Fsp, Ms, Brl, Bt, Fe-Mn phosp, Al-phosp, Nb-Ta oxides, sulfides	**Triphylite**
14	Pedra da Moura (Ponte da Barca, Portugal) Leal Gomes *et al.* (2009)	Beryl-phosphates subtype pegmatites (granite)	Qtz, Ms, Fsp, Brl, Fe-Mn phosp, sulfides	**Triphylite**

(continued)

TABLE 1. (*contd*.)

	Locality	Mineralization type (country rocks)	Mineral association*	Li minerals
15	Cañada (Salamanca, Spain) Roda *et al.* (2004)	Beryl-phosphates subtype pegmatite (gabbro and granite)	Qtz, Ms, Fsp, Tur, Bt, Grt, Brl, Fe-Mn phosp, Nb-Ta oxides, sulfides	**Triphylite** **Ferrisicklerite**
16	Mangualde (Viseu, Portugal) Carvalho and Farinha (2004)	Beryl-phosphates subtype pegmatites (granite)	Qtz, Fsp, Ms, Brl, Bt, Grt, Tur, Fe-Mn phosp, Nb-Ta oxides, sulfides	**Triphylite** Ferrisicklerite
17	Seixeira-Fonte da Cal (Guarda, Portugal) Roda-Robles *et al.* (2008)	Beryl-phosphates subtype pegmatites (granite)	Qtz, Fsp, Ms, Brl, Fe-Mn phosp	**Ferrisicklerite**
18	Pinilla de Fermoselle (Zamora, Spain) Roda-Robles *et al.* (2012*b*)	Pegmatitic cupola over a granite, Li rich in its upper part	Qtz, Ms, Fsp, Tur, Lpd, Bt, Zwd, Fe-Mn phosp	**Lepidolite** **Ferrisicklerite** Elbaite Zinnwaldite
19	Argemela (Guarda, Portugal) Charoy and Noronha (1996)	Microgranite + quartz-albite-dykes with montebrasite	Qtz, Fsp, Ms, Lpd, Mtb, Cst, Nb-Ta oxides	**Lepidolite** Montebrasite
20	Castillejo de Dos Casas (Salamanca, Spain) Martín-Izard *et al.* (1992); Roda-Robles *et al.* (2013)	Stockscheider over a leucogranitic cupola in contact to the micaschists	Qtz, Fsp, Li-Ms, Ptl, Cst, Mtb, Tpz, Fe-Mn phosp	**Li-Muscovite** Petalite Montebrasite Lithiophilite
21	Golpejas (Salamanca, Spain) Martín-Izard *et al.* (1992)	Leucogranitic cupola + quartz dykes with montebrasite	Qtz, Fsp, Mtb, Cst, Nb-Ta oxides, Tpz	**Montebrasite**
22	Valdeflores (Cáceres, Spain) Pesquera *et al.* (1999)	Quartz dykes with montebrasite (micaschists)	Qtz, Mtb, Cst + Zwd, Lpd, Li-Ms in country rock	**Montebrasite** Zinnwaldite Lepidolite
23	Massueime (Guarda, Portugal) Carvalho and Farinha (2004); Roda-Robles *et al.* (2012*c*)	Quartz dykes with montebrasite	Qtz, Mtb, Cst, sulfides	**Montebrasite**
24	Barquilla (Salamanca, Spain) Martín-Izard *et al.* (1992)	Quartz dykes with montebrasite (metasediments)	Qtz, Fsp, Mtb, Cst, Nb-Ta oxides, sulfides	**Montebrasite**
25	El Trasquilón (Cáceres, Spain) Gallego Garrido (1992)	Quartz dykes with montebrasite (granitic cupola)	Qtz, Fsp, Mtb, Cst, Nb-Ta oxides, sulfides	**Montebrasite**

Texto

*Abbreviations: Qtz – quartz; Fsp – feldspar; Brl – beryl; Lpd – lepidolite; Spd – spodumene; Ptl – petalite; Cst – cassiterite; Mtb – montebrasite; Amb – amblygonite; Ms – muscovite; Lpd – lepidolite; Tur – tourmaline; Tpz – Topaz; phosp – phosphates; Ap – Apatite; Grt – garnet, Zwd – zinnwaldite.
** The most abundant Li phases are presented in bold.

natural and synthetic standards were used: fluorite (F); sanidine (K); pollucite (Cs); synthetic $MnTiO_3$ (Ti, Mn); diopside (Ca); synthetic $BaSO_4$ (Ba); synthetic Fe_2O_3 (Fe); albite (Na); periclase (Mg); synthetic SiO_2 (Si); apatite (P); sphalerite (Zn); synthetic Cr_2O_3 (Cr); and synthetic Al_2O_3 (Al). Data were corrected for ZAF values using the procedure of Pouchou and Pichoir (1985). Analytical errors are estimated to be on the order of ±1–2% for major elements and ±10% for minor elements. The Li aluminophosphates and Li-Fe-Mn phosphates were analysed at the Université Paul Sabatier (Toulouse,

France), with a Cameca SX50 electron microprobe. For the phosphates, the operating conditions were: voltage of 15 kV and a beam current of 10 nA for all elements. The standards used for phosphate analyses are: graftonite for P, corundum for Al, hematite for Fe, pyrophanite for Mn, periclase for Mg, wollastonite for Ca and Si, sanidine for K, albite for Na, celestine for S, baryte for Ba and $Pb_2P_2O_7$ for Pb.

The Li content of micas was calculated using different equations based on the positive correlation between Li and F (e.g. Tischendorf *et al.*, 2004, Pesquera *et al.*, 1999; Vieira *et al.*, 2011; Roda-Robles *et al.*, 2006). For other minerals, Li was calculated assuming the ideal content in the structural formulae (for more detail, see Tables 3 to 6).

General geology of the Li mineralization

Lithium mineralization in the Central Iberian Zone is associated mainly with pegmatites, but also with leucogranitic cupolas and quartz-rich hydrothermal veins. Pegmatites are igneous rocks commonly characterized by their coarse, sometimes giant grain size, and commonly by an internal zoning with the development of a massive quartz core, intermediate zone(s) and a wall zone, in the simplest case. Pegmatitic bodies showing these features are common in the Central Iberian Zone, as for example the Puentemocha pegmatite (Salamanca, Spain) (Roda-Robles *et al.*, 2012*a*) or the Nossa Senhora da Assunção pegmatite (Viseu, Portugal) (Roda-Robles *et al.*, 2014). These are Be-P-rich pegmatites, belonging to the beryl-phosphate subtype of the Černý and Ercit classification (2005). However, in the Central Iberian Zone the pegmatite bodies that are most enriched in Li are texturally and compositionally quite different from the more commonly-observed pegmatites. Many of these Li-rich bodies exhibit an aplitic texture, commonly with the development of units with mineralogical layering (line-rock). Coarse crystals are also common, but usually smaller than 10 cm long; and the pegmatites are typically unzoned. However, these bodies are typically notably enriched in Li, with local concentrations exceeding 2 wt.% Li_2O. The different types of Li-rich mineralization from the Central Iberian Zone and the Galicia-Trás-Os Montes Zone are discussed in detail below (Table 1, Fig. 1).

Lithium mineralization in pegmatite fields

This is the most common type of Li mineralization found in the studied region. Lithium-bearing pegmatites crop out in groups of up to a few hundred dykes, hosted in granites and in metasedimentary rocks. These pegmatite dykes are of variable thickness (from a few centimetres up to 30 m), and range from a few metres up to a couple of kilometres long. Their dip is very variable, from sub-horizontal (e.g. Gonçalo and Tres Arroyos fields) to sub-vertical (e.g. Fregeneda-Almendra field). Not all pegmatites in each field are enriched in Li. In some cases the pegmatite fields display a regional zoning, with barren, intermediate and Li-rich pegmatites occurring in different areas of the field, with an enrichment in rare metals mainly including Li and F, but also Sn, P, Nb, Ta, Rb and Cs in some cases, as the distance to the parental granite increases (e.g. Fregeneda-Almendra and Tres Arroyos fields). Usually these Li-rich pegmatites lack internal zoning. The grain size may be very homogeneous (aplitic in some bodies and pegmatitic in others), with crystals only exceptionally >10 cm long; or moderately heterogeneous, with aplitic and pegmatitic facies occurring in the same pegmatite body, without an aparent pattern for the grain size variation inside these bodies. Layering is relatively common in the pegmatites, typically parallel to the contacts with the host rocks. In such cases, the layering is developed throughout the pegmatite (e.g. Fregeneda-Almendra, Gonçalo and Tres Arroyos fields). In the simplest example, the layering consists of two mineral associations (e.g. Li-mica + quartz alternating with albite + quartz, as observed in the Gonçalo and Fregeneda-Almendra fields) (Fig. 2*a*); in other cases there are several different layers forming complex patterns across the dyke. Wedge-shaped crystals of K-feldspar or plagioclase that grew perpendicular to the contacts with the host-rock are common.

The mineralogy of the pegmatites is quite simple, including quartz, albite, K-feldspar and muscovite in the barren dykes; and these minerals together with spodumene, petalite, Li-muscovite and/or lepidolite, in variable proportions, in the Li-rich dykes. Those showing the highest fractionation levels are rich in Li-micas, with up to 35% mica in modal proportions. Amblygonite–montebrasite, cassiterite and Nb-Ta oxides are the commonest accessory minerals in all the dykes of the pegmatite fields.

Beryl-phosphate pegmatites

The beryl-phosphate pegmatites are not usually part of pegmatite fields in the Central Iberian Zone, and belong to the beryl-phosphate subtype defined in

the classification of Černý & Ercit (2005). In these pegmatites, Li is mainly contained in Fe-Mn phosphates, usually of the triphylite–lithiophilite series (e.g. Cañada, Pedra da Moura, Nossa Senhora da Assunção). The phosphate masses are sub-rounded and up to 1.5 m in diameter, typically occurring in the intermediate zone of pegmatites that show a well-developed internal structure and a coarse grain size. The major minerals in the pegmatites include quartz, K-feldspar, plagioclase, beryl, muscovite, biotite, with schorl, Nb-Ta oxides and apatite as minor or accessory phases. The shape of the beryl-phosphate bodies varies from tabular to turnip-shaped, and they are typically hosted by anatectic granitic plutons, frequently with a gradual contact with the host rock.

Lithium mineralization associated with leucogranitic cupolas

This paragenesis is not as common as the pegmatites described above. This type of Li mineralization occurs in the apical or marginal areas of highly-fractionated leucogranites, hosted by metasedimentary rocks of the Schist-Metagreywacke Complex. The associated leucogranites are typically fine grained and enriched in B, Li and F (Martín-Izard *et al.*, 1992, Roda-Robles *et al.*, 2012*b*, 2015). The apical/marginal zones are quite heterogeneous and include a range of mineral associations. The most common association consists of a fine-grained matrix of quartz, albite and Li-mica surrounding coarser crystals of K-feldspar that grew perpendicularly to the contacts with the host-rock. Accessory minerals in this association include topaz, montebrasite, petalite, cassiterite and columbite–tantalite-group minerals. A second typical facies includes fine- to medium-sized layered, sub-horizontal textures (stockscheider), with lepidolite-rich bands alternating rhythmically with feldspar-rich bands (e.g. Castillejo de Dos Casas) (Fig. 2*b*). The two facies may occur in the same intrusion (Roda-Robles *et al.*, 2015). Usually the contact between the granitic and the pegmatitic rocks is gradual, being difficult to establish the limit between both lithologies (Roda-Robles *et al.* 2012*b*, 2015).

Quartz-montebrasite veins

Lithium is locally enriched in quartz-rich hydrothermal veins that occur in association with leucogranitic bodies in the central parts of the Central Iberian Zone (e.g. Golpejas, Valdeflores,

Barquilla, Massueime). The veins typically occur as thin (<1 m thick) subvertical dyke-like bodies, hosted in fractures inside the granites and the metasedimentary rocks of the Schist-Metagreywacke Complex. The main Li-rich minerals in these veins belong to the montebrasite–amblygonite series, corresponding to the OH-rich member montebrasite. Feldspars and cassiterite are commonly present in these dykes, and Nb-Ta oxides plus other oxides and sulfides may be present locally, usually as accessory minerals.

Mineral composition and textures

The major Li-bearing minerals in the various styles of Li mineralization of the Central Iberian Zone and the Galizia-Trás-Os-Montes Zone include Li-micas, spodumene, petalite and phosphates of the triphylite–lithiophilite and amblygonite–montebrasite series. Elbaite, where present, mostly occurs as an accessory mineral. Table 2 lists the different major Li-bearing minerals in the different types of mineralization, their ideal structural formulae, Li contents of these mineral phases and general abundance in the different mineralization styles. Overall, Li-mica is the most common Li phase in the mineralization discussed here. Spodumene and petalite are particularly abundant in some of the dykes in the pegmatitic fields, whereas montebrasite is most commonly found in the hydrothermal veins. The main textural and geochemical features of these minerals are described below.

Li-mica

Most of the Li-micas studied belong to the muscovite-lepidolite series, although zinnwaldite is found in a few pegmatite bodies (Tables 1 and 2). In addition, abundant zinnwaldite, sometimes together with Li-muscovite and/or lepidolite, is found in the metasomatized mica-schists or granites hosting some of the mineralized zones (e.g. Valdeflores, Gonçalo).

In the pegmatite fields of the Central Iberian Zone and of the Galizia-Trás-Os-Montes Zone, Li-mica is usually restricted to the most fractionated bodies (i.e. the most enriched in incompatible elements), especially enriched not only in Li but also in F. These bodies are typically characterized by contact-parallel layering, consisting of a sequence in which Li-mica + quartz-rich layers alternate with albite + K-feldspar-rich bands (Fig. 2*a*). In hand-specimen, the Li-mica exhibits a typical lilac colour, and occurs as prismatic or wedge-shaped crystals
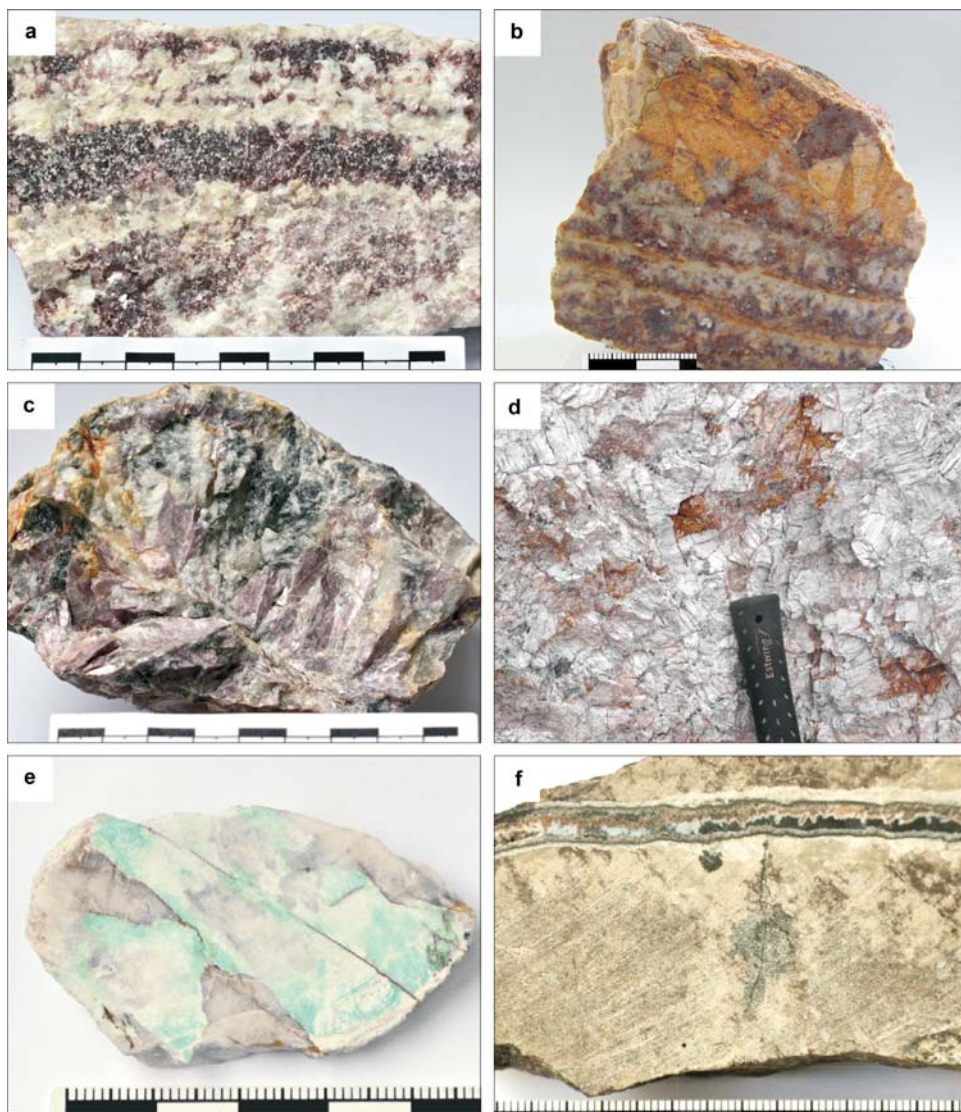
FIG. 2. (*a*) Rythmic layering with alternating lepidolite-rich and albite-rich bands in a aplite-pegmatite dyke from the Gonçalo field; (*b*) similar texture as (*a*) in the lower part, plus some wedge-shaped crystals of K-feldspar in the upper part, from the stockscheider of Castillejo de Dos Casas; (*c*) pinkish primary Li-mica flakes together with greyish K-feldspar crystals and quartz from the Fregeneda-Almendra field; (*d*) cone-shaped crystals of spodumene randomly distributed together with albite crystals, within a pegmatite dyke from the Fregeneda-Almendra field; (*e*) hand sample of weathered montebrasite (white), replaced by turquoise from Valdeflores; and (*f*) massive triphylite crossed by a vein filled by secondary phosphate phases, from the Cañada open pit.

(<2 cm) (Fig. 2*c*) (e.g. Fregeneda-Almendra, Gonçalo, Tres Arroyos, Las Navas). On the basis of these textural features and its relationship to other minerals, mica is considered a primary phase. Li-mica may also form irregular, fine-grained, saccharoidal aggregates with quartz and feldspar, commonly cross-cutting the primary layering of the pegmatites. Mica showing these textures is considered to be a replacement product that originated during an episode of metasomatism. Li-micas

TABLE 2. Structural formulae and abundance of the Li-bearing minerals associated with mineralization in the Central Iberian Zone and in the Galizia-Trás-Os-Montes Zone.

Mineral	Formula	Li_2O (Li) (wt.%)	Li mineralizations associated with granitic cupolas	Beryl-phosphate pegmatites	Pegmatite fields	Qtz-Mtb-Amb veins	Metasomatized country rock
Spodumene	$LiAlSi_2O_6$	8.03 (3.73)	–	–	XXX	–	–
Lepidolite	$K(Li,Al)_3(Si,Al)_4O_{10}(F,OH)_2$	7.70 (3.58)	XX	–	XXX	–	X
Petalite	$LiAlSi_4O_{10}$	4.50 (2.09)	X	–	XXX	–	–
Elbaite	$Na(Li,Al)_3Al_6(BO_3)_3Si_6O_{18}(OH)_4$	4.07 (1.89)	X	–	X	–	X
Zinnwaldite	$KLiFe^{2+}Al(AlSi_3O_{10})(F,OH)_2$	3.42 (1.59)	X	–	X	–	X
Triphylite–lithiophilite	$Li(Fe^{2+}, Mn^{2+})PO_4$	9.47 (4.40)	XX	XXX	X	–	–
Ferrisicklerite–sicklerite	$Li_{1-x}(Fe^{3+}_x, Mn^{2+}_{1-x})PO_4$	< 9.47 (<4.40)	XX	XXX	X	–	–
Amblygonite–montebrasite	$(Li,Na)Al(PO_4)(F,OH)$	7.40 (3.44)	X	X	XX	XXX	–

XXX: very abundant; XX: common; X: accessory; –: absent.

associated with leucogranitic cupolas show quite similar textures, with primary mica flakes forming layers, and secondary fine-grained crystals inter-grown with quartz forming irregular replacement bodies (e.g. Castillejo de Dos Casas). Less commonly, in these cupolas lepidolite forms white, pearly, subhedral flakes which are inter-grown with anhedral quartz crystals in subrounded masses of up to 10 cm in diameter (e.g. Pinilla de Fermoselle). Li-micas have not been found in the beryl-phosphate subtype pegmatites, nor in the quartz-montebrasite veins.

Micas from the pegmatite fields and from Li mineralization associated with granitic cupolas plot on a similar trend in the Tischendorf diagram (Tischendorf *et al.*, 2004), originating from muscovitic compositions and evolving toward Li-rich compositions (Fig. 3). The highest Li contents in micas are those observed in mineralization associated with granitic cupolas (e.g. Castillejo de Dos Casas, Pinilla de Fermoselle), where some of the micas are very close to the polylithionite composition (Table 3, Fig. 3). In contrast, the micas associated with the most fractionated pegmatites in the pegmatite fields do not attain such high Li contents, the micas that are most enriched in Li being intermediate between tri-lithionite and polylithionite compositions (Table 3, Fig. 3), (e.g. Fregeneda-Almendra, Las Navas, Gonçalo, Tres Arroyos and Barroso-Alvão fields). In both cases the dominant mechanism of Li incorporation appears to be the exchange vector $Li_3Al_{-1}Vac_{-2}$, and to a lesser extent Si_2LiAl_{-3} (e.g. Roda-Robles *et al.*, 2006; Vieira *et al.*, 2011, Martins, *et al.* 2012). In the beryl-phosphate pegmatites the mica composition follows the muscovite-biotite trend, with no Li (nor F) enrichment (Fig. 3).

Iron-lithium-rich micas in Li mineralization associated with leucogranite cupolas follows an evolutionary trend from biotite through zinnwaldite toward polylithionite (Fig. 3). In these micas, the Li enrichment is parallel to an Fe decrease, via the $AlLiR_{-2}$, $SiLi_2R_{-3}$ and $SiLiAl_{-1}R_{-1}$ substitution mechanisms (Roda-Robles *et al.*, 2006). In metasomatized mica-schists hosting the quartz-rich hydrothermal veins at Valdeflores, both Fe-Li-rich and Al-Li-rich metasomatic micas can be distinguished. The Fe-Li-rich micas follow a similar trend to the Fe-Li-rich micas in the leucogranitic cupolas, whereas the Al-Li-micas show an evolution from muscovite towards zinnwaldite, with the Li enrichment via the substitution $FeLiAl_{-1}Vac_{-1}$ (Pesquera *et al.*, 1999) (Fig. 3).
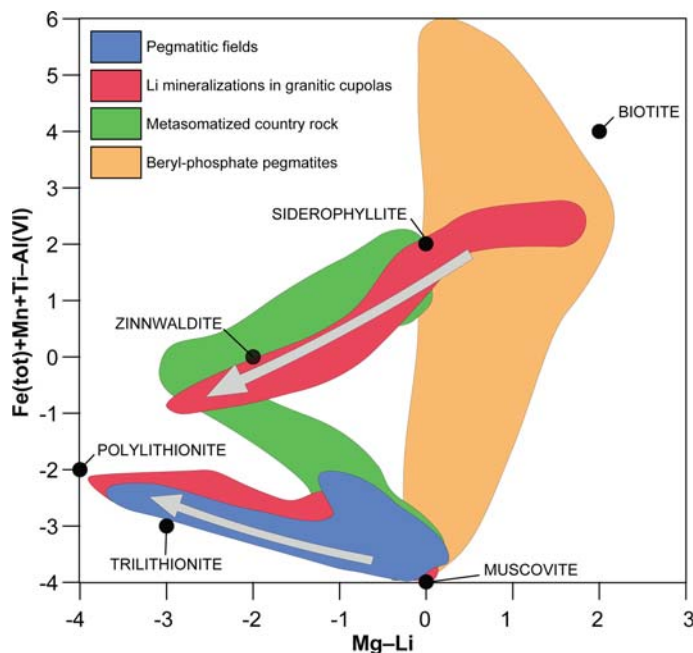
Fig. 3. Mg–Li vs. (Fe + Mn + Ti) – ^{VI}Al for the micas associated with the different types of Li mineralization and their metasomatized country rocks.

Lithium aluminosilicates

The two Li-aluminosilicate mineral phases, spodumene and petalite, are restricted to a few of the aplite-pegmatite dykes occurring in some of the pegmatite fields of the Central Iberian Zone and Galizia-Trás-Os-Montes Zone (Tables 1 and 2). Spodumene is the most common Li-aluminosilicate associated with this type of Li mineralization (e.g. in the Fregeneda-Almendra, Lalín-Forcarei and Barroso-Alvão pegmatite fields). However, petalite is the dominant aluminosilicate in some pegmatites, both in the pegmatite fields mentioned above, and in some other fields (e.g. Queiriga-Lousadela, Seixoso-Vieiros, Dias *et al.*, 2013). It is also quite common for the two phases to coexist in the same body, showing different mutual relationships explained below (e.g. Fregeneda-Almendra and Barroso-Alvão). The abundance of these minerals in parts of the pegmatite is highly variable, from <2 vol.% up to locally ~50 vol.% (Fig. 2*d*). In all cases the crystals have highly-variable grain sizes, from very small crystals (<1 cm) to coarse wedge-shaped crystals up to 20 cm long. The largest grains are typically randomly distributed within the pegmatite, without any preferred orientation. However, in some cases they are perpendicular to

the contacts with the country rock. Petalite and spodumene exhibit similar prismatic or wedge-shaped habits and whitish colours, making it difficult to distinguish between the two in the field. As spodumene is weathered, its cleavage becomes more visible and its colour changes to pale grey. In thin sections several different petrographic varieties of spodumene can be recognized. It appears most commonly as subhedral prismatic crystals, grouped in aggregates, with quartz, mica and plagioclase filling the spaces between the spodumene prisms (Fig. 4*a*). It is locally very fresh, but more commonly shows varying amounts of alteration. This alteration usually begins at the margins of the crystals and in some cases the primary crystals are completely pseudomorphed by cookeite and/or clay minerals. Spodumene commonly appears intergrown with tiny blebs of quartz (Fig. 4*b*), which probably corresponds to the SQUI texture defined by Černý and Ferguson (1972) and interpreted as the result of the breakdown of petalite into spodumene + quartz. Spodumene and petalite also coexist in some pegmatites with intriguing mutual relationships (some of which have already been described by Charoy *et al.*, 2001 for Barroso-Alvão). These two minerals may form a lamella-

TABLE 3. Representative compositions of micas from pegmatite fields (1 and 2); Li mineralization associated with granitic cupolas (18 and 20); and metasomatized host rocks (metasediments) (22).

Locality*	1	1	2	2	18	18	18	20	20	22	22	22
Mica type**	Lpd	Li-Ms	Lpd	Lpd	Lpd	Li-Ms	Zwd	Lpd	Li-Ms	Zwd	Li-Ms	Lpd
Wt.%												
SiO_2	49.72	46.40	50.01	51.70	49.75	45.73	45.75	51.19	47.50	42.48	52.54	50.48
TiO_2	0.00	0.27	0.10	0.03	0.01	0.11	0.12	0.49	0.44	0.54	0.19	0.14
Al_2O_3	24.01	33.36	27.88	24.10	29.86	30.10	21.82	25.85	29.82	22.23	26.64	19.90
FeO(t)	1.08	1.29	0.14	0.16	0.00	5.85	11.33	0.09	2.13	11.45	2.11	6.70
MnO	0.58	0.21	0.54	0.85	0.28	0.16	0.85	0.61	0.96	0.13	0.05	0.16
MgO	0.00	0.00	0.00	0.00	0.00	0.76	0.73	0.00	0.00	4.23	1.12	1.67
CaO	0.00	0.00	0.00	0.08	0.01	0.02	0.04	0.00	0.04	0.03	0.00	0.01
Na_2O	0.16	0.19	0.27	0.40	0.37	0.21	0.16	0.30	0.18	0.26	0.12	0.12
K_2O	10.24	10.64	10.37	10.11	10.51	10.44	9.82	10.67	10.62	7.58	8.49	8.31
Rb_2O	1.18	0.39	1.03	1.18	–	–	–	0.69	0.74	–	–	–
Cs_2O	0.86	0.10	0.21	0.49	0.09	0.07	0.33	–	–	1.64	0.24	0.77
ZnO	–	0.17	0.22	0.20	0.03	0.11	0.18	0.00	0.23	–	–	–
F	8.38	2.52	6.16	7.65	6.11	2.69	6.55	7.76	5.11	6.66	3.56	7.89
Li_2O*	5.39	1.24	3.83	4.76	3.53	1.17	3.87	4.86	2.77	3.96	1.71	4.97
H_2O*	0.43	1.06	1.58	0.84	1.65	3.10	1.15	0.86	2.05	1.05	2.81	0.62
O=F	3.53	3.25	2.59	3.22	2.57	1.13	2.76	3.27	2.15	2.80	1.50	3.32
Total*	98.49	98.97	99.74	99.62	99.47	99.95	100.09	100.44	99.45	98.07	98.43
Atoms per formula unit calculated on the basis of 22 O												
Si	6.78	6.26	6.66	6.93	6.56	6.27	6.45	6.76	6.37	6.05	7.01	6.93
Al(IV)	1.22	1.74	1.34	1.07	1.44	1.73	1.55	1.24	1.63	1.95	0.99	1.07
Al(VI)	2.64	3.56	3.04	2.74	3.21	3.14	2.08	2.79	3.09	1.78	3.19	2.15
Ti	0.00	0.03	0.01	0.00	0.00	0.01	0.01	0.05	0.04	0.06	0.02	0.01
Fe^{2+}	0.12	0.15	0.02	0.02	0.00	0.67	1.34	0.01	0.24	1.36	0.24	0.77
Mn	0.07	0.02	0.06	0.10	0.03	0.02	0.10	0.07	0.11	0.02	0.01	0.02
Mg	0.00	0.00	0.00	0.00	0.00	0.16	0.15	0.00	0.00	0.90	0.22	0.34
Li	2.95	0.67	2.05	2.57	1.87	0.65	2.19	2.58	1.50	2.27	0.92	2.75
Zn	–	0.02	0.02	0.02	0.00	0.01	0.02	0.00	0.02	–	–	–
Σ(Y)	5.78	4.44	5.20	5.45	5.11	4.65	5.90	5.50	5.00	6.38	4.59	6.05
Ca	0.00	0.00	0.00	0.01	0.00	0.00	0.01	0.00	0.01	0.00	0.00	0.00
Na	0.04	0.05	0.07	0.10	0.09	0.06	0.04	0.08	0.05	0.07	0.03	0.03
K	1.78	1.83	1.76	1.73	1.77	1.83	1.77	1.80	1.82	1.38	1.45	1.46
Rb	0.10	0.03	0.09	0.10	–	–	–	0.06	0.06	–	–	–

(continued)

TABLE 3. (*contd.*)

Locality* Mica type**	1 Lpd	1 Li-Ms	2 Lpd	2 Lpd	18 Lpd	18 Li-Ms	18 Zwd	20 Lpd	20 Li-Ms	22 Zwd	22 Li-Ms	22 Lpd
Cs	0.05	0.01	0.01	0.03	0.01	0.00	0.02	–	–	0.10	0.01	0.04
Σ(X)	1.98	1.92	1.93	1.97	1.87	1.89	1.84	1.93	1.93	1.55	1.49	1.53
F	3.61	1.08	2.59	3.24	2.55	1.17	2.92	3.24	2.17	3.00	1.50	3.43
OH*	0.39	2.92	1.41	0.75	1.45	2.83	1.08	0.76	1.83	1.00	2.50	0.57

Locality* = see Table 1; ** Abbreviations: Lpd = lepidolite; Ms = muscovite; Zwd = zinnwaldite; "–" = not determined; H_2O* and Li_2O* = calculated, (OH* = 4 – F).

like rhythmic layering, or mantled textures in which spodumene is rimmed by petalite. Petalite also appears interstitially between spodumene prisms (Fig. 4*c*). In the dykes where petalite is the main Li-aluminosilicate it shows different textures. The large wedge-shaped crystals of petalite that can be observed in hand samples appear in thin sections as very fine- to fine-grained aggregates of anhedral crystals (Fig. 4*d*). In common with spodumene, petalite may be partly or totally replaced by cookeite and clay minerals, or by eucryptite. Petalite has been also observed as an accessory mineral phase in the stockscheider of Castillejo de Dos Casas, where it forms anhedral fine-grained crystals.

Representative compositions of spodumene, petalite and eucryptite associated with Li mineralization from three localities in the Central Iberian Zone are given in Table 4. In general the composition of these phases is quite similar across the different localities. There is some distinct variation in the Fe content of spodumene, which is typically lower in the dykes where it occurs together with Li-mica (<0.06 wt.%), than in those where micas are absent or scarce (up to 0.41 wt.%) (e.g. in the Fregeneda-Almendra field). In the case of eucryptite this difference is more noticeable, with up to 4.62 wt.% FeO in the crystals from pegmatites with no Li-micas (e.g. Barroso-Alvão), whereas in the dykes where Li-mica is abundant the FeO contents in eucryptite are always <0.36 wt.%.

Amblygonite–montebrasite series

Lithium aluminophosphates of the amblygonite–montebrasite series represent probably the ubiquitous Li phase of the Li mineralization of the Central Iberian Zone and Galizia-Trás-Os-Montes Zone (Tables 1 and 2). Amblygonite–montebrasite occurs as the main Li-bearing phase in a number of hydrothermal quartz veins, usually located around or inside leucogranitic cupolas (e.g. Valdeflores, Barquilla, Golpejas, Massueime, El Trasquilón). In these veins, it forms whitish irregular masses of up to 30 cm in diameter, distinguishable from albite by its notably higher density. It is commonly altered and replaced by other secondary phosphates, including lacroixite and turquoise, which gives a characteristic bluish or greenish colour to these phosphate masses (Fig. 2*e*). Members of the amblygonite–montebrasite series constitute a common accessory phase in many dykes of the pegmatite fields (e.g. Fregeneda-Almendra, Barroso-Alvão, Tres Arroyos). In some of these
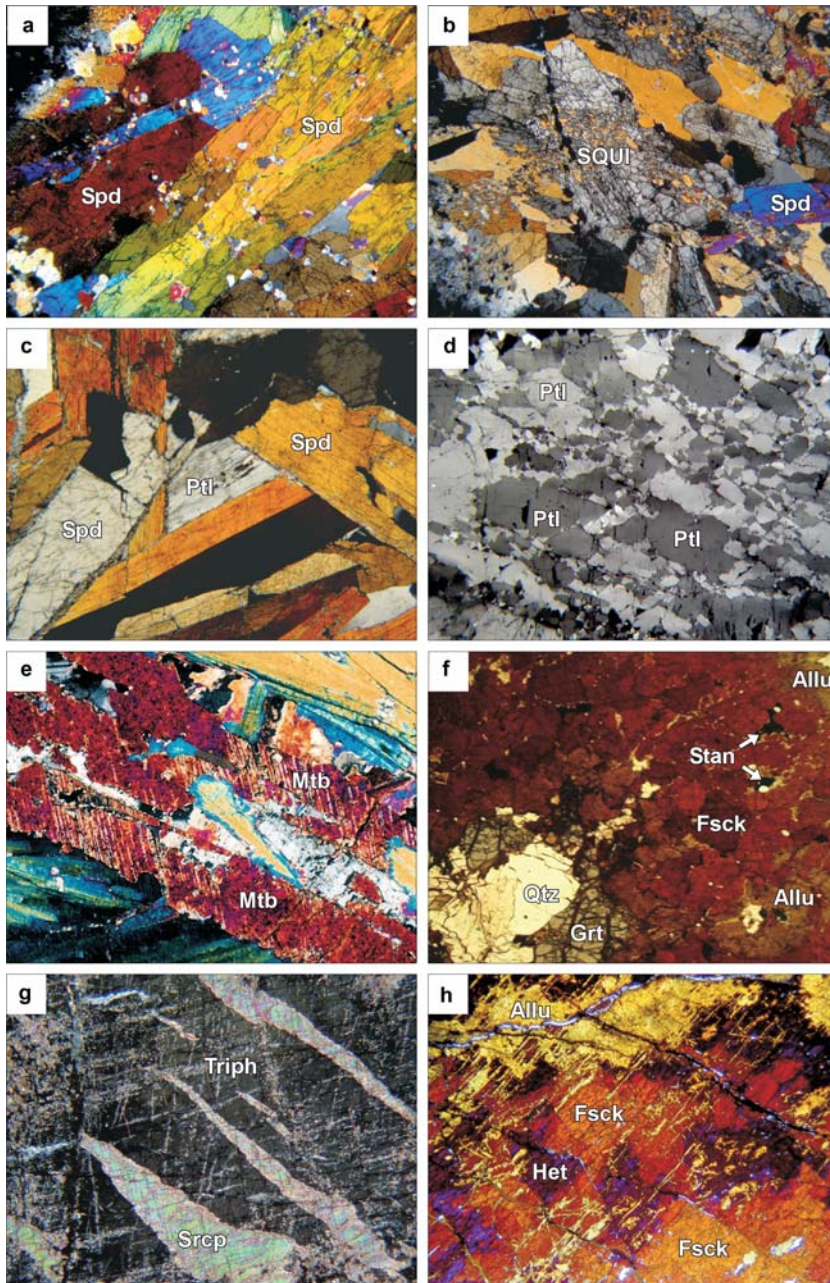
FIG. 4. Photomicrographs of: (*a*) primary prismatic crystals of spodumene; (*b*) crystals of spodumene intergrowth with sub-rounded crystals of quartz, in a SQUI texture (for further explanation see text); (*c*) interstitial petalite crystals between spodumene prisms; (*d*) granular anhedral crystals of petalite; (*e*) montebrasite crystal showing its characteristic polisynthetic twinning; (*f*) granular ferrisicklerite (reddish) together with some garnet crystals (lower-left corner) and quartz; (*g*) sarcopside lamellae inside triphylite (greyish matrix); (*h*) ferrisicklerite (orange) partly-replaced by heterosite (purple) and alluaudite (yellow). (*a*, *b*, *c*, *d*, *e* and *g*: crossed-polarized light; *f* and *h*: plane-polarized light. Scale: 1.8 mm × 2.6 mm). Abbreviations: Spd = spodumene; Ptl = petalite; SQUI = spodumene + quartz blebs intergrowth; Mtb = montebrasite; Allu = alluaudite; Stan = staneckite; Fsck = ferrisicklerite; Qtz = quartz; Grt = Garnet; Triph = triphylite; Het = heterosite.

fields montebrasite may be the only Li-rich phase occurring in some of the less-fractionated pegmatites (e.g. Fregeneda-Almendra, Tres Arroyos). As an accessory phase, amblygonite–montebrasite occurs as whitish, fine-grained crystals. It may be locally very abundant in some of the most Li-enriched dykes; for example, at Gonçalo it occurs in masses of up to 12 cm in diameter. Montebrasite has also been found in some of the beryl-phosphate pegmatites as an accessory mineral, together with other Al phosphates, such as eosphorite–childrenite (e.g. Cañada pegmatite). In these rocks, members of the amblygonite–montebrasite series appear as anhedral to subhedral crystals ranging in size from <1 mm to 5 mm, with high order interference colours and commonly showing polysynthetic twinning (Fig. 4e).

Representative compositions of members of the amblygonite–montebrasite series associated with the four types of Li mineralization are listed in Table 5. The F/OH ratios vary between the different hosting lithologies (Fig. 5a). The lowest F contents are found in the montebrasites associated with the beryl-phosphate pegmatites (0.0–2.18 wt.%). Montebrasite in the quartz-montebrasite veins shows minor variations in the F/OH ratio, with F contents in the range 0.94–2.35 wt.% (Fig. 5a, Table 5). In contrast, in the Li mineralization associated with leucogranitic cupolas and in pegmatite fields, F/OH ratios are rather higher and the F content of amblygonite–montebrasite ranges from 0.43 to 5.33 wt.% and from 0.55 to 7.33 wt.%, respectively (Fig. 5a, Table 5). Nevertheless, the F median values are quite similar for the pegmatite fields, quartz veins and Li mineralization associated with leucogranitic cupolas (1.84, 1.69 and 1.77 wt.% respectively), whereas those of the samples from beryl-phosphate pegmatites are clearly lower (0.68 wt.%). In all cases the median and mean values correspond to the F-poor end-member montebrasite.

Triphylite–lithiophilite series
Members of this series are the most common primary Fe-Mn phosphates associated with pegmatites all over the world. In the Central Iberian Zone they occur mainly associated with the beryl-phosphate pegmatites, forming dark, sub-rounded masses of up to 1.5 m in diameter (e.g. Cañada, Nossa Senhora da Assunção, Mangualde). Inside these masses silicate minerals are scarce or absent, quartz and plagioclase being the most common. More rarely, Fe-Mg-(Mn) silicates, such as

tourmaline, biotite and/or garnet, appear in close contact with these phosphates, sometimes intimately intergrown with them (Fig. 4f) (e.g. Cañada pegmatite). In hand samples, fresh triphylite–lithiophilite ranges from greyish to beige in colour (Fig. 2f). In thin sections, triphylite–lithiophilite minerals are colourless, with very low order interference colours. Triphylite–lithiophilite crystals commonly host lenticular or irregular lamellae of sarcopside that show two preferential crystallographic orientations (e.g. Cañada, Nossa Senhora da Assunção) (Fig. 4g). These lamellae are considered an exsolution product of a higher temperature precursor (Roda-Robles *et al.*, 2011). Triphylite is typically altered following the oxidation sequence described by Quensel (1937) and Mason (1941), with Li leaching and simultaneous progressive oxidation of the transition cations Fe^{2+} and Mn^{2+}, at a high temperature. The products of this alteration are, in succession, ferrisicklerite–sicklerite and heterosite–purpurite. In hand samples members of the ferrisicklerite–sicklerite series are dark brown, whereas in thin sections they show strong orange, yellowish and brownish colours (Fig. 4h). Other common replacement products include members of the alluaudite–varulite series, in addition to long list of late-forming secondary phosphates (e.g. Roda *et al.*, 2004).

Iron-manganese phosphates occur only as accessory phases in the pegmatite fields, and in most of the Li mineralization related to granitic cupolas (e.g. Fregeneda-Almendra, Barroso-Alvão, Tres Arroyos, Castillejo de Dos Casas). Members of the triphylite–lithiophilite series are usually absent in these bodies, but their replacement products, typically members of the ferrisicklerite–sicklerite and heterosite–purpurite series, are relatively common, particularly in pegmatites which show intermediate degrees of fractionation. Only in one example of Li mineralization associated with granitic cupolas, the Pinilla de Fermoselle pegmatite, have volumetrically important amounts of Fe-Mn phosphates been found. In this pegmatite subrounded masses (<1 m in diameter) of ferrisicklerite occur in the intermediate zone of the pegmatite. No relict of triphylite has been observed, and ferrisicklerite has been considered here as a primary phase, subsequently replaced by heterosite and/or alluaudite plus a number of later secondary phosphates (Fig. 4h) (Roda *et al.*, 1996).

Representative compositions of Fe-Mn phosphates associated with beryl-phosphate pegmatites, pegmatite dykes from pegmatite fields and Li mineralization associated with leucogranitic

TABLE 4. Representative compositions of Li-aluminosilicates from pegmatitic fields (1 and 2) and from a Li mineralization associated with a leucogranitic cupola (20).

Locality*	1	1	1	2	2	2	1	2	20	1	1	2	2
Mineral**	Spd-L	Spd-L	Spd	Spd	Spd-L	Spd	Ptl	Ptl	Ptl-L	Eucr-L	Eucr-L	Eucr	Eucr
Wt.%													
SiO_2	65.75	65.69	65.16	65.19	65.42	65.44	79.36	80.68	78.28	47.73	49.97	46.17	45.92
TiO_2	0.08	0.04	0.11	0.03	0.03	0.00	0.00	0.03	0.00	0.00	0.00	0.00	0.02
Al_2O_3	26.40	26.43	27.50	27.33	27.44	27.27	16.13	16.73	16.86	37.36	37.02	36.17	34.33
FeO(t)	0.00	0.03	0.26	0.21	0.06	0.41	0.02	0.08	0.00	0.27	0.14	3.56	4.62
MnO	0.05	0.12	0.10	0.00	0.00	0.06	0.06	0.00	0.00	0.00	0.23	0.00	0.02
MgO	0.00	0.00	0.00	0.00	0.00	0.00	–	0.06	0.00	0.06	0.06	0.61	0.82
CaO	0.00	0.00	0.05	0.02	0.00	0.00	0.00	–	0.00	0.57	0.59	0.18	0.27
Na_2O	0.08	0.10	0.07	0.07	0.08	0.07	0.01	0.00	0.00	0.41	0.36	0.08	0.07
K_2O	0.05	0.05	0.00	0.01	0.00	0.00	0.02	0.00	0.00	0.09	0.18	0.09	0.13
F	0.15	0.03	0.00	0.00	–	–	–	–	0.00	0.00	0.05	0.00	0.00
Cl	0.00	0.00	0.00	0.01	–	–	–	–	0.00	0.00	0.00	0.00	0.00
O=F	0.07	0.01	0.00	0.00	0.00	0.00			0.00	0.00	0.02	0.00	0.00
Li_2O*	8.08	8.07	8.12	8.09	8.12	8.12	4.90	5.00	4.88	11.58	11.86	11.40	11.23
Total*	100.60	100.53	101.39	100.96	101.16	101.37	100.51	102.58	100.02	98.07	100.45	98.25	97.41
Atoms per formula unit calculated on the basis of 6 O (Spd), 10 O (Ptl) and 4 O (Eucr)													
Si	2.02	2.02	2.00	2.00	2.00	2.00	4.02	4.01	3.99	1.03	1.05	1.01	1.02
Ti	0.00	0.00	0.00	0.00	0.00	0.00	0.00	0.00	0.00	0.00	0.00	0.00	0.00
Al	0.96	0.96	0.99	0.99	0.99	0.98	0.96	0.98	1.01	0.95	0.91	0.93	0.90
Fe^{2+}	0.00	0.00	0.01	0.01	0.00	0.01	0.00	0.00	0.00	0.00	0.00	0.06	0.09
Mn	0.00	0.00	0.00	0.00	0.00	0.00	0.00	0.00	0.00	0.00	0.00	0.00	0.00
Mg	0.00	0.00	0.00	0.00	0.00	0.00	–	0.00	0.00	0.00	0.00	0.02	0.03
Ca	0.00	0.00	0.00	0.00	0.00	0.00	0.00	–	0.00	0.01	0.01	0.00	0.01
Na	0.00	0.01	0.00	0.00	0.00	0.00	0.00	0.00	0.00	0.02	0.01	0.00	0.00
K	0.00	0.00	0.00	0.00	0.00	0.00	0.00	0.00	0.00	0.00	0.00	0.00	0.00
F	0.01	0.00	0.00	0.00	–	–	–	–	0.00	0.00	0.00	0.00	0.00
Cl	0.00	0.00	0.00	0.00	–	–	–	–	0.00	0.00	0.00	0.00	0.00
Li*	1.00	1.00	1.00	1.00	1.00	1.00	1.00	1.00	1.00	1.00	1.00	1.00	1.00

Locality* = see Table 1; **Abbreviations: Spd = spodumene; Spd-L = spodumene coexisting with lepidolite; Ptl = petalite; Ptl = petalite coexisting with lepidolite; Eucr = eucryptite;
Eucr-L = eucryptite coexisting with lepidolite; "–" = not determined.
Li* (a.p.f.u.) = 1

TABLE 5. Representative compositions of amblygonite–montebrasite members from pegmatite fields (2 and 3); from a beryl-phosphate pegmatite (15); from Li mineralization associated with a leucogranitic cupola (19 and 20); and quartz-montebrasite veins (22 and 23).

Locality*	2	2	3	15	15	15	19	20	20	22	22	23
Wt.%												
SiO_2	0.12	0.15	0.10	–	–	–	–	–	0.06	–	–	–
Al_2O_3	35.13	34.66	34.24	35.46	34.31	34.37	35.46	35.47	34.19	19.95	35.14	34.42
FeO(t)	0.00	0.04	0.06	0.07	0.23	0.00	0.09	0.03	0.00	0.03	0.00	0.00
MnO	0.00	0.00	0.07	0.09	0.10	0.00	0.11	0.02	0.00	0.00	0.00	0.00
MgO	0.00	0.00	0.02	0.00	0.03	0.00	0.00	–	0.00	0.00	0.00	0.00
CaO	0.01	0.02	0.04	0.03	0.01	0.00	0.01	0.04	0.03	0.07	0.05	0.03
Na_2O	0.04	0.04	0.17	0.10	0.09	0.00	0.03	0.00	0.00	0.06	0.00	0.04
K_2O	0.02	0.01	0.00	–	–	0.00	–	0.14	–	–	–	–
P_2O_5	50.25	49.72	50.26	49.20	49.66	49.87	49.21	48.01	50.45	45.65	48.66	48.98
F	0.55	2.05	7.33	0.00	0.68	2.18	1.25	5.04	0.43	0.94	1.53	2.35
Cl	0.02	0.02	0.01	–	–	0.00	–	–	0.02	–	–	–
O=F	0.24	0.87	3.09	0.00	0.29	0.92	0.53	2.12	0.19	0.39	0.65	0.99
H_2O*	6.06	5.28	2.79	6.26	5.90	5.20	5.67	3.78	6.07	4.50	5.46	5.05
Li_2O*	10.46	10.35	10.32	10.34	10.29	10.34	10.37	10.18	10.41	8.18	10.27	10.21
Total*	102.44	101.47	102.31	101.55	101.01	101.05	101.67	100.63	101.47	78.98	100.48	100.11
Atoms per formula unit calculated on the basis of 5 O												
Si	0.00	0.00	0.00	–	–	–	–	–	0.00	–	–	–
Al	0.98	0.98	0.96	1.00	0.97	0.97	1.00	1.02	0.96	0.71	1.00	0.99
Fe^{2+}	0.00	0.00	0.00	0.00	0.00	0.00	0.00	0.00	0.00	0.00	0.00	0.00
Mn	0.00	0.00	0.00	0.00	0.00	0.00	0.00	0.00	0.00	0.00	0.00	0.00
Mg	0.00	0.00	0.00	0.00	0.00	0.00	0.00	–	0.00	0.00	0.00	0.00
Ca	0.00	0.00	0.00	0.00	0.00	0.00	0.00	0.00	0.00	0.00	0.00	0.00
Na	0.00	0.00	0.01	0.00	0.00	0.00	0.00	0.00	0.00	0.00	0.00	0.00
K	0.00	0.00	0.00	0.00	–	0.00	–	0.00	–	–	–	–
P	1.01	1.01	1.02	1.00	1.01	1.02	1.00	0.99	1.02	1.17	1.00	1.01
F	0.04	0.16	0.55	0.00	0.05	0.17	0.09	0.39	0.03	0.09	0.12	0.18
Cl	0.00	0.00	0.00	–	–	0.00	–	–	0.00	–	–	–
Li*	1.00	1.00	0.99	1.00	1.00	1.00	1.00	1.00	1.00	1.00	1.00	1.00
OH*	0.96	0.84	0.45	1.00	0.95	0.83	0.91	0.61	0.97	0.91	0.88	0.82

Locality* = see Table 1; "–" = not determined; OH* = 1–F–Cl; Li* (a.p.f.u.) = 1–Na–K.
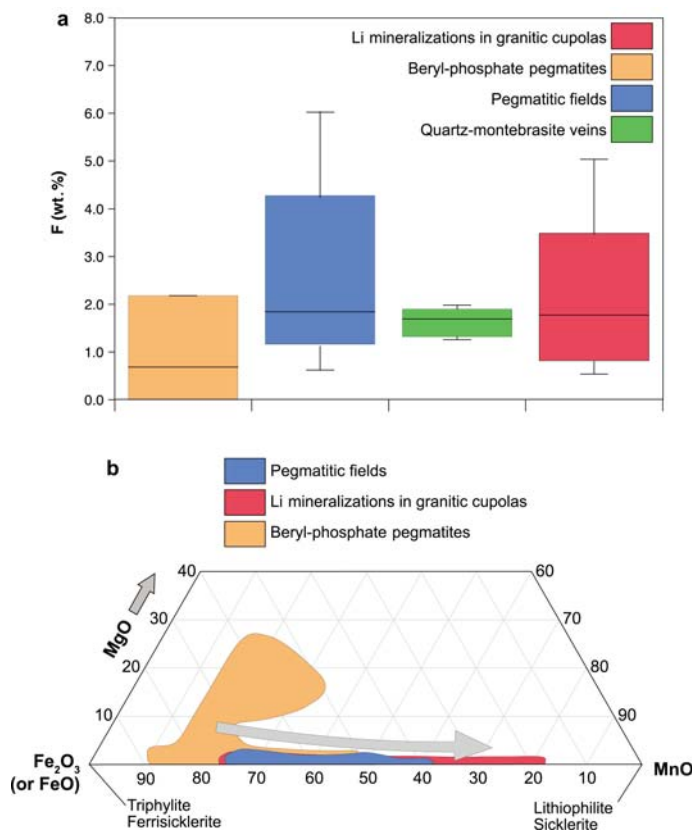
FIG. 5. (*a*) Variation in the F-content for members of the amblygonite–montebrasite series associated with the different types of Li mineralization; and (*b*) ternary plot of the Fe_2O_3–MnO–MgO contents for the Li-Fe-Mn phosphates from the different types of Li mineralization.

cupolas are reported in Table 6 and plotted in Fig 5*b*. The highest Fe and Mg contents are shown by the triphylite and ferrisicklerite crystals associated with the beryl-phosphate pegmatites (FeO from 22.7 to 45.5 wt.% and MgO from 0.0 to 11.7 wt.%). The Mn contents in the phosphates from the beryl-phosphate pegmatites are higher than those of Fe in just a few cases, and always close to the limit between triphylite–lithiophilite and ferrisicklerite–sicklerite (5.4–24.4 wt.% MnO) (Fig. 5*b*). The Fe-Mn phosphates in the pegmatite fields and in the leucogranitic cupolas are in general richer in Mn and poorer in Fe and Mg than those of the beryl-phosphate pegmatites. The lowest Mn and highest Fe values are quite similar for both types of mineralization, whereas the highest Mn and lowest Fe contents are found in the phosphates associated with the Li mineralization in leucogranitic cupolas (13.9–36.6 wt.% MnO and 8.47–43.8 wt.% FeO for

the Li mineralization in leucogranitic cupolas; and 11.0–27.8 wt.% MnO and 18.0–36.5 wt.% FeO for the pegmatite fields) (Table 6, Fig. 5*b*).

Discussion

Classification of the Li-rich bodies in the Central Iberian Zone

On the basis of field relationships, petrographic and mineralogical data, four types of Li mineralization have been established in the Central Iberian Zone. Three of these types, the pegmatite dykes in pegmatite fields, the beryl-phosphate pegmatites and the apical parts of leucogranitic cupolas, are dominated by granitic pegmatites with different mineralogy, textures, and relationships to host rocks. The fourth type, the quartz-montebrasite veins, are better considered as hydrothermal bodies

due to the high proportion of quartz and the scarcity of minerals characteristic of granitic pegmatites, such as feldspars and micas. The mineral assemblage and composition of the three pegmatite types are consistent with the rare-element (*REL*) class, and *REL*-Li subclass, according to the classification of Černý and Ercit (2005). The least Li-enriched pegmatites of the three types are usually those enriched in Fe-Mn phosphates and beryl, which may be classified in the beryl-columbite-phosphate subtype of the beryl type (Černý and Ercit, 2005). The most Li-enriched bodies in the Central Iberian Zone are the most fractionated pegmatites in the pegmatite fields and the Li mineralization associated with leucogranitic cupolas. In these two cases the mineralogy and textures are quite similar, with Li-micas dominating in the most evolved F-rich facies, whereas spodumene and petalite dominate in those bodies with lower F contents. From the mineralogical point of view, these pegmatites could be assigned to the lepidolite, spodumene or petalite subtype of the complex type (Černý and Ercit, 2005). However, the textures, internal structure and whole-rock compositions of these bodies are quite different to the most typical pegmatites of this type. The Central Iberian Zone and Galizia-Trás-Os-Montes Zone pegmatites commonly have aplitic texture, with strong preferred orientation of wedge-shaped feldspar crystals, and more rarely, spodumene and petalite crystals. The pegmatite bodies range from almost homogeneous to strongly layered, and are highly-enriched in albite. These features are more typical of the albite type than of the complex type pegmatites of the Černý and Ercit, (2005) classification. Therefore, the classification of these pegmatites is not easy using the groups established by these authors, as they share features of more than one type and subtype.

Origin and evolution of the pegmatitic melts in the Central Iberian Zone

A magmatic origin for granitic pegmatites is currently the most widely accepted hypothesis for the genesis of pegmatitic melts, even if in some regions an anatectic origin is more probable or at least possible. Granitic pegmatites are mainly located in orogenic belts, being the result of the crystallization of melts that are produced in thickened continental crust due to heating generated by mechanical and/or radiogenic decay processes (Tkachev, 2011). Granitic melts with a

crustal origin are typically generated after the culmination of an orogeny, related to an extensional regime that lasts for 30 to 60 m.y. (Sylvester, 1998; Thompson, 1999; Bea, 2004). These granites may be the parental magmas of some pegmatites enriched in rare elements (Tkachev, 2011). Granites related to rare-element pegmatites are commonly peraluminous leucogranites. A possible source for these granites is found in peraluminous metasedimentary rocks, including greywackes and shales (e.g. Puziewicz and Johannes, 1988; Patiño-Douce and Johnston, 1991). Such rocks represent a potential source for many of the Variscan granitoids in the western European Variscan belt (e.g. Peucat *et al.*, 1988; Bea *et al.*, 2003; Bea, 2004; Tartèse and Boulvais, 2010), including the Central Iberian Zone and the Galizia-Trás-Os-Montes Zone. Variations in the nature and depth of the fertile zone could explain the variety of granitoids in this region (Bea, 2004), with metasedimentary rocks of the Schist-Metagreywacke Complex representing possible candidates for the source of these granitoids (Bea *et al.*, 1999, 2003). Consequently, such source rocks could also be responsible for the rare-element enrichment in the pegmatites derived from those granites. Effectively, marine shales may be a source for rare alkalis, such as Li, Na, K, Rb and Cs, and alkaline earths, such as Be, (mainly contained in micas), and fluxing components (F, B and even P are usually present in black shales) (London, 2008). Further investigation, nevertheless, is necessary to understand the origin of the parental melts, the mechanisms that led to the extremely high concentrations in rare elements and the distribution of the pegmatitic bodies around the parental pluton. Fractionation of granitic melts is the most widely accepted mechanism to explain the composition of rare-element pegmatitic melts. Fractional crystallization is controlled by a number of factors, including the viscosity of magmas, density and size of crystals, concentration of H_2O and fluxing components, and dynamics/ deformation of the granite-pegmatite system. Gravitational settling is considered an effective fractionation mechanism for basic and ultrabasic magmas, as the differences of density among the crystals and melt are high enough to allow the just formed crystals to settle. However, in granitic magmas the high density of the melt, together with the lighter weight of the crystals, probably mean that this mechanism is not effective for fractionation, at least during the earlier stages, before the residual melt has become enriched in fluxes which may notably reduce its viscosity (Dingwell *et al.*,

TABLE 6. Representative compositions of triphylite, and ferrisicklerite/sicklerite from pegmatite fields (1 and 2); from beryl-phosphate pegmatites (12, 13, 15 and 16); and from Li mineralizations associated with leucogranitic cupolas (18 and 20).

Locality*	13	15	16	1	1	2	12	15	15	15	16	18	20
Mineral	Triph	Triph	Triph	Fsck	Fsck	Fsck	Fsck	Fsck	Fsck	Fsck	Fsck	Fsck	Fsck
Wt.%													
Al_2O_3	0.00	0.01	0.00	0.01	0.06	0.01	0.04	0.00	0.00	0.03	0.00	0.02	0.00
FeO(t)	23.49	35.31	22.70										
Fe_2O_3(t)				35.69	22.84	36.33	45.47	41.41	36.50	26.53	24.59	36.13	8.47
MnO	21.30	8.89	22.77	12.60	22.87	13.31	5.75	8.57	11.70	8.10	23.52	14.83	36.57
MgO	0.03	1.20	0.00	0.89	2.26	0.23	0.81	1.66	2.11	11.71	0.00	0.13	0.09
CaO	0.02	0.02	0.17	0.18	0.34	0.09	0.07	0.03	0.29	0.07	0.63	0.16	2.30
Na_2O	0.00	0.04	0.00	0.09	0.27	0.06	0.14	0.00	0.20	0.11	0.00	0.07	0.18
K_2O	0.00	0.01	0.00	0.05	0.00	0.00	0.01	0.04	0.29	0.03	0.04	0.02	0.14
P_2O_5	45.47	45.37	45.27	46.20	45.23	46.17	45.81	45.90	45.18	49.02	45.72	45.29	44.48
Li_2O*	9.52	9.59	9.54	3.02	4.07	2.88	0.24	0.87	1.21	3.85	4.82	1.84	6.44
Total*	99.83	100.45	100.47	98.72	97.94	99.11	98.36	98.49	97.48	99.45	99.32	98.48	98.74
Atomic contents													
Al	0.000	0.000	0.000	0.000	0.002	0.000	0.001	0.000	0.000	0.001	0.000	0.001	0.000
Fe^{2+}	0.513	0.766	0.495										
Fe^{3+}				0.687	0.449	0.699	0.882	0.802	0.718	0.481	0.478	0.709	0.169
Mn	0.471	0.195	0.503	0.273	0.506	0.288	0.126	0.187	0.259	0.165	0.515	0.328	0.823
Mg	0.001	0.046	0.000	0.034	0.088	0.009	0.031	0.064	0.082	0.420	0.000	0.005	0.003
Ca	0.000	0.000	0.005	0.005	0.010	0.002	0.002	0.001	0.008	0.002	0.017	0.004	0.065
Na	0.000	0.002	0.000	0.004	0.014	0.003	0.007	0.000	0.010	0.005	0.000	0.003	0.009
K	0.000	0.000	0.000	0.002	0.000	0.000	0.000	0.001	0.010	0.001	0.001	0.001	0.005
P	1.006	0.996	0.999	1.000	1.000	1.000	1.000	1.000	1.000	1.000	1.000	1.000	1.000
Li*	1.000	1.000	1.000	0.310	0.428	0.297	0.025	0.090	0.127	0.373	0.500	0.193	0.688
	(1)	(1)	(1)	(2)	(2)	(2)	(2)	(2)	(2)	(2)	(2)	(2)	(2)

(1) The a.p.f.u. are calculated on the basis of 4 O and Li* (a.p.f.u.) = 1.
(2) The a.p.f.u. are calculated on the basis of 4 O and P = 1 and Li* (a.p.f.u.) = calculated from charge balance.
Locality* = see Table 1; *Abbreviations: Triph = Triphylite; Fsck = Ferrisicklerite.

1996). The distribution of the rare-element pegmatites in the pegmatite fields, often with the Li-F-richest facies occurring farthest from the parental granite, suggests a previous vertical chemical zonation of the melt within the source pluton. For example, in the Fregeneda-Almendra pegmatite field some Li-rich pegmatites lack zoning across the dyke, but show a clear mineralogical and chemical change along the dyke, with a continuous enrichment in F and Li northwards. This could be explained by the inheritance of a previous compositional zoning in the melt, before it intruded the fractures where it crystallized. The greater enrichment in Li, F, and probably also B and H_2O, would notably reduce the viscosity of the most fractionated melts (Dingwell *et al.*, 1996), and would also lower the liquidus temperature, enhancing the mobility of the melt. A filter-pressing mechanism (Propach, 1976), related to deformation that expels residual melts upwards, would result in a vertical chemical zonation in the magma chamber (Moyen *et al.*, 2003; Bea *et al.*, 2005). If melt were expelled along fractures, the highly fractionated melt in the upper part of the magma chamber would escape first. The exsolution of a fluid phase could also help the extraction of residual melt from mushes (Sisson and Bacon, 1999). Another mechanism that has been proposed to explain fractional crystallization to give a zoning around a pluton is that of differentiation '*en route*' to the surface, with the segregation of solids during magma ascent, which would allow enrichment in incompatible elements in the residual melt (Tartèse and Boulvais, 2010). However, this mechanism probably did not have a significant influence on the chemical evolution of the pegmatites from the pegmatite fields described here, as the occurrence of Li mineralization in the apical parts of leucogranitic cupolas in the Central Iberian Zone, with a clear upwards zoning, indicates that *in situ* fractionation of the melt was an effective mechanism of melt differentiation. The compositional, mineralogical and textural similarities of the Li mineralization in the pegmatite fields and associated with leucogranitic cupolas indicate that the protoliths and fractionation mechanisms of the parental melts were quite similar for both. However, in the case of the mineralization associated with leucogranitic cupolas, most probably the system remained closed until the last stages of pegmatite crystallization (Roda *et al.*, 2005; Roda-Robles *et al.*, 2012*b*). The higher Li and F enrichment attained by micas and the lower Fe/(Fe + Mn) ratios for phosphates from these bodies indicate a higher degree of fractionation. This may

be due to loss of some volatile components, including H_2O and B, from the melts escaping from the parental plutons, during their displacement. Removal of volatile components would have affected fractionation processes, as these fluxing components increase diffusivity and lower the solidus temperature, which enhances fractionation.

The beryl-phosphate pegmatites usually occur inside anatectic granites, frequently with a gradual contact with the host rock. The degree of enrichment in rare elements (e.g. Li, F, B and Sn) for these bodies is much lower than that of the Li pegmatites from pegmatite fields and from leucogranitic cupolas. The volumetrically significant amounts of phosphates in these bodies may be explained by the behaviour of P in peraluminous-perphosphorous granitic melts, where the activity of Ca is low and thus there is more P_2O_5 than CaO to form normative apatite. Crystallization of plagioclase could cause a decrease in the Ca/P ratio in the melt. The excess of P_2O_5 in late differentiates becomes stronger from the point where apatite no longer precipitates, that is, when P first behaves as an incompatible element (Bea *et al.*, 1992). This P is progressively concentrated in the residual melt until intermediate degrees of pegmatite fractionation, when its concentration in the melt decreases by the formation of phosphates and/or through tetrahedral substitution within the lattice of the feldspars. Generally there is a low content of mafic constituents in peraluminous granitic pegmatites. The large masses of Fe-Mn phosphate in these beryl-phosphate pegmatites indicate that, in this case, the concentration of Fe and Mn in the original melt was still moderately important. A scarcity of boron would also favour the crystallization of Fe-Mn phosphates instead of forming Fe-tourmaline (in these dykes, tourmaline is rarely found). Intermediate levels of *in situ* fractionation of anatectic peraluminous granitic melts represent the most plausible genetic model for these pegmatites (Roda-Robles *et al.*, 2012*b*).

Finally, the quartz-montebrasite veins were most probably generated from hydrothermal fluids associated with the latest stages of fractionation of parental granitic and/or pegmatitic melts. According to Černý and Ercit, (2005) a high μPFO2 is required for the crystallization of montebrasite. However, the F content in the montebrasite from these quartz dykes is usually low (Table 5, Fig. 5*a*, median ≈1.69 wt.% F). If the formula proposed by London *et al.* (2001) to estimate the concentration of F in melt from the F content in

amblygonite–montebrasite at 585° and 200 MPa H_2O, is applied, the result is 0.44 wt.% F. This formula was used for calculation in pegmatitic melts, and it may not be appropriate for hydrothermal fluids. The high concentrations of P required to form montebrasite in these dykes could be explained, as in the case of the beryl-phosphate pegmatites, by the fractionation of P as an incompatible element from peraluminous-perphosphorous melts. In this case, a scarcity of mafic components in the original melt may have prevented the formation of Fe-Mn phosphates, allowing P to become enriched in the most fractionated melt.

Lithium exploration clues for the Central Iberian Zone

The most significant potential for Li mineralization in this region, with inferred economic interest, is associated with the pegmatite fields. In general, the pegmatite bodies with Li mineralization in the Central Iberian Zone are relatively small, which makes exploration and extraction more attractive in highly populated areas where a small, relatively short-lived open pit operation might have a lower impact on surrounding communities. At the same time, more than one Li-enriched body is usually present in an area with Li enrichment. Thus, various small operations could potentially bring more benefits and development into economically depressed areas of both Portugal and Spain.

As the pegmatite fields include pegmatites with varying degrees of Li enrichment, it is important to consider some common features for all the pegmatite dykes (barren and Li rich) that may help in the exploration of Li-enriched pegmatite fields: (1) An aplitic character, with high albite content. Plagioclase may be very white and in thin section it commonly forms myrmekitic intergrowths. (2) The presence of wedge-shaped K-feldspar crystals, growing perpendicular to the contacts with the host rocks. Some K-feldspar crystals show greyish colours in hand specimen. In thin sections perthitic textures are usually absent or poorly developed. (3) Graphic quartz-feldspar intergrowths are usually absent. (4) Amblygonite–montebrasite and Fe-Mn phosphates are typical accessory minerals, even in the less-evolved pegmatites of those fields. (5) There are low mica proportions, unless the dyke is Li-mica rich. (6) Pinkish, greenish or, more rarely, bluish soapy masses of cookeite or clay minerals, up to 12 cm long, replacing petalite or spodumene crystals, are key features of some Li-rich pegmatites.

Final remarks

On the basis of field observations, and of the mineralogical, textural and compositional characteristics of the different types of Li mineralization found in the Central Iberian Zone, the following conclusions can be drawn:

(1) Li mineralization in the Central Iberian Zone may be classified in four types: aplite-pegmatite dykes usually grouped in pegmatite fields, Li mineralization associated with leucogranitic cupolas, beryl-phosphate pegmatites and quartz-montebrasite veins.

(2) The main Li minerals of these mineralization types include Li-mica, spodumene and/or petalite in the pegmatite fields and leucogranitic cupolas, triphylite–lithiophilite in the beryl-phosphate pegmatites and amblygonite–montebrasite in the quartz-montebrasite veins.

(3) The origin of the Li-mineralization in this region is probably related to the fractional crystallization of peraluminous melts generated by partial melting of metasedimentary rocks in the middle crust during the Variscan orogeny.

(4) The most fractionated pegmatitic bodies are those occurring in the leucogranitic cupolas and, to a lesser extent, in the pegmatite fields. The beryl-phosphate pegmatites show intermediate degrees of fractionation. The quartz-montebrasite veins are attributed to a later hydrothermal stage.

(5) The highest economic potential for Li is attained by the pegmatite fields, due to the notable Li enrichment shown by some of the dykes and the number of mineralized bodies in each field.

(6) Aspects of texture and mineralogy provide indicators that can be used for Li exploration in the Central Iberian Zone.

Acknowledgements

References

Antunes, I.M.H.R., Neiva, A.M.R., Ramos, J.M.F., Silva, P.B., Silva, M.M.V.G. and Corfu, F. (2013) Petrogenetic links between lepidolite-subtype aplite-pegmatite, aplite veins and associated granites at Segura (central Portugal). *Chemie der Erde – Geochemistry*, **73**, 323–341.

Arenas, R., Martínez Catalán, J.R. and Díaz García, F. (2004) Zona de Galicia Trás Os Montes, introducción. Pp. 133–135 in: *Geología de España* (J.A. Vera, editor). Sociedad Geológica de España, Instituto Geológico y Minero de España, Madrid.

Azor, A., González Lodeiro, F. and Simancas, J.F. (1994) Tectonic evolution of the boundary between the Central Iberian and Ossa-Morena zones (Variscan belt, southwest Spain). *Tectonics*, **13**, 45–61.

Bea, F. (2004) La naturaleza del magmatismo de la Zona Centro Ibérica: consideraciones generales y ensayo de correlación. Pp. 128–133 in: *Geología de España* (J.A. Vera, editor). Sociedad Geológica de España, Instituto Geológico y Minero de España, Madrid.

Bea, F., Fershtater, G.B. and Corretgé, L.G. (1992) The geochemistry of phosphorus in granite rocks and the effect of aluminium. *Lithos*, **29**, 43–56.

Bea, F., Montero, P. and Molina, J.F. (1999) Mafic precursors, peraluminous granitoids, and late lamprophyres in the Avila batholith: A model for the generation of Variscan batholiths in Iberia. *Journal of Geology*, **107**, 399–419.

Bea, F., Montero, P. and Zinger, T. (2003) The nature, origin, and thermal influence of the granite source layer of Central Iberia. *Journal of Geology*, **111**, 579–595.

Bea, F., Fershtater, G.B., Montero, P., Smirnov, V.N. and Molina, J.F. (2005) Deformation-driven differentiation of granitic magma: the Stepninsk pluton of the Uralides, Russia. *Lithos*, **81**, 209–233.

Carvalho, J.M.F. and Farinha, J.A.L.B. (2004) *Lithium potentialities in Northern Portugal*. 17th Industrial Minerals International Congress, Barcelona, Spain, pp. 1–10.

Černý, P. and Ercit, T.S. (2005) The classification of granitic pegmatites revisited. *The Canadian Mineralogist*, **43**, 2005–2026.

Černý, P. and Ferguson, R.B. (1972) The Tanco pegmatite at Bernic Lake, Manitoba; IV, Petalite and spodumene relations. *The Canadian Mineralogist*, **11**, 660–678.

Charoy, B. and Noronha, F. (1996) Multistage growth of a rare-element, volatile-rich microgranite at Argemela (Portugal). *Journal of Petrology*, **37**, 73–94.

Charoy, B., Noronha, F. and Lima, A. (2001) Spodumene – petalite – eucryptite: Mutual relationships and pattern of alteration in li-rich aplite–pegmatite dykes from Northern Portugal. *The Canadian Mineralogist*, **39**, 729–746.

Christmann, P., Gloaguen, E., Labbé, J.-F., Melleton, J. and Piantone, P. (2015) Global lithium resources and sustainability issues. Pp. 1–40 in: *Lithium Process Chemistry. Resources, Extraction, Batteries, and Recycling* (A. Chagnes and J. Swiatowska, editors). Elsevier, 40 pp.

Dias, P.A., Pereira, B., Azavedo, J., Oliveira, J., Leal Gomes, C. and Carvalho, J. (2013) *Pegmatite productive terrains in the variscan granite hosts from northern and central portugal*. 23rd International Mining Congress & Exhibition of Turkey, Pp. 2121–2129.

Díez Balda, M.A., Vegas, R. and González Lodeiro, F. (1990) Structure of the Central Iberian Zone. Autochthonous Sequences. Structure. Pp. 172–188 in *Pre-Mesozoic Geology of Iberia* (R.D. Dallmeyer and E. Martínez García, editor). Springer-Verlag, Berlin.

Dingwell, D.B., Hess, K.U. and Knoche, R. (1996) Granite and granitic pegmatite melts: Volumes and viscosities. *Transactions Of The Royal Society Of Edinburgh – Earth Sciences*, **87**, 65–72.

Farias, P., Gallastegui, G., González Lodeiro, F., Marquínez, J., Martín-Parra, L.M., Martínez Catalán, J.R., de Pablo Maciá, J.G. and Rodríguez-Fernández, L.R. (1987) Aportaciones al conocimiento de la litoestratigrafia y estructura de Galicia central. *Memórias da Faculdae de Ciências, Universidade do Porto*, **1**, 411–431.

Fuertes-Fuente, M. and Martín-Izard, A. (1998) The Forcarei Sur rare-element granitic pegmatite field and associated mineralization, Galicia, Spain. *The Canadian Mineralogist*, **36**, 303–325.

Gallego Garrido, M. (1992) *Las mineralizaciones de Li asociadas a magmatismo ácido en Extremadura y su encuadre en la Zona Centro-Ibérica*. Tesis Doctoral, Universidad Complutense de Madrid, Spain.

Garate-Olave, I., Roda-Robles, E., Gil-Crespo, P.P. and Pesquera, A. (2014) Caracterización petrográfica y geoquímica de las micas asociadas al sistema granito-pegmatitas del área de Tres Arroyos (Alburquerque, Badajoz). *Macla*, 19.

Garção, J.C.S. (1927) Minas de Lítio e estanho. Pp. 25–31 in: *Boletim de Minas.* Imprensa Nacional, Lisbon.

Julivert, M., Fontboté, J.M., Ribero, A. and Nabais-Conde, L.E. (1972) *Mapa tectónico de la Península Ibérica y Baleares scale 1:1.000.000. Memoria explicativa.* Instituto geológico y Minero de España, Spain, pp. 113.

Leal Gomes, C. (1994) *Estudo estructural e paragenético de um sistema pegmatóide granítico. O campo aplito-pegmatitico de Arga Minho, Portugal.* PhD thesis, Universidade do Minho, Portugal.

Leal Gomes, C., Azevedo, A., Lopes Nunes, J. and Dias, P.A. (2009) Phosphate fractionation in pegmatites of Pedra da Moura II claim – Ponte da Barca – Portugal. *Estudos Geológicos*, **19**, 172–176.

Lima, A. (2000) *Estrutura, Mineralogia e Génese dos Filões Aplitopegmatíticos com Espodumena da Região do Barroso-Alvão (Norte de Portugal).* Univ. Porto, Portugal and INPL, Nancy, France, 270 pp.

Lima, A., Rodrigues, R., Guedes, A. and Novák, M. (2009) The rare elements-rich granite of Seixoso Area (Outeiro Mine). Preliminary results. *Estudos Geológicos*, **19**, 182–187.

London, D. (2008) Pegmatites. *The Canadian Mineralogist, Special Publication*, **10**, pp. 347.

London, D., Evensen, J.M., Fritz, E., Icenhower, J.P., Morgan VI, G.B. and Wolf, M.B. (2001) Enrichment and accomodation of manganese in granite-pegmatite systems. *Geochimica Et Cosmochimica Acta*, Eleventh Annual V. M. Goldschmidt Conference, May 20–24, 2001, Hot Springs, Virginia. Abstract n° 3369.

Martín-Izard, A., Reguilón, R. and Palero, F. (1992) Las mineralizaciones litiníferas del oeste de Salamanca y Zamora. *Estudios Geológicos*, **48**, 9–13.

Martínez Catalán, J.R. (1985) *Estratigrafia y estructura del Domo de Lugo : (Sector Oeste de la Zona Asturoccidental-leonesa)*. 324 pp. Fundacion Coruña "Pedro Barrié de la Maza,Conde Fenosa" La Coruña.

Martínez Catalán, J.R., Arenas, R., Díaz García, F., Rubio Pascual, F.J., Abati, J. and Marquínez, J. (1996) Variscan exhumation of a subducted paleozoic continental margin: The basal units of the Ordenes Complex, Galicia, NW Spain. *Tectonics*, **15**, 106–121.

Martínez Catalán, J.R., Martínez Poyatos, D. and Bea, F. (2004) Zona Centroibérica: Introducción. Pp. 68–69 in: *Geología de España* (J.A. Vera, editor). Sociedad Geológica de España, Instituto Geológico y Minero de España, Madrid.

Martínez-Fernández, F.J. (1974) *Estudio del área metamórfica y granítica de los Arribes del Duero (Prov. de Salamanca y Zamora).* PhD Thesis, Univ. de Salamanca, Spain.

Martínez, F.J., Julivert, M., Sebastián, A., Arboleda, M.L. and Gil-Ibarguchi, J.I. (1988) Structural and thermal evolution of high-grade areas in the northwestern parts of the Iberian Massif. *American Journal of Science*, **288**, 969–996.

Martins, T., Roda-Robles, E., Lima, A. and de Parseval, P. (2012) Geochemistry and Evolution of Micas in the Barroso-Alvao Pegmatite Field, Northern Portugal. *The Canadian Mineralogist*, **50**, 1117–1129.

Mason, B. (1941) Minerals of the Varuträsk pegmatite. XXIII. Some iron-manganese phosphate minerals and their alteration products, with special reference to material from Varuträsk. *Geolpgoske Föreniugen i Stockholm Förhandlgar*, **63**, 25–34.

Moyen, J.-F., Martin, H., Jayananda, M. and Auvray, B. (2003) Late Archaean granites: a typology based on the Dharwar Craton (India). *Precambrian Research*, **127**, 103–123.

Neiva, A.M.R. and Ramos, J.M.F. (2010) Geochemistry of granitic aplite-pegmatite sills and petrogenetic links with granites, Guarda-Belmonte area, central Portugal. *European Journal of Mineralogy*, **22**, 837–854.

Neiva, A.M.R., Ramos, J.M.F. and Silva, P.B. (2011) Alguns aplito-pegmatitos graníticos com minerais de Li das regiões centro e norte de Portugal. Pp. 23–26 in: *Valorização de Pegmatitos Litiníferos* (L.M.P. Martins, D.P.S. de Oliveira, R. Silva, H.M.C. Viegas and R.C. Vilas Bôas, editors). Lisbon, Portugal.

Noronha, F., Ramos, J.M.F., Rebelo, J., Ribeiro, A. and Ribeiro, M.L. (1981) Essai de corrélation des phases de déformation hercyniennes dans le nord-ouest Péninsulaire. *Leidse Geologische Mededelingen*, **52** (1), 87–91.

Patiño Douce, A.E. and Johnston, A.D. (1991) Phase equilibria and melt productivity in the pelitic system: implications for the origin of peraluminous granitoids and aluminous granulites. *Contributions to Mineralogy and Petrology*, **107**, 202–218.

Pérez-Estaún, A., Bea, F., Bastida, F., Marcos, A., Martínez Catalán, J.R., Martínez Poyatos, D., Arenas, R., Díaz García, F., Azor, A., Simancas, J.F. and González Lodeiro, F. (2004) La Cordillera Varisca europea: El Macizo Ibérico. Pp. 21–25 in: *Geología de España* (J.A. Vera, editor). Sociedad Geológica de España, Instituto Geológico y Minero de España, Madrid.

Pesquera, A., Torres Ruiz, J., Gil-Crespo, P.P. and Velilla, N. (1999) Chemistry and genetic implications of tourmaline and Li-F-Cs micas from the Valdeflores area (Cáceres, Spain). *American Mineralogist*, **84**, 55–69.

Peucat, J.J., Jegouzo, P., Vidal, P. and Bernard-Griffiths, J. (1988) Continental crust formation seen through the Sr and Nd isotope systematics of S-type granites in the Hercynian belt of western France. *Earth and Planetary Science Letters*, **88**, 60–68.

Pouchou, J.L. and Pichoir, F. (1985) "PAP" $\varphi(\rho z)$ procedure for improved quantitative microanalysis. Pp. 104–106 in: *Microbeam Analysis.* San Francisco Press, San Fransisco, USA.

Propach, G. (1976) Models of filter differentiation. *Lithos*, **9**, 203–209.

Puziewicz, J. and Johannes, W. (1988) Phase equilibria and compositions of Fe-Mg-Al minerals and melts in water-saturated peraluminous granitic systems. *Contributions to Mineralogy and Petrology*, **100**, 156–168.

Quensel, P. (1937) Minerals of the Varuträsk pegmatite. I: The lithium-manganese phosphates. *Geologiska Föreningeni Stockholm Förhandlingar*, **59**, 77–96.

Roda, E., Fontan, F., Pesquera, A. and Velasco, F. (1996) The phosphate mineral association of the granitic pegmatites of the Fregeneda area (Salamanca, Spain). *Mineralogical Magazine*, **60**, 767–778.

Roda, E., Pesquera, A., Velasco, F. and Fontan, F. (1999) The granitic pegmatites of the Fregeneda area

(Salamanca, Spain): characteristics and petrogenesis. *Mineralogical Magazine*, **63**, 535–558.

Roda, E., Pesquera, A., Fontan, F. and Keller, P. (2004) Phosphate mineral associations in the Canada pegmatite (Salamanca, Spain): Paragenetic relationships, chemical compositions, and implications for pegmatite evolution. *American Mineralogist*, **89**, 110–125.

Roda, E., Pesquera, A., Gil-Crespo, P.P., Torres-Ruiz, J. and Fontan, F. (2005) Origin and internal evolution of the Li-F-Be-B-P-bearing Pinilla de Fermoselle pegmatite (Central Iberian Zone, Zamora, Spain). *American Mineralogist*, **90**, 1887–1899.

Roda-Robles, E., Pesquera, A., Gil-Crespo, P.P., Torres-Ruiz, J. and De Parseval, P. (2006) Mineralogy and geochemistry of micas from the Pinilla de Fermoselle pegmatite (Zamora, Spain). *European Journal of Mineralogy*, **18**, 369–377.

Roda-Robles, E., Mateus, S., Vieira, R., Martins, T., Vide, R. and Lima, A. (2008) Phosphate mineral associations in the Seixeira pegmatite (Bendada, Sabugal, Guarda, Portugal): preliminary results. *IX CGPLP— IX Congresso de Geoquímica dos Países de Língua Portuguesa, Abstracts*, p. 39.

Roda-Robles, E., Vieira, R., Lima, A. and Pesquera-Pérez, A. (2009) Petrogenetic links between granites and pegmatites in the Fregeneda-Almendra area (Salamanca, Spain and Guarda, Portugal): new insights from $^{40}Ar/^{39}Ar$ dating in micas. *Estudos Geológicos*, **19**, 305–310.

Roda-Robles, E., Galliski, M., Nizamoff, J., Simmons, W., Keller, P., Falster, A. and Hatert, F. (2011) Cation partitioning between minerals of the triphylite $\pm$ graftonite $\pm$ sarcopside association in granitic pegmatites. *Contributions to the 5th International Symposium on Granitic Pegmatites*, pp. 161–164, Mendoza (Argentina).

Roda-Robles, E., Pesquera, A., Gil-Crespo, P.P. and Torres-Ruiz, J. (2012a) The Puentemocha beryl-phosphate granitic pegmatite, Salamanca, Spain: Internal structure, petrography and mineralogy. *The Canadian Mineralogist*, **50**, 1573–1587.

Roda-Robles, E., Pesquera, A., Gil-Crespo, P.P. and Torres-Ruiz, J. (2012b) From granite to highly evolved pegmatite: A case study of the Pinilla de Fermoselle granite–pegmatite system (Zamora, Spain). *Lithos*, **153**, 192–207.

Roda-Robles, E., Pesquera, A., Gil-Crespo, P.P., Garate-Olave, I. and Ostaikoetxea-Garcia, U. (2013) Textural and mineralogical features of the Li-F-Sn-bearing pegmatitic rocks from Castillejo de Dos Casas (Salamanca, Spain): preliminary results. *6th International Symposium On Granitic Pegmatites*, pp. 118–119.

Roda-Robles, E., Pesquera, A., Lima, A., Vieira, R. and Gil-Crespo, P.P. (2012c) Origin and significance of phosphate minerals in the Central Iberian Zone (Spain and Portugal): implications for the behaviour of P during the Variscan magmatism. *European Mineralogical Conference EMC2012*, **1**, p. 381.

Roda-Robles, E., Pesquera, A., de Madinabeitia, S.G., Ibarguchi, J.I.G., Nizamoff, J., Simmons, W., Falster, A. and Galliski, M.A. (2014) On the geochemical character of primary Fe-Mn phosphates belonging to the triphylite-lithiophilite, graftonite-beusite, and triplite-zwieselite series: First results and implications for pegmatite petrogenesis. *The Canadian Mineralogist*, **52**, 321–335.

Roda-Robles, E., Pesquera, A., Gil-Crespo, Garate-Olave, I., P.P. and Torres-Ruiz (2015) The Li-rich aplopegmatite from Castillejo de Dos Casas (Salamanca, Spain): Example of a highly fractionated granite-pegmatite system. *Proceedings SGA2015*, **vol. 2**, 11–15.

Sisson, T.W. and Bacon, C.R. (1999) Gas-driven filter pressing in magmas. *Geology*, **27**, 613–616.

Sylvester, P.J. (1998) Post-collisional strongly peraluminous granites. *Lithos*, **45**, 29–44.

Tartèse, R. and Boulvais, P. (2010) Differentiation of peraluminous leucogranites "en route" to the surface. *Lithos*, **114**, 353–368.

Thompson, A.B. (1999) Some time-space relationships for crustal melting and granitic intrusion at various depths. *Geological Society, London, Special Publications*, **168**, 7–25.

Tischendorf, G., Rieder, M., Forster, H.J., Gottesmann, B. and Guidotti, C.V. (2004) A new graphical presentation and subdivision of potassium micas. *Mineralogical Magazine*, **68**, 649–667.

Tkachev, A.V. (2011) Evolution of metallogeny of granitic pegmatites associated with orogens throughout geological time. *Geological Society, London, Special Publications*, **350**, 7–23.

Vieira, R., Roda-Robles, E., Pesquera, A. and Lima, A. (2011) Chemical variation and significance of micas from the Fregeneda-Almendra pegmatitic field (Central-Iberian Zone, Spain and Portugal). *American Mineralogist*, **96**, 637–645.

September 12th, afternoon: STOP 1: Feli open-pit

**Travel from the hotel to the Feli open-pit:
30 km; ≈ 45 min**

Locality 1: Fregeneda-Almendra aplite-pegmatite field (Salamanca, Spain)

Stop 1 (12th of September, afternoon) and Stop 4 (14th of September, morning)

General Highlights

-Over two hundreds of aplite-pegmatite dykes, grouped in 11 types from barren to highly enriched in Li+F (Fig. 3 and Table 2).
-Zonal distribution, with a Li+F enrichment northwards (Fig. 3).
-Main Li-rich minerals: spodumene ± petalite, Li-muscovite & lepidolite.
-The origin of the Li-rich aplite-pegmatites is probably related to the extreme fractionation of late-D3 highly peraluminous granite.

Stop 1 Highlights (Feli open pit, 12th of September, afternoon)

-Tin mine closed in the seventies, with cassiterite crystals, some up to 10cm Ø, associated with thin, folded quartz-rich veins and pegmatites (type 11 in Fig. 3 and Table 2).
-Feldspars+Li mine from the beginning of the nineties up to 2012. Nowadays closed.
-Lepidolite±spodumene-rich, subvertical aplite-pegmatite body (type 9 in Fig. 3 and Table 2), up to 20 m thick, with a frequent eye-catching layering, which cuts the Sn-rich veins.
-Overall Li-enrichment of the aplite-pegmatite >1% Li$_2$O. High F contents.

Stop 1: A) General view of the wall of the Feli open-pit (Fregeneda-Almendra) with a Li-mica rich subvertical dique, branched in its upper part, cross-cutting some cassiterite-bearing quartz-rich, folded veins.

Stop 1: B) Zoned quartz-rich vein, with the cassiterite crystals disposed along the contacts with the mica-schists of the hosting rock; C) Li-mica-rich thin dyke, showing the discordant contact with the country rock; D) close-up of the main Li-mica rich aplite-pegmatite dyke from the Feli open pit, showing a subvertical layering with alternating LI-mica-rich and albite-rich bands; and, E) hand sample from the Feli open-pit with coarse-grained Li-mica scales together with greyish K-feldspar.

INTRODUCTION

Numerous studies have been developed during the last three decades on pegmatite bodies that occur in the Fregeneda-Almendra area (FA), Central-Iberian-Zone, (CIZ), Spain and Portugal, (e.g. Roda-Robles, 1993; Roda et al. 1999, 2007, Vieira et al., 2007, Roda-Robles et al., 2010, Vieira, 2010; Vieira et al., 2011). Based on these works, 11 different types of pegmatites have been characterized (Fig. 1, Table 1). Five of these types belong to evolved pegmatites, whereas the other six types correspond to barren and intermediate pegmatitic bodies. Most of these pegmatites intruded pre-Ordovician metasediments of the schist-metagraywacke complex (SGC), showing a zonal distribution from barren to enriched in Li, F, Sn, Rb, Nb>Ta, B, P and Be, with an increase in the evolution degree as the distance to the Meda-Penedono-Lumbrales (MPL) granitic complex increases northwards (Fig. 3). This zonation suggests, at first sight, a parental relationship between the granitic complex and the pegmatites. However, some features are not consistent with the hypothesis of a petrogenetic link between the most evolved pegmatites in the FA field and the MPL granitic complex: 1) a geochemical modelling made on the different granites and pegmatites indicates the existence of at least two different trends of evolution: one for the granite and the barren pegmatites; and the other one for the intermediate and evolved pegmatites (Roda et al., 1999); 2) no more Li-rich pegmatites are observed in relation to the MPL granitic complex along the more than 50 Km of outcrop of this granite, eastwards and westwards from the FA area; and 3) geochronological data obtained by the $^{40}Ar/^{39}Ar$ step-heating method on micas indicate a ≈ 15 Ma gap of time between the MPL granitic complex and the most fractionated pegmatitic bodies in this field, which is too long to consider this granite as the parental melt for such pegmatites.

GEOLOGICAL SETTING AND GENERAL GEOLOGY OF PEGMATITES

The FA area is located in the Central-Iberian-Zone (CIZ), in the western part of a narrow metamorphic belt, with an E-W trend. This belt is bordered by the Variscan MPL granitic complex (Carnicero, 1981) to the south, and by the Saucelle granite to the NE, both two-mica, peraluminous granites, belonging to the group of syntectonic (D3) plutons. These granites and most of the pegmatites intruded pre-Ordovician metasediments of the SGC. In the FA area the metamorphism shows an isograd distribution increasing to the South parallel to the MPL leucogranite contact, reaching locally the sillimanite (fibrolite) isograd.

Most of the pegmatites from the FA field correspond to poorly evolved pegmatites, which may be grouped in two main categories (Table 2, Fig. 3): (i) barren pegmatites with quartz, K-feldspar > albite, muscovite, tourmaline ± andalusite ± garnet, (types 1, 2, 3 and 4); and (ii) albite-rich intermediate discordant aplite-pegmatites (types 5 and 6), characterized by the occurrence of Fe-Mn phosphates, montebrasite, and both micas and K-feldspar with higher Rb and Cs contents than those of the barren pegmatites (Roda et al., 1999). A third category of pegmatites is less abundant but also common. It belongs to (iii) fertile discordant aplite-pegmatites, mainly rich in Li-minerals (types 7, 8, 9 and 10) and/or cassiterite (type 11). It is noteworthy that pegmatites from the first category are well intragranitic (types 1 and 3), well conformable to the hosting-rocks and occurring near the contact with the granite (types 2 and 4). On the contrary, pegmatites from categories (ii) and (iii) are clearly discordant, showing similar strikes, close to N10E, and similar dipping, close to the vertical. They occur as fracture filling, being these fractures attributed to a late tectonic event during the Variscan orogeny. These pegmatites occur further from the contact to the granite, northwards (Fig. 3). The main Li-bearing mineral assemblages in the Li-rich pegmatites include petalite (type 7); spodumene (type 8)(Stop 4, Alberto open pit); lepidolite+spodumene (type 9)(Stop 1, Feli open-pit); and lepidolite (type 10). It is remarkable that the Sn-rich dykes, (type 11, occur folded and are crosscut by one lepidolite+spodumene dyke (type 9) in the Feli open pit)(Stop 1), in the northernmost part of the field (Fig. 3). Some drillings made in this open pit showed the presence of a hidden granitic body under the Sn-rich and the lepidolite+spodumene rich dikes.
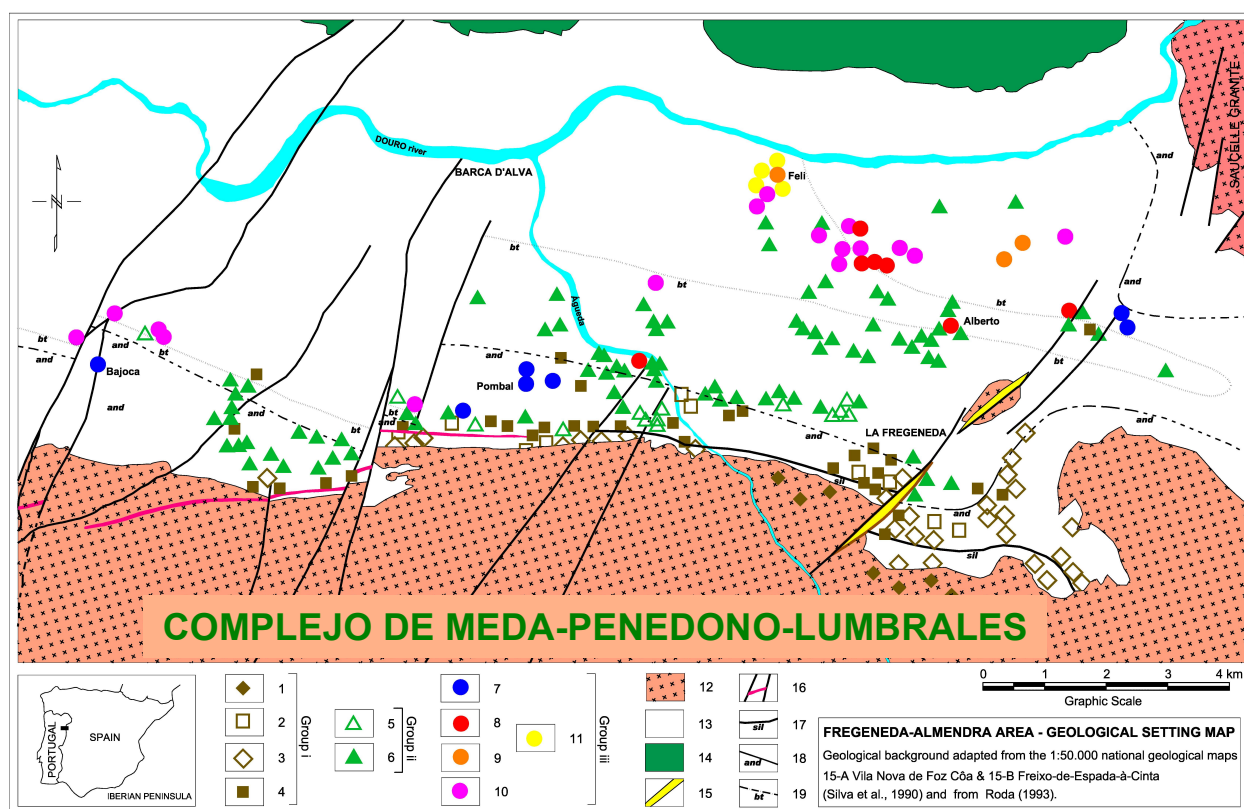
Fig. 3: Distribution of the pegmatite types in the Fregeneda-Almendra area. Legend: Group i) 1– simple interior; 2 – quartz+andalusite conformable dykes; 3 – simple dykes and apophyses; 4 – simple conformable; Group ii) 5– K-feldspar discordant dykes; 6 – simple discordant; Group iii) 7 – petalite-bearing discordant; 8 – spodumene-bearing discordant; 9 –lepidolite-spodumene-bearing discordant; 10 – lepidolite-bearing discordant; 11 – Sn-bearing discordant; 12 – syn-F3 granites; 13 – Pre-Ordovician Schist-Metagraywacke-Complex; 14 – Ordovician formations; 15 – quartz segregations fractures; 16 – porphyry granitic/riolitic and faults; 17 – sillimanite isograd; 18 – andalusite isograd; 19 – biotite isograd.

GEOCHRONOLOGY AND IMPLICATIONS FOR THE PETROGENESIS OF THE PEGMATITES (From Roda-Robles et al., 2009, Vieira 2010)

Micas ^{40}Ar/^{39}Ar geochronology from pegmatites of the FA area yielded concordant spectra with overall 295.1 ± 4.2 Ma to 311.2 ± 3.7 Ma, and ^{40}Ar/^{39}Ar intercept statistically indistinguishable from the atmospheric value of 295.5. The main facies of the MPL granite yields a flat age spectrum and well-defined plateau age of 311.2 ± 3.7 Ma. Intermediate age values are in the range 305.0±3.3 to 300.0±3.1 Ma (hidden granite and Sn-rich dykes of type 11, respectively). Mica spectra for barren pegmatites of the category (i) are mainly composed of concordant steps and yield plateau ages included in this intermediate range. Micas from the (ii) and (iii) pegmatitic categories yield concordant spectra and plateau ages in the range of 295.1±4.2 to 296.4±3.5 Ma. These data are consistent with the Rb-Sr age (292±2.6 Ma) for the lepidolite-rich dyke occurring in the Riba d´Alva scheelite mineralization north from the FA field (Nitschke, 1998). It is noteworthy that all these pegmatites are discordant, (types 6, 7, 8, 9 and 10), showing similar strike, dipping and style.

Based on these results, three different sets of ages have been obtained for the granites and pegmatites from the FA area. The gap between the main facies of the MPL granite and the pegmatites belonging to the (ii) and (iii) categories, close to 15 Ma, makes it difficult to relate the origin of all these pegmatites with this granite. The geochronological results are in agreement with the geological data. The main facies of the MPL is prior to the development of any of the pegmatitic bodies in the FA field. Later granitic facies, with relative ages deduced from structural and mineralogical data, would be more possibly related with the crystallization of the barren pegmatites. In this way, the facies of the hidden granite located under the Feli open pit, with an

age of 305.0±3.3 Ma, could be more probably related to the genesis of the barren pegmatites that have ages between 300.0±3.5 and 304.8±4.7 Ma. It is also possible that this granite is linked to the genesis of the Sn-rich dykes, with an age of 300.0±3.1 Ma and that occur as a stockwork over this granite. These Sn-rich dikes are crosscut by a younger lepidolite-spodumene-rich dyke, with an age of 295.3±3.9 Ma. The origin of the youngest pegmatites is likely to be related to a non-outcropping late-orogenic granite, that are abundant close to this area.

The zonal distribution of pegmatites in relation to the MPL granitic complex in the FA area could be a casual and not causal feature, at least for the most evolved pegmatitic bodies. Anyway, further studies must be done, including dating of all the granitic facies in the MPL complex as well as the nearest late-tectonic granites. Also structural studies on these granites would help the interpretation of the petrogenetic links between granites and pegmatites.

Table 2: Main characteristics of the groups of pegmatites recognized in the Fregeneda-Almendra area (Roda-Robles et al., 2009)

TYPE	MINERALOGY		HOST ROCK METAMORPHISM	MORPHOLOGY AND STRUCTURE	REMARKS	ENRICHMENT
	Main minerals	Other minerals				
(1)	Qtz Kfs	ms ab tur	(intragranitic)	dyke-like thickness < 50 cm	scarce within the Lumbrales granite	K, Al, Si, (B, P)
(2)	Qtz and	ms tur Kfs chl	Andalusite zone	conformable dyke-like thickness < 40 cm	boudinage structures. Qtz & and their main minerals	Al, Si, (B, K)
(3)	Qtz Kfs ms	ab tur bt	Sillimanite, andalusite and biotite zones	irregular and bulbous masses ellipsoidal, lenticular or turnip-shaped forms	abundant; aplite-pegmatite facies; graphic texture	K, Al, Si, (B)
(4)	Qtz Kfs ms ab tur	and chl grt bt	Sillimanite and andalusite zones	conformable dyke-like locally with internal zonation thickness 1 m	abundant; in some cases internal zoning, graphic texture	B, Al, Na
(5)	Kfs	Qtz ms pyrite	Biotite zone	disconformable dyke-like thickness > 1 m	not very abundant; main component is pink K-feldspar	K
(6)	Qtz Kfs ab ms	±pho ±mbs ±tur	Biotite and chlorite zones	disconformable dyke-like thickness < 10 cm - 2 m	most abundant Near the granite internal zoning can be present	K, Na, Al, Si, (P, Li)
(7)	Qtz pet ab ±ecr	ms cst ±mbs	Sillimanite andalusite and andal/biot limit	disconformable dyke-like without internal zonation thickness 5-30 m	main body mined in the Bajoca open-pit	Li, Sn, P
(8)	Qtz spd ab Kfs	ms mbs pet brl	Biotite/chlorite limit zone	disconformable dyke-like without internal zonation thickness 4-15 m	main body mined in the Alberto open-pit	Li, Sn, P, Be
(9)	Qtz ab, Kfs Li-mica ms spd	mbs cst brl ap ±ecr	Biotite and chlorite zones	disconformable dyke-like internal zoning common thickness <15 m	not very abundant; layered internal structure common Li-bearing minerals	Li, Sn, P, Be (Rb, Cs)
(10)	Qtz ab Li-mica Kfs	ms cst mbs	Biotite and chlorite zones	disconformable dyke-like internal zoning common thickness < 3 m	layered internal struct. lepidolite abundant	Li, Sn, P, Be (Rb, Cs)
(11)	Qtz cst ab	ms Kfs ap	Chlorite zone	disconformable dyke-like, thickness < 50 cm locally with internal zoning	scarce, and folded with a reduction in the vertical length	Sn, K, (P)

Qtz-quartz; Kfs-K-feldspar; ms-muscovite; ab-albite; tur-tourmaline; and-andalusite; chl-chlorite; bt-biotite; grt-garnet; py-pyrite; pho-phosphates; mbs-montebrasite; spd-spodumene; cst-cassiterite; ap-apatite; brl-beryl; ecr-eucryptite

MINERAL GEOCHEMISTRY AND PETROGENESIS OF GRANITIC PEGMATITES IN THE FREGENEDA-ALMENDRA AREA (SPAIN AND PORTUGAL)

ROMEU VIEIRA[1§], ENCARNACIÓN RODA-ROBLES[2#], ALFONSO PESQUERA[2] & ALEXANDRE LIMA[3]

[1]Centro de Geologia da Universidade do Porto, Portugal; §romeu.vieira@fc.up.pt
[2]Dpto. Mineralogía y Petrología, Universidad del País Vasco/EHU, España; #encar.roda@ehu.es
[3]Dpto. Geologia, Ambiente e Ordenamento do Território, FCUP, Porto, Portugal

GEOLOGICAL SETTING & PEGMATITES DESCRIPTION

- The **Fregeneda-Almendra** pegmatitic field (FA) is located in the **Central-Iberian Zone**, in the western part of a narrow **metamorphic belt**, with an E-W trend (Figure 1).

- Bordered by the syn-tectonic Variscan **Mêda-Penedono-Lumbrales leucogranite complex (MPL)** to the south, and by the late-tectonic **Saucelle granite** to the NE (Figure 1);

- These granites and most of the pegmatites intruded the pre-Ordovician metasediments of the **Schist-Metagreywacke Complex (SMC)** (Figure 1).
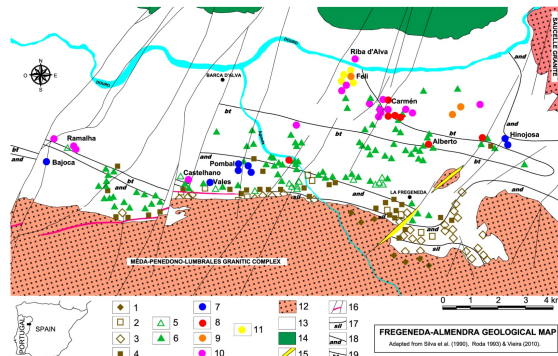

FIGURE 1. Distribution of the pegmatite types in the Fregeneda-Almendra area.
Legend: Group i) 1 – simple interior; 2 – quartz + andalusite conformable dykes; 3 – simple dykes and apophyses; 4 – simple conformable; Group ii) 5 – K-feldspar discordant dykes; 6 – simple discordant; Group iii) 7 – petalite-bearing discordant; 8 – spodumene-bearing discordant; 9 – Li-mica + spodumene discordant; 10 – Li-mica-bearing discordant; 11 – Sn-bearing discordant; 12 – syntectonic Variscan granites; 13 – Pre-Ordovician schist-metagreywacke complex; 14 – Ordovician formations; 15 – quartz segregations fractures; 16 – porphyry granitic/riolitic and faults; 17 – sillimanite isograd; 18 – andalusite isograd; 19 – biotite isograd.

- Most of the veins from the FA pegmatitic field correspond to the **less evolved** ones, grouped in two main groups: **(i) barren pegmatites** (types 1, 2, 3 and 4); and **(ii) intermediate discordant pegmatites** (Figure 1; Table 1);

- A **third group** of pegmatites (Figure 1; Table 1) represents ~10% of the aplite-pegmatite veins from the Fregeneda-Almendra. They are mainly rich in **Li-minerals** (types 7, 8, 9 and 10) and/or **cassiterite** (type 11);

- The main Li-bearing mineral assemblages are **petalite** (type 7), **spodumene** (type 8), *lepidolite* + **spodumene** (type 9), and *lepidolite* (type 10) (Table 1).

TABLE 1. Main characteristics of the types of pegmatites recognized in the Fregeneda-Almendra area.

Type	Mineralogy Main	Other	Morphology and structure	Remarks	Enrichment
(1)	Qtz, Kfs	Ms, Ab, Tur, Bt	Dyke-like; thickness < 50 cm	Scarce; within the MPL granite	K, Al, Si, (B, P)
(2)	Qtz, And	Ms, Tur, Kfs	Conformable dyke-like; thickness < 50 cm	Scarce; boudinage structures	Al, Si, (B, K)
(3)	Qtz, Kfs, Ms	Ab, Tur, Bt, Fe-Mn Pho	Irregular and bulbous masses; ellipsoidal or lenticular forms	More common to east; graphic texture	K, Al, Si, (B, P)
(4)	Qtz, Kfs, Ms, Ab	And, Tur, Grt, Bt	Conformable dyke-like locally with internal zonation; thick. < 1 m	Abundant; graphic texture	Al, Na, B
(5)	Kfs, Qtz	Ms, Py	Discordant dyke-like; thickness > 1m	Scarce; main component is pink Kfs	K
(6)	Qtz, Kfs, Ab, Ms	± Fe-Mn Pho, ± Mbs, ± Tur, Cst, CT	Discordant dyke-like; thickness < 10 cm to 2 m	Most abundant; internal zoning can be present	K, Na, Al, Si, (P, Li)
(7)	Qtz, Pet, Ab, Kfs	Ms, Cst, CT, ± Mbs, Fe-Mn Pho ± Ecr	Discordant dyke-like without internal zonation; thickness 5-30 m	Bajoca, Pombal and Hinojosa del Duero	Li, Sn, P
(8)	Qtz, Spd, Ab, Kfs	Ms, Mbs, Pet, Fe-Mn Pho	Discordant dyke-like without internal zonation; thickness 4-15 m	Alberto and Valdecoso	Li, P (Sn)
(9)	Qtz, Ab, Kfs, Li-mica, Ms, Spd	Mbs, Cst, CT, Ap, ± Ecr, Fe-Mn Pho	Discordant dyke-like; internal zoning common; thick. < 15 m	Feli	Li, Sn, P, F, (Rb, Cs)
(10)	Qtz, Ab, Li-mica, Kfs	Ms, Cst, CT, Mbs	Discordant dyke-like; internal zoning common; thick < 3 m	Cármen, Riba d'Alva and Ramalha	Li, Sn, P, F, (Rb, Cs)
(11)	Qtz, Cst, Ab	Ms, Kfs, CT, Ap	Discordant dyke-like; locally with internal zoning; thick < 50 cm	Only in the eastern part, Feli	Sn, K

Note: Qtz – quartz; Kfs – K-feldspar; Ms – muscovite; Ab – albite; Tur – Tourmaline; And – Andalusite; Chl – chlorite; Bt – biotite; Grt – garnet; Py – pyrite; Pho – phosphates; Mbs – montebrasite; Pet – petalite; Spd – spodumene; Cst – cassiterite; CT – Nb-Ta oxides; Ap – apatite; Ecr – eucryptite. MPL – Meda-Penedono-Lumbrales granitic complex.

GEOCHRONOLOGICAL DATA & PETROGENETIC MODELLING

- **Micas** from the muscovite-*lepidolite* series were separated from the different pegmatite types, as well as from the MPL granitic complex and from another granite detected by drills in the north of the area;

- These mica samples have been used to date their hosting rocks by the step-heating [40]Ar/[39]Ar method (Table 2.).

TABLE 2. [40]Ar*/[39]Ar isotopic data from the Fregeneda–Almendra pegmatite field. (M – MPL granite; F – Feli non-outcroping granite; Ms – muscovite; Ms-Li – lithium-muscovite).

Type	Mica	Plateau age (Ma)	J-value	MSWD	% [39]Ar released	Isochron (Ma)	([40]Ar/[36]Ar)i
M	Ms	311,2 ± 3,7	0,01547 @ 0,4%	0,08	84,40%	311,2 ± 1,7	344,4 ± 43,0
F	Ms	305,0 ± 3,3	0,01547 @ 0,4%	0,52	90,97%	306,3 ± 1,5	264,7 ± 16,0
1	Ms	303,7 ± 4,2	0,01517 @ 0,4%	0,42	90,08%	307,2 ± 6,1	383,4 ± 58,3
2	Ms	302,2 ± 3,6	0,01517 @ 0,4%	0,22	78,30%	302,8 ± 1,9	320,2 ± 56,4
3	Ms	300,0 ± 3,5	0,01517 @ 0,4%	0,40	74,62%	301,1 ± 2,6	308,3 ± 82,0
4	Ms	304,8 ± 4,7	0,01517 @ 0,4%	0,09	50,36%	305,4 ± 2,3	299,5 ± 18,8
6	Ms	303,8 ± 4,4	0,01517 @ 0,4%	0,06	67,06%	304,9 ± 1,8	305,2 ± 14,4
7	Ms	296,4 ± 3,5	0,01517 @ 0,4%	0,33	70,55%	297,0 ± 1,7	308,4 ± 31,6
8	Ms	303,6 ± 4,8	0,01517 @ 0,4%	0,08	81,13%	302,6 ± 2,6	353,6 ± 29,7
9	Ms-Li	295,3 ± 3,9	0,01517 @ 0,4%	0,39	88,99%	292,6 ± 2,4	449,1 ± 20,4
10	Ms-Li	295,1 ± 4,2	0,01517 @ 0,4%	0,34	100,00%	295,0 ± 2,9	307,1 ± 58,9
11	Ms	300,0 ± 3,1	0,01517 @ 0,4%	0,21	95,26%	301,3 ± 1,8	235,5 ± 26,6

- Values of **Li, Rb e Ba** from granites and SMC metasediments from the FA region (Table 3.) the **partial melting** of the SMC materials and subsequent **fractional crystallization** of the generated melts was modelled., using **Rayleigh equation** for fractional crystallization and **batch-melting equation** for partial melting (Figure 2.).
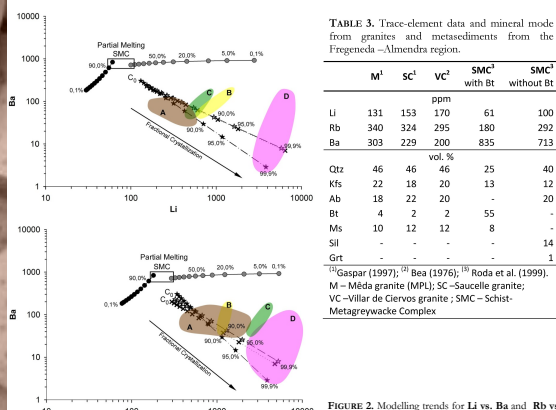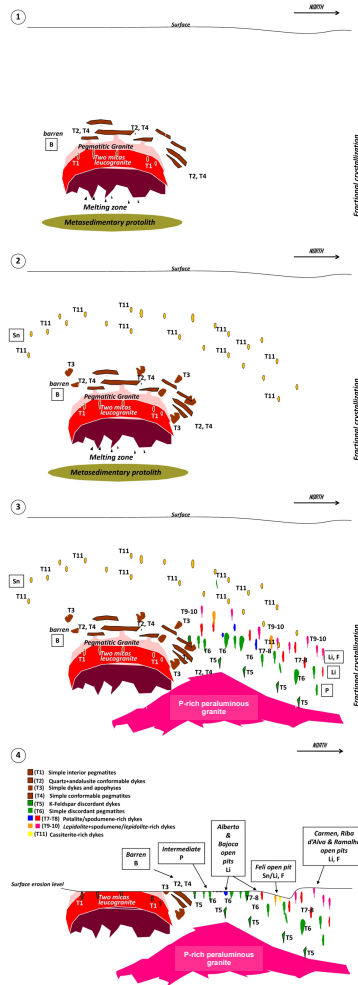

TABLE 3. Trace-element data and mineral mode from granites and metasediments from the Fregeneda –Almendra region.

	M[1]	SC[1]	VC[2]	SMC[3] with Bt	SMC[3] without Bt
			ppm		
Li	131	153	170	61	100
Rb	340	324	295	180	292
Ba	303	229	200	835	713
			vol. %		
Qtz	46	46	46	25	40
Kfs	22	18	22	13	12
Ab	18	22	20	-	20
Bt	4	2	2	55	-
Ms	10	12	12	8	-
Sil	-	-	-	-	14
Grt	-	-	-	-	1

[1]Gaspar (1997); [2] Bea (1976); [3] Roda et al. (1999). M – Mêda granite (MPL); SC –Saucelle granite; VC –Villar de Ciervos granite ; SMC – Schist-Metagreywacke Complex

FIGURE 2. Modelling trends for **Li vs. Ba** and **Rb vs. Ba** for the fractional crystallization of the granitic melts (dashed lines between granites) subsequent to the partial-melting of the SMC (filled lines between SMC). A, B, C and D is for the whole-rock pegmatite types compositions from the Fregeneda-Almendra pegmatite field (Table 3.).

Legend:
- ★ Mêda granite (MPL)
- ✦ Saucelle granite
- ● Villar de Ciervos granite
- ● SMC with biotite residuum
- ● SMC without biotite residuum
- ⬤ barren pegmatites
- ✶ cassiterite T11 veins
- ● intermediate pegmatites
- D Li-bearing pegmatites
- SMC - SMC average values

FIGURE 3. Fregeneda-Almendra model sequence for the metamorphic and magmatic events operating in the pegmatites formation.

- A **first event** of pegmatite formation would be related to the crystallization of the syn- to late-D_3 Variscan MPL granitic complex. **Lower rates of fractional crystallization**, from a melt with similar composition to the MPL, would originate the **T1** and **T3** pegmatites, whereas **higher degrees of fractional crystallization** would be related to the origin of the **Sn-rich dykes**. These bodies, with plateau ages ranging between 300,0±3,5 to 304,8±4,4 Myr, intruded S3 tectonic foliations (N100º-120°E) and are connected to the Variscan poly-harmonic folding and to the MPL emplacement.;

- **T2** and **T4** veins that outcrop in the proximities of the MPL (Alamo Complex) would be coetaneous or preceding this process;

- The **T6** and the **Li-rich pegmatites** represent highly differentiated melts. They infill late-tectonic Variscan structures (NNE-SSW and NE-SW), with plateau ages ranging from 295,1±4,2 to 296,4±3,5 Myr. Modeling demonstrate that these pegmatites would be related to **high rates (≥90%) of fractional crystallization** from melts with compositions analogous to the late- to post-D_3 Variscan granites (e.g., Saucelle or Villar de Ciervo granites). The difference of 10 Myr in the age between the late-D_3 Variscan granites and these pegmatites, exclude those granites as potential generators of the Li-rich pegmatites;

- Thus, the evolved pegmatites could be related to a late-Variscan (300 to 280 Myr) non-outcropping granite as a result of **high rates (≥ 90%) of fractional crystallization.**

Encuadre estructural del enjambre de diques pegmatíticos de La Fregeneda (Zona Centro Ibérica – España)

Structural outline of La Fregeneda pegmatite dyke swarm (Central Iberian Zone – Spain)

Dias da Silva, Í., González Clavijo, E. - Instituto Geológico y Minero de España
if.silva@igme.es

1. Situación Geológica

Esta zona es bastante conocida para la comunidad geológica especialmente por su interés Geominero , sino por las mineralizaciones de Li, Sn y fosfato asociadas al campo pegmatítico de La Fregeneda (figuras 1 y 5).

El área cubierta por los trabajos de campo se compone de las siguientes unidades litoestratigráficas (figura 1):

- Complejo Esquisto-Grauváquico (CEG) o Grupo del Duero – de edad Precámbrico – Cámbrico Inferior (Rebelo y Romano in Escuder, et al., 2000, Escuder, 1999);
- Granito de Lumbrales, pos-D2 varisco a sin-cizalla Juzbado-Penalva do Castelo (D3) (Villar, *et al.*, 2000);
- Granito de Saucelle, tardi-cinemático varisco (Villar, *et al.*, 2000);
- Pegmatitas y aplitas de La Fregeneda (Villar, *et al.*, 2000).

Figura 1 – A) Localización de la área en estudio en el Macizo Ibérico (Adaptado de Robardet, et al. 1990, Rodríguez-Alonso, 2004 y Peréz-Estaún, et al., 2004) con las principales subdivisiones e sus límites; B) Adaptación de las cartografías geológicas 1:50.000 del INETI-IGM (Portugal) y del IGME (MAGNA –España) actualizada con los datos de campo obtenidos en esta investigación.

1.1. La geometría del encajante

- Foliación Sn1 (S1 y/o S2) subhorizontal de plano axial, paralela a la estratificación, sintetizando plegamientos mayores tumbados y vergentes al NNE (Martín-Izard, *et al.* 1992);
- Lineación de estiramiento (Le) en Sn1, marcada por la biotita (figura 2C3) (inclinación y dirección medias: 15°/300°) indicando sentido de transporte hacia el SE;
- Sn1 afectada por D3 con pliegues de ejes subhorizontales de dirección NW-SE y una foliación de plano axial S3 (Sn2) subvertical. (figura 2C1, C2 y C3);
- Conjunto afectado por una red de fallas y fracturas N-S, NNE-SSW, WNW-ESE y ENE-WSW (figura 2B).

Figura 2 – Proyección estereográfica de las principales fabricas planares y filones medidos en La Fregeneda. A) – Principales filones pegmatíticos; B) – Principales direcciones de fallas medidas; C1 – Polos de las foliaciones (Sn1 y/o S2) y Sn2 (o S3); C3 – Lineaciones medidas en el CEG (Le – estiramiento; Li – intersección de Sn1 con Sn2). Se puede observar en A) que las orientaciones principales "filones" medidos corresponden a planos de foliaciones variscas y a direcciones de cizallas N-S hasta NE-SW.

1.2. Metamorfismo, magmatismo y tectónica

1- Metamorfismo regional varísco en la facies de la biotita sin Sn1;

2- Magmatismo tardío varísco y aureola de contacto con greisenización y crecimiento de andalucita en el encajante (Ferreira da Silva, 1994, Roda, *et al.*, 1996);

3- Intrusión del campo aplito-pegmatítico a lo largo de la estructura del encajante con grandes heterogeneidades composicionales y geométricas (Roda, *et al.*, 1996, Martín-Izard, *et al.* 1992) (figura 4A);

4- Deformación frágil a lo largo de fallas de dirección N-S hasta N50ºE, sub-verticales, con cinemática de desgarre dextra y senestra y movimientos verticales (normales y/o inversos) (Pereira, 2000), desplazando las intrusiones (figuras 1, 3 y 4).

2. Discusión

El modelo propuesto en las figuras 4A, B y C, para la geometría actual del campo pegmatítico de La Fregeneda (ver figura 1) es resultado de la superposición de los siguientes eventos tectono-magmáticos:

1 – Periodo de instalación de las pegmatitas en una estructura intensamente foliada, produciendo geometrías complejas con formas anastomosadas en los filones de poco espesor y formas masivas en las intrusiones de mayor volumen (figuras 3 y 4a) con heterogeneidades mineralógicas y geoquímicas (Roda, *et al.*, 1996, Martín-Izard, *et al.* 1992, Ferreira da Silva, 1994);

2 – Desplazamiento vertical y por desgarre de las intrusiones a lo largo de fallas activas durante el periodo tardi y post Varísco, acompañado de intensa fraturación y argilización. Debido a la complejidad cinemática observada en los planos de falla (estrías horizontales y verticales superpuestas) no fue posible definir la cronología de sus periodos de desgarre y levantamiento (figuras 4B y C).
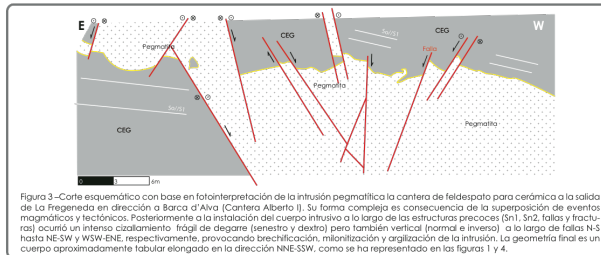

Figura 3 –Corte esquemático con base en fotointerpretación de la intrusión pegmatítica la cantera de feldespato para cerámica a la salida de La Fregeneda en dirección a Barca d'Alva (Cantera Alberto I). Su forma compleja es consecuencia de la superposición de eventos magmáticos y tectónico. Posteriormente a la instalación del cuerpo intrusivo a lo largo de las estructuras precoces (Sn1, Sn2, fallas y fracturas) ocurrió un intenso cizallamiento frágil de desgarre (senestro y dextro) pero también vertical (normal e inverso) a lo largo de fallas N-S hasta NE-SW y WSW-ENE, respectivamente, provocando brechificación, milonitización y argilización de la intrusión. La geometría final es un cuerpo aproximadamente tabular elongado en la dirección NNE-SSW, como se ha representado en las figuras 1 y 4.
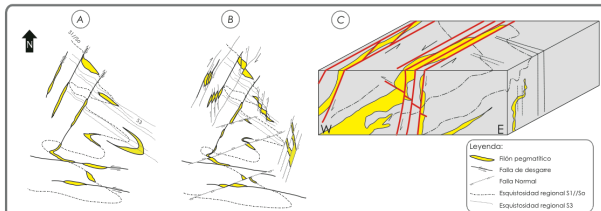

Figura 4 – Modelo esquemático para la geometría final del campo "filoniano" de La Fregeneda. A) – Instalación de intrusiones pegmatíticas a lo largo de las principales discontinuidades existentes como la Sn1 (So//S1 o S2?), la S3 (Sn2), fallas y fracturas de dirección N-S, NW-SE y WNW-ESE; B) – Cizallas frágiles (aquí representadas como dextras) que reactivan las estructuras precoces con tectónica frágil de graben y horst (WSW-ENE) generando el alineamiento de las intrusiones con el patrón observable cartográficamente; C) Bloque diagrama interpretativo de las estructuras observadas en planta y corte, con a representación de algunas fallas senestras. Es una representación simplificada de las geometrías observadas en el enjambre de díques pegmatíticos. Localmente se pueden superponer varias de las relaciones entre fallas representadas.

3. Aspectos relevantes

Figura 5 – Minerales económicos presentes en el campo pegmatítico de La Fregeneda. A) – Lepidolita y cuarzo; B) – Casiterita con sericita y cuarzo de la Mina Feli; C) Apatito azul con cuarzo y sericita presentes en la cantera de feldespato Alberto I (salida de La Fregeneda, dirección a Barca d'Alva).

Figura 6 – Cizallas frágiles de dirección NNE-SSW. A) y B) – Falla del filón mayor de la Mina Feli, con diversos criterios cinemáticos (1º siniestra, 2º normal); C) Falla y respectiva brecha con intensa argilización de la pegmatita. Las flechas blancas indican el movimiento observado en las estrías.
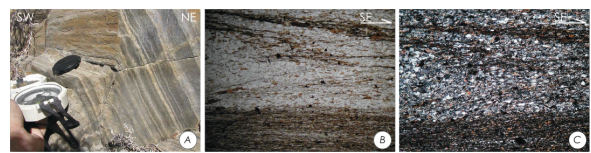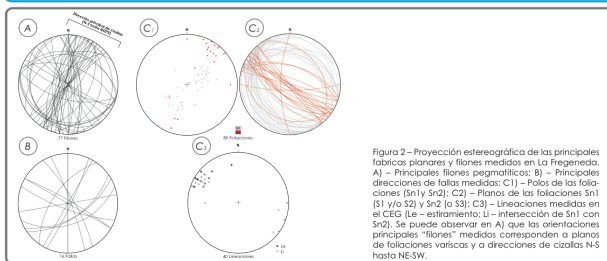

Figura 7 – Fabrica planar Sn1 (So//S1?), A) – Aspecto de Sn1 en una exposición del CEG en bajo a medio grado metamórfico; B) – Lámina delgada de la esquistosidad Sn1 realizada a lo largo de la lineación de estiramiento, mostrando una foliación oblicua a la foliación principal, indicando cinemática del techo para el SE; C) - Misma lámina que B) pero con los polarizadores cruzados, mostrando la asociación mineralógica típica con cuarzo, moscovita, biotita, clorita, cloritóide y opacos. La clorita es el cloritóide son posteriores al pico metamórfico que ha producido la asociación mineralógica de facies de la biotita, mostrando retrogradación de la misma durante el periodo de enfriamiento de los granitos tardivariscos (sin-3ª fase) (Ferreira da Silva, 1994).

Bibliografía

Escuder Viruete, J. Rodríguez Fernández, L.R., Medavilla, R., Díez Montes, A., Bellido, F., Rubio Pascual, F.J., Martín Romera, C., Carrasco, R., González Clavijo, E., Ortega, C., García del Amo, D., Reguero, M., (2000): "Mapa y Memoria explicativa de la Hoja Nº 448/9 (Vilvestre) del Mapa Geológico de España a la escala 1:50.000". ITGE. Madrid;

Escuder Viruete, J. (1999): "Evolución tectonotermal del Domo Gneisico del Tormes, Salamanca, NO del Macizo Ibérico". Lab. Xeol. de Laxe – Serie Terra Nova Nº15. 38pp., Coruña;

Ferreira da Silva, A., Ribeiro, M.L., (1994): "Mapa y Noticia Explicativa da Folha 15-B (Paiso de España 6 Cinta) da Carta geológica de Portugal à escala 1:50.000". IGM. Lisboa;

Peréz-Estaún A., Bea, F., Bastida, F., Marcos, A., Martínez Poyatos, D., Arenas, R., Díaz García, F., Azor, A., Simancas, J.F., González Lodeiro, F. (2004): "La Cordillera Varisca Europea: El Macizo Ibérico" En: "Geología de España (J.A. Vera, Ed.), SGE-IGME. 22-24. Madrid;

Martín-Izard, A., Reguilón, R., Palero, F., (1992): "Las mineralizaciones litríferas del oeste de Salamanca y Zamora". Estudios geológicos, 48: 19-30;

Pereira, E. (coord.) (2006): "Noticia Explicativa da Folha 2 da Carta Geológica de Portugal à escala 1:200.000". INETI. Lisboa

Robardet, M., Gutierez Marco, J.C., (1990): "Sedimentary and faunal domains in the Iberian Peninsula during Lower Paleozoic times" En: "Pre-Mesozoic Geology of Iberia" (Dallmayer, R.D., Martínez García, E., Eds.), Springer-Verlag Berlin Heidelberg: 383-393;

Roda, E., Fontan, F., Pesquiera, A., Velasco, F., (1996): "The phosphate mineral association of the granitic pegmatites of the Fregeneda area (Salamanca, Spain)". Mineralogical Magazine, Vol. 60: 767-778.

Rodríguez-Alonso, M.D., Peinado, M., López-Plaza, M., Franco, P., Carnicero, A., Gonzalo, J.C. (2004): "Neoproterozoic-Cambrian synsedimentary magmatism in the Central Iberian Zone (Spain): geology, petrology and geodynamic significance". International Jour. Earth Sci. (Geol. Rundsch) 93:897-920

Villar, P., Mediavilla, R., Fernández, J., Gallastegui, G., Martín Parra, L., Rubio Pascual, F.J., Bellido, F., Sanz Santos, M.A., González Fernández, L.R., R., González Ramón, A., Rubio Campos, J.C. González Clavijo, E., Ortega, C., Lombardero, M., García del Amo, D. (2000): "Mapa y Memoria explicativa de la Hoja Nº 474/5 (Lumbrales) del Mapa Geológico de España a la escala 1:50.000". ITGE. Madrid.

Chemical variation and significance of micas from the Fregeneda-Almendra pegmatitic field (Central-Iberian Zone, Spain and Portugal)

ROMEU VIEIRA,[1,*] ENCARNACIÓN RODA-ROBLES,[2,†] ALFONSO PESQUERA,[2] AND ALEXANDRE LIMA[1]

[1]Center of Geology, University of Porto, DGAOT, FCUP, Rua do Campo Alegre, 687, 4169-007 Porto, Portugal
[2]Departamento de Mineralogia y Petrologia, Universidad del Pais Vasco/EHU, Apdo. 644, 48080 Bilbao, Spain

ABSTRACT

Field, textural, paragenetic, and chemical data for micas from pegmatites of the Fregeneda-Almendra pegmatitic field (Central-Iberian Zone) are used to characterize and evaluate their petrogenesis. These pegmatites show a zonal distribution from barren to evolved, with an increase in degree of evolution with increasing distance from the Mêda-Penedono-Lumbrales leucogranite. Five types of evolved pegmatites have been recognized: (1) petalite-rich, (2) spodumene-rich, (3) Li-mica + spodumene-rich, (4) Li-mica-rich, and (5) cassiterite-rich pegmatites, plus six types of barren and intermediate pegmatites. Representative micas from the different pegmatite types and from the leucogranite were analyzed for major and trace elements. All micas belong to the muscovite-*lepidolite* series. Lithium is incorporated into Li-micas via the $Li_3Al_{-1}\square_{-2}$ and Si_2LiAl_{-3} substitutions, where $\square$ represents vacancies. The $Al_4Si_{-3}\square_{-1}$ and $Al_2\square_1R^{2+}_{-3}$ substitutions, where R^{2+} = (Fe + Mg + Mn), account for the compositional variability of micas from the Li-mica-free pegmatites. The Li, Rb, Cs, Be, Ta, and Nb contents of micas increase in the order: leucogranites and barren pegmatites < intermediate pegmatites < spodumene-bearing and petalite-bearing dikes < Li-mica-bearing pegmatites. The Ba content decreases in the same order, and Sn and Zn are relatively abundant in the intermediate pegmatites. These variations are consistent with rare-element enrichment via fractionation processes combined with partitioning of rare elements from the pegmatite melt into the minerals and volatile phases. However, some pegmatite types occurring in this area, such as the cassiterite-rich dikes, do not seem to form part of the same evolutionary trend.

Keywords: Micas, pegmatites, compositional variations, petrologic implications, degree of evolution, Fregeneda-Almendra area

INTRODUCTION

In the Fregeneda-Almendra area (FA) (Salamanca, Spain, and Guarda, Portugal), 11 pegmatite types have been recognized. They show a zonal distribution northward from the Mêda-Penedono-Lumbrales granitic complex (MPL). Less evolved dikes occur inside or close to the contact of the granite, and the content in lithophile elements increases northward with increased distance from the granite. In the northernmost part of the field, Li- and/or Sn-rich pegmatites are common (petalite-rich, spodumene-rich, Li-mica + spodumene-rich, Li-mica-rich, and cassiterite-rich) (Roda 1993; Roda et al. 1999; Vieira 2010). The evolution observed in the FA field with increased distance from the MPL granite is mineralogical, textural, and compositional. All rock-forming minerals of these pegmatites reflect clearly this evolution, which is especially apparent in mica, ubiquitous minerals in all the pegmatites from the FA field. Physical properties, chemical composition, and paragenetic relations of micas

have been frequently used to establish the degree of evolution and crystallization conditions of pegmatites (e.g., Černý and Burt 1984; Foord et al. 1995; Wise 1995; Jolliff et al. 1987, 1992; Henderson et al. 1989; Roda et al. 1995, 2006, 2007a; Kile and Foord 1998; Brigatti et al. 2000).

This paper is concerned with micas from the different pegmatite types in the FA field. This field is a good example to better understand the chemical, paragenetic, and textural evolution of micas during pegmatitic crystallization in zoned pegmatitic fields. We focus on the paragenetic and textural relations, and chemical composition in relation to pegmatite petrogenesis. We also propose an order of crystallization for the different pegmatite types in the area.

GEOLOGICAL SETTING AND GENERAL GEOLOGY OF THE PEGMATITES

The FA area represents a typical section of the metamorphic Variscan basement in the Central-Iberian Zone, which is located in the western part of a narrow EW trending belt (Fig. 1). It consists largely of psammopelites, with abundant intercalations of quartzites, conglomerates and, less frequently, amphibolites and calc-silicate rocks from the pre-Ordovician Schist-Greywacke Complex

---

* Present address: DGAOT, FCUP, Rua do Campo Alegre, 687, 4169-007 Porto, Portugal. E-mail: romeu.vieira@fc.up.pt
† E-mail: encar.roda@ehu.es
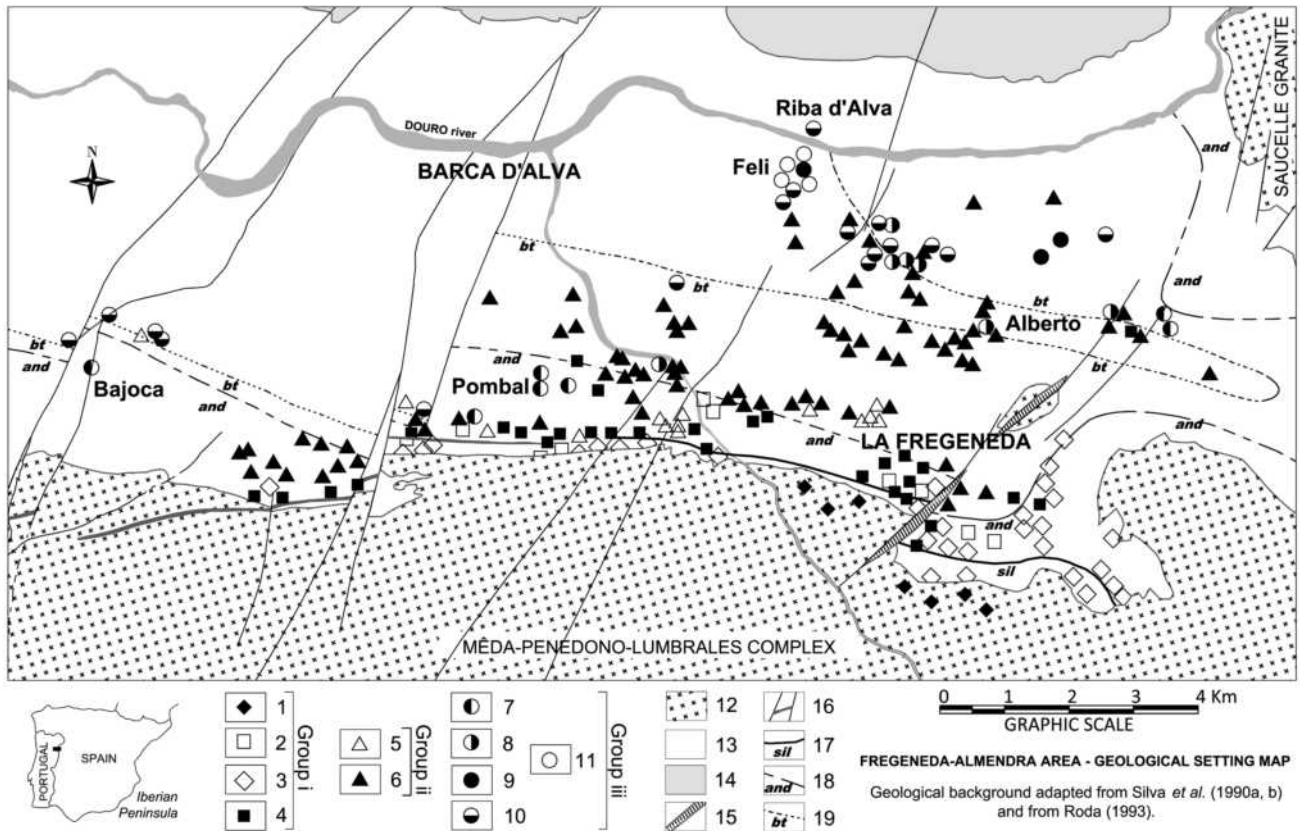
FIGURE 1. Distribution of the pegmatite types in the Fregeneda-Almendra area. Group i legend: 1 = simple interior; 2 = quartz + andalusite conformable dikes; 3 = simple dikes and apophyses; 4 = simple conformable. Group ii legend: 5 = K-feldspar discordant dikes; 6 = simple discordant. Group iii legend: 7 = petalite-bearing discordant; 8 = spodumene-bearing discordant; 9 = Li-mica + spodumene-bearing discordant; 10 = Li-mica-bearing discordant; 11 = Sn-bearing discordant; 12 = syntectonic Variscan granites; 13 = Pre-Ordovician Schist-Greywacke complex; 14 = Ordovician formations; 15 = quartz segregations fractures; 16 = porphyry granite/rhyolite and faults; 17 = sillimanite isograd; 18 = andalusite isograd; 19 = biotite isograd.

TABLE 1. Main characteristics of the types of pegmatites recognized in the Fregeneda-Almendra area

Type	Mineralogy		Host rock metamorphism	Morphology and structure	Remarks	Enrichment
	Main	Other				
(1)	Qtz, Kfs	Ms, Ab, Tur, Bt	(Intragranitic)	Dike-like; thickness < 50 cm	Scarce; within the MPL granite	K, Al, Si, (B, P)
(2)	Qtz, And	Ms, Tur, Kfs	Andalusite zone	Conformable dike-like; thickness < 50 cm	Scarce; boudinage structures	Al, Si, (B, K)
(3)	Qtz, Kfs, Ms	Ab, Tur, Bt, Fe-Mn Pho	Sillimanite, andalusite and biotite zones	Irregular and bulbous masses; ellipsoidal or lenticular forms	More common to the east; graphic texture	K, Al, Si, (B, P)
(4)	Qtz, Kfs, Ms, Ab	And, Tur, Grt, Bt	Sillimanite and andalusite zones	Conformable dike-like locally with internal zonation; thick. < 1 m	Abundant; graphic texture	Al, Na, B
(5)	Kfs, Qtz	Ms, Py	Biotite zone	Discordant dike-like; thickness > 1m	Scarce; main component is pink Kfs	K
(6)	Qtz, Kfs, Ab, Ms	± Fe-Mn Pho, ± Mbs, ± Tur, Cst, CT	Biotite and chlorite zones	Discordant dike-like; thickness < 10 cm to 2 m	Most abundant; internal zoning can be present	K, Na, Al, Si, (P, Li)
(7)	Qtz, Pet, Ab, Kfs	Ms, Cst, CT, ± Mbs, Fe-Mn Pho ± Ecr	Sillimanite, andalusite and andal./biotite limit	Discordant dike-like without internal zonation; thickness 5–30 m	Bajoca, Pombal and Hinojosa del Duero	Li, Sn, P
(8)	Qtz, Spd, Ab, Kfs	Ms, Mbs, Pet, Fe-Mn Pho	Biotite/chlorite limit zone	Discordant dike-like without internal zonation; thickness 4–15 m	Alberto and Valdecoso	Li, P (Sn)
(9)	Qtz, Ab, Kfs, Li-mica, Ms, Spd	Mbs, Cst, CT, Ap, ± Ecr, Fe-Mn Pho	Biotite and chlorite zones	Discordant dike-like; internal zoning common; thick. < 15 m	Feli	Li, Sn, P, F, (Rb, Cs)
(10)	Qtz, Ab, Li-mica, Kfs	Ms, Cst, CT, Mbs	Biotite and chlorite zones	Discordant dike-like; internal zoning common; thick. < 3 m	Cármen, Riba d'Alva and Ramalha	Li, Sn, P, F, (Rb, Cs)
(11)	Qtz, Cst, Ab	Ab, Ms, Kfs, CT, Ap	Chlorite zone	Discordant dike-like; locally with internal zonation; thick. < 50 cm	Only in the eastern part, Feli	Sn, K

Notes: Qtz = quartz; Kfs = K-feldspar; Ms = muscovite; Ab = albite; Tur = Tourmaline; And = Andalusite; Chl = chlorite; Bt = biotite; Grt = garnet; Py = pyrite; Pho = phosphates; Mbs = montebrasite; Pet = petalite; Spd = spodumene; Cst = cassiterite; CT = Nb-Ta oxides; Ap = apatite; Ecr = eucryptite. MPL = Mêda-Penedono-Lumbrales granitic complex.

(SGC). This belt is bordered by the Variscan MPL granitic complex to the south and by the Saucelle granite to the northeast (Fig. 1). Both granites and most of the pegmatites intrude the SGC.

Deformation and metamorphism

Overall, the rocks from the FA area record a Variscan polyphasic deformation accompanied by regional metamorphism. The earliest phase—D_1—produced WNW-ESE polyharmonic folds with subhorizontal axes and a subvertical axial-planar foliation. This initial folding gave rise to an important set of sinistral ductile shear faults along WNW-ESE strike. The second phase is characterized by the development of a subhorizontal penetrative foliation. It has been related to ductile-shearing processes of extensional origin that account for the mylonitic foliation in the granitic rocks. D_3 was a discontinuous, localized deformation that produced open to tight folds with NW-SE to EW trending axes, characterized by a crenulation superimposed on the previous foliation (Silva and Ribeiro 1991, 1994; Ábalos et al. 2002). Finally, a late deformation gave rise to ductile-brittle Variscan sinistral shears (NNE-SSW to NE-SW).

During D_1 the rocks underwent a prograde metamorphism with the development of a metamorphic sequence typical of >4 kbar at temperatures of ≈ 600–700 °C followed by a nearly isothermal decompression during D_2 that led to low-pressure conditions (≈2 kbar) recorded by the stability of andalusite (Ábalos et al. 2002). In the FA area, the metamorphic grade increases toward the MPL leucogranite contact, locally reaching the sillimanite zone (Fig. 1).

Granites and pegmatites

The granitic rocks of the Central-Iberian Zone may be classified according to their relation to Variscan deformation, and two main groups can be distinguished: (1) pre- to syntectonic intrusions; and (2) late- to post-tectonic intrusions. The MPL and Saucelle granites are two-mica, peraluminous granites belonging to the first group of syntectonic intrusions.

Most of the pegmatites from the FA field are poorly evolved and fall into two main categories (Table 1; Fig. 1) (Roda et al. 2007b; Vieira 2010): (1) barren pegmatites that consist of quartz, K-feldspar > albite, muscovite, tourmaline ± andalusite ± garnet, (types 1, 2, 3, and 4); and (2) intermediate-discordant pegmatites (types 5 and 6), the latter characterized by the occurrence of Fe-Mn phosphates, montebrasite, and both micas and feldspars with higher Rb and Cs contents than those of the barren pegmatites (Roda et al. 1999). A third category of pegmatites, although less abundant, is common; it comprises fertile discordant pegmatites, mainly enriched in Li-minerals (types 7, 8, 9, and 10) and/or cassiterite (type 11). Except for the pegmatites belonging to type 3, whose shapes are quite variable, ranging from irregular and bulbous masses to ellipsoidal, lens-like, or turnip-shaped forms, the rest of the pegmatitic bodies in the FA field are clearly dike-like. It is noteworthy that pegmatites from the first category are intragranitic (types 1 and 3), as well as conformable to the host rocks, occurring near the contact with the granite (types 2 and 4). Conversely, pegmatites from categories 2 and 3 are clearly discordant, showing similar strike, close to N010-030°E, and close to vertical. These pegmatites occur further north from the contact of the MPL granite (Fig. 1). They are fracture infillings

generated during a late Variscan tectonic event. Some of the conformable barren pegmatites are affected by these fractures (López Plaza et al. 1982). Therefore, we can assume that the barren pegmatites are older than the discordant pegmatites. The main Li-bearing mineral assemblages in the Li-rich pegmatites include petalite (type 7), spodumene (type 8), Li-mica + spodumene (type 9), and Li-mica (type 10). It is remarkable that the Sn-rich dikes (type 11) are folded and crosscut by one Li-mica + spodumene dike (type 9) at the Feli open pit, in the northernmost part of the field (Fig. 1).

OCCURRENCE AND TEXTURES

Most of the micas occurring in the pegmatites from the FA field belong to the muscovite-*lepidolite* series, with the exception of *biotite* in a few barren pegmatite bodies (types 3 and 4) and some very fine-grained, secondary *zinnwaldite* crystals in the Bajoca open pit (type 7). Muscovite is widespread in all pegmatite types, either in the contact zones or in the internal zones. Normally, crystals are variable in size, up to 4 cm—book-like, flakes, and laths—of silvery colors. Fine aggregates of greenish muscovite, locally replacing pre-existing minerals, e.g., feldspars or Li-aluminosilicates, are also common, but are not considered here. The cassiterite-rich pegmatites (type 11) contain small flakes (<1 cm) of a white-yellowish muscovite. Lithium-mica occurs exclusively in two of the 11 pegmatite types (types 9 and 10), which are particularly enriched in Li and F. This type of pegmatite is characterized by a layering consisting of a sequence in which Li-mica + quartz-rich layers alternate with albite + K-feldspar-rich layers. Li-mica has a typical lilac color, occurring as prismatic or wedge-shaped crystals (≈1 cm) or as fine saccharoidal aggregates with quartz and feldspar. The micas are optically homogeneous, even the biggest crystals.

TABLE 2. Representative mica compositions (major, minor, and trace elements) of the different pegmatite types from the Fregeneda-Almendra field

Type	Granite	T1	T2	T3	T4	T6	T7	T8	T9
Sample	Mêda-9	10-6	136-6	269-5	clall-2	252-2	11-34	ma-8	fr-4
Mica type	Ms	Ms	Ms	Ms	Ms	Ms	Ms	Ms	Li-ms
					(wt%)				
SiO$_2$	45.26 ± 0.22	45.15 ± 0.22	45.50 ± 0.22	45.99 ± 0.23	45.82 ± 0.22	45.81 ± 0.22	44.53 ± 0.33	45.73 ± 0.61	47.19 ± 0.23
TiO$_2$	0.39 ± 0.04	0.21 ± 0.04	0.17 ± 0.04	0.14 ± 0.04	0.20 ± 0.04	b.d.	0.06 ± 0.02	b.d.	b.d.
Al$_2$O$_3$	34.72 ± 0.16	35.17 ± 0.16	35.52 ± 0.16	35.56 ± 0.16	35.37 ± 0.16	36.47 ± 0.16	37.15 ± 0.44	36.81 ± 0.47	30.63 ± 0.15
FeO	1.57 ± 0.12	1.86 ± 0.13	0.86 ± 0.09	1.52 ± 0.12	1.20 ± 0.10	1.03 ± 0.11	0.71 ± 0.10	0.62 ± 0.16	0.30 ± 0.07
MnO	b.d.	b.d.	b.d.	b.d.	b.d.	b.d.	b.d.	b.d.	0.28 ± 0.08
MgO	0.78 ± 0.03	0.43 ± 0.02	0.64 ± 0.02	0.51 ± 0.02	0.48 ± 0.02	0.07 ± 0.01	b.d.	b.d.	b.d.
ZnO	b.d.	0.10 ± 0.08	b.d.	b.d.	b.d.	b.d.	b.d.	b.d.	b.d.
CaO	b.d.	b.d.	0.02 ± 0.01	b.d.	b.d.	b.d.	b.d.	b.d.	b.d.
Li$_2$O*	0.05	0.15	0	0.19	0.19	0	0.09	0.04	2.1
Na$_2$O	0.56 ± 0.03	0.72 ± 0.02	1.11 ± 0.04	0.60 ± 0.03	0.85 ± 0.03	0.39 ± 0.03	0.33 ± 0.06	0.55 ± 0.07	0.19 ± 0.02
K$_2$O	10.30 ± 0.14	9.73 ± 0.14	9.08 ± 0.13	10.09 ± 0.14	9.57 ± 0.14	10.26 ± 0.14	10.61 ± 0.35	10.44 ± 0.30	9.80 ± 0.14
BaO	0.09 ± 0.03	0.09 ± 0.03	0.18 ± 0.03	0.11 ± 0.03	0.04 ± 0.03	b.d.	b.d.	n.a.	0.06 ± 0.03
Rb$_2$O	b.d.	b.d.	b.d.	b.d.	b.d.	b.d.	0.34 ± 0.06	0.11 ± 0.09	0.51 ± 0.07
Cs$_2$O	b.d.	b.d.	b.d.	b.d.	b.d.	0.09 ± 0.04	b.d.	b.d.	0.21 ± 0.05
F	0.31 ± 0.04	0.50 ± 0.04	b.d.	0.58 ± 0.04	0.58 ± 0.04	0.15 ± 0.04	0.38 ± 0.09	0.30 ± 0.25	4.12 ± 0.08
O=F	0.13	0.21	0	0.24	0.24	0.06	0.16	0.13	1.73
H$_2$O*	4.27	4.19	4.43	4.21	4.18	4.4	4.25	4.34	2.41
Total*	98.17	98.09	97.51	99.26	98.24	98.61	98.29	98.84	96.06
			Structural formulas on the basis of 24 (O, OH, F) atoms						
Si	6.139	6.12	6.153	6.149	6.164	6.145	6.018	6.12	6.493
^{IV}Al	1.861	1.88	1.847	1.851	1.836	1.855	1.982	1.88	1.507
(Z)	8	8	8	8	8	8	8	8	8
^{VI}Al	3.689	3.739	3.815	3.753	3.773	3.91	3.935	3.926	3.459
Ti	0.04	0.021	0.017	0.014	0.02	0	0.006	0	0
Fe^{2+}	0.178	0.211	0.097	0.17	0.135	0.115	0.08	0.069	0.035
Mn	0	0	0	0	0	0	0	0	0.033
Mg	0.157	0.087	0.128	0.101	0.097	0.015	0	0	0
Li	0.026	0.081	0	0.104	0.104	0	0.046	0.023	1.161
Zn	0	0.01	0	0	0	0	0	0.003	0
(Y)	4.09	4.149	4.058	4.142	4.128	4.041	4.067	4.021	4.688
Ca	0	0	0.003	0	0	0	0	0	0
Na	0.146	0.189	0.292	0.156	0.222	0.102	0.087	0.142	0.049
K	1.782	1.683	1.567	1.721	1.642	1.756	1.829	1.783	1.72
Rb	0	0	0	0	0	0	0.03	0.009	0.045
Cs	0	0	0	0	0	0.005	0	0	0.012
(X)	1.928	1.872	1.861	1.877	1.865	1.863	1.946	1.934	1.827
F	0.135	0.214	0	0.246	0.246	0.062	0.163	0.128	1.793
OH	3.866	3.786	4	3.754	3.754	3.939	3.835	3.872	2.207

Notes: b.d. = below detection limit. n.a. = not analyzed.
* Calculated.

ANALYTICAL RESULTS

In general, the micas show compositional differences with pegmatite type for major, minor, and trace elements (Tables 2 and 3; Figs. 2, 3, and 4). As shown in Figure 2a with [(Fe + Mn + Ti) − ^{VI}Al] vs. (Mg − Li) (Tischendorf et al. 1997), the compositions of the micas from Li-mica + spodumene-rich pegmatites (type 9) and Li-mica-rich pegmatites (type 10) define a trend from the muscovite end-member toward Li-muscovite, frequently quite close to the trilithionite end-member. The rest of micas associated with the other pegmatite types and granite plot around muscovite (Table 2; Fig. 2). On average, muscovite shows a clear cation-deficiency at the interlayer site Σ(Ca + Na + K + Rb + Cs), especially for micas from the granite (1.82 to 1.93 apfu) and pegmatite types 1 to 4 (1.77 to 1.96 apfu) (Table 2). The octahedral site-occupancy for muscovite associated with the granite, barren (type 1 to type 4), intermediate (type 6), petalite (type 7), and spodumene (type 8) pegmatites varies from 4.055 to 4.148 apfu, close to the 4.0 apfu of ideal dioctahedral muscovite. The micas from type 9 (Li-mica + spodumene) and type 10 (Li-mica) pegmatites show the highest octahedral site-occupancies, with muscovite showing average values of 4.289 apfu, indicative of a mixed-layer structure (Foord et al. 1995). Lithium-muscovite, exclusive of type 9 and 10 pegmatites, has

octahedral site occupancies between dioctahedral (4.518 apfu) and trioctahedral values (5.494 apfu). When compared to muscovite from other FA pegmatite types and the granite, the muscovite from the pegmatite types 9 and 10 show the highest content of Li$_2$O [<1.83 wt% (av. 0.86) n = 43], F [<3.63 wt% (av. 1.82) n = 43], Rb$_2$O [<0.99 wt% (av. 0.38) n = 43], and Cs$_2$O [<0.65 wt% (av. 0.12) n = 43] and the lowest content of Al$_2$O$_3$ [>30.74 wt% (av. 34.20) n = 43]. Moreover, Li-muscovite from these pegmatite types (9 and 10) shows enrichment in Li$_2$O and F [av. 2.67 and 5.17 wt% (n = 50), respectively], reaching a maximum of 4.74 wt% (Li$_2$O) and 9.02 wt% (F) close to trilithionite. Li-muscovite is also characterized by the highest contents in MnO (0.75 wt%), Rb$_2$O (1.40 wt%) and Cs$_2$O (0.82 wt%).

The K/Rb ratio for micas (Fig. 3, Table 3) decreases from the MPL granite and the barren pegmatites (types 1, 2, 3, and 4) (49 to 147) through the intermediate pegmatites (type 6) (48), the petalite-rich (type 7), and the spodumene-rich pegmatites (type 8) (39 and 33, respectively). The lowest K/Rb values are found in the Li-mica + spodumene-rich (type 9) and the Li-mica-rich (type 10) pegmatites (12 and 8, respectively). In Figure 3, an enrichment in Li (14 681 and 14 774 ppm), Rb (7075 and 10 388 ppm), Cs (1375 and 1891 ppm), Be (64 and 38 ppm), and Tl (43 and 53 ppm) is observed for Li-muscovite of types 9 and 10,

TABLE 2.—_EXTENDED_

Type	T9	T10	T10	T11
Sample	fr-6	89-3	89-5	ala-1
Mica type	Li-ms	Li-ms	Li-ms	Ms
(wt%)				
SiO_2	48.97 ± 0.23	49.46 ± 0.64	51.80 ± 0.64	45.65 ± 0.33
TiO_2	0.06 ± 0.04	b.d.	b.d.	0.06 ± 0.03
Al_2O_3	29.11 ± 0.15	27.44 ± 0.42	23.64 ± 0.42	36.12 ± 0.25
FeO	b.d.	b.d.	b.d.	1.38 ± 0.11
MnO	0.37 ± 0.07	0.13 ± 0.11	0.14 ± 0.11	b.d.
MgO	0.05 ± 0.01	b.d.	b.d.	0.16 ± 0.02
ZnO	b.d.	b.d.	b.d.	b.d.
CaO	b.d.	b.d.	b.d.	b.d.
Li_2O*	2.57	3.38	4.74	0.11
Na_2O	0.17 ± 0.02	0.35 ± 0.07	0.29 ± 0.07	0.42 ± 0.04
K_2O	10.07 ± 0.15	10.01 ± 0.29	9.83 ± 0.29	11.12 ± 0.20
BaO	0.09 ± 0.03	b.d.	b.d.	n.a.
Rb_2O	0.61 ± 0.07	1.30 ± 0.21	1.36 ± 0.21	0.21 ± 0.12
Cs_2O	0.18 ± 0.05	0.53 ± 0.16	0.62 ± 0.16	b.d.
F	4.99 ± 0.09	6.50 ± 0.95	9.02 ± 0.95	0.42 ± 0.24
O=F	2.1	2.74	3.8	0.18
H_2O*	2.05	1.32	0.15	4.28
Total*	97.12	97.82	97.88	99.79
Structural formulas on the basis of 24 (O, OH, F) atoms				
Si	6.658	6.73	7.024	6.107
^{IV}Al	1.342	1.27	0.976	1.893
(Z)	8	8	8	8
^{VI}Al	3.322	3.129	2.801	3.802
Ti	0.006	0	0	0.006
Fe^{2+}	0	0.004	0.009	0.154
Mn	0.043	0.015	0.016	0.003
Mg	0	0	0	0.032
Li	1.404	1.851	2.583	0.057
Zn	0	0.009	0	0
(Y)	4.775	5.009	5.41	4.055
Ca	0	0	0.004	0
Na	0.044	0.093	0.077	0.109
K	1.747	1.738	1.701	1.898
Rb	0.053	0.114	0.118	0.018
Cs	0.01	0.031	0.036	0.001
(X)	1.854	1.975	1.935	2.025
F	2.146	2.799	3.866	0.178
OH	1.855	1.201	0.134	3.822

Notes: b.d. = below detection limit. n.a. = not analyzed.
* Calculated.

respectively. On the other hand, Ba shows a negative correlation with the K/Rb ratio, with the higher values (1614 ppm) in the quartz-andalusite type 2 veins.

The highest values in Sn (896 ppm) occur in muscovites from the cassiterite-bearing pegmatites (type 11). Enrichment in Sn is found from the MPL granite (175 ppm) to the intermediate type 6 pegmatites (669 ppm) and petalite and spodumene-bearing pegmatite types (508 and 730, respectively).

Micas from the different pegmatite types and the MPL granite are depleted in REE (Table 3), with values for ΣLREE ranging from 0.37 to 12.13 for the pegmatites and to 31.34 ppm for the granite, whereas the content in heavy rare earth elements is much lower, with ΣHREE ranging from 0.04 to 1.29 for the pegmatites, and to 3.72 ppm for the granite. The REE pattern is characterized by a relative enrichment in LREE, the $(La/Yb)_N$ ratio ranging from 3.83 to 111.55. A negative Eu anomaly is observed for most of the pegmatites and for the MPL granite (Eu/Eu* = 0.28–0.98 and 0.16, respectively), a typical feature of evolved melts. However, the cassiterite-rich dikes (type 11) and the quartz-andalusite dikes (type 2) exhibit a clear positive Eu anomaly (Eu/Eu* = 5.67 and 2.37, respectively), which in the case of the cassiterite-rich dikes, could be related to the activity of high-temperature hydrothermal fluids (Sverjensky 1984).

DISCUSSION

Substitution mechanisms

All the studied micas belong to the K-Li-Al-Si compositional space (Al-rich, Fe-free micas). In the pegmatites where muscovite is the only mica present, its chemical composition is generally quite homogeneous, with the most significant variations observed in the spodumene-rich dikes (type 8) and in the intermediate discordant pegmatites (type 6) (Figs. 2 and 4). Compositional changes in Li-poor muscovite associated with all of the pegmatite types involves the substitutions $Al_4Si_{-3}\square_{-1}$, and, to a lesser extent, $Al_2\square(R^{2+})_{-3}$ where R^{2+} = (Fe + Mg + Mn) and $\square$ represents vacancies (Figs. 4a and 4b).

The micas from the Li-rich mica-bearing pegmatites (types 9 and 10) define a clear compositional trend from muscovite to a composition close to ideal trilithionite (Fig. 2). The ^{VI}Al contents show a clear negative correlation with Li (and F) for all micas from type 9 and 10 pegmatites (R = –0.983). In addition, the good negative correlations between Al and (Si + Li) (R = –0.989) and between Li and (^{VI}Al + $^{VI}\square$) (R = –0.993) (Figs. 4b and 4c) indicate that Li was incorporated into the micas by a combination of the $Li_3Al_{-1}\square_{-2}$ and Si_2LiAl_{-3} substitutions (Figs. 4b and 4c). However, these two mechanisms did not operate to the same extent for the two Li-mica bearing pegmatite types. For type 9 pegmatites, the slope of the regression line for Li vs. (^{VI}Al + $^{VI}\square$) (m_{slope} = –1.01) (Figs. 4b and 4c) is slightly higher than the slope for the micas from type 10 pegmatites (m_{slope} = –1.00). This suggests that the $Li_3Al_{-1}\square_{-2}$ substitution was more important in pegmatites where the only Li-rich mineral is mica (type 10) than in the pegmatites where spodumene occurs together with the Li-rich mica (type 9).

Petrogenetic implications

The K/Rb ratio of micas, together with the content in Li or F and some trace elements such as Cs, Sn, Ba, and Zn, have been used frequently as petrogenetic indicators of the degree of pegmatite evolution (e.g., Gaupp et al. 1984; Foord et al. 1995; Wise 1995; Roda et al. 1995, 2006, 2007a, 2007b; Pesquera et al. 1999; Kile and Foord 1998; Clarke and Bogutyn 2003; Černý 2004). In general, micas show the same general evolutionary trends as those of feldspars, with an increase in Li, Rb, Cs, and F and a decrease in Ba with decreasing K/Rb ratio.

A decrease in K/Rb is observed from micas associated with the granite and adjacent barren pegmatites, through intermediate pegmatites, to the Li and F richest bodies furthest from the MPL granite (Figs. 1 and 3). Some trace elements, such as Li, F, Cs, Be, Nb, and Ta, show a clear negative correlation with the K/Rb ratio in the micas from the FA pegmatites. The highest values in these elements are observed in the micas from the Li-mica-rich pegmatites (types 9 and 10), with intermediate values for the other Li-bearing pegmatites (types 7 and 8) (Fig. 3). It is noteworthy that, contrary to what was observed by Smeds (1992) and proposed by London (2008), the micas richest in Be in the FA are those associated with the most evolved pegmatites (Fig. 3g). K/Rb is positively correlated with Ba (Fig. 3f), with the highest values for the micas associated with the barren pegmatites (types 1 to 4) and with the granite.
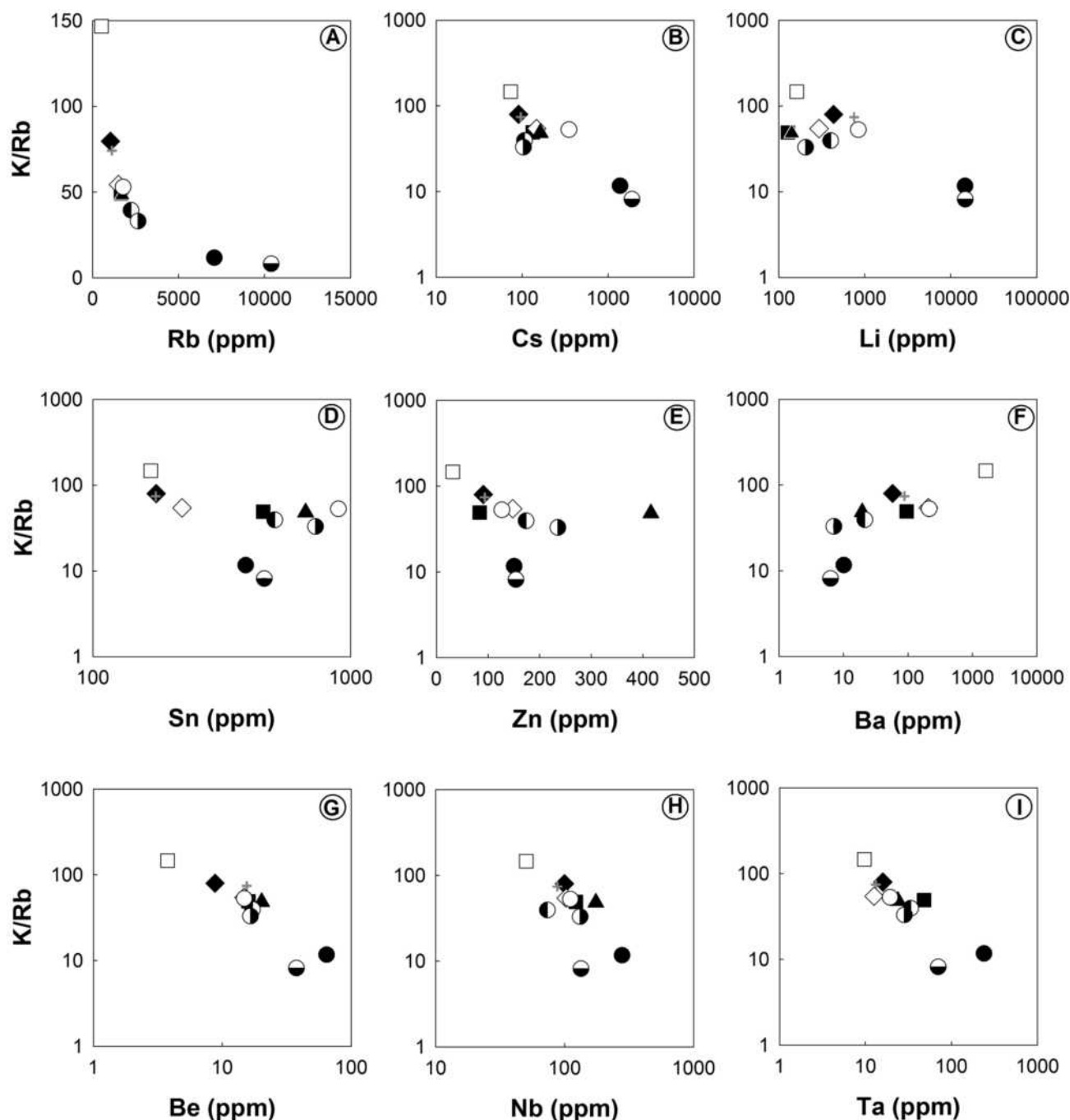
TABLE 3. Trace elements and rare-earth elements from representative micas of the different pegmatite types from the Fregeneda-Almendra field

Type	Granite	T1	T2	T3	T4	T6	T7	T8	T9	T10	T11
Sample	Mêda-9	10-6	136-6	269-5	clall-2	252-3	11-34	ma-8	fr-4/6	89-3/5	ala-1
Mica type	Ms	Ms	Ms	Ms	Ms	Ms	Ms	Ms	Li-ms	Li-ms	Ms
Trace elements											
Li	752 ± 0.5	435 ± 0.5	162 ± 0.5	294 ± 0.5	128 ± 0.5	142 ± 0.5	401 ± 0.5	205 ± 0.5	14681 ± 0.5	14774 ± 0.5	843 ± 0.5
Rb	1121 ± 39.2	1028 ± 36.0	516 ± 18.1	1494 ± 52.3	1639 ± 57.4	1714 ± 60.0	2230 ± 78.1	2633 ± 92.1	7075 ± 241.6	10388 ± 363.6	1761 ± 61.6
Cs	97 ± 4.9	91 ± 4.6	73 ± 3.7	147 ± 5.2	133 ± 4.7	163 ± 5.71	107 ± 3.8	104 ± 3.6	1375 ± 48.1	1891 ± 66.2	350 ± 12.3
Sn	175 ± 6.1	176 ± 6.2	167 ± 5.9	222 ± 7.8	458 ± 16.0	669 ± 23.4	508 ± 17.8	730 ± 25.6	392 ± 13.7	462 ± 16.2	896 ± 31.4
Zn	94 ± 4.7	91 ± 4.6	32 ± 1.6	148 ± 5.2	84 ± 4.2	416 ± 14.6	174 ± 6.1	236 ± 8.2	151 ± 5.3	154 ± 5.4	127 ± 4.5
Ba	88 ± 4.4	58 ± 2.9	1614 ± 56.5	207 ± 7.3	96 ± 4.8	20 ± 1.0	21 ± 1.1	7 ± 0.4	10 ± 0.5	6 ± 0.3	213 ± 7.4
Be	15 ± 0.8	9 ± 0.5	4 ± 0.2	15 ± 0.8	16 ± 0.8	20 ± 1.0	17 ± 0.9	17 ± 0.9	64 ± 3.2	38 ± 1.9	15 ± 0.8
Nb	88 ± 4.4	100 ± 5.0	50 ± 2.5	103 ± 3.6	122 ± 4.3	175 ± 6.1	73 ± 3.7	132 ± 4.6	279 ± 9.8	134 ± 4.7	111 ± 3.9
Ta	13 ± 0.7	16 ± 0.8	10 ± 0.5	13 ± 0.7	48 ± 2.4	24 ± 1.2	34 ± 1.7	28 ± 1.4	239 ± 8.4	70 ± 3.5	19 ± 1.0
Zr	24 ± 1.2	7 ± 0.4	7 ± 0.4	20 ± 1.0	5 ± 0.3	5 ± 0.3	1 ± 0.1	4 ± 0.2	2 ± 0.1	20 ± 1.0	1 ± 0.1
Ni	87 ± 4.4	220 ± 7.7	77 ± 3.9	124 ± 4.3	121 ± 4.2	116 ± 5.8	217 ± 7.6	118 ± 4.1	111 ± 3.9	117 ± 4.1	216 ± 7.6
Tl	4 ± 0.2	4 ± 0.2	2 ± 0.1	6 ± 0.3	7 ± 0.4	21 ± 1.1	11 ± 0.6	12 ± 0.6	43 ± 2.2	53 ± 2.7	8 ± 0.4
Pb	99 ± 5.0	1136 ± 39.8	546 ± 19.1	432 ± 15.1	297 ± 10.4	55 ± 2.8	121 ± 4.2	112 ± 3.9	39 ± 2.0	67 ± 3.4	34 ± 1.7
REE ppm											
Y	4.229 ± 0.01	0.666 ± 0.01	1.699 ± 0.01	1.702 ± 0.01	0.473 ± 0.01	0.846 ± 0.01	0.240 ± 0.01	0.279 ± 0.01	0.281 ± 0.01	1.069 ± 0.01	0.088 ± 0.01
La	6.399 ± 0.01	1.000 ± 0.01	2.690 ± 0.01	1.196 ± 0.01	0.613 ± 0.01	1.724 ± 0.01	0.156 ± 0.01	0.548 ± 0.01	0.821 ± 0.01	0.351 ± 0.01	0.118 ± 0.01
Ce	14.513 ± 0.01	3.054 ± 0.01	5.422 ± 0.01	2.582 ± 0.01	1.376 ± 0.01	3.812 ± 0.01	0.362 ± 0.01	0.876 ± 0.01	1.545 ± 0.01	0.387 ± 0.01	0.152 ± 0.01
Pr	1.793 ± 0.01	0.304 ± 0.01	0.660 ± 0.01	0.307 ± 0.01	0.147 ± 0.01	0.429 ± 0.01	0.032 ± 0.01	0.103 ± 0.01	0.187 ± 0.01	0.078 ± 0.01	0.012 ± 0.01
Nd	6.613 ± 0.01	1.246 ± 0.01	2.383 ± 0.01	1.072 ± 0.01	0.593 ± 0.01	1.662 ± 0.01	0.078 ± 0.01	0.467 ± 0.01	0.583 ± 0.01	0.268 ± 0.01	0.048 ± 0.01
Sm	1.930 ± 0.01	0.254 ± 0.01	0.575 ± 0.01	0.271 ± 0.01	0.122 ± 0.01	0.270 ± 0.01	0.036 ± 0.01	0.107 ± 0.01	0.097 ± 0.01	0.046 ± 0.01	b.d.
Eu	0.095 ± 0.01	0.074 ± 0.01	0.401 ± 0.01	0.093 ± 0.01	0.028 ± 0.01	0.054 ± 0.01	0.016 ± 0.01	0.018 ± 0.01	0.016 ± 0.01	0.006 ± 0.01	0.036 ± 0.01
Gd	1.728 ± 0.01	0.242 ± 0.01	0.422 ± 0.01	0.308 ± 0.01	0.089 ± 0.01	0.234 ± 0.01	0.046 ± 0.01	0.060 ± 0.01	0.081 ± 0.01	0.090 ± 0.01	0.024 ± 0.01
Tb	0.281 ± 0.01	0.036 ± 0.01	0.060 ± 0.01	0.045 ± 0.01	0.017 ± 0.01	0.038 ± 0.01	0.004 ± 0.01	0.007 ± 0.01	0.010 ± 0.01	0.015 ± 0.01	b.d.
Dy	1.039 ± 0.01	0.094 ± 0.01	0.380 ± 0.01	0.264 ± 0.01	0.087 ± 0.01	0.157 ± 0.01	0.008 ± 0.01	0.034 ± 0.01	0.048 ± 0.01	0.081 ± 0.01	b.d.
Ho	0.152 ± 0.01	0.018 ± 0.01	0.091 ± 0.01	0.052 ± 0.01	0.015 ± 0.01	0.027 ± 0.01	0.002 ± 0.01	0.008 ± 0.01	0.008 ± 0.01	0.025 ± 0.01	0.002 ± 0.01
Er	0.256 ± 0.01	0.020 ± 0.01	0.146 ± 0.01	0.163 ± 0.01	0.045 ± 0.01	0.053 ± 0.01	0.006 ± 0.01	0.019 ± 0.01	0.017 ± 0.01	0.058 ± 0.01	0.004 ± 0.01
Tm	0.035 ± 0.01	0.002 ± 0.01	0.025 ± 0.01	0.027 ± 0.01	0.005 ± 0.01	0.009 ± 0.01	0.004 ± 0.01	0.003 ± 0.01	0.003 ± 0.01	0.008 ± 0.01	b.d.
Yb	0.205 ± 0.01	0.016 ± 0.01	0.150 ± 0.01	0.212 ± 0.01	0.044 ± 0.01	0.046 ± 0.01	b.d.	0.004 ± 0.01	0.005 ± 0.01	0.028 ± 0.01	0.006 ± 0.01
Lu	0.026 ± 0.01	0.002 ± 0.01	0.019 ± 0.01	0.033 ± 0.01	0.006 ± 0.01	0.006 ± 0.01	b.d.	0.001 ± 0.01	b.d.	0.005 ± 0.01	b.d.
K/Rb	74	80	147	54	49	48	39	33	12	8	53
†(La/Yb)$_N$	21.2	42.46	12.18	3.83	9.46	25.46	–	93.07	111.55	8.52	13.36
†Eu/Eu*	0.16	0.9	2.37	0.98	0.78	0.64	1.2	0.62	0.53	0.28	5.67

Note: b.d. = below detection limit.
† McDonough and Sun (1995) = Chondrite (Cl).
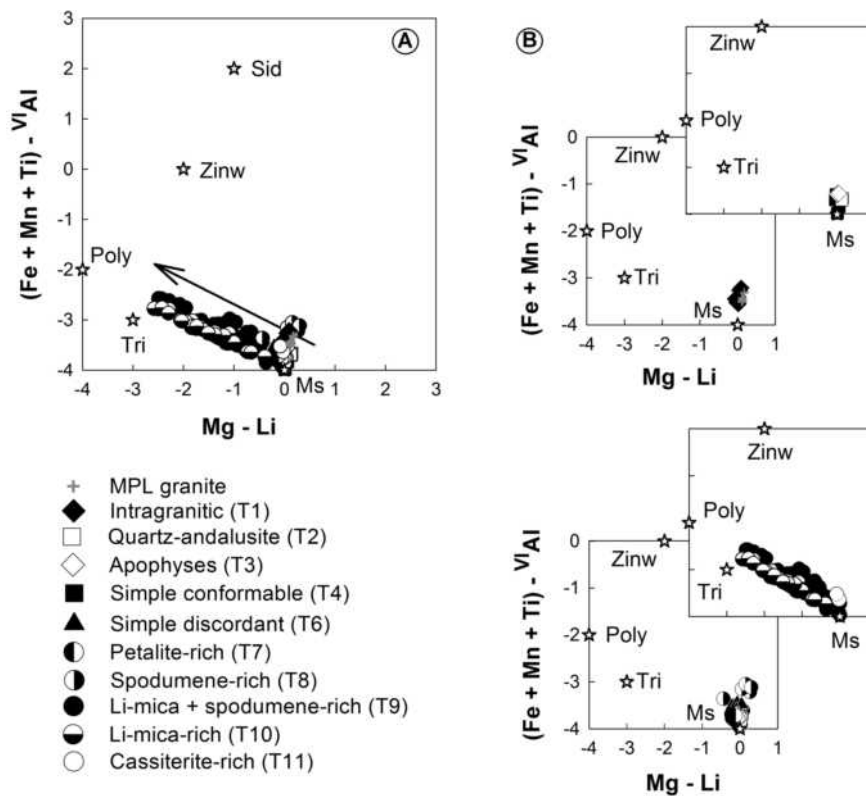
FIGURE 2. (**a**) Mg – Li vs. (Fe + Mn + Ti) – ^{VI}Al and (**b**) Figure 2a inset, for the micas associated with the different pegmatite types from the Fregeneda-Almendra field. (All data in apfu.)

Legend:
- + MPL granite
- ◆ Intragranitic (T1)
- □ Quartz-andalusite (T2)
- ◇ Apophyses (T3)
- ■ Simple conformable (T4)
- ▲ Simple discordant (T6)
- ◑ Petalite-rich (T7)
- ◐ Spodumene-rich (T8)
- ● Li-mica + spodumene-rich (T9)
- ⊖ Li-mica-rich (T10)
- ○ Cassiterite-rich (T11)

FIGURE 3. Plot of the trace element concentrations for the micas associated with the different pegmatite types from the Fregeneda-Almendra field. (Symbols legend as in Fig. 2.)

Field geologic data combined with geochemical data of micas suggest that all of the discordant pegmatites were derived under the same petrogenetic process, with the exception of type 11. Some data from the cassiterite-rich dikes (type 11) are not consistent with the evolutionary trend defined by the other discordant pegmatite types. These dikes are cassiterite + albite rich and should be the most evolved, bearing in mind their mineral association and the scheme established by Černý (1991) for zoned pegmatite fields. However, they are folded and cut by some Li-bearing dikes (type 9) in the Feli open pit (northernmost part

of the FA field) (Fig. 1), which clearly shows that they predate Li-rich bodies. Moreover, the K/Rb ratio in micas from the cassiterite-rich dikes is higher than this ratio in micas from the Li-bearing pegmatites (types 7 to 10), and similar to the micas from the simple discordant pegmatites (type 6). In addition, not only is the K/Rb ratio in micas from the cassiterite-rich dikes higher than expected, but the content of some trace elements (such as Li and Cs) are lower than in micas from Li-mica-bearing pegmatites, whereas Ba values are higher. These facts suggest that the FA pegmatites do not conform to a single crystallization
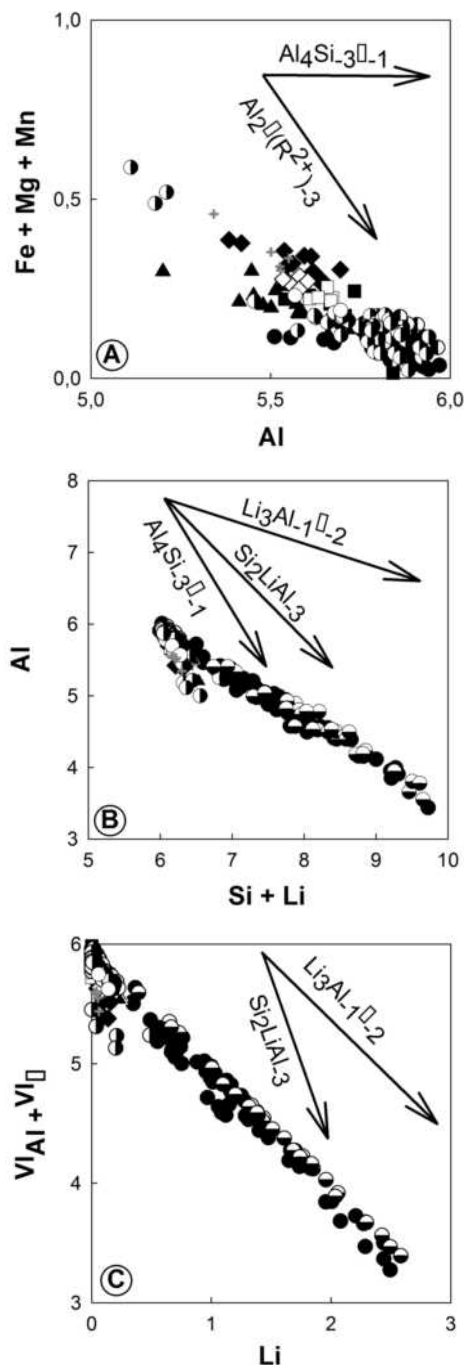
FIGURE 4. (**a**) Al vs. Fe + Mg + Mn (F wt% < 1), (**b**) Si + Li vs. Al, and (**c**) Li vs. $^{VI}Al + ^{VI}\square$, for the micas associated with the different pegmatite types from the Fregeneda-Almendra field. The arrows labeled with the exchange vectors represent the direction of the vector that reflects the evolutionary trend of the micas. (Symbols as in Fig. 2; all data in apfu; R^{2+} = Fe + Mg + Mn.)

path, in accord with the petrogenetic model of Roda (1993) and Roda et al. (1999) for the eastern part of this pegmatitic field, where at least two different evolution trends were proposed.

The discordant pegmatites, with strikes around NS to N030°E, and belonging to the types 6 to 10, are more evolved than the barren pegmatites (types 1 to 4), and they clearly belong to the same evolutionary trend. Based on these considerations,

we propose an order of pegmatite evolution as follows: MPL leucogranite, barren pegmatites (types 1, 2, 3, and 4), intermediate pegmatites (type 6), petalite- and spodumene-rich pegmatites (types 7 and 8, respectively), Li-mica + spodumene-rich (type 9), and Li-mica-rich, (type 10). The differences between the two types of Li-mica-bearing pegmatites do not seem to be very important. As documented above, the highest contents in Li, F, Rb, Cs, and volatiles are found in the Li-mica-bearing dikes (type 10) followed by the Li-mica + spodumene dikes (type 9). This progressive enrichment in large-ion-lithophile elements is consistent with the appearance of a fluid phase during pegmatite crystallization. For these elements, the silicate-melt/fluid-phase partition coefficients are not at unity, and large-ion-lithophile elements partition into the fluid, unlike the high-field-strength elements (Bau 1996). The occurrence of such liquids at late stages of crystallization is revealed by melt inclusion studies (Thomas et al. 2000; Banadina et al. 2004; Kamenetsky et al. 2004). The fluids may become strongly enriched in incompatible elements such as F, B, P, Be, and Li (Veksler 2004). The greater availability of Li and F during crystallization of the Li-mica-rich pegmatites (type 10) could be related to the stronger influence of the $Li_3AL_1\square_{-2}$ substitution in these micas, in comparison to the micas from the Li-mica + spodumene-rich dikes (type 9). This exchange vector implies incorporation of a higher amount of Li at the octahedral sites of micas than the Si_2LiAL_{-3} vector, which seems to be more operative during the crystallization of the Li-micas from the Li-mica + spodumene-rich pegmatites (type 9).

Li-mica-rich pegmatites (types 9 and 10) are hosted in metasediments of the biotite and/or chlorite metamorphic facies (Fig. 1). Nevertheless, the occurrence of Li-mica depends not on the degree of metamorphism, but on the Li and F activities and to water content of the pegmatite-forming melt. Based on experimental studies, London (1982, 2008) argues that lithium aluminosilicates remain stable with respect to *lepidolite* or topaz at up to ~2 wt% F in melt. Accordingly, in the case of the Li-mica-rich pegmatites (type 10), where no other Li-rich silicates have been identified, we can assume that the F content in the melt was over this value. The occurrence of spodumene, more stable than petalite or eucryptite under higher activity of F (Burt and London 1982), along with the presence of Li-mica in the type 9 pegmatites, would indicate lower F (and Li) in the melt (close to 2 wt% F). Moreover, the occurrence of primary spodumene in these dikes (type 9) could be related to the low degree of regional metamorphism attained by the host rocks in the Feli open pit.

Petalite- and spodumene-rich pegmatites (types 7 and 8, respectively) have similar mica compositions (Figs. 3 and 4). This similarity, together with field, mineralogical, and geochemical data, suggests that the evolutionary degrees of types 7 and 8 are identical. The scarcity of micas (only minor muscovite is found) could indicate that crystallization proceeded under water-undersaturated conditions, also with lower F content than in the Li-mica-rich pegmatites (below 2 wt% in F). In this case, there seems to be a close relation between the degree of metamorphism of the host rocks and the lithium aluminosilicate assemblages in the pegmatites: petalite-bearing pegmatites occur in the andalusite-sillimanite (fibrolite) zone, whereas spodumene-bearing veins are associated with metasediments of the biotite and/or chlorite zone.

Although the relations between the MPL leucogranite and the different pegmatite types are not completely understood, it is clear that pegmatites of the FA field show a zoned regional distribution with respect to the MPL granite. The discordant pegmatites occupy late-Variscan structures, whereas the MPL granite is considered to be syntectonic. Therefore, further investigation, particularly geochronological data, on pegmatites and granites is required to shed light on petrogenetic relations among the pegmatite types and to clarify if the zonation is causal or simply casual, for all or some of the different types of pegmatites occurring in the FA field.

ACKNOWLEDGMENTS

REFERENCES CITED

Ábalos, B., Carreras, J., Druguet, E., Escuder Viruete, J., Gómez Pugnaire, M.T., Lorenzo Alvarez, S., Quesada, C., Rodríguez Fernández, L.R., and Gil-Ibarguchi, J.I. (2002) Variscan and Pre-Variscan Tectonics. In W. Gibbons and T. Moreno, Eds., The Geology of Spain, p. 155–183. The Geological Society of London.

Banadina, E.V., Veksler, I.V., Thomas, R., Syritso, L.F., and Trumbull, R.B. (2004) Magmatic evolution of Li-F, rare-metal granites: a case study of melt inclusions in the Khangilay complex, Eastern Transbaikalia (Russia). Chemical Geology, 210, 113–134.

Bau, M. (1996) Controls on the fractionation of isovalent trace elements in magmatic and aqueous systems; evidence from Y/Ho, Zr/Hf, and lanthanide tetrad effect. Contributions to Mineralogy and Petrology, 123, 323–333.

Brigatti, M.F., Lugli, C., Poppi, L., Foord, E.E., and Kile, D.E. (2000) Crystal chemical variations in Li- and Fe-rich micas from Pikes Peak Batholith (central Colorado). American Mineralogist, 85, 1275–1286.

Burt, D.M. and London, D. (1982) Subsolidus equilibria. In P. Černý, Ed., Granitic Pegmatites in Science and Industry, vol. 8, p. 329–346. Short Course Handbook, Mineralogical Association of Canada.

Černý, P. (1991) Rare-element granitic pegmatites. Part II: regional to global environments and petrogenesis. Geoscience Canada, 18, 49–62.

Černý, P. (2004) The Tanco rare-element pegmatite deposit, Manitoba: regional context, internal anatomy, and global comparisons. In R.L. Linnen and I.M. Samson, Eds., Rare Element Geochemistry and Mineral Deposits, vol. 17, p. 184–231. Short Course Notes, Geological Association of Canada.

Černý, P. and Burt, D.M. (1984) Paragenesis, crystallochemical characteristics, and geochemical evolution of micas in granite pegmatites. In S.W. Bailey, Ed., Micas, vol. 13, p. 257–297. Reviews in Mineralogy, Mineralogical Society of America, Chantilly, Virginia.

Clarke, D.B. and Bogutyn, P.A. (2003) Oscillatory epitactic-growth zoning in biotite and muscovite from the Lake Lewis leucogranite, South Mountain batholith, Nova Scotia, Canada. Canadian Mineralogist, 41, 1027–1047.

Foord, E.E., Černý, P., Jackson, L.L., Sherman, D.M., and Eby, R.K. (1995) Mineralogical and geochemical evolution of micas from miarolitic pegmatites of the anorogenic Pikes Peak batholith, Colorado. Mineralogy and Petrology, 55, 1–26.

Gaupp, R., Möller, P., and Morteani, G. (1984) Tantal-pegmatite. Geologische, petrologische und geochemische Untersuchungen. Monograph Series on Mineral Deposits, 124 p. Gebrüder Borntraeger-Berlin-Stuttgart, Germany.

Henderson, C.M.B., Martin, J.S., and Mason, R.A. (1989) Compositional relations in Li-micas from S. W. England and France: an ion- and electron-microprobe study. Mineralogical Magazine, 53, 427–449.

Jolliff, B.L., Papike, J.J., and Shearer, C.K. (1987) Fractionation trends in mica and tourmaline as indicators of pegmatite internal evolution: Bob Ingersoll pegmatite, Black Hills, South Dakota. Geochimica et Cosmochimica Acta, 51, 519–543.

——— (1992) Petrogenetic relationships between pegmatite and granite based on geochemistry of muscovite in pegmatite wall zones, Black Hills, South Dakota, USA. Geochimica et Cosmochimica Acta, 56, 1915–1939.

Kamenetsky, V.S., Naumov, V.B., Davidson, P., van Achterbergh, E., and Ryan, C.G. (2004) Immiscibility between silicate magmas and saline fluids: a melt inclusion microprobe into magmatic-hydrothermal transition in the Omsukchan Granite (NE Russia). Chemical Geology, 210, 73–90.

Kile, D.E. and Foord, E.E. (1998) Micas from the Pikes Peak Batholith and its cogenetic granitic pegmatites, Colorado: optical properties, composition, and correlation with pegmatite evolution. Canadian Mineralogist, 36, 463–482.

London, D. (1982) Stability of spodumene in acidic and saline fluorine-rich environments, 331–334. Carnegie Institution of Washington Year Book 81.

——— (2008) Pegmatites, 347 p. The Canadian Mineralogist Special Publication, Québec, Canada.

López Plaza, M., Carnicero, A., and Gonzalo, J.C. (1982) Estudio geológico del campo filoniano de La Fregeneda (Salamanca). Stvdia Geologica Salmanticensia, 17, 89–98.

McDonough, W.F. and Sun, S.-s. (1995) The composition of the Earth. Chemical Geology, 120, 223–254.

Monier, G., and Robert, J.L. (1986) Evolution of the miscibility gap between muscovite and biotite solid solutions with increasing lithium content: and experimental study in the system $K_2O-Li_2O-MgO-FeO-Al_2O_3-SiO_2-H_2O-HF$ at 600 °C, 2 kbar PH_2O:comparison with natural lithium micas. Mineralogical Magazine, 50, 641–651.

Pesquera, A., Torres-Ruiz, J., Gil-Crespo, P., and Velilla, N. (1999) Chemistry and genetic implications of tourmaline and Li-F-Cs micas from the Valdeflores area (Cáceres, Spain). American Mineralogist, 84, 55–69.

Roda, E. (1993) Características, distribución y petrogénesis de las pegmatitas de La Fregeneda (Salamanca, Spain), 200 p. Ph.D thesis, Univ. Pais Vasco, Spain.

Roda, E., Pesquera, A., and Velasco, F. (1995) Micas of the muscovite-lepidolite series from the Fregeneda pegmatites (Salamanca, Spain). Mineralogy and Petrology, 55, 145–157.

Roda, E., Pesquera, A., Velasco, F., and Fontan, F. (1999) The granitic pegmatites of the Fregeneda area (Salamanca, Spain): characteristics and petrogenesis. Mineralogical Magazine, 63, 535–558.

Roda, E., Pesquera, A., Gil-Crespo, P.P., Torres-Ruiz, J., and de Parseval, P. (2006) Mineralogy and geochemistry of micas from the Pinilla de Fermoselle pegmatite (Zamora, Spain). European Journal of Mineralogy, 18, 36–377.

Roda, E., Keller, P., Pesquera, A., and Fontan, F. (2007a) Micas of the muscovite-lepidolite series from Karibib pegmatites, Namíbia. Mineralogical Magazine, 71, 41–62.

Roda E., Vieira R., Lima A., Pesquera A., Noronha F., and Fontan F. (2007b) The Fregeneda–Almendra pegmatitic field (Spain & Portugal): mineral assemblages and regional zonation, 81–82. Granitic Pegmatites: the state of the art, Book of Abstracts. Memórias 8, Univ. Porto, Portugal.

Silva, A.F. and Ribeiro, M.L. (1991) Notícia explicativa da folha 15-A—Vila Nova de Foz Côa—da carta Geológica de Portugal na escala 1/50.000. Serviços Geológicos de Portugal, 52 p.

——— (1994) Notícia explicativa da folha 15-B—Freixo de Espada à Cinta—da carta Geológica de Portugal na escala 1/50.000. Instituto Geológico e Mineiro, Lisboa, Portugal, 48 p.

Silva A.F., Santos A.J., Ribeiro A., and Ribeiro M.L. (1990a) Carta Geológica de Portugal na escala 1/50.000—folha 15-A—Vila Nova de Foz Côa. Serviços Geológicos de Portugal.

Silva A.F., Santos A.J., Ribeiro A., Cabral J., and Ribeiro M.L. (1990b) Carta Geológica de Portugal na escala 1/50.000—folha 15-B—Freixo de Espada à Cinta. Serviços Geológicos de Portugal.

Smeds, S.-A. (1992) Trace elements in potassium-feldspar and muscovite as a guide in the prospecting for lithium- and tin-bearing pegmatites in Sweden. Journal of Geochemical Exploration, 42, 351–469.

Sverjensky, D.A. (1984) Europium redox equilibria in aqueous solution. Earth and Planetary Science Letters, 67, 70–78.

Tindle, A.G. and Webb, P.C. (1990) Estimation of lithium contents in trioctahedral micas using microprobe data: application to micas from granitic rocks. European Journal of Mineralogy, 2, 595–610.

Tischendorf, G., Gottesmann, B., Förster, H.J., and Trumbull, R.B. (1997) On Li-bearing micas: estimating Li from electron microprobe analyses and an improved diagram for graphical representation. Mineralogical Magazine, 61, 809–834.

Thomas, R., Webster, J.D., and Heinrich, W. (2000) Melt inclusions in pegmatite quartz: complete miscibility between silicate melts and hydrous fluids at low pressure. Contributions to Mineralogy and Petrology, 139, 394–401.

Veksler, I.V. (2004) Element enrichment and fractionation by magmatic aqueous fluids: experimental constraints on melt-fluid immiscibility and element partitioning. In R.L. Linnen and I.M. Samson, Eds., Rare Element Geochemistry and Mineral Deposits, vol. 17, p. 103–129. Short Course Notes, Geological Association of Canada.

Vieira, R. (2010) Aplitopegmatitos com elementos raros da região entre Almendra (V. N. de Foz-Côa) e Barca D'Alva (Figueira de Castelo Rodrigo). Campo aplitopegmatítico da Fregeneda-Almendra, 275 p. Ph.D thesis, Univ. of Porto, Portugal.

Wise, M.A. (1995) Trace element chemistry of lithium-rich micas from rare-element granitic pegmatites. Mineralogy and Petrology, 55, 203–215.

September 13th, morning:
STOP 2: Senhora da Assunçao Mine
(Aldeia Nova, Sátão, Portugal)

Travel from the Hotel to the Senhora da Assunçao Mine: 154 km, ≈ 2h35'

Locality 2: The Senhora da Assunçao beryl-phosphate pegmatites (Sátão, Portugal)

Stop 3 Highlights (13th of September, morning)

- Coarse grained, internally zoned pegmatites with a prominent massive quartz-core.
- Giant beryl crystals (up to 5 m long) and subrounded Fe-Mn phosphate masses of up to 1,5 m Ø.
- Intragranitic within the porphyritic biotite-muscovite monzogranite-syenogranite from Ferreira de Aves (292 Ma).
- The pegmatites are being mined for feldspar.

Stop 3: A) Giant euhedral quartz crystals from the core zone of the Nossa Senhora da Assunçao pegmatite; B) pseudographic intergrowth of K-feldspar inside a beryl hexagonal prism; C) and D) giant beryl crystal, up to six m long. (Pictures A and B by Pedro-Pablo Gil-Crespo).

INTRODUCTION

The Senhora da Assunção pegmatite group, located at Ferreira de Aves (Sátão, Viseu district) (Fig. 4), consists of a pair of coupled intra-granitic pegmatite bodies (Fig. 5). These pegmatites belong to a pegmatitic belt that extends at the western margin of the Aguiar da Beira Massif, passing from Sátão, up to Fornos de Algodres (Trabulo et al., 1995). The biggest pegmatitic bodies in this belt appear scattered, with irregular to turnip shapes, occasionally grouped or beaded. These pegmatites have been mined for decades for industrial quartz and feldspar. They show also Nb+Ta-enrichment, with the common occurrence of Nb-Ta-oxides as well as abundant masses of Fe-Mn-phosphates, mainly from the triplite-zwieselite and trihylite-lithiophilite series. These pegmatites, with a well-developed internal structure and a coarse, sometimes giant, grain size, show the features usually observed in many pegmatites worldwide. The Senhora da Assunção pegmatite group constitutes a good example of the beryl-phosphate pegmatites from the CIZ. Despite the clear scientific and economic interest of this pegmatite group, a comprehensive study of this pegmatite, including a detailed mineralogy, geochemistry and petrogenetic model has not been published yet in an international magazine. However, some interesting publications in Portuguese give detail on these pegmatites (e.g. Trabulo et al., 1995; Hochleitner & Fehr, 2005; Alves, 2013; Ferreira et al., 2014)
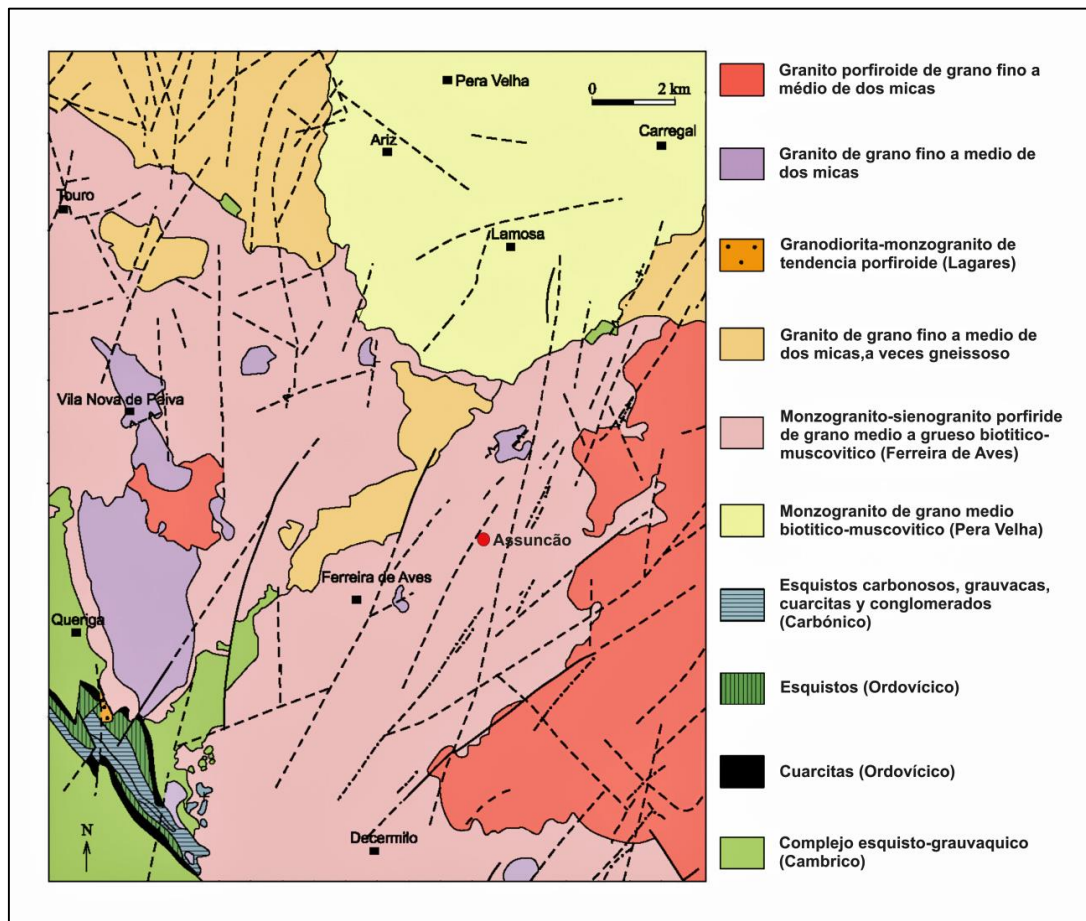

Fig. 4: Geological setting of the Senhora da Assunçao mine (Alves, 2013; modified from Costa, 2006)

GENERAL GEOLOGY OF THE HOSTING GRANITE AND THE PEGMATITES

The Senhora da Assunçao pegmatites are hosted by the Ferreira de Aves granite (Fig. 4), which is a porphyritic biotite>muscovite monzogranite-syenogranite (Teixeira et al., 1972, Costa, 2006). It is late- to post D3, with an age of 292 Ma (Rb/Sr, Costa, 2006). This granite is crossed by abundant pegmatitic and quartz-rich dykes of different thicknesses, including the Senhora da Assunçao pegmatitic bodies. Many of these dykes were emplaced along some of the numerous fractures (Ne-SW and NNE-SSW) that occur in the whole area (Teixeira, 1972).

According to the information offered by Trabulo et al., (1995), the axis joining the two pegmatites from the Senhora da Assunçao group shows a N25E strike, parallel to the border of the hosting granitic massif and to the fluidal trends of such granitic rocks (Fig. 5). The two pegmatitic bodies show a major lenticular subhorizontal shape, up to 100m long, with some shorter subvertical branches and/or apophyses (Fig. 5). These pegmatites show a well developed zoned internal structure, with a all zone of simple mineralogy (Qz+K-Fd+Ab+Mus+Bio+oxides); a Qz+K-Fd-rich intermediate zone, with minor beryl, columbite-tantalite and muscovite; a K-Fd-rich intermediate zone, with minor beryl, Fe-Mn-phosphates, pyrite and ilmenite; and a massive quartz core. Besides these primary zones, some replacement bodies may be observed, with chlorite, pitchblende, caolinite and secondary Fe-Mn-phosphates, among others (Trabulo et al., 1995).
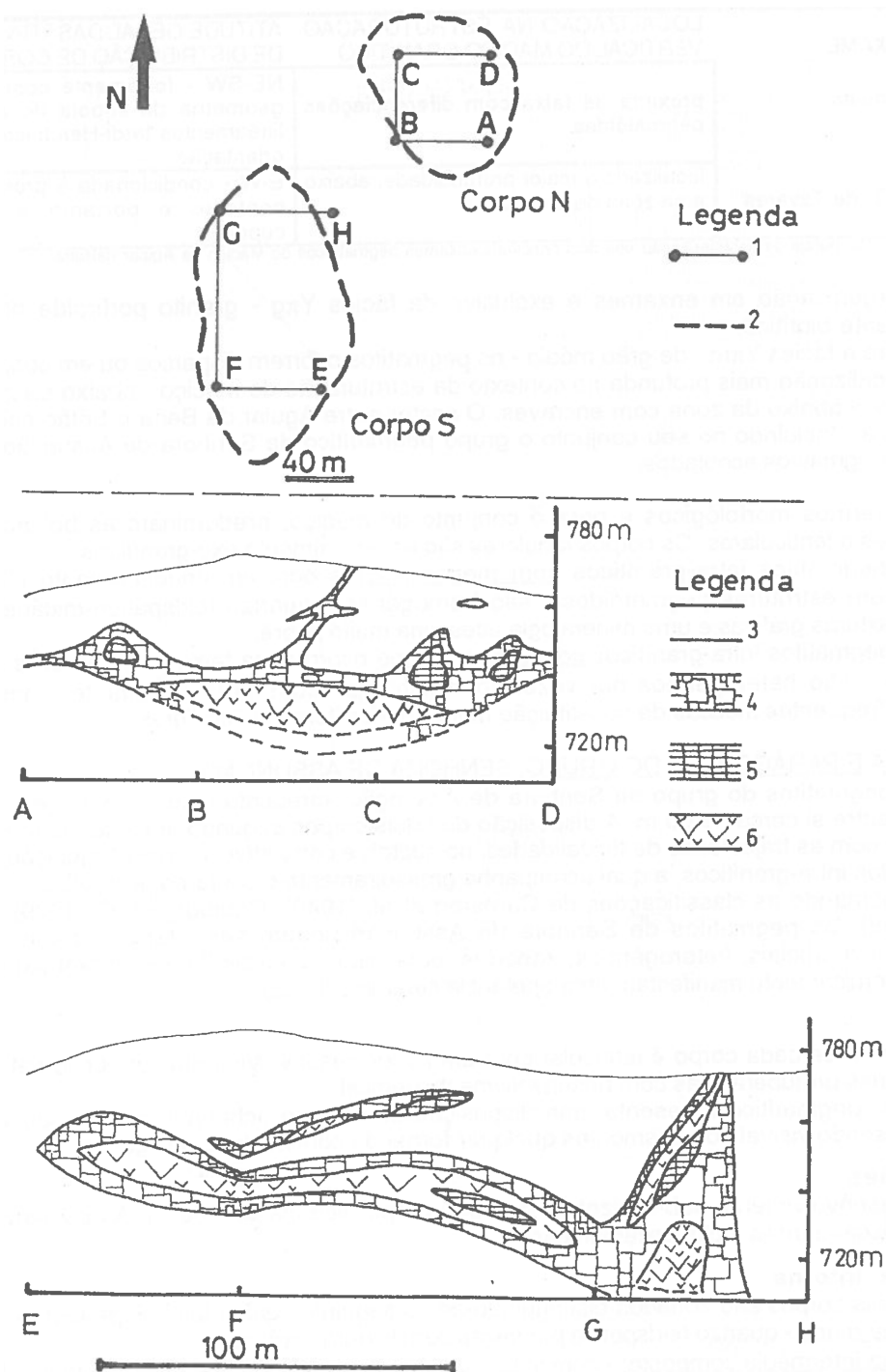

Fig. 5. Idealized cross-cut of the Senhora da Assunçao pegmatitic group. 3) Medium grained porphyritic granite; 4) qz+K-fd-rich outer zones; 5) K-feldspar rich intermediate zone; 6) quartz core. (Taken from Trabulo et al., 1995).

Geoquímica do Ta e estrutura da sua distribuição no Grupo Pegmatítico Granítico de Senhora da Assunção, Sátão, Centro de Portugal

Ta geochemistry and pattern of its distribution in the Senhora da Assunção Granitic Pegmatite Group of Satão, Center of Portugal

J. Ferreira[1*], P. Araújo[1], F. Guimarães[1], M. Pereira[1], C. Leal Gomes[1]

Artigo Curto
Short Article

Resumo: O grupo pegmatítico de Senhora da Assunção situado em Ferreira de Aves, Sátão, é composto por um par de pegmatitos intra-graníticos que foram objecto de exploração mineira dedicada ao quartzo e feldspato. No decurso da actividade extractiva foram encontrados conteúdos não negligenciáveis de nióbio-tantalatos com potencial para rentabilização como sub-produtos de lavra mineira, muito embora, nunca tenham sofrido aproveitamento. Este potencial económico justifica uma análise integrada da distribuição espacial dos teores de Nb-Ta nas diferentes unidades internas do pegmatito, assim como da sua composição e tendências de fraccionação.
As unidades mais ricas em óxidos de Nb-Ta são as unidades albíticas da zona intermédia, a periferia dos gigacristais de berilo, as unidades fosfáticas e uma brecha de colapso tardio que ocorre no corpo Sul. Os teores de Ta em rocha total situam-se frequentemente acima de 150 ppm, barreira razoável para equacionar uma potencialidade económica. A fraccionação dos Nb-tantalatos é coerente com uma linhagem híbrida LCT - NYF para os pegmatitos, tendendo para termos ricos em molécula tapiolítica e microlítica. Estes resultados sugerem que a exploração dos pegmatitos deveria ter em conta o aproveitamento de concentrados de columbite-tantalite com valores prováveis de Ta_2O_5 superiores a 30%, portanto em condições de extracção lucrativa desde que baseada numa lavra selectiva e ordenada. É de supor que outros pegmatitos da mesma região apresentem o mesmo potencial.

Palavras-chave: Pegmatito, Nb-Tantalatos, Tendência de fraccionação, Potencial tantalífero.

Abstract: The Senhora da Assunção pegmatite group located at Ferreira de Aves, Sátão, consists of a pair of coupled intra-granitic pegmatite bodies whose exploration was focused on industrial quartz and feldspar. In the course of mining activity considerable amounts of niobium-tantalates were detected with a profitable potential as by-products. This economic potential justifies the integrated analysis of the distribution of Nb-Ta contents in the different units of the pegmatite, as well as their occurrence modes and trends of fractionation.
Nb-Ta phase minerals are concentrated in albite units of intermediate zones, in giant beryls, in phosphatic units and in a collapse breccia on the southern body. The whole-rock Ta contents are frequently above 150 ppm, which is a reasonable cut-off threshold. The Nb-Ta fractionation is consistent with a LCT – NYF hybrid suite, trending toward tapiolite and microlite members. These results suggest an Nb-Ta potential for the ceramic pegmatites from the entire pegmatite field.

Keywords: Pegmatite, Nb-Tantalates, Fraccionation trends, Ta potential.

CIG-R, Escola de Ciências, Universidade do Minho, Campus de Gualtar, 4710-057 Braga, Portugal.
*Autor correspondente / Correspondent Author: nestafacil@hotmail.com

1. Introdução

Na região de Aguiar da Beira – Penalva do Castelo, os pegmatitos intra-graníticos concentram-se ao longo de uma faixa em arco que passa por Sátão, até Fornos de Algodres, coincidindo com o bordo ocidental do Maciço de Aguiar da Beira. Este maciço é essencialmente constituído por um granito porfiróide de duas micas (mas essencialmente biotítico) tardi-tectónico, cuja granularidade varia de média a grosseira. Nas suas zonas apicais e cúpulas, este maciço exibe estruturas bandadas com feldspatos plumosos em *comb* e diferenciações pegmatóides difusas ou corpos pegmatíticos bem delimitados cujas atitudes acompanham o contorno do plutão granítico. Estas estruturas típicas da cristalização de diferenciados graníticos residuais apresentam por vezes uma configuração em *stocksheider*. Nas zonas com estruturações pegmatóides difusas os encraves são raros. Nas porções imediatamente abaixo os encraves tornam-se mais abundantes e dissipam-se as estruturas pegmatóides. Os xenólitos predominantes são sobremicáceos, *schlieneíticos,* podendo ocorrer também encraves granulares elipsoidais de tendência meso a melanocrata e grão fino – encraves homoeógenos (Trabulo *et al.*, 1995). Em níveis topográficos mais profundos os encraves também se tornam raros, observando-se ligeiro aumento da quantidade relativa dos que são granulares, por vezes aglomerados em corredores - corredores de *mingling* (Guimarães, 2012). Neste nível granítico os pegmatitos de maiores dimensões ocorrem dispersos, com formas irregulares a isodiamétricas, por vezes organizados em rosários ou grupos e pares acoplados. O grupo pegmatítico Senhora da Assunção, constituído por um par de pegmatitos acoplados, corresponde a esta situação (Fig. 1). Os pegmatitos deste grupo podem ser incluídos numa linhagem evolutiva de tipo híbrido LCT/NYF (pegmatitos especializados em Li, Cs e Ta e em Nb, Y e F, respectivamente), e num agrupamento tipológico com berilo, columbite, fosfatos de Li e molibdenite.

No decurso da actividade extractiva sobre quartzo e feldspato que se verificou na jazida de Senhora da

Assunção intersectaram-se unidades paragenéticas com conteúdos não negligenciáveis de nióbio-tantalatos, sugerindo que jazidas deste tipo podem ser encaradas como produtivas em concentrados de Nb e Ta, pelo menos na acepção de subprodutos da lavra dirigida a materiais cerâmicos. Por isso se apresenta uma análise descritiva da

localização destes minérios no jazigo, sugerindo um modelo conceptual para a distribuição e génese das concentrações desses metais, o qual pode ser extrapolado e usado em contexto de valorização de outras jazidas de materiais cerâmicos ocorrentes no mesmo contexto pegmatítico.
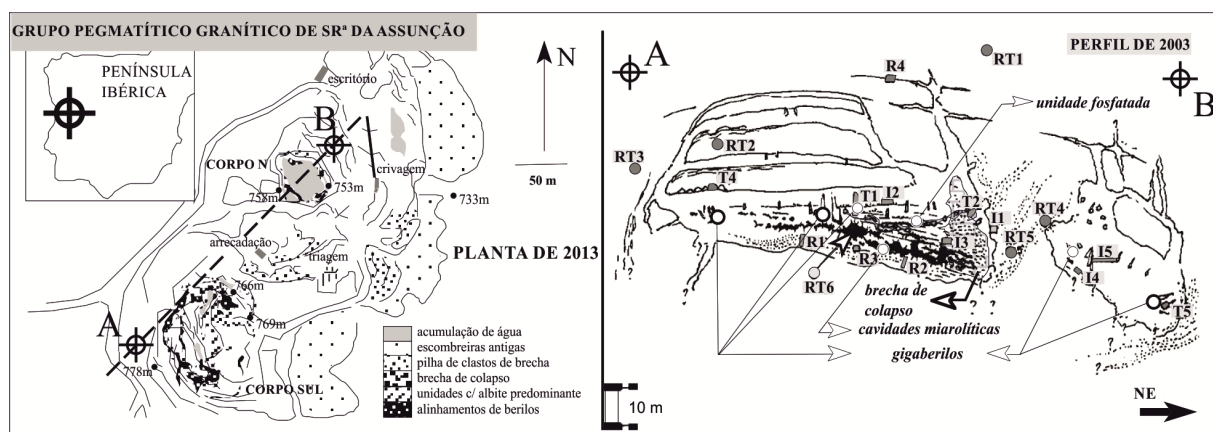

Fig. 1. Esquema representativo do conjunto pegmatítico Senhora de Assunção. Com localização aproximada e planta da exploração em 2013, indicando um perfil A-B executado em 2003. Tipologia das unidades amostradas: RT1 – granito porfiróide essencialmente biotítico de grão médio a grosseiro; RT2 – granito de grão grosseiro a médio essencialmente biotítico; RT3 – *cluster* de fenocristais com alinhamento fluidal e fácies granitóide biotítica; RT4 – granitóide bandado essencialmente moscovítico, com plagioclase; RT5 - granitóide bandado essencialmente moscovítico; RT6 – *mush* cimentado por calcedónia e montmorilonite acumulado em pavimento de megacavidade miarolítica; I1 – Unidade sobremicácea com fosfatos da série triplite-zwiezelite; I2 – moscovite *comb* intercrescida com albite na transição zona intermédia – núcleo de quartzo; I3 – clastos e argilas do bordo de brecha de colapso com crustificações hidrotermais; I4 – banda de moscovite *comb* intercrescida com albite, similar a I2, mas extraída no corpo N; I5 – transição quartzo – feldspática (Na,K) entre zona intermédia e núcleo de quartzo entre dois berilos (gigaberilos); T1 – totalidade de um conjunto de eflorescências periféricas de um berilo – concentrado; T2 – totalidade de um cristal compósito de "ambligonite-montebrasite" com fosfatos secundários e mineralização; T3 – totalidade de uma porção hidrotermalizada (alteração filítica predominante) num gigaberilo; T4 – totalidade de uma protuberância ascendente de pegmatito zonado *pillow*; R1 – roço em *line-rock* com feldspato rubro (canal subvertical transverso à estrutura bandada); R2 - roço em *line-rock* com feldspato claro (canal subvertical transverso à estrutura bandada); R3 – roço em conjunto de duas bandas de relaxação com moscovite+albite predominantes; R4 – roço total transverso em pegmatito com 9 cm de possança e núcleo essencialmente constituído por volframite.

Fig. 1. Schematic representation of the Senhora de Assunção pegmatite group with approximate location and mine draw from 2013, indicating an A-B section from 2003. Typology of sampled units: RT1 - porphyritic biotite granite, mainly medium to coarse grained; RT2 - biotite granite medium to coarse grained; RT3 – phenocrysts cluster with fluidal alignment in biotitic granitoid facies; RT4 - muscovitic banded granitoid, with plagioclase predominance; RT5 - muscovite layered granitoid with plagioclase; RT6 - mush cemented by chalcedony and montmorillonite accumulated in a miarolitic megacavity; I1 – micaceous unit with phosphate from triplite - zwiezelite series; I2 – comb muscovite with intergrown albite in the intermediate zone to quartz core transition; I3 – clasts and clays from collapse breccia edge, with hydrothermal crustifications; I4 - comb muscovitic band intergrown with albite similar to I2 , extracted from the N body; I5 - quartz -feldspar (Na, K) transition from intermediate zone to quartz core, between two beryl cristals; T1 - set of pheryferic efflorescences over beryl – Ta minerals concentrate; T2 - composite crystal of ambligonite - montebrasite with secondary phosphates and associated mineralization; T3 - hydrotermalized portion of a giant beryl crystal; T4 - totality of an ascendent bulbous, zoned pegmatite (pillow); R1 - line-rock with reddish feldspar (subvertical channel tranverse to the banded structure); R2 line-rock with clear feldspar (subvertical channel tranverse to the banded structure); R3 – channel of two relaxation strips with predominant muscovite + albite; R4 – crosscut trench in 9 cm width pegmatite with essentially wolframitic core.

2. Variabilidade geoquímica de metais pegmatófilos no sistema – análise química de rocha total

A análise química de rocha total de amostras recolhidas ao longo do perfil A-B, figura 1, permitiu caracterizar a variação e dispersão dos elementos químicos associados a zonas específicas dos pegmatitos (Tabela 1). De entre a diversidade de elementos analisados, os teores de Nb, Ta, Ti, Sc, W, Pb e U mostram tendências bastante sugestivas de fraccionação interna consistentes com as observações feitas no estudo paragenético e indiciam um padrão de comportamento que pode ser considerado reprodutível e

susceptível de ser extrapolado para jazigos similares do mesmo campo pegmatítico.

Nióbio e Tântalo – os menores teores foram detectados nas amostras de granito biotítico (RT1, RT2 e RT3), sendo evidente um aumento no sentido da zona intermédia - núcleo de quartzo (I2, I4, I5, T2 e T3) e da brecha de colapso (I3 e T2), onde foram determinados os teores mais elevados;

Titânio – os teores apresentam uma redução gradual desde o granito encaixante (RT1, RT2, RT3, RT4 e RT5) até às unidades do interior do pegmatito;

28

Escândio – os maiores teores correspondem às amostras atribuídas a eflorescências (T1) e porções hidrotermalizadas (T3) obtidas nas proximidades de gigacristais de berilo;

Tungsténio – os maiores teores correspondem às amostras I3, T2, R3 e R4 tardias na paragénese e relacionadas com a expressão mineralógica de fosfatos;

Chumbo – os teores mais elevados ocorrem na amostra I1, que incidiu sobre unidades sobremicáceas e fosfatadas e, na amostra R4, correspondente a um roço de veio composto essencialmente por volframite. O Pb aparece, pois, muito relacionado com a presença e génese precoce de minerais de U ou com a formação muito tardia de microlites e pirocloros;

Urânio – teores significativos em diversas unidades do pegmatito, sendo os teores máximos registados na amostra RT6, extraída de uma cavidade miarolítica; os mais reduzidos foram detectados nas amostras de granito encaixante, parecendo existir um claro enriquecimento na transição de granito para pegmatito, mas depois no interior do pegmatito numerosas oscilações podem estar relacionadas com a grande mobilidade do U em ambientes hidrotermais de baixa temperatura e supergénicos.

Tabela 1. Quadro selectivo de análises realizadas em unidades internas diversificadas do pegmatitos de Senhora de Assunção (valores em ppm). * - valores como % em massa de óxidos; n. d. – não determinado; n. a. – não analisado.

Table 1. Selected chemical analysis of samples from diversified inner units of Senhora de Assunção pegmatites (values in ppm). * - values in weight per cent; n.d.- non determinated; n. a. – non analized.

	Ta	Nb	Ti	Sc	Y	W	Zr	Mo	Sn	Bi	Pb	Cu	Zn	U	Rb	Cs	Ba	Sr
RT1	31	46	2920	12	41	26	102	60	30	n.d.	n.d.	11	76	8	299	44	455	173
RT2	18	30	1063	16	30	39	100	n.d.	91	n.d.	n.d.	16	90	12	301	38	190	89
RT3	16	28	841	15	35	56	94	n.d.	26	n.d.	n.d.	22	81	18	425	121	202	112
RT4	161	180	1304	32	42	204	44	n.d.	251	19	n.d.	n.d.	n.d.	107	430	325	216	312
RT5	263	171	918	49	42	212	46	n.d.	312	45	n.d.	n.d.	n.d.	200	612	423	104	89
RT6	301	425	443	291	35	353	458	669	23	502	45	1540	1829	6804	46	2022	30	17
I1	194	254	1352	307	4612	38	1200	4705	19	687	412	1160	410	3020	n.a.	n.a.	n.a.	n.a.
I2	675	532	361	140	2250	112	2341	30	25	28	118	67	46	1324	n.a.	n.a.	n.a.	n.a.
I3	426	484	64	31	240	2308	215	67	n.d.	55	88	86	53	2750	n.a.	n.a.	n.a.	n.a.
I4	500	621	217	136	2306	18	2854	58	21	22	200	33	n.d.	1263	n.a.	n.a.	n.a.	n.a.
I5	183	308	73	30	120	n.d.	53	1023	n.d.	19	n.d.	n.d.	n.d.	103	n.a.	n.a.	n.a.	n.a.
T1	*Ta_2O_5 = 32,8%	*Nb_2O_5 = 45,1%	1200	4025	326	36	325	139	41	22	812	n.d.	n.d.	453	n.a.	n.a.	n.a.	n.a.
T2	412	569	189	20	293	4888	714	29	n.d.	n.d.	162	376	111		n.a.	n.a.	n.a.	n.a.
T3	286	563	73	2250	156	42	236	66	74	44	3601	1017	1150		n.a.	n.a.	n.a.	n.a.
T4	190	303	641	565	321	88									n.a.	n.a.	n.a.	n.a.
R1	101	178	146	36	73	312	66	20	70	n.d.	n.d.	95	104	800	n.a.	n.a.	n.a.	n.a.
R2	96	112	154	n.d.	80	420	34	21	54	n.d.	n.d.	40	114	712	n.a.	n.a.	n.a.	n.a.
R3	843	913	166	32	74	1634 *WO_3	34	26	69	n.d.	n.d.	n.d.	1008		n.a.	n.a.	n.a.	n.a.
R4	88	155	521	31	65	> 63,1%	46	207	144	634	437	1111	288	46	n.a.	n.a.	n.a.	n.a.

Numa selecção de material na exploração foram realizadas separações hidrogravíticas que originaram concentrados de minerais densos. Uma análise química direcionada ao potencial económico foi realizada e os resultados obtidos estão patentes na tabela 2. Constata-se que para o Ta_2O_5 foram apurados teores de 20,64 e 21,669

e para o Nb_2O_5 42,334 e 29,177, o que sugere a viabilidade do aproveitamento destes metais.

Tabela 2. Caracterização composicional de alguns concentrados *coltan* segundo especificações de mercado (normalizadas). Nota: estas amostras são consideradas parageneticamente representativas de concentrados que podem ser obtidos com regularidade – valores em %. n.a. – não analisado.

Table 2. Compositional characterization of some "coltan" concentrates according to market specifications (standard). Note: these samples are considered to be representative of concentrates that can be obtained regularly - (% values). n.a. – non analized.

Nb_2O_5	42,334	29,177
Ta_2O_5	20,64	21,669
MnO	10,353	13,087
FeO	25,446	24,792
U_3O_8	1,227	1,011
Ti	n.a.	5,473
Bi	n.a.	2,93
Pb	n.a.	2,11

2.1. Paragéneses portadoras da mineralização em Ta

De acordo com a terminologia proposta por Cameron *et al.* (1949), que caracteriza as variações texturais e mineralógicas ao longo de um pegmatito com zonamento interno, as mineralizações de Nb e Ta, bem como as suas paragéneses portadoras, encontram-se geralmente mais concentradas nas zonas intermédias dos pegmatitos, podendo também ocorrer na zona nuclear. Nos pegmatitos de Assunção, as paragéneses e unidades portadoras de espécies com Nb-Ta, podem ser muito variadas. A mineralização surge tanto com minerais principais como também com minerais acessórios, em inclusões ou eflorescências. Foram identificaram-se as seguintes unidades portadoras de mineralizações de Nb-Ta (Fig. 2):

Unidades moscovíticas – albíticas – nestas unidades foram identificadas Mn-columbite/tantalite e Fe-columbite com zonamento progressivo;

Unidades inclusas ou em eflorescências na periferia de gigaberilos – apresentam a maior diversidade de mineralizações, desde Fe-columbite, (Ti,Sc)-ixiolite, (Sn,Ti)-ixiolite, (Pb,U)-microlite, Fe-tapiolite e U-pirocloro tanto em inclusão como em eflorescência sobre gigacristais de berilo;

Unidades fosfáticas (litiofilite-trifilite / triplite – zwiezelite) - destaca-se a ocorrência de (Fe, Mn)-columbite e epitaxias de (Sn,W)-ixiolite + Mn-tantalite + Ti-ixiolite + Fe-columbite;

Unidades quartzosas tardias do tipo brecha colapso – nesta unidade predomina largamente Fe-tapiolite.

29

Fig. 2. Representação da diversidade paragenética associada às mineralizações de Nb-Ta, em fotografias de lupa binocular e microscopia de luz reflectida.

Fig. 2. Paragenetic diversity representation of the assemblages with Nb- Ta minerals in reflected light and set of binoculars.

3. Tendências de fraccionação e evolução da mineralização

As tendências de fraccionação dos óxidos de Nb/Ta neste sistema pegmatítico encontram-se sintetizadas no quadrilátero [Ta/(Ta+Nb) vs Mn/(Mn+Fe)] patente na figura 3. Aqui, os diversos vectores de fraccionação representam o ajuste de linhas de tendência às projecções de composições pontuais determinadas em microssonda electrónica. Os programas analíticos foram orientados por imagens de MEV-ER (electrões retrodifundidos) obtidas para secções polidas de cristais extraídos em diferentes unidades internas dos corpos pegmatíticos.

Em termos gerais, o diagrama mostra uma tendência de fraccionação dirigida ao pólo Mn-tantalite, que é truncada nas fases terminais da fraccionação, invertendo para o pólo tapiolite. Detalhadamente, os termos mineroquímicos menos evoluídos encontram-se próximos do pólo Fe-columbite evoluindo no sentido de um enriquecimento em Mn e Ta, originando termos Mn-columbíticos, progressivamente enriquecidos em Ta. Com o decorrer da fraccionação, o enriquecimento em Ta acaba por originar composições atribuíveis à Mn-tantalite. É importante salientar que estas tendências, embora gerais, não são seguidas pela totalidade das amostras analisadas. De facto, a nível intra-cristalino, observam-se algumas tendências de fraccionação inversas, como é o caso de RT6 e I1 (empobrecimento em Ta). Ainda a nível de tendências mais generalizadas é de salientar uma convergência paroxismal de todas as tendências no sentido da Fe – tapiolite que é um óxido típico das unidades paragenéticas mais evoluídas e, em especial, da brecha de colapso (I3) e das eflorescências sobre gigacristais de berilo (T1).
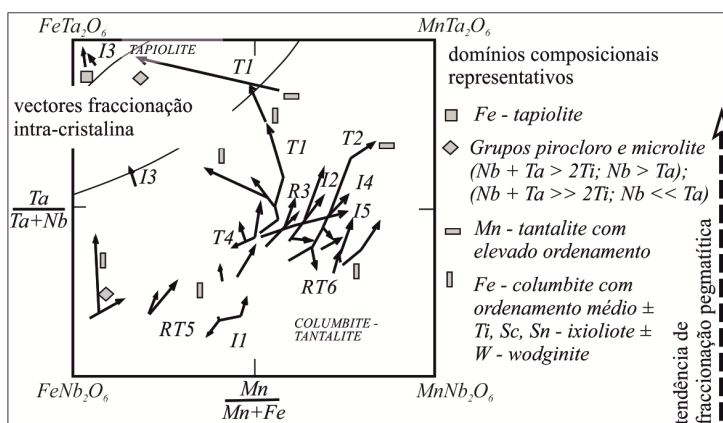

Fig. 3. Composições de minerais portadores de Nb-Ta representadas no quadrilátero da columbite-tantalite, destacando tendências de fraccionação intra-cristalinas e intrapegmatíticas. Composições obtidas por análise em microssonda electrónica de cristais individualizados. Valores em apfu. Para a representação das microlites, piocloros e ixiolites só foram ponderados os teores de Nb, Ta, Mn e Fe.

Fig. 3. Analysis of Nb-Ta bearing minerals plotted in columbite-tantalite quadrilateral. Fractionation trends highlighted corresponds to individual crystal and pegmatite units. Compositions obtained by electron microprobe and exposed as apfu. For microlites, pyrochlores and ixiolites only the contents of Nb, Ta, Mn and Fe were considered.

4. Discussão e conclusões

Os teores de Nb e Ta, (Tabela 1), aumentam de forma generalizada no sentido da maior fraccionação pegmatítica. Os teores mais elevados ocorrem em zonas intermédias e em unidades tardias onde também ocorrem os valores mais altos da razão Ta/Nb. A elevada solubilidade do Nb e Ta em diferenciados graníticos residuais, comprovada em trabalhos experimentais é consistente com as constatações acima expostas (Tindle & Breaks, 2000).

No decurso da fraccionação, para além da variação dos teores, verifica-se ainda diversificação das espécies minerais que expressam aqueles metais, não só correspondendo à evolução dos domínios de estabilidade das fases portadoras, mas também como uma resposta aos produtos de solubilidade e variações de abundância relativa localizadas, seguindo sempre uma tendência geral de enriquecimento tantalífero. Os baixos teores de Nb-Ta encontrados no granito encaixante podem ser explicados pela escassez de minerais acessórios que possam alojar Ta e Nb (especialmente, rutilo e ilmenite), mas também devido ao marcado comportamento higromagmáfilo destes metais, quando estão disponíveis fluidos residuais abundantes.

Em ambiente pegmatítico, no decurso da fraccionação interna, desenvolve-se uma sequência de cristalização oscilatória que é comum neste tipo de pegmatitos (Tindle & Breaks, 2000), marcada pela ocorrência inicial de Fe-columbite e Mn – columbite (evidenciando por vezes um zonamento interno inverso), que evolui posteriormente para termos mais ricos em Mn e Ta (Mn - columbite e mesmo Mn - tantalite). O zonamento oscilatório pode ser atribuído à imiscibilidade incompleta ou à existência de ambientes de cristalização caracterizados por equilíbrio flutuante da incorporação de Nb, Ta, Mn e Fe, que resulta na distribuição rítmica de zonas com diferentes relações Nb/Ta - sem que sejam necessárias grandes variações de P e T. A incorporação do Sc-Ti-Sn em ixiolites circunscreve-se a epitaxias na periferia ou inclusão em berilo. A presença destes metais nos diferenciados residuais, manifestam-se também em ocorrências de bazzite e thortveitite identificadas em eflorescências no berilo. Existe, aparentemente, uma muito marcada favorabilidade da partilha destes metais raros no sentido dos ambientes onde crescem os gigaberilos.

O pirocloro, a U- Pb microlite e ferberite, restringem-se à fase final da fraccionação, já em *subsolidus*. A incorporação de U e Pb nestas fases marca a evolução para um estado pneumatolítico/hidrotermal que se pode considerar característico de linhagens híbridas LCT/NYF, por sua vez também típicas de pegmatitos internos, relativamente a plutões graníticos, tardi-tectónicos Variscos. Também, caracteristicamente, a ferberite e a volframite acompanham as parágéneses terminais destes pegmatitos

As unidades parageneticas mais enriquecidas em Nb-tantalatos situam-se nas zonas intermédias: em faixas periféricas onde nucleiam os gigaberilos e na transição entre a moscovite em bandas e a albite monominerálica.

Esta distribuição revela-se consistente com o zonamento paragenético proposto por Cameron *et al.* (1949), no qual os enriquecimentos em Nb-tantalatos tendem a ocorrer nas zonas intermédias dos pegmatitos.

A formação de Fe-tapiolite generaliza-se na brecha de colapso e representa a tendência evolutiva final da fraccionação dos Nb-tantalatos. Ter-se-á provavelmente originado no decurso da interacção hidrotermal promovida pelo colapso e digestão parcial da zona intermédia afectada, possivelmente, pela contaminação dos fluidos face a reacções de dissolução da Fe-columbite primitiva. A presença de F controla a fraccionação do Mn, promovendo a sua cristalização e sequestro após o Fe (Cerny *et al.*, 1986; Tindle & Breaks, 2000). A ocorrência de pirocloro e sobretudo da microlite comprovam um enriquecimento ainda mais tardio em F e OH, responsável pela cristalização de ambas as fases minerais, em regime *subsolidus*.

No que respeita à estrutura cristalina dos portadores de Nb-Ta, a tendência de fraccionação desenvolve-se no sentido do menor ordenamento, iniciando-se com a cristalização de columbite-tantalite (típica de alto a médio ordenamento), evoluindo posteriormente para a ixiolite (baixo ordenamento) e mais tardiamente para pirocloro e microlite.

Embora o aproveitamento das mineralizações em Nb-Ta não se tenha verificado na mina de Assunção, os teores de Ta encontrados na generalidade das amostras de rocha total (Tabela 1) sugerem a possibilidade de prevalecerem teores médios acima de 150 ppm, que representa um teor de corte razoável em muitas jazidas pegmatíticas consideradas produtivas para Ta. Os valores de Ta_2O_5 encontrados em análises de concentrados apurados por fraccionação hidrogravítica, localizam-se acima da barreira de 30%, (Tabela 2), que condiciona a atribuição dos mais altos preços unitários, aos concentrados de columbite-tantalite. Justifica-se pois equacionar o aproveitamento de Nb e Ta em muitos dos pegmatitos intra-graníticos cerâmicos do maciço de Aguiar da Beira.

Referências

Cameron, E.N., Jahns, R.H., McNairn, A.H., Page, L.R., 1949**.** Internal structure of granitic pegmatites. *Economic Geology*, Monograph, 2 p.

Cerny, P., Goad, B.E., Hawthorne, F.C., Chapman, R., 1986. Fractionation trends of the Nb- and Ta-bearing oxide minerals in the Greer Lake pegmatitic granite and its pegmatite aureole, southeastern Manitoba. *American Mineralogist*, **71**, 501-517.

Guimarães, D., 2012. *Cinemática da mobilidade pegmatítica em enxames epi a mesocorticais: modelos conceptuais aplicados à prospecção.* Tese de mestrado, Universidade do Minho (não publicada), 104 p.

Tindle, A.G., Breaks, F.W., 2000. Columbite-tantalite mineral chemistry from rare-element granitic pegmatites: Separation Lake area, N.W. Ontario, Canada. *Mineralogy and Petrology*, **70**, 165-198.

Trabulo, L.C., Leal Gomes, C., Lopes Nunes, J.E., 1995. Enquadramento geológico, estrutura e paragénese do grupo pegmatítico de Senhora da Assunção – Aguiar da Beira – centro de Portugal. *Publicações do Museu e Laboratório Mineralógico e Geológico da Universidade do Porto*, **Memoria nº4**, 837-841.

31

September 13th, afternoon: STOP 3: Gonçalo Mine
(Gonçalo pegmatitic field, Guarda-Belmonte, Portugal)

**Travel from Senhora da Assunçao pegmatite to Gonçalo mine:
100km; ≈ 1h30min**

Locality 3: Gonçalo pegmatitic field (Guarda-Belmonte, Portugal)
Stop 3 (13th of September, afternoon)

General Highlights
-Over one hundred of aplite-pegmatite subhorizontal sills, grouped in 3 types: simple, amblygonite-rich and lepidolite ± petalite-rich.
-Tabular bodies with thicknesses between a few centimeters up to 15 m, hosted by a late-D3, biotite>muscovite granite, locally strongly metasomatized.
-Blue topaz and montebrasite centimetric pods may be common.
-Usually no internal structure or quartz core is observed. In the lepidolite-rich sills a layering with alternating lepidolite-rich and albite-rich fine grained bands may be observed.
-The sills are related to the extreme fractional crystallization of a fine- to medium-grained porphyritic biotite>muscovite granite (late D3).
-The sills are being mined for feldspar + Li.

Stop 3: A) Intragranitic aplite-pegmatite sill showing a layered internal structure with alternating lepidolite-rich and albite-rich bands; and, B) Detail of A, where a coarse K-feldspar crystals grows perpendicularly to the layers, and these envelope it upwards (in the sense of the crystallization of the dyke).

INTRODUCTION
Lithium-rich aplite-pegmatite sills are abundant in the Gonçalo field of the Guarda-Belmonte region. The high Li+F contents attained by the most fractionated melts allowed the massive crystallization of F-rich, F+Li-rich and Li-rich phases, such as topaz, lepidolite, amblygonite and petalite, in proportions >35 % volume of the rocks. This is one of the most extreme enrichment in

these elements observed in the CIZ. The occurrence in this area of four different granites, one of the acting as the hosting rock of the sills, add even a higher scientific interest to try to decipher the petrogenetic relationship between these granites and between them and the aplite-pegmatites. In this sense, the Gonçalo field has been studied extensively by some Portuguese geologists, with a number of interesting publications, including the Ph D. Thesis of Ramos (1998), and some international papers (e.g. Neiva & Ramos, 2009; 2010). Besides the scientific interest, these pegmatites show an important economic interest. They are being mined during the last decade for feldspar + Li by the Portuguese company FELMICA. Moreover, the layered texture that may be observed in the most fractionated sills, with deep-purple lepidolite-rich bands alternating with pure-whitish ones, gives some of these outcrops an outstanding beauty. All this taken together makes the Gonçalo aplite-pegmatite field one of the most interesting places to be visited in the Central Iberian Zone from a geological point of view.

GENERAL GEOLOGY OF THE GRANITES AND THE APLITE-PEGMATITES
(taken from Neiva & Ramos, 2009)
"The Guarda-Belmonte area lies within the Central Iberian Zone of the Iberian Massif. Granites intruded the Cambrian schist-metagraywacke complex, and were emplaced relatively to the third Variscan deformation phase (D3) (Fig. 6). Coarse- to very coarse-grained porphyritic biotite>muscovite granite (G1), fine- to medium-grained porphyritic biotite>muscovite granite (G2) and coarse-grained porphyritic biotite >muscovite granite (G3) are late-D3 and medium- to coarse-grained muscovite>biotite granite (G4) is post D3. U-Th-Pb age by SHRIMP for G1 and U-Pb ages by ID-TIMS for the other granites indicate 301±3 Ma for G1, G2 and G3 and 293.9±0.5 Ma for G4. G1 passes gradually to G4. G2 intruded G1 showing sharp contacts and passes gradually to G3. G4 intruded G3 nd the contacts are sharp. Granites G1, G3 and G4 are cut by many aplite-pegmatite sills and quartz veins and some mafic rock veins.
Aplite-pegmatite sills from Gonçalo intruded G1, are subhorizontal, trending NE-SW, 10-25°NE, N-S, 20°E and NNE-SSW, 20°E and up to 4 km long (Fig. 7). The sills are from a few centimetres up to 15 m thick for amblygonite-subtype and up to 5 m thick for lepidolite-subtype."…"The aplite-pegmatite sills produced a metasomatic zone enriched in zinnwaldite, albite and tourmaline of 2-3 cm up to 20 m thick in host granite G1. The sills are cut by late aplite, pegmatites veins, quartz veins and mafic rock veins (Ramos, 1998)."
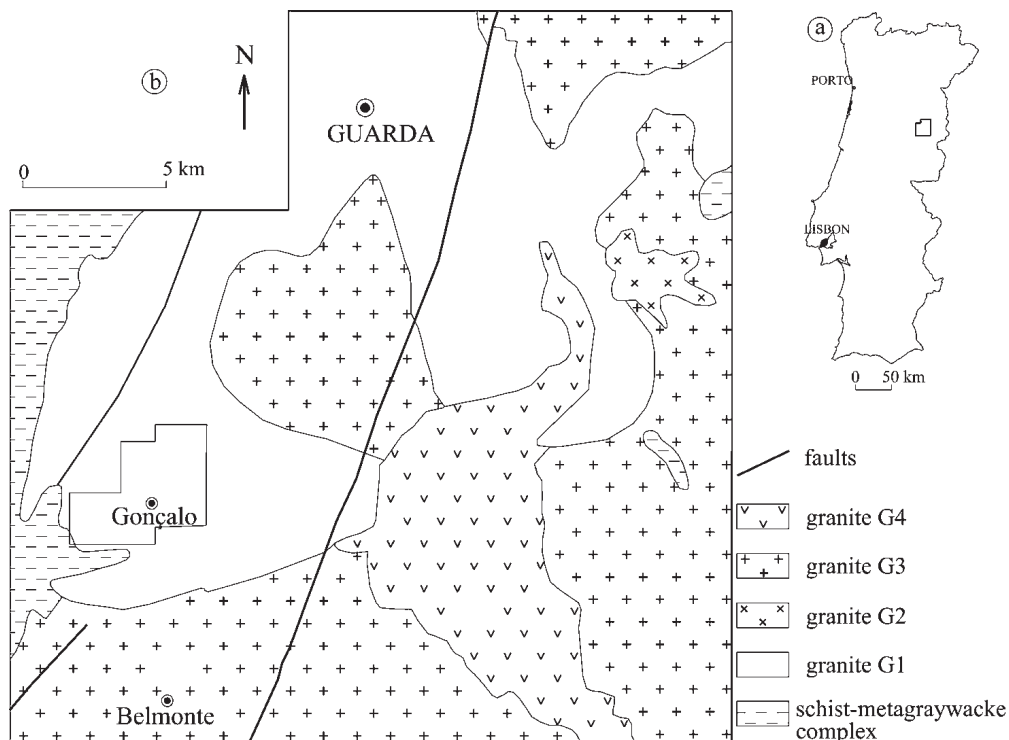

Fig. 6: (a) Location of the Guarda-Belmonte area on the map of Portugal. (b) Simplified geological map of the Guarda-Belmonte area, mainly to show the granites and location of the Gonçalo area. (Neiva & Ramos, 2010).

PETROGENESIS
(taken from Neiva & Ramos, 2009)
"Fractionation trends in variation diagrams of major and trace elements for granites G2 and G3 and aplite-pegmatite sills (Fig. 8), subparallel whole-rock REE patterns, similar ^{18}O values and compositions of feldspars and primary muscovite suggest that aplite-pegmatite sills are derived from granite G2 magma by fractional crystallization of quartz, potash feldspar, plagioclase, biotite and ilmenite, which is supported by modelling of trace elements. There was also fractionation of: a) monazite responsible for depletion in LREE; b) zircon that caused decrease in HREE and Zr contents; c) apatite responsible for depletion in MREE and HREE from G2 to G3 to aplite-pegmatite sills. Fractional crystallization was responsible for Sn and Li enrichments in granite G3 and aplite-pegmatite sills (Fig. 8) reaching the highest concentrations in lepidolite-subtype sills."
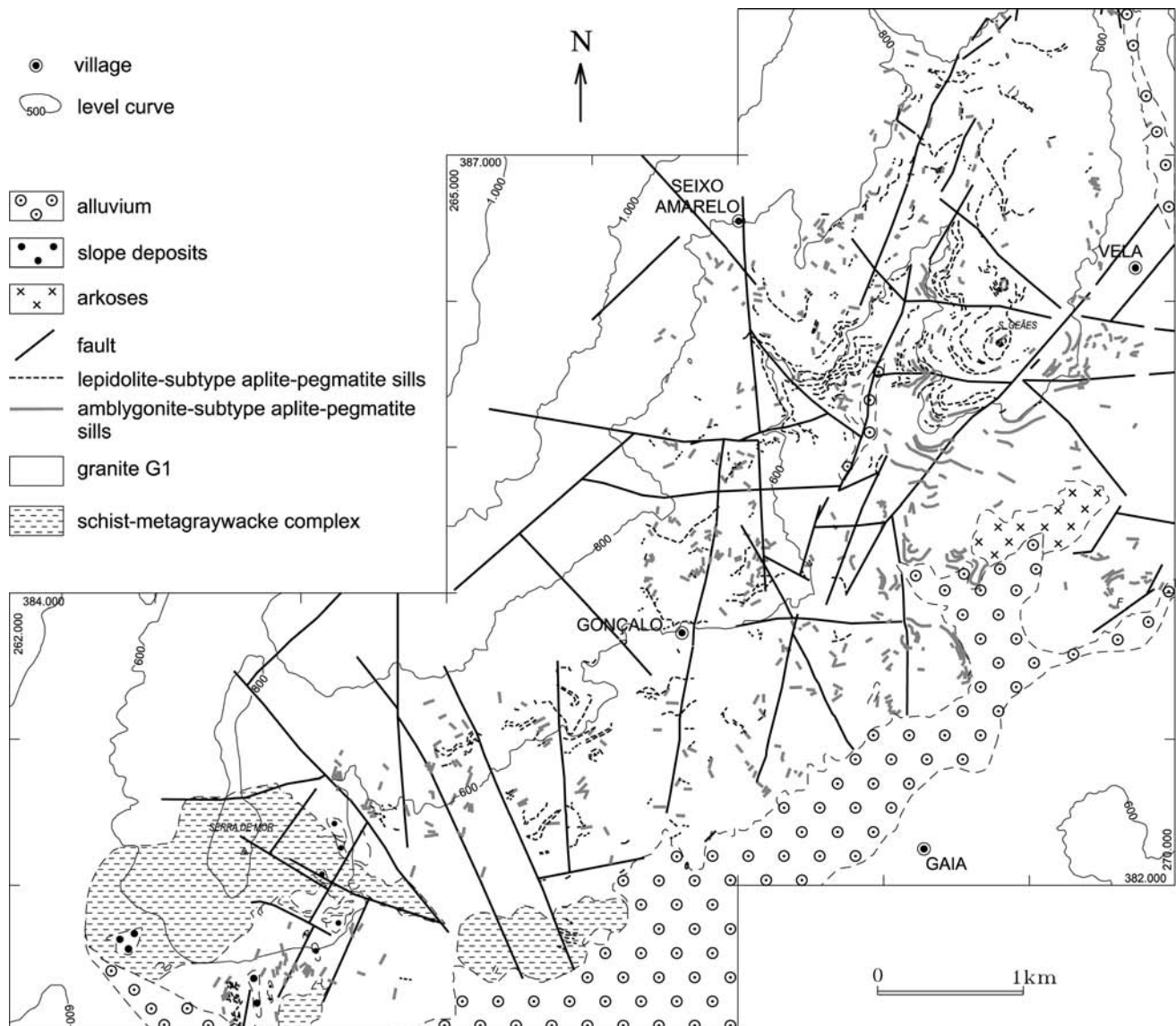

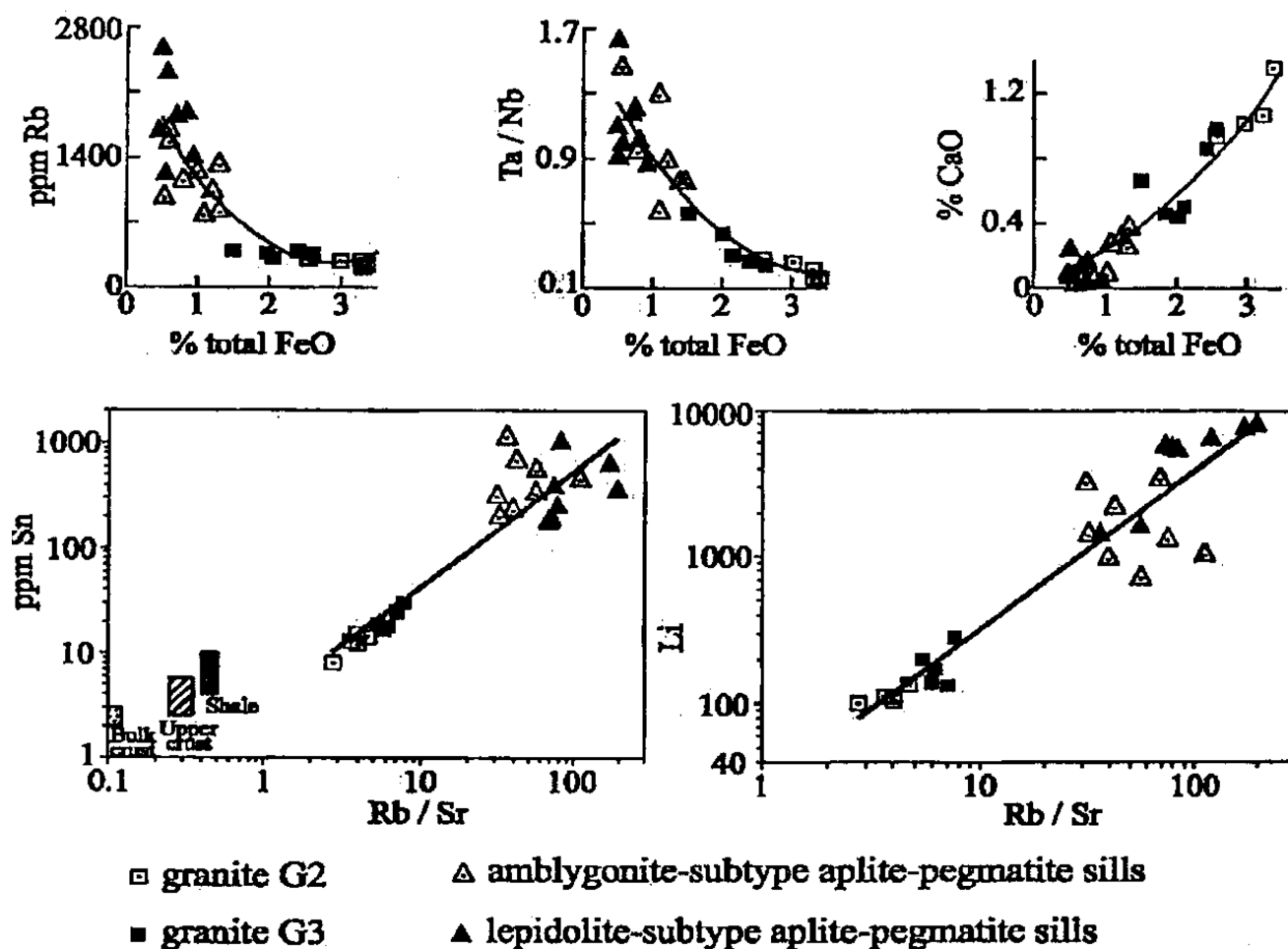Fig. 7. Geological map of the Gonçalo (Guarda) area. (Neiva & Ramos, 2010)

Fig. 8: Selected variation diagrams and log Rb/sr-log Sn and log Rb/Sr-log Li correlations for two biotite>muscovite granites from Guarda-Belmonte area and granitic aplite-pegmatite sills from Gonçalo, central Portugal, indicating a crystal fractionation series. (Neiva & Ramos, 2009)

Geochemistry of granitic aplite-pegmatite sills and petrogenetic links with granites, Guarda-Belmonte area, central Portugal

ANA M.R. NEIVA[1,*] and JOÃO M.F. RAMOS[2]

[1] Department of Earth Sciences, and Geosciences Centre, University of Coimbra, 3000-272 Coimbra, Portugal
*Corresponding author, e-mail: neiva@dct.uc.pt
[2] LNEG, National Laboratory of Energy and geology 4466-956 S. Mamede de Infesta, Portugal

Abstract: Granitic amblygonite-subtype and lepidolite-subtype, aplite-pegmatite sills intruded a biotite>muscovite granite (G1). Two other biotite>muscovite granites (G2 and G3) and a muscovite>biotite granite (G4) crop out in the area. Variation diagrams for major and trace elements of the Variscan rocks show fractionation trends for a) G1 and G4; b) G2, G3 and aplite-pegmatite sills. The two series are confirmed by the two trends defined by major elements of primary muscovite. The sills also contain Li-bearing muscovite, which has higher Mn, Li, F and paragonite contents and lower Al^{VI} content than primary muscovite from G2, G3 and sills. All sills have pure albite and P_2O_5 content of K-feldspar and plagioclase increases in the series G2, G3 and sills. Beryl occurs in all sills, but lepidolite and a nearly pure petalite only occur in lepidolite-subtype sills, which are the most evolved sills. Primary topaz and amblygonite have a similar composition in all sills. Aplite-pegmatite sills contain cassiterite, which shows sequences of alternating darker and lighter zones. The former are richer in (Nb + Ta + Fe + Mn) than the latter. Manganocolumbite is common in all sills, but ferrocolumbite only appears in amblygonite-subtype sills and manganotantalite in lepidolite-subtype sills. The sills richest in Li contain reversely-zoned crystals with a homogeneous microlite core and a heterogeneous uranmicrolite rim. Least squares analysis of major elements shows that granite G3 and amblygonite-subtype and lepidolite-subtype aplite-pegmatite sills can be derived from granite G2 magma by fractional crystallization of quartz, plagioclase, K-feldspar, biotite and ilmenite. Modelling of trace elements shows good results for Sr, but magmatic fluids controlled the Rb and Ba contents of the aplite-pegmatite sills and probably also their Li, F, Sn and Ta contents and crystallization of lepidolite, cassiterite and Nb–Ta oxide mineral assemblage. Schorl from the lepidolite-subtype sills that cut granite G1 has higher Mg/(Mg + Fe) than schorl from metasomatised granite at sill walls and resulted from the mixing of magmatic fluids carrying B and some Fe with a meteoric fluid that has interacted with the host granite G1 and carried Fe and Mg. Schorl and dravite, respectively from metasomatised granite and micaschist at sill walls, were also formed from the mixing processes.

Key-words: granites, aplite-pegmatite sills, feldspars, micas, Sn- and Li-enrichments.

1. Introduction

Most researchers are of the opinion that pegmatites are derived from granitic melts (*e.g.*, Jahns & Burnham, 1969; London, 1992, 2005, 2008; Simmons & Webber, 2008). The chemical composition of granites, aplites, pegmatites and their feldspars and micas gives important information for petrogenesis and favours fractional crystallization of a granite magma (*e.g.*, Breaks *et al.*, 2005; Černý, 2005; Neiva *et al.*, 2008 and references therein). Experimental work also supports this mechanism and, according to London (2008), the rare element pegmatites can only be derived by the protracted and very efficient fractional crystallization of large volumes of granite magma (London, 2008). However this mechanism is difficult to test for pegmatites (*e.g.*, Shearer *et al.*, 1992; Neiva *et al.*, 2008), due to the presence of fluxes such as B, F, P and Li in addition to H_2O in the formation of rare element pegmatites

(London, 1992, 2005), which are responsible for the crystallization of several minerals such as tourmaline, topaz, montebrasite-amblygonite and lepidolite, and influence in the crystallization of cassiterite, columbite-tantalite and microlite (*e.g.*, Linnen & Cuney, 2005). This paper presents the mineralogy, geochemistry and petrology of granites from the Guarda-Belmonte area and aplite-pegmatite sills from Gonçalo within this area, using the data to identify the possible mechanisms responsible for the origin of these rare-element pegmatites.

2. Geology

The Guarda-Belmonte area (Fig. 1a) lies within the Central Iberian Zone of the Iberian Massif. This massif corresponds
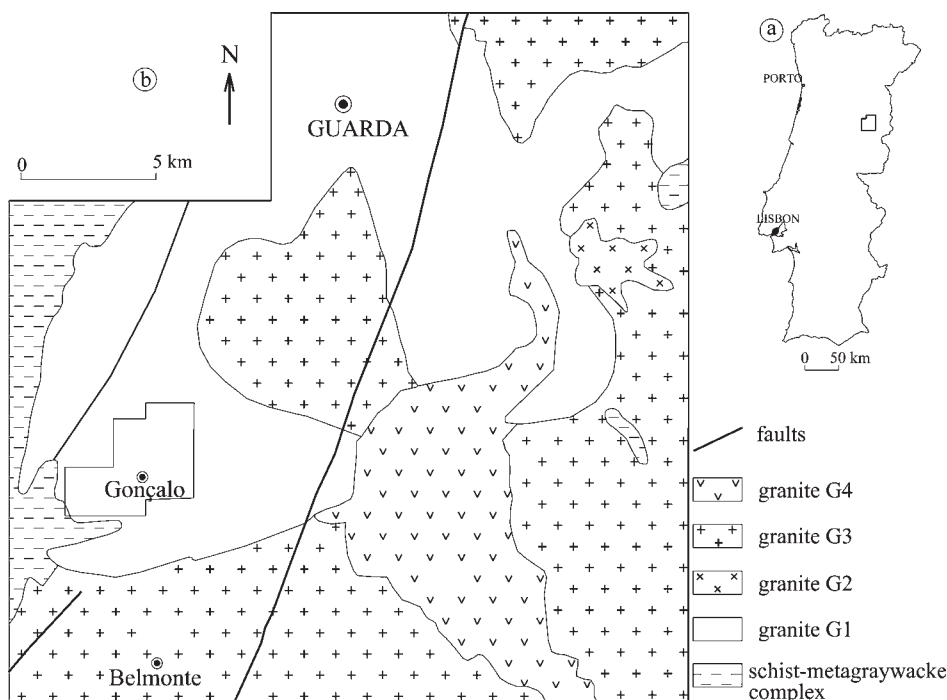
Fig. 1. (a) Location of the Guarda-Belmonte area on the map of Portugal. (b) Simplified geological map of the Guarda-Belmonte area, mainly to show the granites and location of the Gonçalo area.

to the south-western extension of the European Variscan Belt. Variscan granites predominate in the area and intruded the Cambrian schist-metagraywacke complex (Fig. 1b). The coarse- to very coarse-grained porphyritic biotite>muscovite granite (G1), fine- to medium-grained porphyritic biotite>muscovite granite (G2) and coarse-grained porphyritic biotite>muscovite granite (G3) are late-D3 and the medium- to coarse-grained muscovite>biotite granite (G4) is late- to post-D3. The SHRIMP U–Th–Pb monazite age from G1 is 304.1 ± 3.9 Ma. The ID-TIMS U–Pb zircon and monazite ages are 299.8 ± 0.6 Ma from G2, 301.1 ± 2.2 Ma from G3 and 299 ± 3 Ma from G4. Granite G2 intruded G1 showing sharp contacts and passes gradually to G3. Granite G4 intruded G1 and G3 and the contacts are sharp with G3. Granite G2 also crops out in the east of this area outside of Fig. 1. Granites G1, G3 and G4 are cut by numerous aplite-pegmatite sills, some quartz veins and some mafic rock veins (Ramos, 1998).

The Gonçalo area (Fig. 1b) was selected to study aplite-pegmatite sills (Fig. 2), which are subhorizontal, trending NE–SW, 10°–25° NE, N–S, 20° E and NNE–SSW, 20° E, up to 4 km long and from a few centimetres to 15 m thick in amblygonite-subtype sills, and up to 5 m thick in lepidolite-subtype sills. Most sills intruded granite G1, showing sharp and quite lineal contacts and locally produced a metasomatic zone enriched in zinnwaldite, albite and tourmaline from 2–3 cm up to 20 cm thick at footwall and hanging wall. Only a few sills intruded the Cambrian schist-metagraywacke complex and produced a metasomatic zone up to 10 cm thick at footwall and hanging wall and enriched in zinnwaldite and tourmaline. The lepidolite-subtype aplite-pegmatite sills crop out

at higher levels than the amblygonite-subtype aplite-pegmatite sills, and they do not cut each other anywhere because they intruded subhorizontal faults of the same vein field. The number of aplite-pegmatite sills is hard to define, but there are tens of them. The lepidolite-subtype aplite-pegmatite sill tends to be the most abundant in the Gonçalo area (Fig. 2). The simplest sill consists of either amblygonite-subtype or lepidolite-subtype pegmatite (Fig. 3a, b). Others are more complex, some with alternating layers of aplite, amblygonite-subtype pegmatite and lepidolite-subtype pegmatite (Fig. 3c, d) and others with a layer of early aplite at the footwall followed by alternating layers of lepidolite-bearing aplite and lepidolite-subtype pegmatite (Fig. 3e, f). The most common number of layers is 6–7, but some sills have up to 14–15 alternating layers (Fig. 3e, f). Rarely, an enclave of metasomatised granite occurs between layers (Fig. 3f), but all sills show metasomatised granite at the contact with footwall and hanging wall (Fig. 3). In general, aplite is found at the footwall (Fig. 3c, e, f) and either aplite or pegmatite occur at the hanging wall (Fig. 3c–f). Pegmatite is more abundant than aplite. Aplite-pegmatite sills are cut by late aplite, pegmatite veins, quartz veins and mafic rock veins (Ramos, 1998).

3. Petrography

The granites from Guarda-Belmonte area (Fig. 1) contain quartz, microperthitic microcline, plagioclase, biotite, chlorite, muscovite, zircon, apatite, monazite, ilmenite and rutile. Andalusite only occurs in G3. They have subhedral granular texture and show some evidence of cataclasis, particularly in
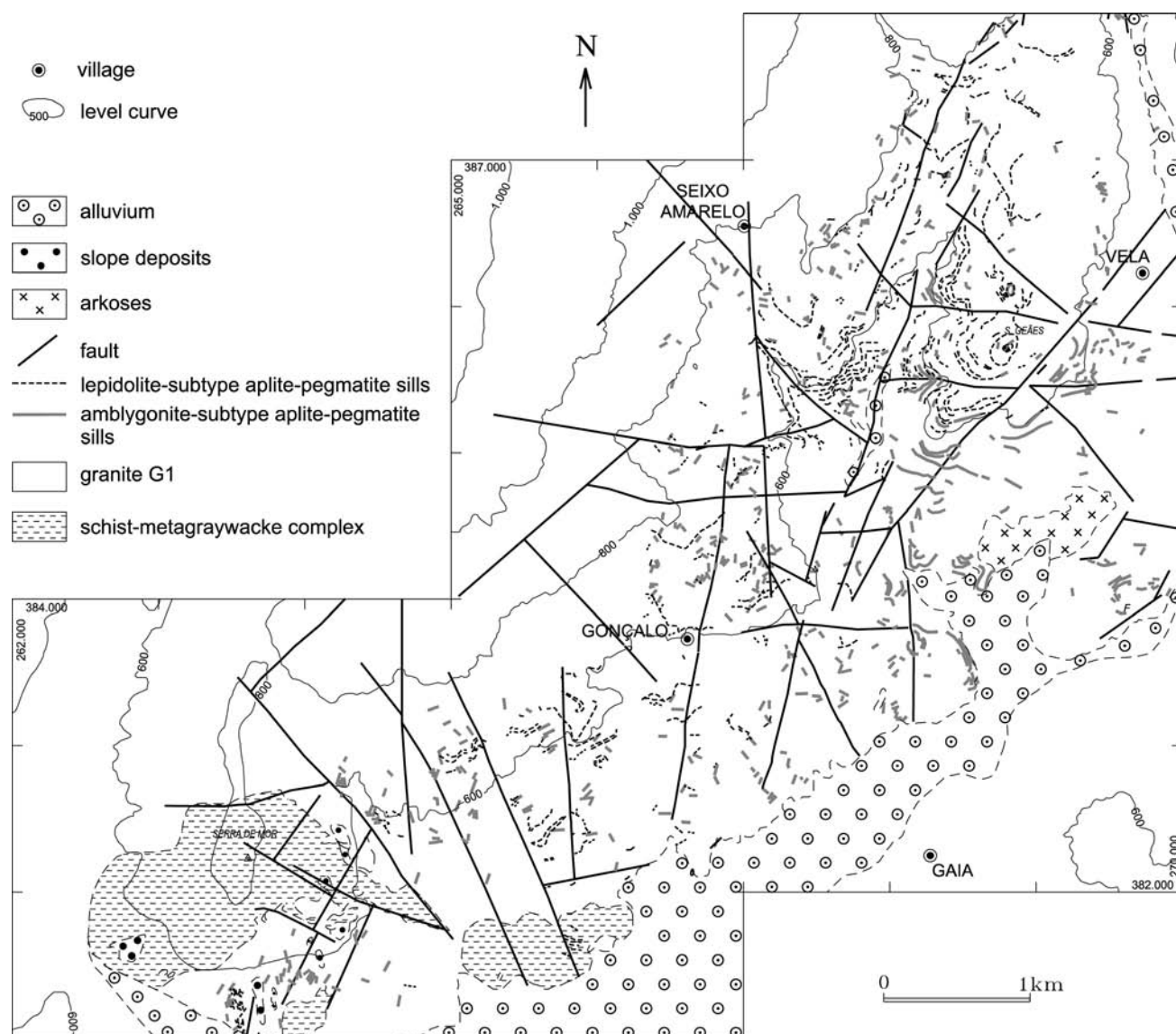
Fig. 2. Geological map of the Gonçalo (Guarda) area.

the quartz. Most of them contain phenocrysts of microcline and plagioclase, except G4 (Ramos, 1998). Some petrographic characteristics of the two main aplite-pegmatite sills from Gonçalo (Fig. 2 and 3) are given in Table 1.

3.1. Quartz

Quartz is anhedral and contains inclusions of all minerals in granites and aplites. Quartz from pegmatites is mainly milky and anhedral, but grey quartz locally zoned and rare pink quartz forming aggregates with albite also occur. Four generations of quartz are distinguished. Quartz is associated with albite and muscovite in aplitic layers at the footwall and hanging wall. Euhedral quartz occurs included in K-feldspar. Subhedral, but mainly anhedral

quartz is associated with albite. Late fine-grained quartz replaces albite and lepidolite.

3.2. Feldspars

In general, K-feldspar and plagioclase are subhedral, except in aplites where they are anhedral but euhedral feldspars also occur in pegmatites. Microperthitic microcline in granites, aplites and pegmatites shows well defined cross-hatch twinning, but orthoclase from aplites and pegmatites is twinned according to the Carlsbad law. K-feldspar from pegmatites is mainly microcline with triclinicity ($\Delta = 12.5\ (d_{131} - d_{1\bar{3}1})$) of 0.89–1.0. The amount of K-feldspar decreases and that of albite increases towards lepidolite-subtype sills. Microperthitic K-feldspar presents albite lamellae and contains inclusions of plagioclase. Late
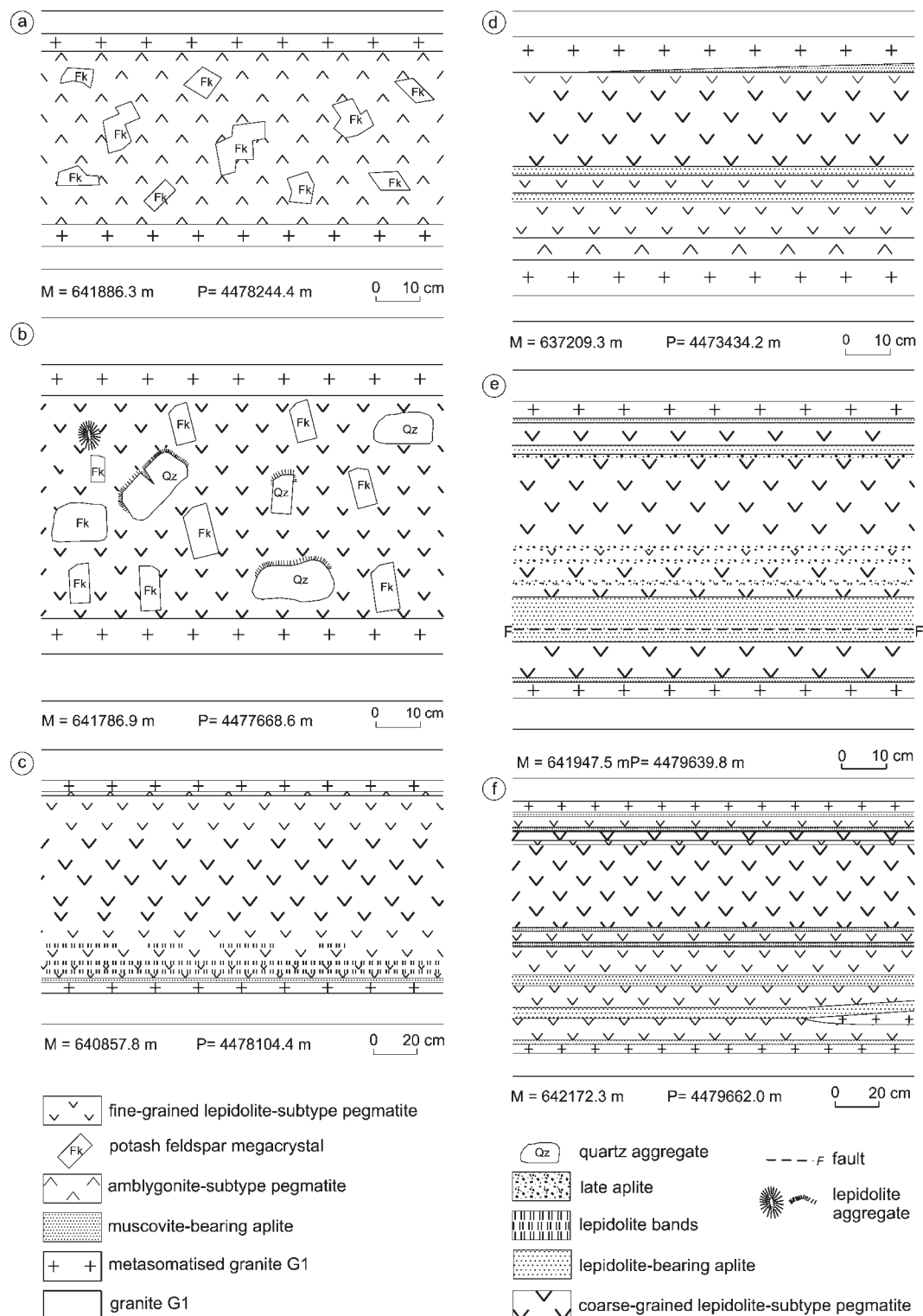
Fig. 3. Sketches of aplite-pegmatite sills from Gonçalo (Guarda). (a–f) From the simplest to those containing up to 14–15 layers.

albite replaces K-feldspar in pegmatites. Granites contain albite-oligoclase in the groundmass, except G4 which has albite. All granites contain phenocrysts of microcline, which are rare in G4. Granites G1 and G3 also contain phenocrysts of albite-oligoclase and granite G2 has phenocrysts of albite-andesine.

3.3. Micas

Biotite and primary muscovite from granites are subhedral and have inclusions of zircon, apatite and monazite. Locally biotite is transformed into chlorite. Primary muscovite is anhedral in aplites and subhedral in pegmatites. Muscovite

Table 1. Some petrographic characteristics of the two main granitic aplite-pegmatite sills from Gonçalo, central Portugal.

	Amblygonite-subtype	Lepidolite-subtype
Main constituents	quartz, microperthitic orthoclase and microcline, albite	quartz, microperthitic orthoclase and microcline, albite
Subordinate and accessory minerals	muscovite, Li-bearing muscovite, topaz, beryl, schorl, zircon, apatite, amblygonite, monazite, cassiterite and columbite-tantalite	muscovite, Li-bearing muscovite, topaz, beryl, schorl, zircon, apatite, amblygonite, monazite, petalite, lepidolite, cassiterite, columbite-tantalite, microlite, torbernite, antunite and rare arsenopyrite, pyrite and chalcopyrite
Texture	anhedral granular in aplite and subhedral granular in pegmatite	anhedral granular in aplite and subhedral granular in pegmatite
Grain size	fine-grained aplite and mainly coarse-grained, but locally fine-grained pegmatite (< 2mm)	fine-grained aplite and mainly coarse-grained, but locally fine-grained pegmatite (< 2mm)

The petrographic characteristics are given by Ramos (1998). Orthoclase and microcline were identified by XRD and chemically.

occurs associated with albite and quartz in all sills, but is more abundant in lepidolite-subtype aplite-pegmatite sills than in the amblygonite-subtype sills. Two generations of lepidolite were found, one coarse-grained and the other late fine-grained (Fig. 4a), in pegmatites, which are abundant and locally radial. The fine-grained lepidolite occurs within the sills and locally it is the only lepidolite. It occurs neither at the hanging wall or in concentrations, suggesting that it was not formed during greisenization.

3.4. Tourmaline

Schorl is very rare in amblygonite-subtype aplite-pegmatite sills and rare in lepidolite-subtype aplite-pegmatite sills. Crystals are < 1 mm in the former and < 2 × 1 mm in the latter. Schorl is subhedral, interstitial, unzoned, dark in colour and does not show any preferential orientation. It occurs associated with albite and muscovite in sills, but close to the contact with the host rock. Schorl from

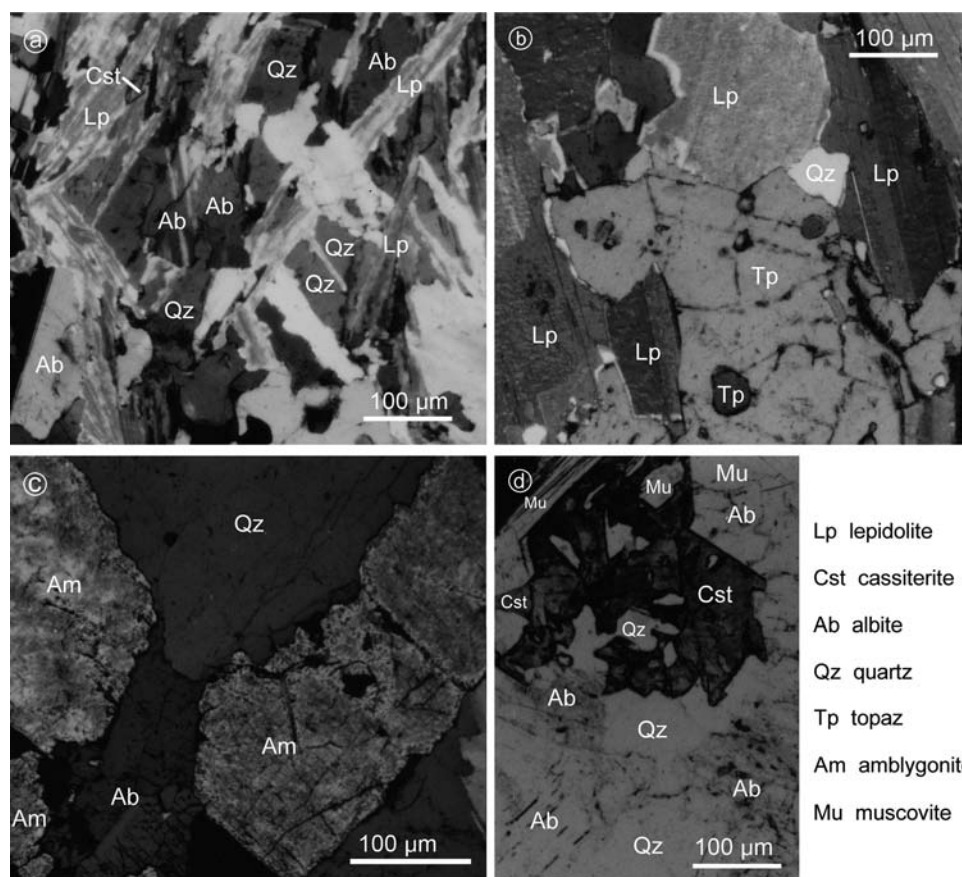
Fig. 4. Images of some minerals from the Gonçalo aplite-pegmatite sills. (a) Lepidolite (Lp) containing inclusions of cassiterite (Cst) and penetrating albite (Ab) and quartz (Qz); (b) topaz (Tp) crystal containing inclusions of an earlier topaz and penetrated by lepidolite (Lp); (c) amblygonite (Am) penetrated by quartz and albite; (d) zoned cassiterite crystal replacing quartz and muscovite.

metasomatised granite and dravite from metasomatised micaschist at the aplite-pegmatite sill walls are subhedral to anhedral, dark in colour, 1–5 mm long and 0.3–0.5 mm thick, replace muscovite and are more abundant than schorl in sills.

3.5. Other silicates

Subhedral greenish blue topaz occurs in all sills and is more abundant in the hanging wall than the footwall. It is particularly abundant in lepidolite-subtype sills. Locally, topaz forms aggregates up to 5 cm in diameter. Two generations of topaz occur, with the earlier one included in a later generation (Fig. 4b). It is associated with quartz and surrounded by albite. Locally it is penetrated by late fine-grained lepidolite and albite. Beryl occurs associated with quartz and K-feldspar in the aplite-pegmatites sills. It is euhedral to subhedral, mainly green in colour, but very rare pink crystals also occur in sills containing lepidolite. Some crystals are partially replaced by albite. Petalite occurs in euhedral to subhedral crystals of 2×1 cm in the lepidolite-subtype aplite-pegmatite sills.

3.6. Amblygonite

Amblygonite occurs in subhedral to anhedral single crystals, often twinned, associated with K-feldspar and quartz in the aplite-pegmatite sills. Some crystals are partially replaced by albite, quartz (Fig. 4c) and muscovite, but also by Li-bearing muscovite and lepidolite in some lepidolite-subtype sills.

3.7. Sn–Nb–Ta oxides

Subhedral to anhedral cassiterite occurs mainly interstitially associated with albite and micas (Fig. 4a, d) in the aplite-pegmatite sills. The crystals are between 1 and 2 mm across, are zoned and exhibit parallel alternating darker and lighter zones. Both zones are pleochroic, but pleochroism is more intense in the former (ε red, ω translucent and colourless) than in the latter (ε light brown, ω beige). Some crystals are partially replaced by albite and quartz. Anhedral columbite-tantalite crystals occur associated with cassiterite, albite and lepidolite.

Microlite is subhedral, only occurs in a few lepidolite-subtype aplite-pegmatite sills, the richest in Li. It is associated with zircon and columbite-tantalite and surrounded by lepidolite, albite and quartz. Most brownish crystals are concentrically zoned and fractured.

4. Analytical methods

The major and trace elements of granitic rocks were determined by XRF using the Tertian & Claisse (1982) method, with relative percent accuracy better than $\pm 1\%$ for major elements and Rb and $\pm 4\%$ for the other trace elements.

Lithium in whole rocks was determined by atomic absorption with the accuracy of $\pm 2\%$. Fluorine in the granitic rocks was measured by selective ion electrode analysis with an accuracy of $\pm 2\%$. All these determinations were carried out at INETI, S. Mamede de Infesta, Portugal.

FeO of granitic rocks was determined by titration with a standardized potassium permanganate solution with the accuracy of $\pm 1\%$. Loss on ignition (LOI) for rocks was determined using the method described by Lechler & Desilets (1987). These determinations were carried out at the Department of Earth Sciences, University of Coimbra, Portugal. Rare earths in the granitic rocks were determined by ICP-MS with an accuracy of $\pm 5\%$ in the SGS Laboratory, Toronto, Canada. Whole rock oxygen isotope analysis of granitic rocks was carried out at the Department of Earth Sciences, the University of Western Ontario, Canada, with the reproducibility of ± 0.2 ‰, using a quartz standard.

The major element composition of the minerals was determined using a Cameca Camebax electron microprobe at INETI, S. Mamede de Infesta, operating at 15 kV accelerating voltage and a 15 nA beam current. Detection limits (3σ above mean background) were 0.03 wt% oxide for most components, except F (0.1 wt%) and BaO (0.06 wt%), with counting times of 80 s for F and BaO.

Li$_2$O content for muscovite and Li-bearing muscovite from some granitic rocks was calculated using the equation $Li_2O = 0.3935 \, F^{1.326}$ (Tischendorf *et al.*, 1997), while the Li content of lepidolite was determined by atomic absorption and the other trace elements by XRF, with accuracies of $\pm 2\%$ and $\pm 4\%$, respectively.

5. Whole-rock geochemistry

The chemical analyses and trace elements of the four granites from the Guarda-Belmonte area and aplite-pegmatites sills from Gonçalo (Fig. 5–7) are given in Table 2. The granites present molecular A/CNK ratio = molecular Al$_2$O$_3$/(CaO + Na$_2$O + K$_2$O) of 1.18–1.56 and amblygonite-subtype aplite-pegmatite sills have A/CNK values ranging between 1.18 and 1.38, and lepidolite-subtype
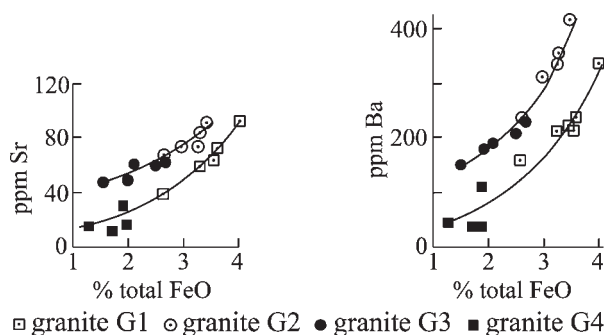

Fig. 5. Selected variation diagrams of granites from Guarda-Belmonte. Granites G1 and G4 define one series, and granites G2 and G3 define another series.
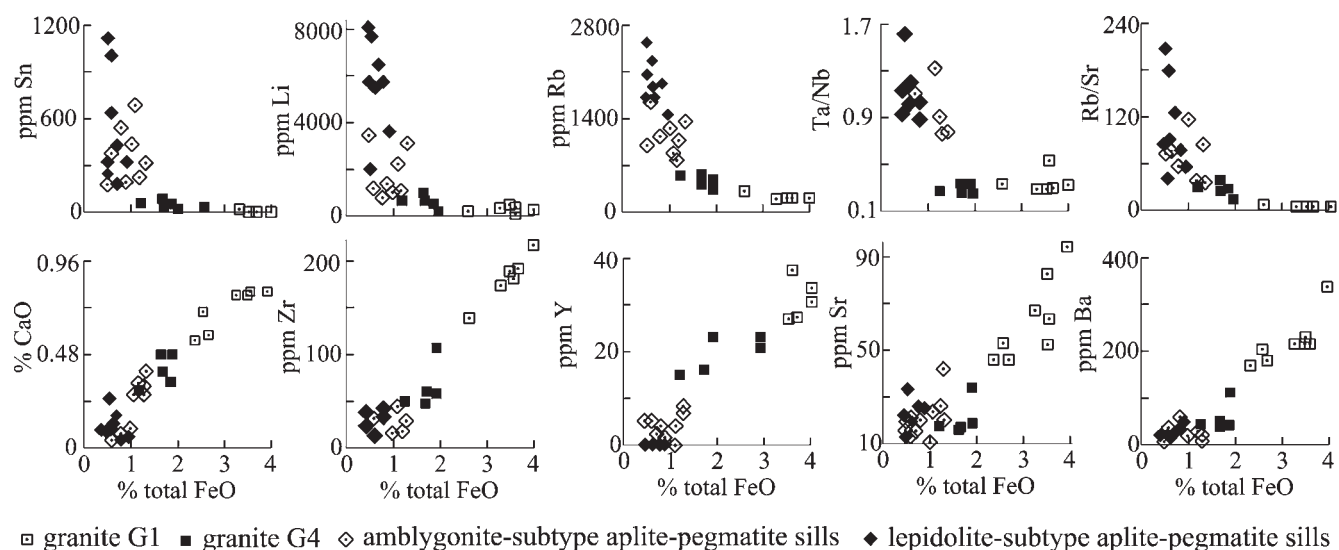
Fig. 6. Selected variation diagrams of granites G1 and G4 from Guarda-Belmonte and granitic aplite-pegmatite sills from Gonçalo, suggesting that aplite-pegmatite sills are not related to this series G1–G4.
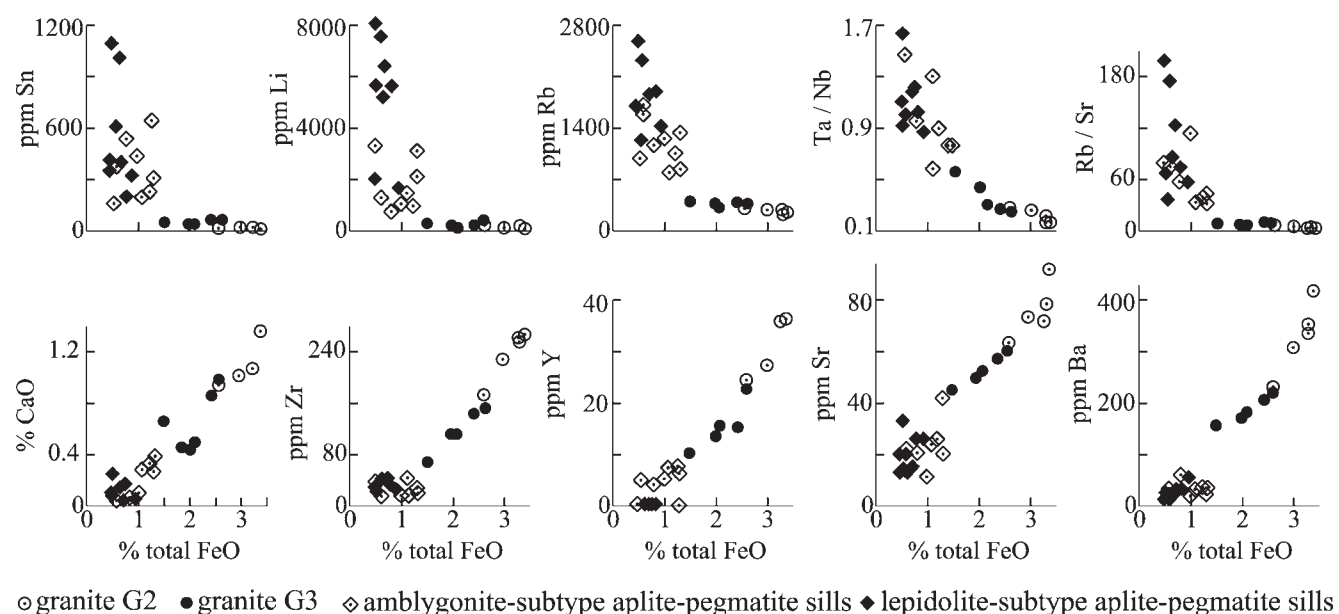
Fig. 7. Variation diagrams of granites G2 and G3 from Guarda-Belmonte and granitic aplite-pegmatite sills from Gonçalo, suggesting a crystal fractionation model.

sills have A/CNK values of 1.46–1.72 and one value of 2.13. Therefore, the granitic rocks are peraluminous.

Aplite-pegmatite sills from Gonçalo have higher Na_2O, Li, F, Nb, Ta, Sn, Rb contents, similar to higher MnO, Al_2O_3, P_2O_5 contents and lower TiO_2, total FeO, MgO, CaO, Zr, Y, Sr and Ba contents than the granite G1 they cut (Table 2; Fig. 6).

Granites G1 and G4 seem to exhibit fractionation trends (Fig. 5) as do granites G2 and G3. The difference between the correlation coefficients for granites G2–G3 and sills, and for granites G1–G4 and sills are very slight (Table 3, Fig. 6 and 7). The F, Sn, Li and Rb contents and Ta/Nb and Rb/Sr values show wide ranges in aplite-pegmatite sills

(Table 2, Fig. 7) and the highest values occur in lepidolite-subtype sills. The pegmatites studied belong to the LCT family, rare-element class (REL), REL-Li subclass, complex type. Some belong to the amblygonite-subtype and others to the lepidolite-subtype of Černý & Ercit (2005).

Rare earth element contents of selected samples of granites from Guarda-Belmonte area and aplite-pegmatite sills from Gonçalo are given in Table 4 and the chondrite normalized rare-earth-element patterns are presented in Fig. 8. They are enriched in LREE with respect to HREE (La_N/Yb_N of 6.9–28.4). Those for granites G1 and G4 are subparallel, and all REE contents decrease while the negative Eu anomaly increases from the former to the latter.

Table 2. Chemical analyses in wt% and trace elements in ppm of granites from the Guarda-Belmonte area and aplite-pegmatite sills from Gonçalo, central Portugal.

	Granites								Aplite-pegmatite sills (AP)			
	G1	σ	G2	σ	G3	σ	G4	σ	1	Range	2	Range
SiO_2	69.78	1.50	70.76	0.96	71.95	0.87	73.55	0.65	71.74	69.55–73.19	69.54	67.31–71.63
TiO_2	0.45	0.07	0.44	0.07	0.29	0.08	0.13	0.05	0.01	0–0.02	0.01	0.01–0.02
Al_2O_3	14.88	0.38	14.48	0.25	14.86	0.55	14.34	0.43	15.82	14.43–16.98	17.24	16.04–18.05
Fe_2O_3	0.66	0.29	0.90	0.19	0.54	0.20	0.19	0.23	0.06	0–0.24	–	0
FeO	2.84	0.37	2.30	0.30	1.65	0.46	1.52	0.24	0.93	0.53–1.33	0.65	0.49–0.93
MnO	0.05	0.01	0.05	0.01	0.04	0.01	0.07	0.01	0.10	0.06–0.20	0.15	0.07–0.29
MgO	0.63	0.11	0.52	0.16	0.39	0.07	0.17	0.06	0.02	0.00–0.05	0.01	0.01–0.02
CaO	0.87	0.09	1.08	0.16	0.69	0.22	0.39	0.08	0.20	0.04–0.39	0.12	0.05–0.25
Na_2O	2.49	0.35	2.81	0.09	2.74	0.31	3.17	0.16	4.81	3.52–6.15	4.12	3.03–5.30
K_2O	4.84	0.44	5.19	0.18	5.10	0.54	4.73	0.38	3.41	1.92–4.96	3.47	3.04–4.70
P_2O_5	0.20	0.05	0.23	0.05	0.22	0.05	0.28	0.07	0.61	0.15–1.50	0.85	0.17–1.66
Li_2O	0.06	0.02	0.02	0.01	0.04	0.01	0.11	0.05	0.38	0.15–0.71	1.14	0.35–1.74
F	0.10		0.10		0.12		0.12		0.47	0.44–0.57	1.54	1.49–1.64
LOI	2.18	0.49	1.25	0.21	1.46	0.50	1.21	0.12	1.82	1.33–2.40	2.10	1.34–3.50
Total	100.03		100.13		100.09		99.98		100.38		100.94	
$O \equiv F$	0.04		0.04		0.05		0.05		0.20		0.65	
	99.99		100.09		100.04		99.93		100.18		100.29	
Nb	18	2	19	1	16	2	23	4	42	25–101	58	31–104
Ta	6	2	4	1	6	2	5	0	45	12–150	68	42–166
Sn	13	4	12	3	21	5	39	13	364	174–659	532	192–1098
Zr	183	26	237	40	117	32	65	24	27	15–43	27	17–34
Y	30	5	31	7	15	5	19	4	4	*–7	*	*
Sr	66	18	76	11	54	4	21	8	22	11–42	21	13–33
Ba	226	66	329	70	190	26	56	30	30	15–58	25	16–51
Rb	263	26	285	16	337	16	465	68	1126	786–1595	1834	1213–2305
n	6		5		5		5		8		8	

G1 – coarse- to very coarse-grained porphyritic biotite>muscovite granite; G2 – fine- to medium-grained porphyritic biotite>muscovite granite (G2); G3 – coarse-grained porphyritic biotite>muscovite granite; G4 – medium- to coarse-grained muscovite>biotite granite; 1 – amblygonite-subtype aplite-pegmatite sills; 2 – lepidolite-subtype aplite-pegmatite sills. LOI – loss on ignition; – not detected; * below the detection limit, which is of 2 ppm for Ta and 4 ppm for Y. F was only determined in two samples of each granite.

Table 3. Correlation coefficients for the two trends of granites from the Guarda-Belmonte area and aplite-pegmatite sills from Gonçalo, central Portugal.

wt% total FeO *versus*	G1, G4 and sills	G2, G3 and sills
wt% MnO	0.465	0.506
wt% CaO	0.982	0.971
wt% P_2O_5	0.685	0.697
ppm Li	0.742	0.759
ppm Nb	0.788	0.816
ppm Ta	0.765	0.773
ppm Sn	0.688	0.698
ppm Zr	0.977	0.990
ppm Y	0.942	0.985
ppm Sr	0.937	0.951
ppm Ba	0.974	0.978
ppm Rb	0.872	0.876
Ta/Nb	0.857	0.904
Rb/Sr	0.757	0.772
n	27	26

n – number of samples.

The REE patterns for granites G2 and G3 are also subparallel and all REE contents decrease from G2 to G3. The aplite-pegmatite sills are impoverished in REE, as expected, and their REE contents are lower than the granitic contents for G1, G2, G3 and G4, except for Eu in one sample of G4. Lepidolite-subtype sills are the poorest in all REE contents.

The whole rock $\delta^{18}O$ and total FeO values of selected samples of granites from Guarda-Belmonte area and aplite-pegmatite sills from Gonçalo are given in Table 5 and plotted in Fig. 9. The correlation coefficient for the trend of $\delta^{18}O$ versus total FeO is higher (0.972) for G2, G3 and aplite-pegmatite sills than for G1, G4 and sills (0.891).

6. Geochemistry of minerals

6.1. Feldspars

Compositions of feldspars from granites of Guarda-Belmonte area and aplite-pegmatite sills from Gonçalo are given in Table 6. There is a decrease in anorthite from phenocryst to matrix plagioclase, an increase in orthoclase content and a decrease in Ba content from phenocryst to matrix microcline, showing that granites G1, G2 and G3 have plagioclase phenocrysts and all granites contain microcline phenocrysts (Ramos, 1998). The anorthite content of phenocryst and matrix plagioclase

Table 4. Rare-earth element concentrations (ppm) of selected samples of granites from the Guarda-Belmonte area and aplite-pegmatite sills from Gonçalo, central Portugal.

	Granites				Aplite-pegmatite sills			
	G1	G2	G3	G4	1a	1b	2a	2b
La	23.7	55.2	25.8	10.65	8.80	7.80	5.60	4.40
Ce	53.8	116	50.7	24.4	11.8	9.10	8.00	5.80
Pr	6.40	13.7	5.99	2.90	1.33	1.05	0.67	0.45
Nd	24.2	54.3	23.7	10.8	5.80	4.20	2.80	1.80
Sm	5.20	9.36	4.60	2.60	1.30	1.05	0.70	0.50
Eu	0.57	1.17	0.65	0.15	0.16	0.15	0.10	0.07
Gd	4.30	8.06	4.04	2.45	1.07	0.91	0.60	0.47
Tb	0.73	1.34	0.60	0.42	0.16	0.12	0.09	0.08
Dy	4.10	6.60	3.13	2.65	0.86	0.57	0.37	0.33
Ho	0.77	1.47	0.68	0.45	0.12	0.09	0.06	0.06
Er	1.90	3.43	1.54	1.15	0.28	0.20	0.14	0.13
Tm	0.30	0.51	0.23	0.17	<0.05	<0.05	<0.05	<0.05
Yb	1.80	3.30	1.50	1.00	0.20	0.18	0.13	0.12
Lu	0.30	0.48	0.22	0.15	<0.05	0.07	<0.05	<0.05

Column headings as in Table 2. 1a, b – amblygonite-subtype aplite-pegmatite sills; 2a, b – lepidolite-subtype aplite-pegmatite sills.
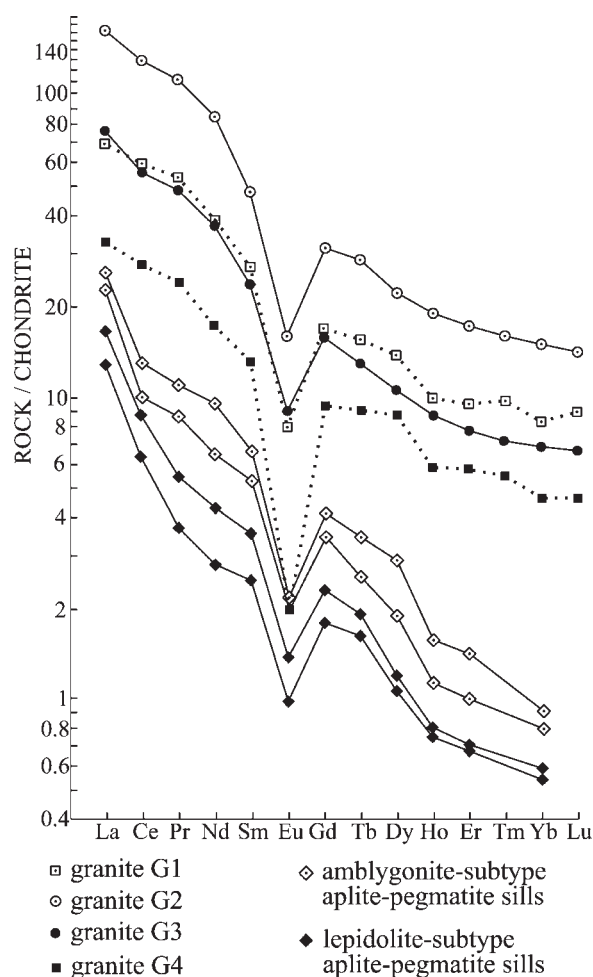

Fig. 8. Chondrite-normalized REE abundances of selected samples of granites from Guarda-Belmonte and granitic aplite-pegmatite sills from Gonçalo, confirming that granites G1 and G4 define one series and granites G2 and G3 define another series. Aplite-pegmatite sills are the poorest in REE.

Table 5. $\delta^{18}O$ and total FeO of selected samples of granites from the Guarda-Belmonte area and aplite-pegmatite sills from Gonçalo of central Portugal.

		$\delta^{18}O$ ‰	total FeO wt%
G1		11.02	2.60
G2		10.79	3.28
		10.84	3.00
G3		10.87	2.09
		11.02	1.99
		11.04	1.47
G4		11.09	1.90
		11.14	1.71
AP	1	11.21	0.80
	1	11.34	0.59
	2	11.18	0.71
	2	11.31	0.63

G1, G2, G3, G4 and AP as in Table 2. Correlation coefficient for G1, G4 and sills is 0.891 and for G2, G3 and sills is 0.972.
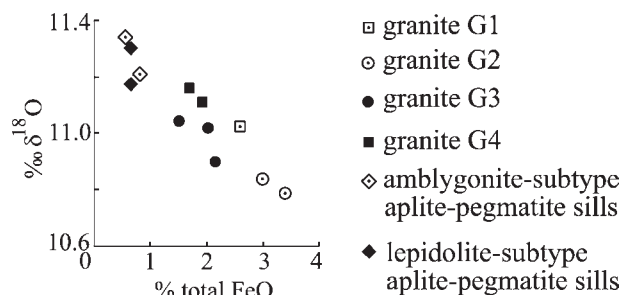

Fig. 9. Diagram of total FeO versus $\delta^{18}O$ of granites from Guarda-Belmonte and granitic aplite-pegmatite sills from Gonçalo.

decreases from G1 to G4 and from G2 to G3. The barium content of phenocryst and matrix microcline decreases from G1 to G4 and from G2 to G3. Phenocryst and matrix plagioclase from G2 has a higher anorthite content than phenocryst

Table 6. Compositions of feldspars from granites from the Guarda-Belmonte area and aplite-pegmatite sills from Gonçalo, central Portugal.

| | | Granites | | | | Aplite-pegmatite sills |
		G1	G2	G3	G4	
Anorthite content of plagioclase	Phenocryst	5–30	6–42	4–27	–	–
	Matrix	3–19	4–23	1–15	0–4	0–1
Orthoclase content of K-feldspar	Phenocryst	89–94	85–94	88–95	88–96	–
	Matrix	88–97	90–97	91–98	91–98	90–99
wt% BaO of K-feldspar	Phenocryst	≤ 0.06–0.29	≤ 0.06–0.33	≤ 0.06–0.29	≤ 0.06–0.16	–
	Matrix	≤ 0.06–0.14	≤ 0.06–0.26	≤ 0.06–0.20	≤ 0.06–0.10	–

Column headings as in Table 2. – not found. G4 only has rare microscopic potash feldspar phenocrysts. There is no significant distinction in albite and potash feldspar compositions from amblygonite-subtype and lepidolite-subtype aplite-pegmatite sills.

and matrix plagioclase from G1. Furthermore, phenocryst and matrix microcline from G2 and G3 have similar to higher Ba content than that from G1. Of the granites, G4 has the poorest anorthite in plagioclase content and the poorest Ba in microcline content, as it is the most evolved granite. The anorthite content of albite from sills is lower than that of plagioclase from granites. The Ba content of K-feldspar from sills is lower than that of microcline from granites.

The P_2O_5 content of feldspars from granites G2 and G3 and aplite-pegmatite sills (Table 7), determined by electron microprobe, does not show significant distinction between the phenocryst and matrix. P_2O_5 contents of feldspars may depend on phosphorus content in the crystallizing melt (Bea *et al.*, 1994), because the P_2O_5 content of K-feldspar is not dependent on the orthoclase content and the P_2O_5 content of plagioclase is not related to the anorthite content. The P_2O_5 contents of K-feldspar and plagioclase increase from G2 to G3 and to aplite-pegmatite sills. No significant fractionation of phosphorus took place between coexisting feldspars, because D[P]Kf/Pl ranges between 1.00 and 1.33, but equilibrium was only attained for the distribution of P between Kf-Pl pairs from granites G2 and G3 (*e.g.*, London *et al.*, 1999).

6.2. Micas

Selected chemical analyses of primary muscovite from granites of Guarda-Belmonte area and primary muscovite, Li-bearing muscovite and lepidolite from granitic aplite-pegmatite sills of Gonçalo are given in Table 8. Primary

Table 7. Phosphorous content of feldspars from granites G2 and G3 from the Guarda-Belmonte area and aplite-pegmatite sills from Gonçalo, central Portugal.

| Rock type | | P_2O_5 wt% | | | D[P] Kf/Pl |
		Mean	Min / Max	n	
G2	Kf	0.09	0 / 0.32	48	1.00
	Pl	0.09	0 / 0.26	88	
G3	Kf	0.17	0 / 0.43	45	1.06
	Pl	0.16	0 / 0.76	93	
AP	Kf	0.48	0.05 / 0.80	52	1.33
	Pl	0.36	0 / 0.70	95	

G2, G3 and AP as in Table 2. Min – minimum, Max – maximum, n – number of analyses. D[P]Kf/Pl – empirical distribution coefficient.

muscovite from granites G2 and G3 and granitic aplite-pegmatite sills define a trend (Fig. 10a), whereas primary muscovite from granites G1 and G4 define another trend. Primary muscovite from aplite-pegmatite sills has higher Al^{VI}, Mn, Li, F contents and lower Ti, Fe and Mg contents than primary muscovite from granites G2 and G3.

Li-bearing muscovite from aplite-pegmatite sills has higher Mn, Li, F and paragonite contents and lower Al^{VI} content than primary muscovite from the granites G2 and G3 and aplite-pegmatite sills (Table 8, Fig. 1b). Lepidolite has higher Li, F contents and lower Al^{VI} and Al^{VI} + Ti contents than them. The later fine-grained lepidolite has higher Mn, Li, F, $\sum$(Fe + Mn + Mg) contents and lower Sn, Rb contents than the earlier lepidolite (Table 8, Fig. 10b).

6.3. Other silicate minerals and amblygonite

Topaz occurs in all studied aplite-pegmatite sills from Gonçalo and their compositions are given in Table 9. There are no chemical distinctions between the two generations of topaz and it has a similar composition in all aplite-pegmatite sills.

Petalite occurs in lepidolite-subtype aplite-pegmatite sills from Gonçalo and is a nearly pure phase (Table 9) (Ramos, 1998).

Compositions of tourmaline from lepidolite-subtype aplite-pegmatite sills cutting granite G1 and metasomatised G1 and micaschist at sill walls are given in Table 9. Schorl from the sills has a distinct composition from the metasomatic schorl of granite and dravite of micaschist at the sill walls (Fig. 11, Table 9).

Amblygonite shows some deficiency in Al, which is attributed to a slight alteration (Ramos, 1998). The amblygonite composition is similar in all aplite-pegmatite sills from Gonçalo (Table 10).

6.4. Oxides

The cassiterite is zoned (Fig. 4d) and in general the darker zone has higher (Nb + Ta + Fe + Mn) content than the lighter zone (Table 11). The incorporation of these elements and Ti in cassiterite is probably explained by the main mechanism $2(Nb, Ta)^{5+} + (Fe + Mn)^{2+} \rightleftarrows 3(Sn,$

Table 8. Representative chemical analyses in wt% of micas from granites from the Guarda-Belmonte area and aplite-pegmatite sills from Gonçalo, central Portugal.

	Muscovite from						Li-bearing muscovite from			Lepidolites from				
	Granites				Aplite-pegmatite sills		Aplite-pegmatite sills			Aplite-pegmatite sills			Early	Late
	G1	G2	G3	G4	1	2	1	1	2	Early 2	Late 2		2	2
SiO_2	47.26	46.68	46.63	46.27	46.99	46.16	45.90	46.63	46.00	50.60	49.90	ppm		
TiO_2	0.98	0.57	0.21	0.77	0.10	0.05	0.10	0.10	0.05	0.05	0.10	Nb	47	40
Al_2O_3	33.59	33.77	34.31	34.71	34.87	38.20	30.70	33.14	35.00	26.50	25.70	Ta	24	20
FeO	1.97	1.42	1.23	1.27	1.21	0.05	3.60	2.63	0.05	0.05	1.20	Sn	96	64
MnO	0.03	0.05	0.05	0.01	0.40	0.10	0.90	0.71	0.05	0.20	1.60	Zr	10	10
MgO	1.22	0.85	0.72	0.81	0.10	0.05	0.05	0.05	0.20	0.05	0.10	Ba	20	20
Li_2O	0.36	0.07	0.08	0.43	0.39	0.90	2.43	1.20	1.33	5.03*	5.40*	Rb	3404	2865
CaO	–	0.01	–	0.01	0.05	0.05	0.05	0.05	0.05	–	0.05			
Na_2O	0.39	0.40	0.40	0.42	0.20	0.40	0.45	0.40	0.50	0.20	0.30			
K_2O	10.69	10.22	10.70	10.60	9.90	10.50	10.50	9.30	10.60	9.80	8.40			
F	0.94	0.28	0.30	1.04	1.00	0.34	3.95	2.32	2.50	5.80	6.60			
Total	97.43	94.32	94.63	96.34	95.21	96.80	98.63	96.53	96.28	98.28	99.35			
	0.39	0.12	0.13	0.44	0.42	0.14	1.66	0.97	1.05	2.44	2.77			
Total	97.04	94.20	94.50	95.90	94.79	96.66	96.97	95.56	95.23	95.84	96.58			
Si	3.089	3.133	3.119	3.047	3.110	2.994	2.998	3.065	3.010	3.196	3.138			
Al^{IV}	0.911	0.867	0.881	0.953	0.890	1.006	1.002	0.935	0.990	0.804	0.862			
T	4.00	4.00	4.00	4.00	4.00	4.00	4.00	4.00	4.00	4.00	4.00			
Al^{VI}	1.677	1.804	1.824	1.741	1.830	1.913	1.361	1.633	1.710	1.169	1.043			
Ti	0.048	0.029	0.011	0.038	0.005	0.002	0.005	0.005	0.002	0.002	0.005			
Fe^{2+}	0.108	0.080	0.069	0.070	0.067	0.003	0.197	0.145	0.003	0.003	0.063			
Mn	0.002	0.003	0.003	0.001	0.022	0.006	0.050	0.040	0.011	0.011	0.085			
Mg	0.119	0.085	0.072	0.080	0.010	0.005	0.005	0.005	0.011	0.005	0.009			
Li	0.095	0.019	0.022	0.114	0.104	0.235	0.638	0.317	0.350	1.277	1.366			
$\sum R$	2.05	2.02	2.00	2.04	2.04	2.16	2.26	2.15	2.08	2.47	2.57			
Ca	–	0.001	–	0.001	0.004	0.003	0.003	0.004	0.004	–	0.003			
Na	0.049	0.052	0.053	0.054	0.026	0.050	0.057	0.051	0.063	0.024	0.037			
K	0.891	0.875	0.938	0.891	0.836	0.869	0.875	0.780	0.885	0.790	0.674			
$\sum A$	0.94	0.93	0.99	0.95	0.87	0.92	0.94	0.84	0.95	0.81	0.71			
F	0.194	0.059	0.066	0.217	0.209	0.069	0.816	0.482	0.517	1.159	1.313			
OH**	1.806	1.941	1.934	1.783	1.791	1.931	1.184	1.518	1.483	0.841	0.687			

G1, G2, G3, G4 and aplite-pegmatite sills as in Table 2. Li content was mainly calculated, except for lepidolites, *, for which it was measured by atomic absorption. – not detected. Number of ions calculated on the basis of 11 oxygen atoms. ** – calculated by difference to 2.000.
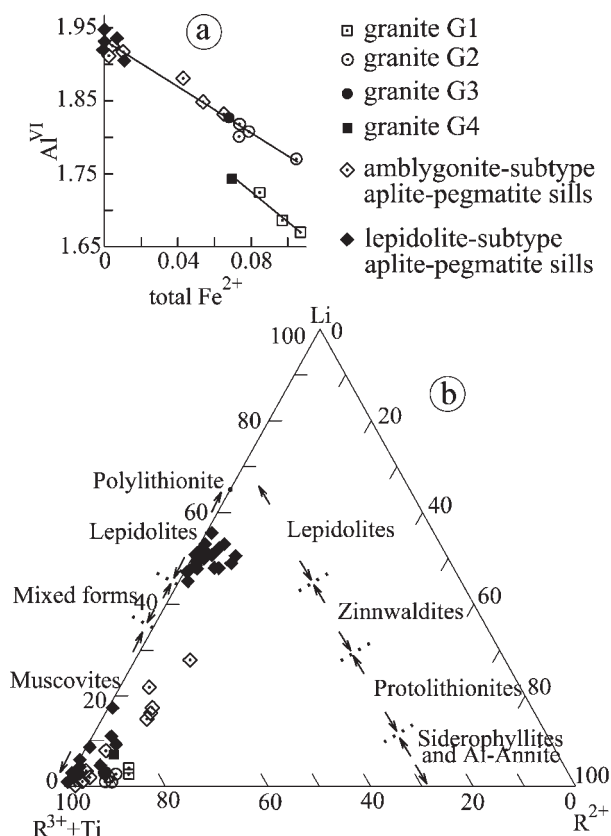
Fig. 10. Crystal chemistry of micas from granites from Guarda-Belmonte and granitic aplite-pegmatite sills from Gonçalo. (a) Al^{VI} vs. Fe diagram showing two trends for magmatic muscovites, one for G1 and G4 and another for G2, G3 and sills; (b) octahedral cation plot for micas from these granitic rocks, according to the classification of Foster (1960); however, zinnwaldite is a series name for trioctahedral mica on, or close to, the siderophyllite-polylithionite join (Rieder et al., 1999); $R^{3+} = Al^{VI}$, $R^{2+} = (Fe_t^{2+} + Mn^{2+} + Mg)$.

Ti)$^{4+}$ (Černý et al., 1985), as cassiterite compositions plot close to the trend defined by this ideal substitution. The cassiterite with the highest Nb and Ta contents has Mn>Fe and belongs to the lepidolite-subtype aplite-pegmatite sills (Fig. 12a, Table 11) (Ramos, 1998).

Compositions of manganocolumbite dominate, but very rare ferrocolumbite also occurs in amblygonite-subtype aplite-pegmatite sills, whereas manganotantalite only occurs in a few lepidolite-subtype sills (Table 11, Fig. 12b) (Ramos, 1998). There is a general trend from manganocolumbite to manganotantalite in lepidolite-subtype aplite-pegmatite sills in agreement with the trend defined by Černý (1989). There is also enlargement of the Mn-rich part of the quadrilateral (Fig. 12b) due to changes in the Mn/(Mn + Fe) ratio. This is attributed to the precipitation of Fe-bearing minerals as found in the columbite-tantalite compositions from the lepidolite-subtype granitic pegmatites of the Massif Central (Raimbault, 1998).

Most microlite crystals from lepidolite-subtype aplite-pegmatite sills of Gonçalo are zoned (Fig. 13a). Microlite compositions are Ta-rich with Mn and Ba almost absent and Ti, Fe, Sr, Pb and K absent. In the A-group of cations,

Na dominates over Ca, with Na/Ca values varying between 1.2 and 2.5. The U content is up to 0.243 apfu in the composition with the highest Nb content (Table 12) (Ramos, 1998). The core has a homogeneous microlite composition and the rim presents a heterogeneous uranmicrolite composition (Fig. 13b–d). The rim has higher U, Sn, Nb, OH contents and lower Ca, Na, Ta, F contents, and a lower Ta/(Ta + Nb) value than the core (Table 12, Fig. 13b–d). This indicates a reverse zoning because the continuum of crystal-melt fractionation causes a concentration of C_{Nb}/C_{Ta} in melt that decreases with the progress of crystallization, and the crystallizing phases in which Nb and Ta are compatible become progressively richer in Ta (London, 2008). There is a compositional gap between the microlite core and the uranmicrolite rim. The heterogeneous composition of uranmicrolite suggests that there is no single stage of uranmicrolite crystallization and this mineral may not be related to a metasomatic stage. The crystals have several fractures. The reverse-zoning is explained by the nucleation and growth of the evolved microlite core within boundary layers depleted in Nb by the growth of other crystals and its back-reaction with the more primitive bulk magma once the boundary layer is removed.

7. Discussion and conclusions

The variation diagrams for Sr and Ba suggest that granites G1 and G4 define one series and granites G2 and G3 define another series (Fig. 5), which is supported by the subparallel REE patterns within each series (Fig. 8) and the two
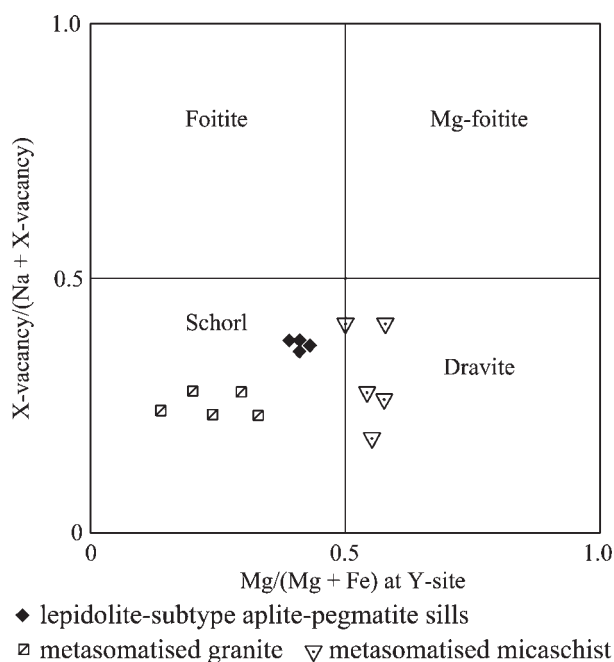

Fig. 11. Tourmaline compositions from lepidolite-subtype aplite-pegmatite sills from Gonçalo and adjacent granite and micaschist. Schorl from sills has a composition distinct from metasomatic schorl of granite and metasomatic dravite of micaschist.

Table 9. Representative electron-microprobe analyses of some other silicate minerals from granitic aplite-pegmatite sills from Gonçalo (Guarda), central Portugal.

Topaz

Mineral / Sill no.	1	2
SiO_2	32.29	33.14
Al_2O_3	56.17	55.63
FeO	0.05	0.05
MnO	0.05	0.05
MgO	0.05	0.05
CaO	0.05	0.05
Na_2O	0.05	0.05
K_2O	0.05	0.05
F	12.88	13.18
H_2O+	3.74	3.64
	105.38	105.89
$O\equiv F$	5.41	5.54
Total	99.97	100.35
Si	3.934	4.019
Al	0.066	–
Σ	4.00	4.02
Al	7.998	7.951
Fe^{2+}	0.005	0.005
Mn	0.005	0.005
Mg	0.009	0.009
Ca	0.007	0.006
Na	0.012	0.012
K	0.008	0.008
Σ	8.04	8.00
F	4.962	5.055
OH	3.038	2.945
Σ	8.00	8.00

Petalite

Mineral / Sill no.	2
SiO_2	78.36
Al_2O_3	16.90
FeO	–
MnO	0.03
MgO	0.02
CaO	0.02
Li_2O	4.89
Na_2O	0.05
K_2O	0.03
Total	100.30
Si	7.972
Al	0.028
Σ	8.00
Al	1.999
Mg	0.003
Fe^{2+}	–
Mn	0.003
Σ	2.01
Li	2.000
Na	0.010
Ca	0.002
K	0.004
Σ	2.02

Tourmaline

Mineral / Sill no.	2	MG	MS
SiO_2	34.40	34.87	35.50
TiO_2	0.50	1.09	0.70
Al_2O_3	34.70	32.29	34.10
FeO	9.90	11.39	7.90
MgO	3.80	3.07	5.40
CaO	0.30	0.59	0.30
MnO	0.10	0.10	–
Na_2O	1.80	2.08	2.10
K_2O	0.05	0.05	0.10
F	0.50	0.50	0.85
H_2O^*	3.37	3.34	3.26
$B_2O_3^*$	10.45	10.36	10.63
Li_2O^*	0.11	0.38	0.22
Sum	99.98	100.11	101.06
$O\equiv F$	0.21	0.21	0.36
Total	99.77	99.90	100.70
T Si	5.724	5.848	5.804
Al	0.276	0.152	0.196
B	3.000	3.000	3.000
Z Al	6.000	6.000	6.000
Y Al	0.528	0.231	0.375
Ti	0.063	0.137	0.086
Mg	0.943	0.768	1.316
Mn	0.014	0.014	–
Fe^{2+}	1.378	1.598	1.080
Li^*	0.074	0.252	0.143
ΣY	3.000	3.000	3.000
X Ca	0.053	0.106	0.053
Na	0.581	0.676	0.666
K	0.011	0.011	0.021
$\square$	0.355	0.207	0.260
OH	3.737	3.735	3.560
F	0.263	0.265	0.440

1 – Amblygonite-subtype aplite-pegmatite sills; 2 – lepidolite-subtype aplite-pegmatite sills, MG – metasomatised granite, MS – metasomatised micaschist, both at the sill walls. Atomic contents for topaz normalized to 24 oxygen atoms and H_2O estimated assuming that $F + OH = 8.00$. Topaz has a similar composition in all aplite-pegmatite sills. Ion contents of petalite calculated on the basis of 20 oxygen atoms and a fixed content of 2 lithium atoms. Structural formula of tourmaline calculated on the basis of 31 anions. – Not detected. *– Calculated.

muscovite trends, one for each series (Fig. 10a), suggesting that the two series are independent. Granite G2 cannot be derived from the older and more evolved granite G1 (Tables 2 and 6). Anorthite content of phenocryst and matrix plagioclase and Ba content of phenocryst and matrix microcline decrease within each series G1–G4 and G2–G3 (Table 6). Both series were successfully modelled for major and trace elements, and G4 is derived from G1 magma while G3 is derived from G2 magma by fractional crystallization of quartz, plagioclase, microcline, biotite and ilmenite.

Some aplite-pegmatite sills have lower P_2O_5 content and similar to higher Sr content than granite G4 (Table 2, Fig. 6), suggesting that sills cannot be derived from G4. This is supported by the fact that there is no trend of muscovite for G1, G4 and sills (Fig. 10a). The correlation coefficient for the $\delta^{18}O$ versus the total FeO of G2, G3 and sills is higher than

for that of G1, G4 and sills (Table 5; Fig. 9), the diagram of muscovite compositions shows a trend for those from G2, G3 and all aplite-pegmatite sills (Fig. 10a) and P_2O_5 contents of K-feldspar and plagioclase increase from G2 to G3 to sills (Table 7), suggesting that the sills are related to G2 and G3. The increase in $\delta^{18}O$ values in the series G2, G3 and aplite-pegmatite sills is up to 0.55 ‰, consistent with fractional crystallization (White, 2003).

The possibility of the granites G2–G3 as possible parental melts of the studied aplite-pegmatite sills was tested. Major elements were modelled using a least-squares regression method and taking into account compositions of micas (biotite with $Mg/(Mg + Fe^{2+} + Fe^{3+}) = 0.37$) and ilmenite from the sample poorest in SiO_2 from G2, determined by electron microprobe, and pure quartz, K-feldspar, albite and anorthite. The sample with the lowest SiO_2 content for G2 was selected as the parent magma. Samples

Table 10. Representative electron-microprobe analyses and formula of amblygonite from granitic aplite-pegmatite sills from Gonçalo (Guarda), of central Portugal.

Mineral	Amblygonite	
Sill no.	1	2
Al_2O_3	34.26	34.65
FeO	0.01	0.01
MnO	–	–
MgO	–	–
CaO	–	–
Na_2O	0.01	0.01
P_2O_5	48.88	49.23
F	6.60	6.55
	89.76	90.45
O≡F	2.77	2.75
Total	86.99	87.70
Al	0.976	0.980
Fe	–	–
Mn	–	–
Mg	–	–
Ca	–	–
Na	0.001	0.001
Li	0.999	0.999
P	1.000	1.000
F	0.504	0.497
OH	0.496	0.503

1 – Amblygonite-subtype aplite-pegmatite sills; 2 – lepidolite-subtype aplite-pegmatite sills. Ion contents of amblygonite normalized to 1P. Amblygonite has a similar composition in amblygonite-subtype and lepidolite-subtype aplite-pegmatite sills. – Not detected.

of G2, G3, amblygonite-subtype and lepidolite-subtype sills, which do not contain metasomatic effects, represent residual liquids. The sum of the squares of the residuals ($\sum R^2$) was always ≤0.64 (Table 13). The model calculates the composition of the parent granite magma. Therefore, all the contents in major elements calculated are nearly similar for G2, G3, amblygonite-subtype and lepidolite-subtype sills and also for the determined composition of parent granite magma (Table 13), indicating that the test is successful. Furthermore, the anorthite content of plagioclase of the cumulate is similar to the highest anorthite content of plagioclase from G2. The percentages of quartz and K-feldspar increase and those of plagioclase and biotite decrease in the cumulate versus the decrease in weight fraction of the remaining melt during fractional crystallization (Table 13, Fig. 14a, b). Granite G3 and amblygonite-subtype and lepidolite-subtype aplite-pegmatite sills seem to be derived from the granite G2 magma by fractional crystallization of quartz, plagioclase, K-feldspar, biotite and ilmenite. Granite G2 has $(^{87}Sr/^{86}Sr)_0 = 0.7078 \pm 0.0005$ and $\delta^{18}O = 10.82 \pm 0.04$ ‰, showing that is S-type.

A similar test for major elements was applied to find out if the aplite-pegmatite sills could be related to the G1 and G4 granites. $\sum R^2$ values range between 1.43 and 13.23, confirming that the sills are not derived from these granites, because the $\sum R^2$ must be <1 for the test to be accepted.

Table 11. Representative compositions of cassiterite and columbite-tantalite crystals from aplite-pegmatite sills from Gonçalo (Guarda area), central Portugal.

Sills	Cassiterite				Columbite-tantalite				
	1		2		1		2		
	a	b	c	d	e	f	g	h	i
Nb_2O_5	2.09	1.00	2.30	0.58	41.30	61.00	58.80	44.90	19.70
Ta_2O_5	0.40	0.10	6.90	0.88	37.90	15.70	20.60	36.20	63.50
TiO_2	0.10	0.10	–	–	2.30	1.00	0.70	0.05	0.70
SnO_2	97.21	99.10	90.20	98.41	0.80	0.20	0.80	0.05	0.20
WO_3	0.10	–	–	0.20	0.10	2.10	1.20	–	–
MnO	0.30	0.10	1.00	0.05	8.00	19.00	10.30	18.50	14.80
FeO	–	–	0.05	–	9.30	1.10	7.50	–	1.00
Total	100.20	100.40	100.45	100.12	99.70	100.10	99.90	99.70	99.90
Nb	0.023	0.011	0.026	0.007	1.228	1.647	1.621	1.336	0.668
Ta	0.003	0.001	0.047	0.006	0.678	0.255	0.342	0.648	1.295
Ti	0.002	0.002	–	–	0.114	0.045	0.032	0.002	0.040
Sn	0.961	0.982	0.898	0.981	0.021	0.005	0.019	0.001	0.006
W	0.001	–	–	0.001	0.002	0.033	0.019	–	–
Mn	0.006	0.002	0.021	0.001	0.446	0.961	0.532	1.032	0.940
Fe	–	–	0.001	–	0.512	0.055	0.382	–	0.063
Total	0.996	0.998	0.993	0.996	3.001	3.001	2.947	3.019	3.012
Mn/(Mn + Fe)					0.47	0.95	0.58	1.00	0.94
Ta/(Ta + Nb)					0.36	0.13	0.17	0.33	0.66

1 – Amblygonite-subtype aplite-pegmatite sills; 2 – lepidolite-subtype aplite-pegmatite. Oxides in wt%. – not detected. Cation formula based on two and six atoms of oxygen for cassiterite and columbite-tantalite, respectively. Cassiterite: crystals 1 and 2 from amblygonite-subtype and lepidolite-subtype aplite-pegmatite sills, respectively; a, c – darker; b, d – lighter zone. Columbite-tantalite: e – ferrocolumbite; f, g and h – manganocolumbite; i – mangano-tantalite.
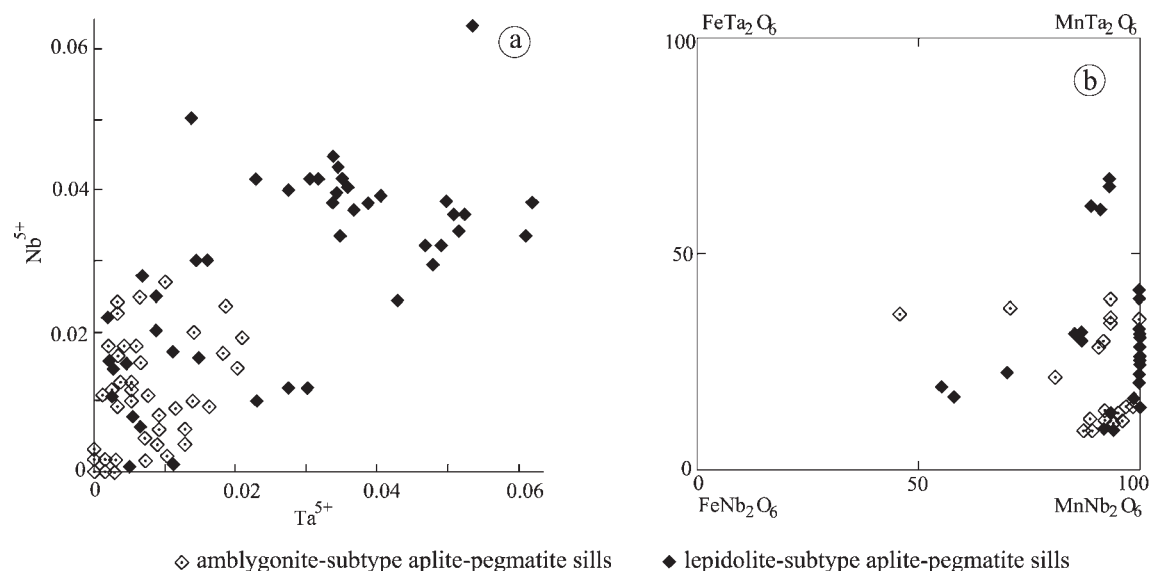
Fig. 12. Diagrams for cassiterite and columbite-tantalite from granitic aplite-pegmatite sills from Gonçalo (Guarda). (a) Nb *vs.* Ta of cassiterite showing that cassiterite with the highest Nb and Ta contents belongs to lepidolite subtype aplite-pegmatite sills; (b) columbite quadrilateral, showing that most compositions are of manganocolumbite.
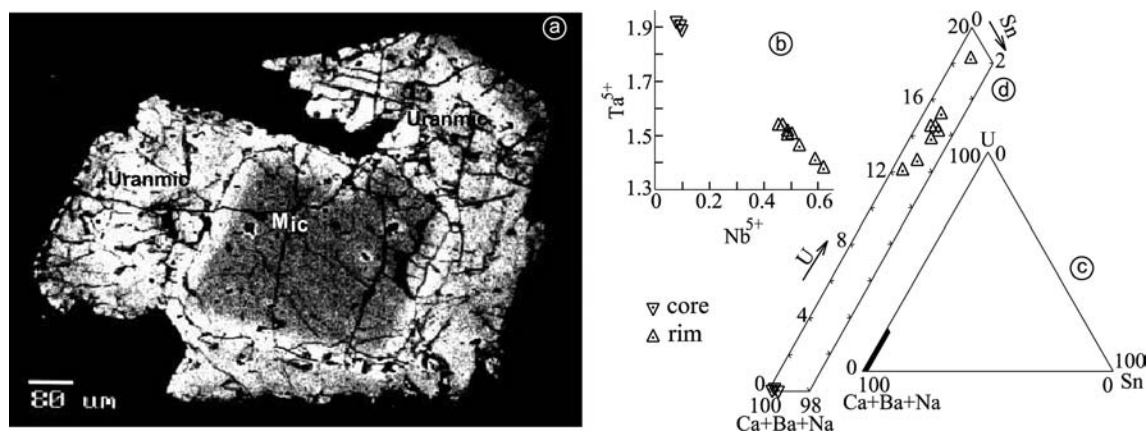

Fig. 13. Zoned microlite crystals from granitic aplite-pegmatite sills from Gonçalo (Guarda). (a) Backscattered image of a zoned crystal showing the core and rim; (b) Ta *vs.* Nb diagram; (c) U–Sn–(Ca + Ba + Na) diagram showing the location of diagram d; (d) U – Sn – (Ca + Ba + Na) diagram for a zoned microlite crystal. Diagrams show that there is a compositional gap between the microlite core and uranmicrolite rim.

The trace elements Rb, Sr and Ba were modelled using the equation for perfect fractional crystallization, the modal compositions of the cumulate, the weight fractions of the remaining melt during fractional crystallization, the distribution coefficients given in Table 13 and Rb, Sr and Ba contents of the sample with the lowest SiO$_2$ of G2. The bulk distribution of Sr is controlled by plagioclase and Rb and Ba by K-feldspar and biotite (Table 13). The calculated value of Rb increases and that of Sr and Ba decreases as the weight fraction of the remaining melt falls during fractional crystallization from G3 to aplite-pegmatite sills (Fig. 14c, d, Table 13). As the distribution coefficients and the weight fraction of the remaining melt during fractional crystallization have large errors, the modelling only shows general trends (Table 13, Fig. 14a–d), which suggest fractional crystallization. The determined Sr contents of the sills are close to the calculated values. However, the determined Ba contents of the sills, tend to be lower than the calculated values and the determined Rb contents for the amblygonite-subtype and the lepidolite-subtype sills are approximately two and three times higher than the respective calculated values (Table 13, Fig. 14e, f), indicating that this model is not good and probably also another mechanism took place. Magmatic fluxes and fluids probably controlled the behaviour of LIL elements, particularly of Ba and Rb. The aplite-pegmatite sills caused metasomatism in the host granite G1, showing that a mobile vapour phase was present in the pegmatite-forming magma and diffused from the magma into the host rock, a process which occurs even if the magma is not vapour-saturated (London, 2008).

The decrease in HREE from G2 to G3 and aplite-pegmatite sills (Fig. 8) is attributed to zircon fractionation

Table 12. Representative analyses and formula of zoned crystals of microlite crystals from lepidolite-subtype aplite-pegmatite sills from Gonçalo (Guarda area), central Portugal.

	Core	Rim				Core	Rim			Atomic ranges	
		a	b	c			a	b	c	Core	Rim
WO_3	0.30	0.10	0.30	0.20	U^{4+}	0.001	0.243	0.239	0.217	0–0.002	0.214–0.243
Nb_2O_5	2.20	15.40	11.90	11.30	Ca^{2+}	0.922	0.584	0.406	0.618	0.901–0.923	0.387–0.619
Ta_2O_5	78.90	56.60	61.50	62.60	Ba^{2+}	0.002	–	–	–	0	0–0.002
UO_2	0.05	12.20	11.90	10.80	Mn^{2+}	–	0.004	–	0.004	0–0.004	0–0.004
CaO	9.70	6.10	4.20	6.40	Sn^{2+}	0.002	0.021	0.014	0.018	0.002–0.007	0.011–0.021
MnO	–	0.05	–	0.05	Na^+	1.066	0.866	0.996	0.717	1.061–1.071	0.717–1.071
SnO	0.04	0.54	0.36	0.45	$\sum$A site	1.993	1.718	1.655	1.574		
BaO	0.05	–	–	–	W^{6+}	0.007	0.002	0.007	0.005	0.003–0.011	0.002–0.012
Na_2O	6.20	5.00	5.70	4.10	Nb^{5+}	0.088	0.622	0.485	0.461	0.077–0.089	0.461–0.622
F	3.70	2.80	1.70	2.00	Ta^{5+}	1.905	1.376	1.508	1.535	1.905–1.917	1.376–1.535
	101.14	98.79	97.56	97.90	$\sum$B site	2.000	2.000	2.000	2.001		
$O\equiv F$	1.55	1.18	0.71	0.84	F^-	1.038	0.792	0.483	0.570	0.964–1.063	0.485–0.825
Total	99.59	97.61	96.85	97.06	$(OH)^-$	0.028	0.149	0.716	0.560	0.024–0.126	0.149–0.817
					O^{2-}	5.934	6.059	5.801	5.870	5.891–5.934	5.698–6.046
					$\sum$ anion	7.000	7.000	7.000	7.000		
					Ta/(Ta + Nb)	0.96	0.69	0.76	0.77	0.96	0.69–0.77
									N	4	8

Oxides and F in wt%, – not detected. Formula contents based on (Ta + Nb + W) = 2; OH^- – calculated as charge-balanced complement to $\sum$ anions = 7; N – number of analyses.

Table 13. Results of fractional crystallization modellings of granitic rocks from the Guarda-Belmonte area of central Portugal.

	Determined	Calculated composition of parent magma for			
	Parent granite G2	Biotite>	Aplite-pegmatite sills		
		muscovite granite G3	1	1	2
SiO_2	70.6	70.6	70.7	70.6	70.6
TiO_2	0.6	0.6	0.6	0.6	0.6
Al_2O_3	14.8	14.8	14.8	14.8	14.8
Fe_2O_3t	3.8	3.8	3.8	3.8	3.8
MgO	0.8	0.9	0.9	0.9	1.0
CaO	1.4	1.3	1.4	1.4	1.3
Na_2O	2.8	2.8	2.8	2.8	2.8
K_2O	5.2	5.1	5.1	5.1	5.1
Fr		0.523 ± 0.107	0.428 ± 0.046	0.352 ± 0.040	0.343 ± 0.085
$\sum R^2$		0.18	0.42	0.64	0.56
Modal composition of cumulate					
Quartz		28.5 ± 7.1	30.3 ± 2.4	32.8 ± 1.5	35.9 ± 2.6
Plagioclase		30.7 ± 8.2	25.0 ± 3.6	17.9 ± 3.9	20.8 ± 7.6
K-feldspar		17.8 ± 6.3	23.6 ± 1.9	30.1 ± 0.8	22.7 ± 3.2
Biotite		22.2 ± 1.9	20.2 ± 0.7	18.4 ± 0.6	19.8 ± 0.9
Ilmenite		0.8 ± 0.4	0.9 ± 0.2	0.8 ± 0.2	0.8 ± 0.3

Concentration of residual metals									
ppm	Det	Det.	Calc.	Det.	Calc.	Det.	Calc.	Det.	Calc.
Rb	257	351	361	1046	414	857	481	1213	476
Sr	92	51	44	26	33	20	25	33	32
Ba	422	172	100	30	57	31	29	16	38

1 – Amblygonite-subtype aplite-pegmatite sill; 2 – lepidolite-subtype aplite-pegmatite sill. Fr – weight fraction of remaining melt during fractional crystallization. $\sum R^2$ – sum of the squares of the residuals. Det. – determined, Calc. – calculated. The calculated parent magma has always a similar composition to that determined for the parent granite. Distribution coefficients for plagioclase (Rb 0.06, Sr 4, Ba 0.05 of Peccerillo *et al.*, 1994); K-feldspar (Rb 0.07 of London, 2005; Sr 5 of Long, 1978; Ba 6 of Peccerillo *et al.*, 1994); biotite (Rb 2, Sr 0.06, Ba 9 of Icenhower & London, 1995).
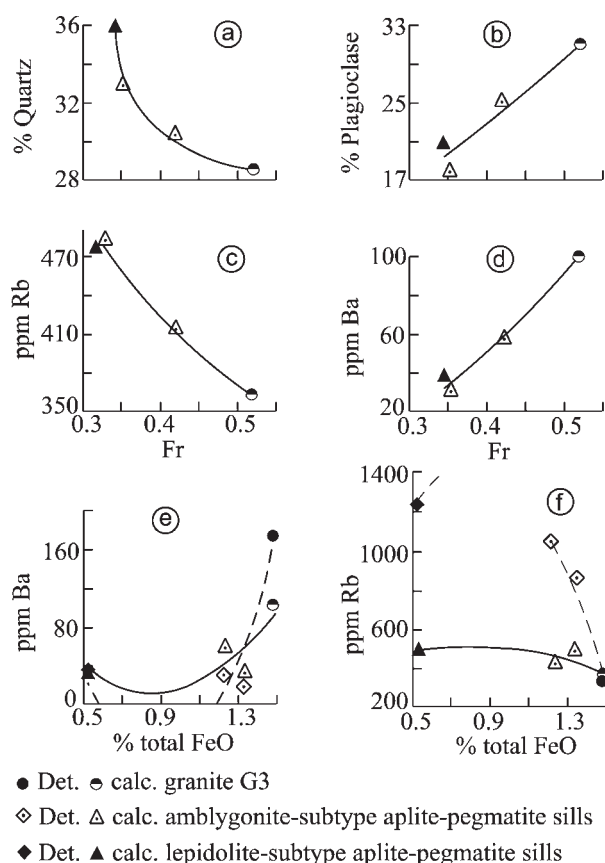
Fig. 14. Plot of: (a), (b) modal quartz and plagioclase of cumulate *versus* Fr; (c), (d) calculated Rb and Ba concentrations in granite G3 and amblygonite-subtype and lepidolite-subtype aplite-pegmatite sills from Gonçalo *versus* the weight fraction (Fr) of remaining melt during fractional crystallization; (e), (f) determined Rb and Ba concentrations compared with results from modelling calculations.

(*e.g.*, Mittlefehldt & Miller, 1983) supported by the Zr trend (Fig. 7), whereas the decreases in MREE and LREE are respectively explained by the fractionation of apatite and monazite (*e.g.*, Bea, 1996). The whole rock P, La and Ce contents (Tables 2, 4) are consistent with monazite saturation and appropriate modes of the fractionating zircon, apatite and monazite make the model feasible.

The aplite-pegmatite sills exhibit increasing fractionation in the contents of Sn, Li, Rb, Ta and F (Table 2, Fig. 7), mica compositions (Table 8, Fig. 10) and in the Nb–Ta oxide mineral assemblage from ferrocolumbite-manganocolumbite to manganocolumbite-manganotantalite + microlite (Fig. 12b, 13). In the aplite-pegmatite sills F is compatible in micas and topaz is a primary mineral and a good monitor of fluorine. The activity of F increased as indicated by the F contents of aplite-pegmatite sills (Table 2) and the appearance of lepidolite and microlite (Tables 8, 12). The activity of F was probably relatively high before the emplacement of the pegmatite melt. Columbite-tantalite compositions (Fig. 12b) indicate that a higher activity of F promotes fractionation of Mn from Fe (*e.g.*, Černý *et al.*, 1986; Spilde & Shearer, 1992). Ta-rich phases occur in the most fractionated assemblages because the addition of Li and F enhances the

solubility of manganotantalite in the melts (Linnen & Cuney, 2005). The solubility of the Sn–Nb–Ta oxides in melt declines quickly as the temperature falls (*e.g.*, Linnen, 1998) and the pegmatite-forming magmas crystallize at temperatures well below their equilibrium solidus; the oxide phases can therefore precipitate from melt as primary phases (London, 2008). However, magmatic fluids must have caused an increase in the Rb, Li, F, Sn and Ta contents of aplite-pegmatite sills, which attained their highest levels in lepidolite-subtype sills (Table 2, Fig. 7), and also influenced the crystallization of lepidolite, cassiterite and the Nb–Ta oxide mineral assemblage.

Schorl from lepidolite-subtype aplite-pegatite sills cutting granite G1 occurs close to the sill walls and has higher Mg content and Mg/(Mg + Fe) ratio than schorl from metasomatised granite at the sill walls (Table 9, Fig. 11), suggesting that schorl from sills resulted from the mixing of magmatic fluids carrying B, Na and some Fe, but depleted in Mg, with a meteoric fluid enriched in Fe and Mg that has interacted with the host granite G1, particularly with biotite. The higher mobility of Mg compared with Fe is responsible for the higher Mg content and Mg/(Mg + Fe) ratio of schorl from sills than schorl from the metasomatised granite. Tourmaline is more abundant in metasomatised granite and micaschist at the sill walls than in the sills. Boron is highly soluble in the fluid, whereas Mg and Fe will be much less soluble (Neiva *et al.*, 2007). Magmatic fluids carrying B migrated towards the country rocks, controlling tourmaline formation by B, and these rocks provided Fe and Mg. At the sill walls metasomatic dravite formed in micaschist, whereas metasomatic schorl occurs in granite because micaschist is richer in Mg (Ramos, 1998).

References

Bea, F. (1996): Residence of REE, Y, Th and U in granites and crustal protoliths: implications for the chemistry of crustal melts. *J. Petrol.*, **77**, 521–552.

Bea, F., Pereira, M.D., Corretgé, L.G., Fershtater, G.B. (1994): Differentiation of strongly peraluminous, perphosphorus granites. The Pedrobernardo pluton, central Spain. *Geochim. Cosmochim. Acta*, **58**, 2609–2628.

Breaks, F.W., Selway, J.B., Tindle, A.C. (2005): Fertile peraluminous granites and related rare-element pegmatites, Superior Province of Ontario. *in* "Rare Element Geochemistry and Mineral Deposits", R.L. Linnen & I.M. Sampson, eds. *Geol. Soc. Can. Short Course Notes, St. Catharines*, **17**, 87–125.

Černý, P. (1989): Characteristics of pegmatite deposits of tantalum. *in* "Lanthanides, Tantalum and Niobium", P. Möller, P. Černý, F. Saupé, eds. Springer-Verlag, Berlin, Germany, 195–239.

— (2005): REE-enriched granitic pegmatites. *in* "Rare-Element Geochemistry and Mineral Deposits", R.L. Linnen & I.M. Sampson, eds. *Geol. Soc. Can. Short Course Notes, St. Catharines*, **17**, 175–199.

Černý, P. & Ercit, T.S. (2005): The classification of granitic pegmatites revisited. *Can. Mineral.*, **43**, 2005–2026.

Černý, P., Roberts, W.L., Ercit, T.S., Chapman, R. (1985): Wodginite and associated oxide minerals from the Peerless pegmatite, Pennington Country, South Dakota. *Am. Mineral.*, **70**, 1044–1049.

Černý, P., Goad, B.E., Hawthorne, F.C., Chapman, R. (1986): Fractionation trends of the Nb- and Ta-bearing oxide minerals in the Greer Lake pegmatite granite and its pegmatite aureole, southeastern Manitoba. *Am. Mineral.*, **71**, 501–517.

Foster, M.D. (1960): Interpretation of the composition of lithium micas. *U.S. Geol. Surv. Prof. Paper*, **354-E**, 115–147.

Icenhower, J. & London, D. (1995): An experimental study of element partitioning between biotite, muscovite and coexisting peraluminous granitic melt at 200 MPa (H_2O). *Am. Mineral.*, **80**, 1229–1251.

Jahns, R.H. & Burnham, C.W. (1969): Experimental studies of pegmatite genesis: I. A model for the derivation and crystallization of granite pegmatites. *Econ. Geol.*, **64**, 843–864.

Lechler, P.J. & Desilets, M.O. (1987): A review of the use of loss on ignition as a measurement of total volatiles in whole rock analysis. *Chem. Geol.*, **63**, 341–344.

Linnen, R.L. (1998): The solubility of Nb–Ta–Zr–Hf–W in granitic melts with Li and Li + F; constraints for mineralization in rare metal granites and pegmatites. *Econ. Geol.*, **93**, 1013–1025.

Linnen, R.L. & Cuney, M. (2005): Granite-related rare-element deposits and experimental constraints on Ta–Nb–W–Sn–Zr–Hf mineralization. *in* ''Rare-element geochemistry and mineral deposits'', R.L. Linnen & I.M. Sampson, eds. *Geol. Soc. Can. Short Course Notes, St. Catharines*, **17**, 45–68.

London, D. (1992): The application of experimental petrology to the genesis and crystallization of granitic pegmatites. *Can. Mineral.*, **30**, 499–540.

London, D. (2005): Geochemistry of alkali and alkaline earth elements in ore-forming granites, pegmatites and rhyolites. *in* ''Rare-element geochemistry and mineral deposits'', R.L. Linnen & I.M. Sampson, eds. *Geol. Soc. Can. Short Course Notes, St. Catharines*, **17**, 17–44.

London, D. (2008): Pegmatites. *The Canadian Mineralogist, Special Publication*, **10**, 347 pp.

London, D., Wolf, M.B., Morgan VI, G.B., Garrido, M.G. (1999): Experimental silicate-phosphate equilibria in peraluminous granitic magmas, with a case study of the Albuquerque batholith at Tres Arroyos, Badajoz, Spain. *J. Petrol.*, **40**, 215–240.

Long, P.E. (1978): Experimental determination of partition coefficients for Rb, Sr and Ba between alkali feldspar and silicate liquid. *Geochim. Cosmochim. Acta*, **42**, 833–846.

Mittlefehldt, D.W. & Miller, C.F. (1983): Geochemistry of the Wash Pluton, California: implications for ''anomalous'' trace element behaviour during differentiation of felsic magmas. *Geochim. Cosmochim. Acta*, **47**, 109–124.

Neiva, A.M.R., Silva, M.M.V.G., Gomes, M.E.P. (2007): Crystal chemistry of tourmaline from Variscan granites, associated tin-tungsten- and gold deposits, and associated metamorphic and metasomatic rocks from northern Portugal. *N. Jb. Miner. Abh.*, **184**, 45–76.

Neiva, A.M.R., Gomes, M.E.P., Ramos, J.M.F., Silva, P.B. (2008): Geochemistry of granitic aplite-pegmatite sills and their minerals from Arcozelo da Serra area (Gouveia, central Portugal). *Eur. J. Mineral.*, **20**, 465–485.

Peccerillo, A., Rotura, S., Pinarelli, L., Del Moro, A. (1994): Interaction between mafic and silic magmas in granitoid plutons as inferred from geochemical and Sr–Nd isotopic study of granitoids and host enclaves from Cima d'Asta, Southern Alps, Italy. *in* ''Some Contributions to Circum-Mediterranean Basements and Granitoids'', F.P. Sassi & A. Peccerillo, eds. *Period. Mineral.*, **63**, 93–111.

Raimbault, L. (1998): Composition of complex lepidolite-type granitic pegmatites and of constituent columbite-tantalite, Chèdeville, Massif Central, France. *Can. Mineral.*, **36**, 563–583.

Ramos, J.M.F. (1998); Mineralizações de metais raros de Seixo Amarelo-Gonçalo (Guarda). Unpublished PhD thesis, University of Lisbon, Portugal, 659 p.

Rieder, M., Cavazzini, G., D'Yakonov, Yu S., Frank-Kamenetskü, V.A., Gottardi, G., Guggenheim, S., Koval, P.V., Müller, G., Neiva, A.M.R., Radoslovich, E.W., Robert, J.-L., Sassi, F.P., Takeda, H., Weiss, Z., Wones, D.R. (1999): Nomenclature of the micas. *Mineral. Mag.*, **63**, 267–279.

Shearer, C.K., Papike, J.J., Jolliff, B.L. (1992): Petrogenetic links among granites and pegmatites in the Harney Peak rare-element granite-pegmatite system, Black Hills, South Dakota. *Can. Mineal.*, **30**, 785–810.

Simmons, Wm. B. & Webber, K.L. (2008): Pegmatite genesis: state of the art. *Eur. J. Mineral.*, **20**, 421–438.

Spilde, M.N. & Shearer, C.K. (1992): A comparison of tantalum-niobium oxide assemblages in two mineralogically distinct rare-element granitic pegmatites, Black Hills, South Dakota. *Can. Mineral.*, **30**, 719–737.

Tertian, R. & Claisse, F. (1982): Principles of Quantitative X-Ray Fluorescence Analysis. Heyden & Son Ltd, UK, 355 p.

Tischendorff, G., Gattesmann, B., Förster, H.-J., Trumbull, R.B. (1997): On Li-bearing micas: estimating Li from electron microprobe analyses and an improved diagram for graphical representation. *Mineral. Mag.*, **61**, 809–834.

White, V.M. (2003): High temperature applications. II. Oxygen isotopes as an indicator of assimilation. *Geol. 656 Isot. Geochem.*, **Lecture 30**, 227–231.
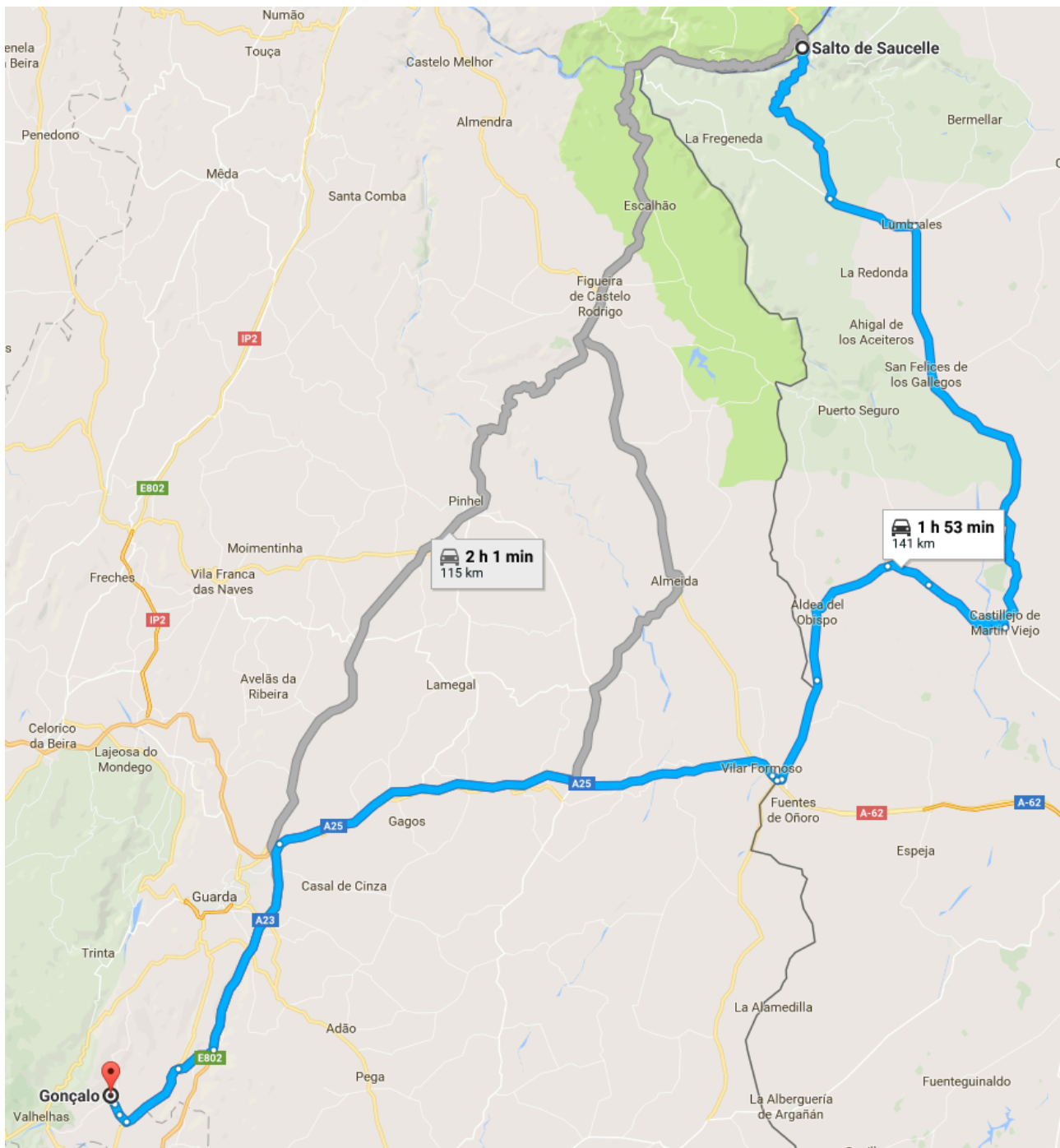
Travel back to the hotel: ≈ 141 km, 2h

September 14th, morning: STOP 4: Alberto I open-pit (Locality 1: Fregeneda-Almendra aplite-pegmatite field)

Travel from the Hotel to the Alberto I open-pit: 26 km, ≈ 35min

# Locality 1: Fregeneda-Almendra aplite-pegmatite field (Salamanca, Spain)

Stop 1 (12th of September, afternoon) and Stop 4 (14th of September, morning)

General Highlights

-Over two hundreds of aplite-pegmatite dykes, grouped in 11 types from barren to highly enriched in Li+F (Fig. 3 and Table 2).

-Zonal distribution, with a Li+F enrichment northwards (Fig. 3).

-Main Li-rich minerals: spodumene ± petalite, Li-muscovite & lepidolite.

-The origin of the Li-rich aplite-pegmatites is probably related to the extreme fractionation of a late-D3 highly peraluminous granitic melt.

Stop 4 Highlights (Alberto I open pit, 14th of September, morning)

-Feldspars+Li mine from the mid nineties up to now.

-Spodumene ± petalite-rich (type 8 in Fig. 3 and Table 2), subvertical aplite-pegmatites bodies, up to 6 m thick.

-No internal zoning or layering is observed, just some feldspars and Li-aluminosilicates comb crystals, growing perpendicular to the contacts wit the country-rock.

-Overall Li-enrichment of the aplite-pegmatite >1% Li_2O. Low F contents.
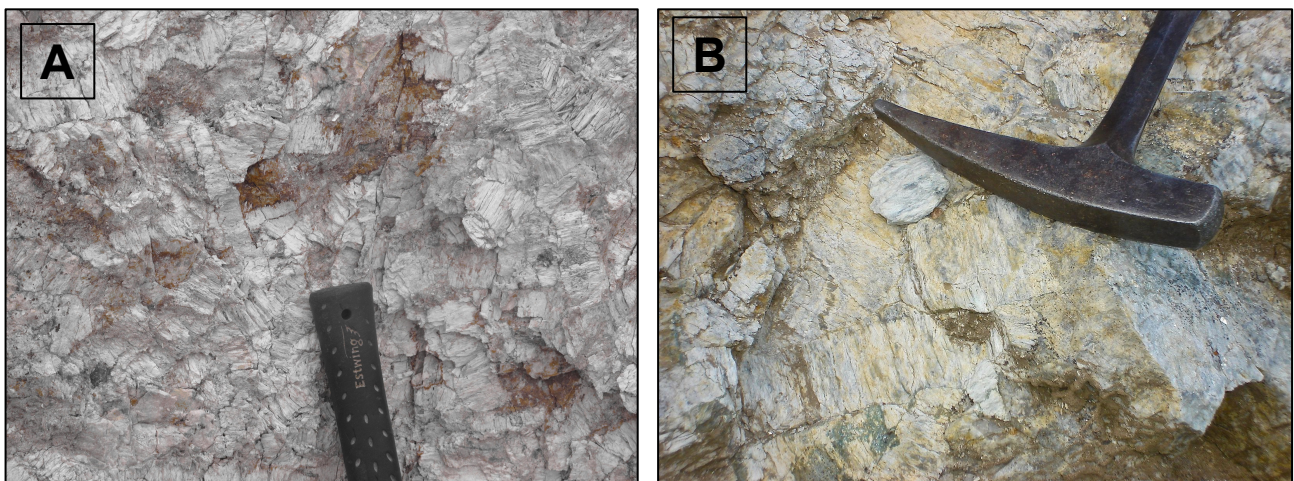
Stop 4: A) Spodumene prismatic crystals, randomly distributed together with albite ± quartz in one of the dykes from Alberto I open pit; and, B) idem with petalite crystals instead of spodumene.
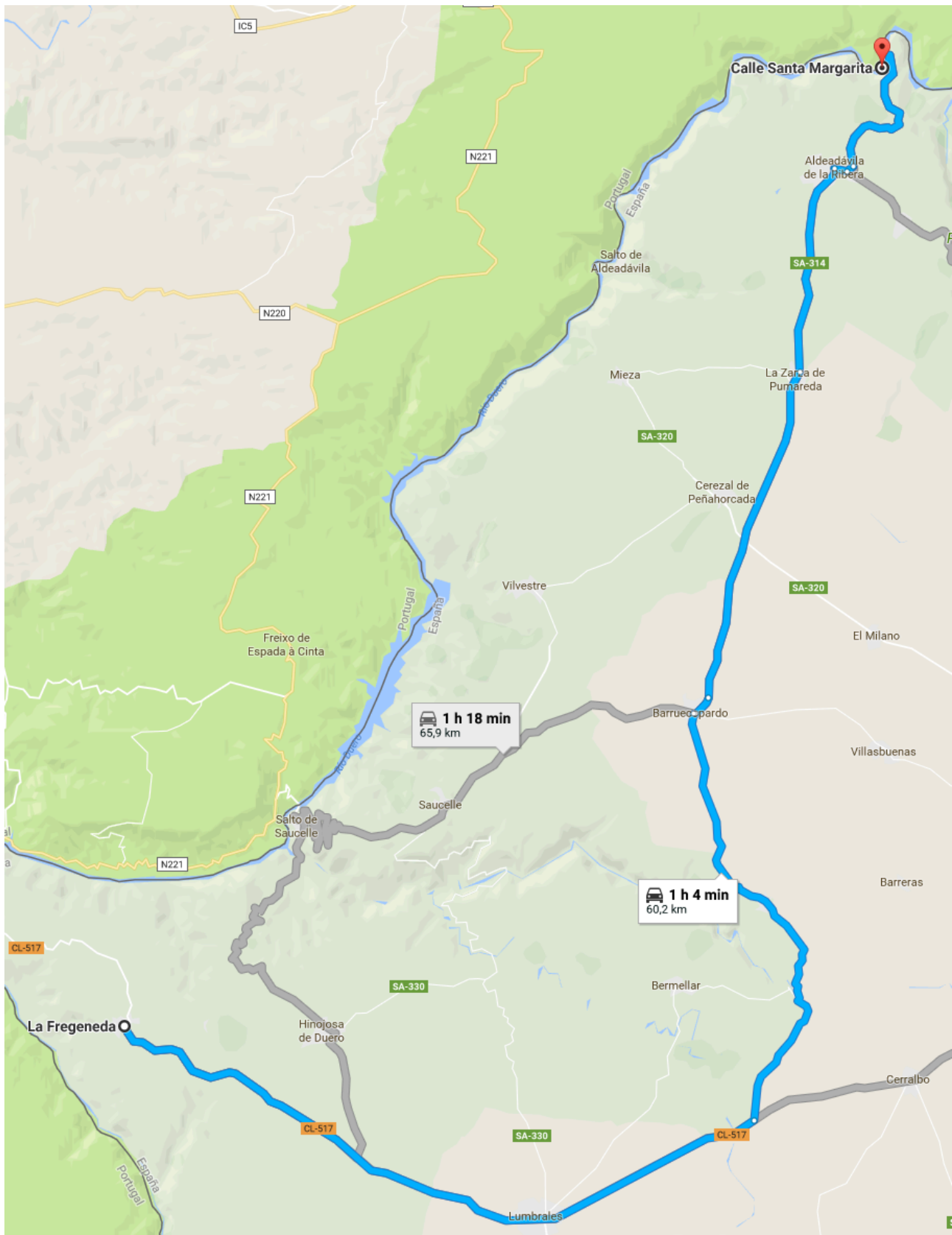
**Travel to the boat for the trip along the Duero river: ≈ 63 km, 1h10min
and later lunch at "El Zebadero" Restaurant**

BIBLIOGRAPHY

Alves, P. 2013 Morinita de la mina "Senhora da Assunção", Ferreira de Aves (Viseu, Portugal). Acopios 4, 73-84

Antunes, I.M.H.R., Neiva, A.M.R., Farinha Ramos, J.M., Silva, P.B., Silva, M.M.V.G. and Corfu, F., 2013. Petrogenetic links between lepidolite-subtype aplite-pegmatite, aplite veins and associated granites at Segura (central Portugal). Chem der Erde - Geochemistry 73, 323–341.

Bea, F., Montero, P. and Molina, J.F., 1999. Mafic precursors, peraluminous granitoids, and late lamprophyres in the Avila batholith: A model for the generation of Variscan batholiths in Iberia. Journal of Geology 107(4), 399.

Caravalho J.M.F. and Farinha J.A.L.B. (2004) Lithium potentialies in notherns Portugal, 17th Industrial Minerals International Congress,

Carnicero, M. A. 1981. Granitoides del Centro Oeste de la Provincia de Salamanca. Clasificación y correlación. Cuad. Lab. Xeol. Laxe. 2, 45-49.

Černý, P. and Ercit, T.S., 2005. The classification of granitic pegmatites revisited. Canadian Mineralogist 43, 2005-2026.

Charoy, B. and Noronha, F., 1996. Multistage Growth of a Rare-Element, Volatile-Rich Microgranite at Argemela (Portugal). Journal of Petrology 37(1), 73-94.

Costa M. M. (2006) - Geoquímica de granitóides de Pera Velha – Vila Nova de Paiva – Ferreira de Aves. Tese de Mestrado. Univ. de Aveiro. 150p.

Dias, G., Leterrier, J., Mendes, A., Simões, P.P. and Bertrand, J.M., 1998. U-Pb zircon and monazite geochronology of post-collisional Hercynian granitoids from the Central Iberian Zone (Northern Portugal). Lithos 45(1-4), 349-369.

Dias, G., Simões, P.P., Ferreira, N. and Leterrier, J., 2002. Mantle and Crustal Sources in the Genesis of Late-Hercynian Granitoids (NW Portugal): Geochemical and Sr-Nd Isotopic Constraints. Gondwana Research 5(2), 287-305.

Dias, P.A. et al., 2013. Pegmatite Productive Terrains in the Variscan Granite Hosts From Northern and Central Portugal, 23rd International Mining Congress & Exhibition of Turkey, pp. 2121-2129.

Ferreira, J., Araújo, P., Guimarães, F., Pereira, M., Leal Gomes, C. 2014. Geoquímica do Ta e estrutura da sua distribuição no Grupo Pegmatítico Granítico de Senhora da Assunção, Sátão, Centro de Portugal. Comunicaçoes Geológicas, 101, Especial 11, 781-785.

Fuertes-Fuente, M. and Martín-Izard, A., 1998. The Forcarei Sur rare-element granitic pegmatite field and associated mineralization, Galicia, Spain. Can Mineral, 36: 303-325.

Gallego-Garrido, M., 1992. Las mineralizaciones de Li asociadas a magmatismo ácido en Extremadura y su encuadre en la Zona Centro-Ibérica. PhD Thesis, Universidad Complutense de Madrid, Spain, 323 pp.

Garate-Olave, I., A., M., Roda-Robles, E., Gil-Crespo, P.P. and Pesquera, A., 2017. Extreme fractionation in a granite-pegmatite systema documented by quartz chemistry: The cas study of Tres Arroyos (Central Iberuan Zone, Spain). Lithos 286-287, 162-174.

Garate-olave, I., Roda-robles, E., Gil-crespo, P.P. and Pesquera, A., 2014. Caracterización petrográfica y geoquímica de las micas asociadas al sistema granito-pegmatitas del área de Tres Arroyos.

Hochleitner R. and Fehr K.T. 2005 Isokite, CaMg[F|PO4], from Senhora de Assunção, Portugal: new find and new data. N. Jb. Miner. Abh, 182/1: 103-108

Leal Gomes, C., 1994. Estudo estrutural e paragenético de um sistema pegmatóide granítico. O campo aplito-pegmatiítico de Arga Minho, Portugal, Ph. D. Universidade do Minho, 695 pp.

Leal Gomes, C., Azevedo, A., Lopes Nunes, J. and Dias, P.A., 2009. Phosphate fractionation in pegmatites of Pedra da Moura II claim – Ponte da Barca – Portugal. Estudos Geológicos 19(2), 172-176.

Lima, A., 2000. Estrutura, Mineralogia e Génese dos Filões Aplitopegmatíticos com Espodumena da Região do Barroso-Alvão (Norte de Portugal), Univ. Porto, Portugal and INPL, Nancy, France, 270 p.

Lima, A., Rodrigues, R., Guedes, A. and Novák, M., 2009. The Rare Elements-Rich Granite Of Seixoso Area (Outeiro Mine). Preliminary results. Estudos Geológicos 19(2), 182-187.

Martín-Izard, A., Reguilón, R. and Palero, F., 1992. Las mineralizaciones litiníferas del oeste de Salamanca y Zamora. Estudios Geológicos 48, 9-13.

Martínez Catalán, J.R., Fernández-Suárez, J., Jenner, G.A., Belousova, E. and Díez Montes, A., 2004. Provenance constraints from detrital zircon U-Pb ages in the NW Iberian Massif: implications for Palaeozoic plate configuration and Variscan evolution. Journal of the Geological Society 161(3), 463-476.

Martins, T., Roda-Robles, E., Lima, A. and de Parseval, P., 2012. Geochemistry and Evolution of Micas in the Barroso-Alvao Pegmatite Field, Northern Portugal. The Canadian Mineralogist 50(4), 1117-1129.

Neiva, A., & Ramos., 2009. Petrogenetic links of granitic aplite-pegmatite sills from Gonçalo with granites from Guarda-Belmonte area, central Portugal. Estudos Geológicos, 19(2), 251-255.

Neiva, A.M.R. and Ramos, J.M.F., 2010. Geochemistry of granitic aplite-pegmatite sills and petrogenetic links with granites, Guarda-Belmonte area, central Portugal. European Journal of Mineralogy 22(6), 837-854.

Neiva, A.M.R., Silva, P.B. and Ramos, J.M.F., 2011. Geochemistry of granitic aplite-pegmatite veins and sills and their minerals from Cabeço dos Poupos, Sabugal, Central Portugal. Contributions to the 5th International Symposium on Granitic Pegmatites 143(May), 141-143.

Nitschke, 1998. Tungsten and fluorine in calc-silicate rocks at Riba d'Alva, NE Portugal.

Ramos, J.M.F. (1998); Mineralizaçoes de metais raros de Seixo Amarelo-Gonçalo (Guarda). Unpublished PhD thesis, University of Lisbon, Portugal, 659 pp.

Roda, E., Pesquera, A., Fontan, F. and Keller, P., 2004. Phosphate mineral associations in the Canada pegmatite (Salamanca, Spain): Paragenetic relationships, chemical compositions, and implications for pegmatite evolution. American Mineralogist 89(1), 110-125.

Roda, E., Pesquera, A., Velasco, F. and Fontan, F., 1999. The granitic pegmatites of the Fregeneda area (Salamanca, Spain): characteristics and petrogenesis. Mineralogical Magazine 63(4), 535-558.

Roda, E. Vieira, R. Lima, A. Pesquera, A. Noronha, F. Fontan, F., 2007. The Fregeneda – Almendra pegmatitic field (Spain & Portugal): mineral assemblages and regional zonation. Granitic Pegmatites: The State of the Art–International Symposium(May), 3-4.

Roda-Robles, E., 1993. Distribución, características y petrogénesis de las pegmatitas de La Fregeneda (Salamanca). PhD Thesis, Universidad del País Vasco, Spain, 199 pp.

Roda-Robles, E. Mateus, S. Vieira, R. Martins, T. Vide, R. Lima, A,. 2008. Phosphate mineral associations in the Seixeira pegmatite (Bendada, Sabugal, Guarda, Portugal): preliminary results, IX CGPLP—IX Congresso de Geoquímica dos Países de Língua Portuguesa, pp. 39.

Roda-Robles, E., Pesquera, A., Gil-Crespo, P. and Torres-Ruiz, J., 2012a. From granite to highly evolved pegmatite: A case study of the Pinilla de Fermoselle granite–pegmatite system (Zamora, Spain). Lithos 153, 192-207.

Roda-Robles, E., Pesquera, A., Gil-Crespo, P.P., Garate-Olave, I. and Ostaikoetxea-Garcia, U., 2013. Textural and mineralogical features of the Li-F-Sn-bearing pegmatitic rocks from Castillejo de Dos Casas (Salamanca, Spain): preliminary results, 6th International Symposium on granitic pegmatites. Contributions to the 6th international symposiumon granitic pegmatites, pp. 118-119.

Roda-Robles, E., Pesquera, A., Gil-Crespo, Garate-Olave, I., P.P. and Torres-Ruiz (2015) The Li-rich aplopegmatite from Castillejo de Dos Casas (Salamanca, Spain): Example of a highly fractionated granite-pegmatite system. Proceedings SGA2015, vol. 2, 11–15

Roda-Robles, E., Pesquera, A., Gil-Crespo, P.P. and Torres-Ruiz, J., 2012b. The Puentemocha Beryl-Phosphate Granitic Pegmatite, Salamanca, Spain: Internal Structure, Petrography and Mineralogy. The Canadian Mineralogist 50(6), 1573-1587.

Roda-Robles, E. Pesquera, A. Gil-Crespo, P. P. Vieira, R. Lima, A. Garate-Olave, I. Martins, T. Torres-Ruiz, J.2016. Geology and mineralogy of Li mineralization in the Central Iberian Zone (Spain and Portugal). Mineralogical Magazine 80(1), 103-126.

Roda-Robles, E., Vieira, R., Lima, A. and Pesquera-Pérez, A., 2009. Petrogenetic links between granites and pegmatites in the Fregeneda-Almendra area (Salamanca, Spain and Guarda, Portugal): new insights from 40Ar/39Ar dating in micas. Estudos Geologicos 19(2), 305-310.

Roda-Robles, E., Vieira, R., Pesquera, A. and Lima, A., 2010. Chemical variations and significance of phosphates from the Fregeneda-Almendra pegmatite field, Central Iberian Zone (Spain and Portugal). Mineralogy and Petrology 100(1-2), 23-34.

Roda-Robles, E. Villaseca, C. Pesquera, A. Gil-Crespo, P.P. Vieira, R. Lima, A. Garate-Olave, I., Submitted. Petrogenetic relationships among Variscan granitoids and Li-(F-P)-rich aplite-pegmatites in Central Iberian Zone: geological and geochemical constraints and implications for the other regions from the European Variscides. Ore geology Reviews.

Roda-Robles, E., Pesquera, A., García De Madinabeitia, S., Gil Ibarguchi, J. I., Nizamoff, J., Simmons, W., Falster, A., Galliski, M. A. 2014. On the geochemical character of primary Fe-Mn phosphates belonging to the triphylite-lithiophilite, graftonite-beusite, and triplite-zwieselite series: First results and implications for pegmatite petrogenesis. Canadian Mineralogist 52(2), 321-335.

Teixeira, C., Santos, J.P., Lopes, J.V.T., Pilar, L., Pereira, V.C. (1972) – Carta Geológica de Portugal, escala 1: 50000, Folha 14D (Aguiar da Beira) e respectiva notícia explicativa. Serv. Geol. Portugal, Lisboa.

Trabulo, L. C., Gomes, C. L. & Nunes, J. L. (1995) Enquadramento geológico, estrutura e paragénese do grupo pegmatítico de Senhora da Assunção – Aguiar da Beira – Centro de Portugal. Memória Mus. Lab. Min. Geol. Univ. Porto, 4, pp. 837-841.

Vieira, R., 2010. Aplitopegmatitos com elementos raros da região entre Almendra (V. N. de Foz-Côa) e Barca d'Alba (Figueira de Castelo Rodrigo). Campo aplitopegmatítico da Fregeneda-Almendra. PhD Thesis, Universidade do Porto, Portugal, 275 pp.

Vieira, R., Lima, A., Robles, E.R. and Martins, T., 2007. Lithium-bearing pegmatite resources at Fregeneda-Almendra pegmatitic field (Spain & Portugal). Geochimica Et Cosmochimica Acta 71(15), A1066-A1066.

Vieira, R., Roda-Robles, E., Pesquera, A. and Lima, A., 2011. Chemical variation and significance of micas from the Fregeneda-Almendra pegmatitic field (Central-Iberian Zone, Spain and Portugal). American Mineralogist 96(4), 637-645.

Villaseca, C., 2011. On the origin of granite types in the Central Iberian Zone: contribution from integrated U-Pb and Hf isotope studies of zircon, VIII Congresso Ibérico de Geoquímica, Livro de Actas 1,271-276.